

Functional characterization of the inverse FBAR-containing proteins
srGAP1 and Carom

Dissertation

der Mathematisch-Naturwissenschaftlichen Fakultät
der Eberhard Karls Universität Tübingen
zur Erlangung des Grades eines
Doktors der Naturwissenschaften
(Dr. rer. nat.)

vorgelegt von
Anitha Jeyanthan, geb. Jeganantham
aus Hof (Bayern)

Tübingen

2015

Gedruckt mit Genehmigung der Mathematisch-Naturwissenschaftlichen Fakultät der Eberhard Karls Universität Tübingen.

Tag der mündlichen Qualifikation:

13.05.2015

Dekan:

Prof. Dr. Wolfgang Rosenstiel

1. Berichterstatter:

Dr. Yvonne Groemping

2. Berichterstatter:

Prof. Dr. Thilo Stehle

For my family

ACKNOWLEDGEMENTS

First, I want to thank my supervisor Dr. Yvonne Groemping for this challenging and exciting research project and for her guidance throughout the years. I want to thank Professor Dr. Andrei Lupas for letting me work in his department, for being a member in my TAC committee and for his constant support. I would also like to thank the other members of my TAC committee Dr. Christian Soellner and Professor Dr. Thilo Stehle for their invaluable guidance, discussion and support during critical times.

I would like to thank the members of the Soellner research group: Horst Geiger, Paolo Panza and my dear friend Xuefan Gao for teaching me to how to work with zebrafish, the fruitful discussions and the nice working atmosphere. Xuefan, thank you for always supporting me and for being a great friend.

Then, I want to thank Dr. Wolfram Antonin for letting me work in his research group. I am sincerely thankful to Dr. Nathalie Eisenhardt for introducing me to the GUV assays. Thank you for spending your last days at the institute with helping me to improve the assays.

I also want to thank Dr. Matthias Floetenmeyer and Juergen Berger as well as Dr. Christian Liebig for introducing me to EM and light microscopy

Next, I want to thank Johannes Madlung of the mass spectrometry facility of the proteome centre in Tuebingen for analysing my pulldown experiments.

I also would like to thank Dr. Aleksander Czogalla of the Hertie Institute in Dresden, who carried out the initial GUV assays.

I want to thank the International PhD programme coordinator Dagmar Sigurdardottir for her support and guidance, especially in my final year.

A big thanks to Reinhard Albrecht and Kerstin Baer for setting up the crystallization screens and to Dr. Marcus Hartmann for trying to solve the structure of the Carom FBAR domain.

I would also like to thank Dr. Moritz Ammelburg for showing me how to carry out bioinformatical analysis and Silvia Wuertenberger, who introduced me to several new methods in the lab.

My sincere thanks to Dr. Murray Coles, who measured all the NMR experiments, which are a big part in this thesis.

I would like to thank my RISE internship students Arjun Sharma and Aimee Landry. It was a great experience to have you here.

Special thanks to Iuliia Boichenko, Dr. Birte Hernandez-Alvarez, Beatrice Laudenbach and Eva Sulz for their invaluable friendship and their constant support. It means a lot to me.

I want to thank the current and former members of the Department I for the nice and enjoyable working atmosphere. In alphabetical order: Jyoti Adlakha, Vikram Alva, Harshul Arora, Jens Baßler, Professor Dr. Volkmar Braun, Manish Chaubey, Silvia Deiss, Mohammed ElGamacy,

Carolin Ewers, Dara Foruozan, Adrian Fuchs, Claudia Gehring, Ioanna Karamichali, Klaus Kopec, Mateusz Korycinski, Amit Kumar, Karin Lehmann, Joerg Martin, Martin Michelke, Juthaporn Sangwallek, Franka Scharfenberg, Martin Schueckel, Edgardo Sepulveda, Astrid Ursinus and Hongbo Zhu.

At the end, I want to thank my family and friends. Words cannot describe how thankful I am to my parents, my sister Jenitta and my beloved husband Jeyanthan, who were always there for me throughout the good and bad times. Without you I would not have come so far. Thank you for always supporting me and believing in me.

TABLE OF CONTENTS

1. LIST OF ABBREVIATIONS	1
2. ABSTRACT	4
3. INTRODUCTION	5
3.1 NEURONAL DEVELOPMENT	5
3.2 THE SLIT-ROBO PATHWAY	7
3.2.1 THE SLIT LIGAND	7
3.2.2 THE ROUNDABOUT RECEPTOR	8
3.3 THE DISCOVERY OF THE SRGAP FAMILY	10
3.3.1 THE DOMAINS OF THE SRGAP FAMILY	10
3.3.1.1 The srGAP FBAR domain	10
3.3.1.1.1 The Classical BAR/NBAR domain	11
3.3.1.1.2 The FBAR domain	12
3.3.1.1.3 The I-BAR domain	12
3.3.1.2 The srGAP GAP domain	14
3.3.1.2.1 The RhoGTPases	14
3.3.1.2.2 The RhoGAP family	16
3.3.1.3 The srGAP SH3 domain	17
3.3.1.4 The srGAP C-terminal domain	18
3.4 THE FCH AND DOUBLE SH3 DOMAIN FAMILY-ANOTHER MEMBER OF THE I-FBAR CONTAINING PROTEINS	20
3.4.1 NERVOUS WRECK	20
3.4.2 THE HUMAN NWK HOMOLOG-THE FCHSD2 PROTEIN	22
4. GOAL OF THE PROJECT	23
5. CONTRIBUTIONS	24
6. MATERIALS AND METHODS	26
6.1 MATERIALS	26
6.1.1 CHEMICALS AND ENZYMES	26
6.1.2 USED BACTERIAL STRAINS	26
6.1.3 PLASMIDS	27
6.1.4 OLIGONUCLEOTIDES	28
6.1.5 CLONING VECTORS	28
6.1.5.1 pET28b	28
6.1.5.2 pET47b	29
6.1.5.3 pGEX4T1	29
6.1.5.4 pGEX6P1	29
6.1.6 MEDIA AND ADDITIVES	30
6.1.7 BUFFERS	30
6.1.7.1 Agarose Gel Buffer	30

6.1.7.2 SDS Gel buffer	31
6.1.7.3 Western Blot	32
6.1.7.4 Buffer for silver staining of SDS-gels	32
6.1.7.5 Buffer for protein purification	33
6.1.7.5.1 srGAP1 FBAR domain 21-469 of <i>Homo sapiens</i>	33
6.1.7.5.2 srGAP1 FBAR domain 20-460 of <i>Pristionchus pacificus</i>	34
6.1.7.5.3 srGAP1 FBAR domain 21-475 of zebrafish	35
6.1.7.5.4 Purification buffers for GST-tagged proteins	36
6.1.7.5.5 Carom FBAR domain	37
6.1.7.6 Buffer for rat brain and zebrafish pulldown	37
6.1.7.7 Buffers for single and double <i>in-situ</i> hybridization	38
6.2 METHODS	38
6.2.1 METHODS IN MOLECULAR BIOLOGY	38
6.2.1.1 Polymerase chain reaction	38
6.2.1.2 Restriction digest	39
6.2.1.3 Ligation	40
6.2.1.4 Competent <i>E. coli</i> cells	40
6.2.1.5 Transformation in competent <i>E. coli</i> cells	41
6.2.1.6 Preparation of plasmid DNA	41
6.2.1.7 Sequencing of target DNA	41
6.2.2 METHODS IN PROTEIN BIOCHEMISTRY	41
6.2.2.1 Overexpression of the proteins in <i>E. coli</i> in LB-Medium	41
6.2.2.2 Overexpression of proteins in M9-Medium	42
6.2.2.3 Purification of 6-His-tagged proteins	43
6.2.2.4 Purification of GST-tagged proteins	43
6.2.2.5 Purification of ¹³ C and ¹⁵ N labelled proteins for NMR	43
6.2.2.6 Preparation of nucleotide-free RhoGTPases	43
6.2.2.6.1 Nucleotide-free RhoGTPases with alkaline phosphatase	43
6.2.2.6.2 Nucleotide-free RhoGTPases with EDTA	44
6.2.2.7 SDS Polyacrylamide gelelectrophoresis	44
6.2.2.8 Silver staining	45
6.2.3 BIOPHYSICAL METHODS	45
6.2.3.1 Circular Dichroism Spectroscopy	45
6.2.3.2 Nuclear Magnetic Resonance	46
6.2.3.3 Crystallography	46
6.2.3.4 Mass spectrometry analysis	47
6.2.4 BIOINFORMATICS	48
6.2.5 <i>IN VIVO</i> AND <i>IN VITRO</i> ASSAYS	48
6.2.5.1 Pulldown	48
6.2.5.2 <i>In-situ</i> hybridization in zebrafish embryos	49
6.2.5.2.1 Handling of zebrafish embryos	49
6.2.5.2.2 Generating template for <i>in-vitro</i> transcription	49

6.2.5.2.3 Single <i>in-situ</i> hybridization	49
6.2.5.2.4 Double <i>in-situ</i> hybridization	50
6.2.5.3 Assays with liposomes	51
6.2.5.3.1 Generating the liposomes	51
6.2.5.3.2 Co-sedimentation with high speed centrifugation	52
6.2.5.3.3 Negative stain electron microscopy	53
6.2.5.3.4 Giant unilamellar vesicle assay	53
7. RESULTS	54
7.1 CHARACTERIZATION OF THE SRGAP1 PROTEIN	54
7.1.1 BIOINFORMATICAL CLUSTER ANALYSIS OF THE SRGAP FAMILY	54
7.1.2 DEVELOPMENTAL AND TISSUE-SPECIFIC EXPRESSION ANALYSIS OF <i>SRGAP1</i> IN ZEBRAFISH EMBRYOS	59
7.1.2.1 Gene expression pattern analysis in developing zebrafish embryos	59
7.1.2.1.1 Expression of <i>srgap1</i> in developing zebrafish embryos	59
7.1.2.1.2 Comparison of the expression pattern of <i>srgap1</i> with <i>robo1-3</i>	61
7.1.2.2 <i>srgap1</i> co-localizes with <i>robo1</i> in developing zebrafish embryos	66
7.1.3 STRUCTURAL ANALYSIS OF THE SRGAP1 FBAR DOMAIN	70
7.1.3.1 The human srGAP1 FBAR domain	70
7.1.3.2 The SRGAP1 FBAR domain of <i>Pristionchus pacificus</i>	73
7.1.3.3 The srGAP1 FBAR domain of zebrafish	74
7.1.4 FUNCTIONAL CHARACTERIZATION OF THE SRGAP1 FBAR DOMAIN OF ZEBRAFISH	77
7.1.4.1 The srGAP1 FBAR domain of zebrafish co-sediments with negatively charged liposomes	77
7.1.4.2 The srGAP1 FBAR domain of zebrafish leads to indentations of charged liposomes	79
7.1.4.3 The srGAP1 FBAR domain of zebrafish causes invagination of giant unilamellar vesicles	80
7.1.4.4 Time-dependent invagination of GUVs by the srGAP1 FBAR domain	81
7.1.5 COMPARISON OF THE BINDING SPECIFICITY OF THE HUMAN SRGAP1 GAP DOMAIN AND ITS ZEBRAFISH HOMOLOG TO THREE MEMBERS OF THE RHOGTPASES	83
7.1.5.1 The human srGAP1 GAP domain binds to the human Cdc42, but not to human RhoA and Rac1	83
7.1.5.2 The human srGAP1 GAP domain is active and increases the intrinsic hydrolysis rate of the human Cdc42	87
7.1.5.3 The zebrafish srGAP1 GAP domain increases the intrinsic hydrolysis rate of the zebrafish Cdc42	91
7.1.5.4 No effect observed on the intrinsic hydrolysis activity of the Cdc42 proteins in cross-organism ³¹ P-NMR measurements	95
7.1.5.5 Mapping of the srGAP1 GAP domain binding sites on the homologous Cdc42 proteins	96

7.1.5.5.1 Mapping of the human srGAP1 GAP domain binding sites on the human Cdc42	97
7.1.5.5.2 Mapping of the zebrafish srGAP1 GAP domain binding sites on the zebrafish Cdc42.....	99
7.1.6 POSSIBLE NEW INTERACTION PARTNERS FOR THE HUMAN SRGAP1 PROTEIN AND ITS ZEBRAFISH HOMOLOG	103
7.1.6.1 Prediction of protein binding motifs in the human srGAP1 C-terminus	103
7.1.6.2 Rat brain pulldown with the human srGAP1 C-terminus hints to possible new interaction partners	105
7.1.6.3 Prediction of protein binding motifs in the C-terminal domain of the zebrafish srGAP1	110
7.1.6.4 No relevant hints for potential interaction partners for the zebrafish srGAP1 C-terminus	111
7.2 STRUCTURAL AND FUNCTIONAL CHARACTERIZATION OF THE FBAR DOMAIN OF THE HUMAN CAROM PROTEIN	114
7.2.1 BIOCHEMICAL CHARACTERIZATION OF THE FBAR DOMAIN OF THE HUMAN CAROM PROTEIN	114
7.2.1.1 Purification and biochemical analysis of the FBAR domain of the human Carom protein	114
7.2.1.2 First crystals for the human Carom FBAR domain	117
7.2.2 MEMBRANE DEFORMING ACTIVITY OF THE HUMAN CAROM FBAR DOMAIN	121
7.2.2.1 The Carom FBAR domain induces scalloping of giant unilamellar vesicles	121
7.2.2.2 The Carom FBAR domain binds to giant unilamellar vesicles	122
7.2.2.3 Time-dependence of the deformation of giant unilamellar vesicles by the Carom FBAR domain	124
8. DISCUSSION	126
8.1 <i>SRGAP1</i> IS EXPRESSED IN NEURONAL TISSUES OF ZEBRAFISH EMBRYOS	126
8.2 THE SRGAP1 FBAR DOMAIN BELONGS TO THE INVERSE FBAR SUBFAMILY	127
8.3 THE SRGAP1 GAP DOMAIN BINDS TO THE RHOGTPASE CDC42 AND INCREASES ITS INTRINSIC HYDROLYSIS RATE	132
8.4 POTENTIAL NEW PATHWAY INVOLVEMENTS FOR THE SRGAP1 PROTEIN	134
8.5 OUTLOOK	138
9. REFERENCES	139

1. LIST OF ABBREVIATIONS

A	Ampere
Å	Ångström
Aa	Amino acid
<i>A. dest.</i>	Distilled water
APS	Ammonium persulfate
β-DDM	n-Dodecyl β-D-maltoside
BA	Branchial arches
bp	Base pair
BDNF	Brain-derived neurotrophic factor
BDT	Big Dye Terminator
BSA	Bovine Serum Albumin
°C	Celsius
CaCl ₂	Calcium chloride
<i>C.elegans</i>	<i>Caenorhabditis elegans</i>
Ca(OA ₂)	Calcium acetate
CD	Circular dichroism
Cdc42	Cell division control protein 42 homolog
CNS	Central nervous system
comm	Commissureless
C-term	C-terminus
Da	Dalton
DiD	Dicarbocyanine
DNA	Deoxynucleic acid
Dnase	Deoxyribonuclease
dNTP	deoxynucleoside triphosphate
<i>E. coli</i>	<i>Escherichia coli</i>
EDTA	Ethylenediaminetetraacetic acid
EGF	Epidermal growth factor
<i>et al.</i>	<i>et alii</i>
FB	Forebrain
FBAR	FCH Bin-Amphiphysin-Rvs
FISH	Fluorescent <i>in-situ</i> hybridization
fw	Forward
GAP	GTPase activating protein
GEF	Guanine exchange factor
GDI	Guanine nucleotide dissociation inhibitor
GppNHp	5'Guanylyl imidodiphosphate
GTP/GDP	Guanosine triphosphate/Guanosine diphosphate
GTPase	Guanosine triphosphatase
h	Hour
HB	Hindbrain
Hs/ <i>H. sap.</i>	<i>Homo sapiens</i>
HEPES	4-(2-hydroxyethyl)-1-piperazineethanesulfonic acid
hpf	Hours post fertilization
HSQC	Heteronuclear Single Quantum Coherence

IMAC	Immobilized metal ion affinity chromatography
IPTG	Isopropyl- β -D thiogalactopyranoside
K	Kilo
kDa	Kilo Dalton
L	Liter
LB	Lysogeny broth
LRR	Leucine-rich repeat
M	Molar
MABT	Maleic acid buffer containing Tween 20
MAD	Multi-wavelength anomalous diffraction
MB	Midbrain
MgCl ₂	Magnesium chloride
MHB	Mid-hindbrain boundary
mM	Millimolar
Min	Minute
<i>M. mus</i>	<i>Mus musculus</i>
μ	Micro
mRNA	Messenger RNA
MS	Mass spectrometry
N	Nano
NBT-BCIP	Nitro-blue tetrazolium chloride and 5-bromo-4-chloro-3'-indolyphosphate p-toluidine salt
NaCl	Sodium chloride
NaOAc	Sodium acetate
Ni-NTA	Nickel nitrilotriacetic acid
NMR	Nuclear Magnetic Resonance
N-term	N-terminus
Nwk	Nervous Wreck
OB	Olfactory bulb
OE	Olfactory epithelium
OP	Olfactory pit
PBS	Phosphate buffered saline
PBST	Phosphate buffered saline with Tween 20
PS	Phosphatidylcholine
PCR	Polymerase chain reaction
PCW	Post conception week
PDB	Protein data base
PE	Phosphatidylethanolamine
PEG	Polyethylene glycol
PEP	Posterior error probability
PF	Pectoral fin
PFA	Paraformaldehyde
pH	<i>Potentia Hydrogenii</i>
PI	Phosphatidylinositol
PI(4,5)P ₂	Phosphatidylinositol-4,5-biphosphate
PMSF	Phenylmethansulfonylfluoride
PP	<i>Pristionchus pacificus</i>

PS	Phosphatidylserine
R2/R3	Rhombomere 2/3
RNA	Ribonucleic acid
RhoA	Ras homolog gene family, member A
Robo	Roundabout receptor
RT	Retina
rv	Reverse
<i>S. cer.</i>	<i>Saccharomyces cerevisiae</i>
SC	Spinal cord
SDS	Sodium dodecyl sulfate
SDS-PAGE	Sodium dodecyl sulfate-polyacrylamide-gel electrophoresis
Sec	Second
SeMet	Selenomethionine
SH2	Src Homology 2
SH3	Src Homology 3
SHH	Sonic hedgehog
SLS	Swiss Light Source
srGAP	Slit-Robo GTPase activating protein
SVZa	subventricular zone
T	Tail
Tab	Table
TAE	Tris-Acetate-EDTA
TEMED	N, N, N', N'-Tetramethylethylenediamine
TeO	Tectum
Tris	Tris(hydroxymethyl) aminomethan
U	Unit
UV	Ultra violet
V	Volt
VZ	Ventricular zone
W	Watt
WT	Wild type
WW	Domain with two conserved tryptophans

2. ABSTRACT

The Slit-Robo GTPase activating protein family (srGAPs) consists of four members and are important multi-domain adaptor proteins, which are involved in axonal pathfinding and various other neuronal processes. This thesis explores the function of the human srGAP1 protein as well as its zebrafish homolog in three ways: 1) examining of the membrane deforming activity of the FBAR domain, 2) analysing the specific activity of the srGAP1 GAP domain towards three members of RhoGTPases, and 3) identifying potential novel interaction partners for the srGAP1 protein with the intention to determine new pathway involvements for the protein.

The work presented in this thesis shows that the srGAP1 FBAR domain can induce vesicle deformation in vesicle-based *in vitro* assays. Compared to the results of another FBAR domain-containing protein, the Carom protein, the srGAP1 FBAR domain is less potent in inducing invaginations of giant unilamellar vesicles. Both proteins do not induce formation of tubules as seen for classical FBAR domains, but lead to invaginations of the vesicles. Based on these results both proteins can be assigned to the recently found inverse FBAR subfamily. This work also measures the intrinsic GTP hydrolysis accelerating activity of the srGAP1 GAP domain with different NMR approaches. A comparison of the srGAP1 GAP domains of human and zebrafish showed species-specific interaction with Cdc42. Cross-interactions between the GAP domains and Cdc42 from different organism, namely human and zebrafish, was observed to a low extent. Finally, this work identifies possible new interaction partners for the srGAP1 protein with mass spectrometry analysis, which indicate that the srGAP1 protein might have a more complex and diverse role than assumed so far.

Die Slit-Robo GAP Proteinfamilie besteht aus vier Mitgliedern und ist an der Slit-Robo vermittelten repulsiven Wegfindung von Axonen und weiteren neuronalen Prozessen beteiligt. In dieser Arbeit wurden die Domänen des humanen srGAP1-Proteins sowie dessen Homolog aus Zebrafisch funktionell untersucht. Es wurde die membranbindende Aktivität der FBAR Domäne mit einem auf Vesikeln basierenden *in-vitro* System analysiert. Weiterhin wurde die Affinität der srGAP1 GAP Domäne zu drei Mitgliedern der RhoGTPase-Familie mit verschiedenen NMR-Methoden untersucht. Für die Suche nach neuen Interaktionspartnern für srGAP1 wurde ein GST-Pulldown Experiment mit der bis dato wenig charakterisierten C-terminalen Domäne des Proteins durchgeführt.

Die Ergebnisse dieser Arbeit zeigen, dass die FBAR Domäne von srGAP1 aktiv zur Deformierung von Vesikeln führt. Untersuchungen an einem weiteren FBAR-Domäne enthaltenden Protein, dem humanen Carom Protein, zeigen jedoch eine schwächere Deformierungsaktivität der srGAP1 FBAR Domäne. Die Interaktion beider Proteine mit den Vesikeln führt jedoch nicht zur Bildung von Tubulen, wie bei klassischen FBAR-Domänen, sondern zu deren Einstülpung. Deshalb können beide Proteine aufgrund der hier vorliegenden Ergebnisse zu der neuen Unterfamilie, den Inversen FBAR-Domänen gezählt werden. Die srGAP1 GAP-Domäne zeigt eine starke Affinität zu der RhoGTPase Cdc42. Diese Affinität wird auch für die homologen Proteine aus Zebrafisch bestätigt und weist daher auf eine entwicklungs geschichtlich konservierte Interaktion hin. Die vorläufigen Ergebnisse von Pulldown-Experimenten zur Identifizierung neuer Interaktionspartner liefern neue Hinweise auf die Beteiligung von srGAP1 an anderen Signaltransduktionswegen und weisen somit auf eine weitaus komplexere Rolle für das Protein hin.

3. INTRODUCTION

3.1 NEURONAL DEVELOPMENT

The human brain is a complex network of interconnected neurons, which are important for the processing and signalling of information. The structure of a neuron is presented in Fig. 3.1 A. A neuron is divided into three sectors: the dendrites, the cell body (soma) and the axons. Dendrites are the primary target for synaptic input from other neurons. They forward the incoming signal to the axon hillock, which combines all incoming inputs and transmits them to the axon. After reaching the presynaptic side the signal is transferred to the next neuron. Axons, which are not synaptically interconnected, are guided through their growth cone to their synaptic target (Purves et al., 2008). The axons end into the growth cone, which can be divided into three zones: the central domain, the transition zone and the peripheral domain (Fig 3.1 B). The central domain contains bundles of microtubules, which come from the axon shaft. The actin arcs in the transition zone form a ring from which the long actin filaments of the peripheral domain originate and form filopodia and F-actin networks.

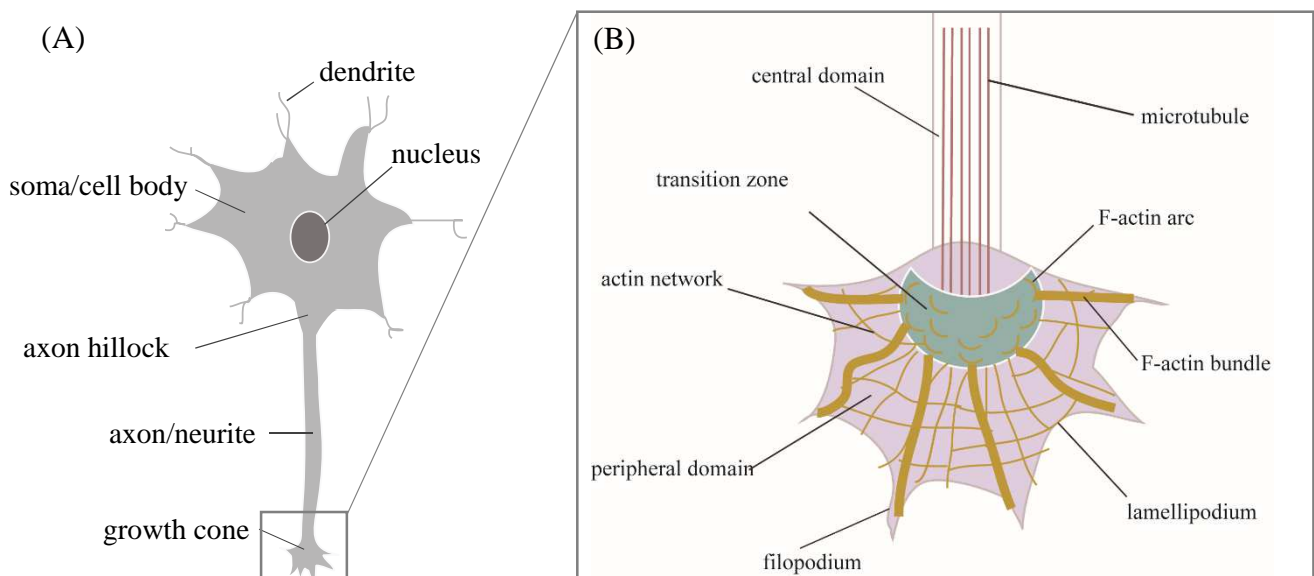


Fig. 3.1: Schematic representation of a neuron

A) The cell body (soma) of a neuron contains the nucleus. Dendrites are the primary target for synaptic input from other neurons. The axon originates in the axon hillock and permits signal transmission over long distances. The growth cone contains bundles of microtubules and actin inside, and directs the axon to its synaptic target.

B) The growth cone can be separated into three zones: the central domain (white), the transition zone (green) and the peripheral domain (purple). The central domain contains bundles of microtubules, which come from the axon shaft. The transition zone contains a ring of actin arcs. The peripheral domain has long bundles of actin filaments, which form the filopodia and the F-actin networks, which lead to the lamellipodial structures (modified, Lowery and Van Vactor, 2009).

The growth cone explores the environment and determines the direction of the axon growth and the recognition of the target. This process is termed migration, an ubiquitous feature of development, which guides cells to their appropriate spatial relationships. The motility of the

growth cone reflects modulation of the actin and microtubule cytoskeleton through different signalling mechanisms, which involve changes in the intracellular Ca^{2+} concentration (Purves et al., 2008). Adhesive, chemotropic, chemo-repulsive and trophic molecules lead to the response of the growth cone. These molecules can be found in extracellular matrixes on cell surfaces or are secreted to diffuse in extracellular spaces (Fig. 3.2). They ensure that axon pathways are formed from one structure to another and inappropriate connections are prevented.

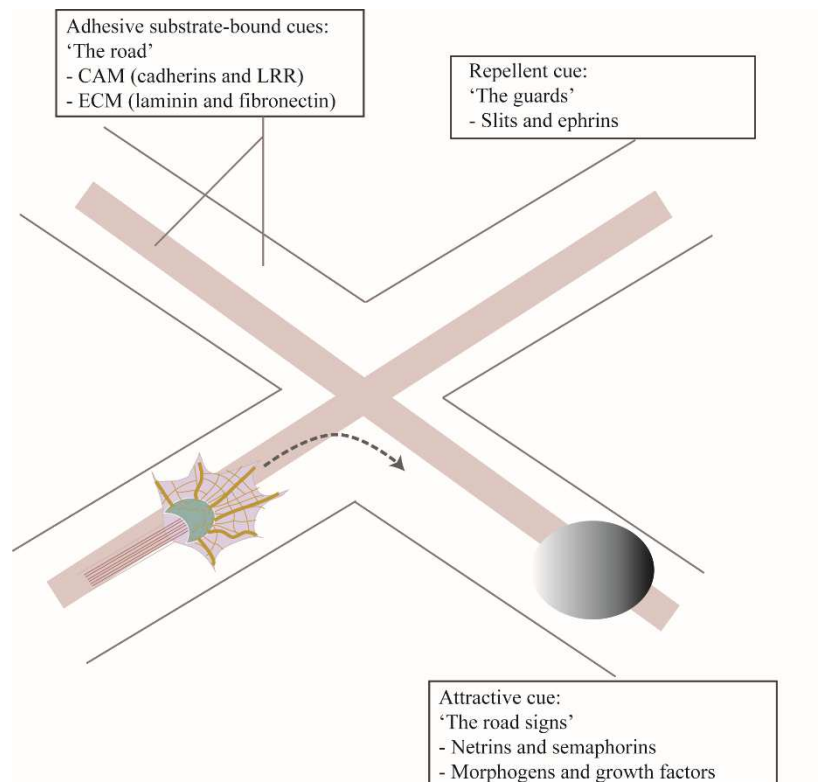


Fig. 3.2: The way of a growth cone

The growth cone encounters many different types of cues in its environment. It travels on a 'road' that is made of adhesive molecules, that are either directly on a cell surface, for example, transmembrane cell adhesion molecules (CAMs) or assembled into a complex extracellular matrix (ECM), for example laminin. Repellent molecules such as slits can prohibit growth cone advance and thus provide the guards that determine the road boundaries. Diffusible chemotropic cues present further instructions to the growth cone and include various diffusible chemotropic molecules such as netrins as well as morphogens such as Wnt, sonic hedgehog (SHH) and growth or neurotrophic factors (such as brain-derived neurotrophic factor (BDNF), secreted transcription factors 6–9 and neurotransmitters (modified, Lowery and Van Vactor, 2009).

There are four families of guidance cues, netrins, semaphorins, ephrins and slits, which are divided into attractive and repellent guidance cues. The following chapter gives insight into the repellent guidance cue Slit and its involvement with the Roundabout (Robo) receptor.

3.2 THE SLIT-ROBO PATHWAY

In the central nervous system there are two different interneuron groups described: the association neurons and the commissural neurons. Association neurons project axons ipsilaterally and never cross the midline, whereas commissural neurons send the axons contralaterally and form a commissure across the midline. The latter mentioned neurons need repulsive guidance cues to cross the midline (Long et al., 2004). In *Drosophila* the midline repellent, which expels commissural axons and prevents them from re-crossing, is the Slit ligand. Slit mediates repulsive effects through the Roundabout receptor family (Kidd et al., 1998; Kidd et al., 1999). Robo receptors are kept away from the axon surface by the commissureless protein when the commissural neuron grows towards the midline. In the moment it crosses the midline, the inhibition of Robo is removed and the Robo proteins are expressed at the surface of commissural growth cones, which then sense the Slit repellent and expel them from the midline (Fig. 3.3) (Kidd et al., 1998).

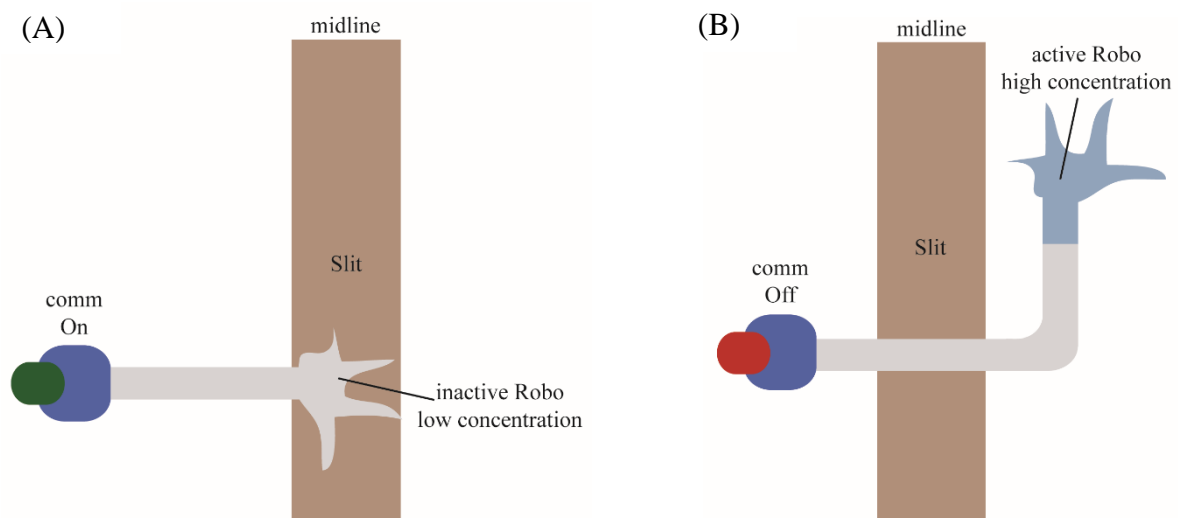


Fig. 3.3: Model for Slit-Robo function in midline crossing

The commissureless (comm) protein is the switch, which controls the midline crossing. When comm is on (A), the level of the Robo protein is low (grey) and allows crossing of neurons. Once it crosses the midline, comm is turned off and the level of Robo is increased (blue), thus inhibiting recrossing (B) (modified, Keleman et al., 2002).

3.2.1 THE SLIT LIGAND

Drosophila slit was identified in a screen for embryonic patterning and defects in commissural axon pathfinding (Hummel et al., 1999; Nuesslein-Vollhardt et al., 1984; Seeger et al., 1993). Invertebrates contain a single Slit, whereas vertebrates have three homologous proteins, Slit1, Slit2 and Slit3 (Dickson et al., 2006). The hallmark of the Slit proteins is a tandem of four leucine-rich repeats (LRR) at the N-terminus, termed D1-D4. This region is

followed by six epidermal growth factor like domains (EGF), a laminin G-like domain (either one in invertebrates or two in vertebrates), EGF-like domains and a cysteine knot domain at the C-terminus (Fig. 3.4).



Fig. 3.4: Domain composition of the mammalian Slit protein

Schematic drawing of the mammalian Slit protein. The cleavage site of Slit is indicated with a black line. Abbreviations: D1-D4: Leucine-rich repeat domains, EGF: epidermal growth factor like, LG: laminin G-like domain, CT: C-terminal cysteine knot domain (modified Hohenester et al., 2008).

3.2.2 THE ROUNDABOUT RECEPTOR

Robo is highly conserved in different species, regarding its sequence and function (Kidd et al., 1998). *Caenorhabditis elegans* has a single Robo protein (Sax-3), *Drosophila* has three (Robo1, Robo2 and Robo3) and vertebrates have four Robo receptors (Robo1, Robo2, Robo3/Rig-1 and Robo4/Magic Roundabout). All Robo receptors, except Robo4, share the



same domain architecture (Fig. 3.5), containing five immunoglobulin-like domains (IG), three fibronectin type 3 repeats (FN3) and four cytosolic domains. The cytosolic domains are poorly conserved, besides some conserved linear motifs (Hohenester et al., 2008). These motifs named CC0-CC3, can occur in different combinations in different Robos (Dickson et al., 2006). Previous studies in different embryonic stages of rats, mice, zebrafish embryos and human foetuses (Ip et al., 2011; Lee et al., 2001) showed that all *robo* receptors except *robo4* are expressed in the developing nervous system (Tab. 3.1). *robo4*, however, shows expression mainly in endothelial cells (Huminiacki et al., 2002; Okada et al., 2007).

Fig. 3.5: Domain composition of the mammalian Robo receptor

Schematic drawing of the mammalian Robo receptor. The cytosolic domain is mainly unstructured, containing four motifs, here shown as squares, and labelled with CC0-CC3. Abbreviations: IG1-5: Immunoglobulin like domain 1-5 (brown), FN1-3: fibronectin type 3 (blue), CC0-3: cytosolic domain CC0-CC3 (bisque) (modified Hohenester et al., 2008).

Tab. 3.1: Expression pattern of Robo receptors in mice, rats, zebrafish embryos and human fetuses

	ZEBRAFISH	MICE	RATS	HUMAN
EXPRESSION PATTERN OF ALL ROBO RECEPTORS	hindbrain	cortical plate	striatum	cortical plate
	cranial ganglia	subventricular zone	cortex	subventricular zone
	olfactory system	intermediate zone	hippocampus	intermediate zone
	visual system	corticospinal axons	thalamus	corticospinal axons
	spinal cord	dorsal thalamus	hindbrain	
	somites	developing hippocampus	olfactory system	
	fin buds	roof of midbrain		
		spinal chord		
		olfactory system		

All four genes show similar expression patterns in neuronal tissues of different organisms, indicating a conserved expression pattern.

Besides their function as repulsive cue both Slit and Robo are involved in neuronal migration, cell death, angiogenesis and also have a role in the development of different organs, such as kidney, lungs or liver (Avcı et al., 2004; Grieshammer et al., 2004; Xian et al., 2004). Recently, it was shown that the Slit Robo GTPase activating family 1 (srGAP1) protein binds to the cytosolic domain CC3 of the mammalian Robo receptor and leads to Slit-dependent inactivation of the RhoGTPase Cell division cycle 42 (Cdc42) (see chapter 3.3) (Wong et al., 2001).

3.3 THE DISCOVERY OF THE SRGAP FAMILY

The srGAP family consists of three members, srGAP1, srGAP2 and srGAP3. All members are multi-domain containing proteins, consisting of a FBAR, GAP, SH3 and C-terminal domain. Figure 3.6 shows a scheme of the multi-domain protein with the sequence identities of all members.

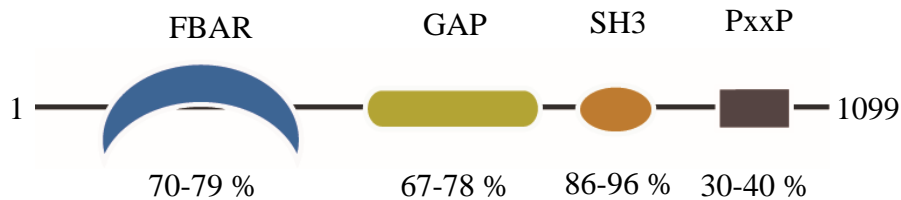


Fig. 3.6: Domain composition of the srGAP family

The srGAP family contains a FBAR domain, a GAP domain, a SH3 domain and a C-terminal domain. The sequence identities between the three members of the srGAP family vary between 70-79 % for the FBAR domain, 67-78 % for the GAP domain, 86-96 % for the SH3 domain and 30-40 % for the C-terminus, containing PxxP motifs.

Recently, a new member was added to the srGAP family on the basis of its function, ARHGAP4, also termed srGAP4. ARHGAP4 has the same domain composition, though the sequence identity between the domains is low: FBAR domain 46-48 %, GAP domain 53-59 %, SH3 domain 55-56 % and the C-terminus 8-11 %.

3.3.1 THE DOMAINS OF THE SRGAP PROTEINS

3.3.1.1 The srGAP FBAR domain

The srGAP FBAR domain belongs to the BAR superfamily, which not only induce membrane deformation, but link the membrane to the cytoskeleton, thus becoming regulators of cell morphology and function (Lee et al., 2007; Scita et al., 2008; Suetsugu et al., 2006; Tsujita et al., 2006; Yamagishi et al., 2004). The BAR superfamily can be divided into three subfamilies: the classical BAR/N-BAR proteins, the Fer-CIP4 Homology (FBAR) proteins and the inverse BAR (I-BAR) proteins. In Fig. 3.7 the characteristic curvature of each subfamily is displayed.

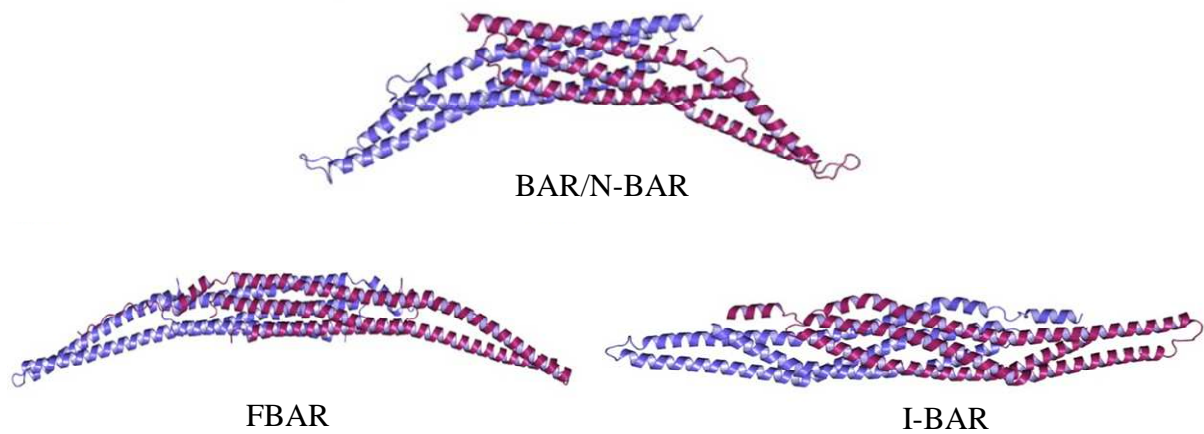


Fig. 3.7: The BAR domain superfamily

Structures of the three subfamilies of the BAR superfamily: the Amphiphysin N-BAR domain (PDB: 1URU, Peter et al., 2004), the FBP17 FBAR domain (PDB: 2EFL, Shimada et al., 2007) and the IRSp53/missing-in-metastasis I-BAR domain (PDB: 1Y2O, Millard et al., 2005). The membrane-binding surface is directed to the bottom, emphasizing the classical banana-shaped appearance of the BAR domain and the different characteristic curvature of the FBAR and I-BAR domains (Moravcevic et al., 2012).

3.3.1.1.1 The classical BAR/NBAR domain

The classical BAR domain consists of three anti-parallel α -helical bundles in each monomer, which form crescent-shaped dimers, consisting of 6 α -helices (Suetsugu et al., 2009). Positively charged residues can be found on the concave surface of the BAR domain, which allows it to directly interact with negatively charged PI(4,5)P₂ containing membranes via electrostatic interaction (Fig. 3.8). It has been reported that the dimers oligomerize to induce membrane invagination (Itoh et al., 2005; Shimada et al., 2007).

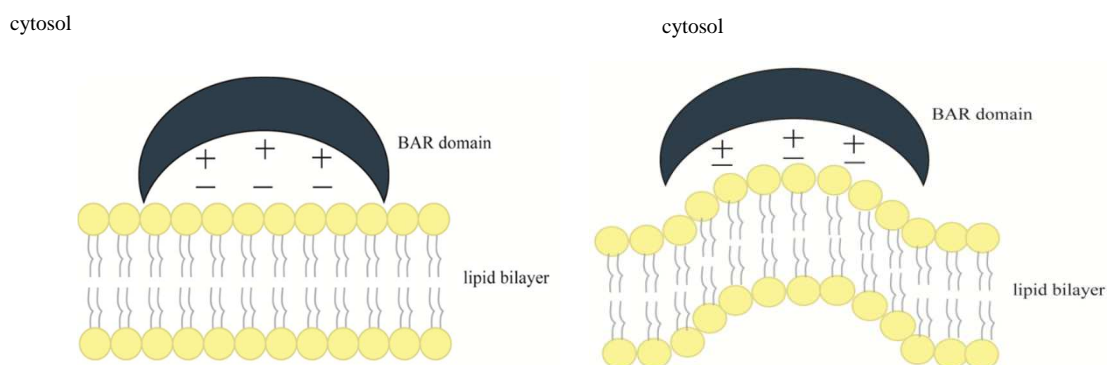


Fig. 3.8: Schematic models for membrane deformation by BAR domains

BAR domains bind to the negatively charged membrane with their concave surface through electrostatic interaction and lead to membrane invaginations, like caveolae or clathrin-coated pits.

The N-BAR domains contain an additional N-terminal amphipathic α -helix, which can insert into the membrane, thus increasing membrane curvature (Itoh et al., 2006). Various proteins, which contain a BAR or N-BAR domain, such as amphiphysin or endophilin, have been

implicated in membrane deforming activities related to synaptic vesicle formation (Di Paolo et al., 2002; Schuske et al., 2003).

3.3.1.1.2 The FBAR domain

FBAR domains contain a FCH domain which is followed by a coiled-coil domain. This C-terminal coiled-coil domain has been predicted to fold in a similar way to BAR domains (Frost et al., 2007). FBAR dimers consist of 5 α -helices and are longer and shallower curved in comparison to “classical” BAR domains, though they still exhibit the banana-shaped form. This difference in length and curvature of the FBAR domain, leads to a larger diameter of the induced tubules (Henne et al., 2007). *In vitro* assays with FBAR domains showed deformation of liposomes (Couthino-Budd et al., 2012; Henne et al., 2007). To understand the ability of the FBAR domains to induce membrane tubules, structural information of the protein have been combined with cryo-electron microscopy (Frost et al., 2008; Shimada et al., 2007;). These studies report that FBAR dimers can bind with their tips end-to-end and form strings of oligomers (Fig. 3.10). Most of the FBAR containing proteins, like formin-binding protein 17 (FBP17) or Cdc42-interacting protein (CIP4), are involved in endocytosis, regulation of the actin cytoskeleton and signalling (Itoh and De Camilli, 2006).

3.3.1.1.3 The I-BAR domain

I-BAR domains contain three anti-parallel α -helices, like classical BAR domains. But instead of the familiar banana-shape, I-BAR domains show a zeppelin-shaped appearance, with positive amino acids located on their convex surface (Millard et al., 2005). Hence, this subfamily was named inverse BAR (Fig. 3.9).

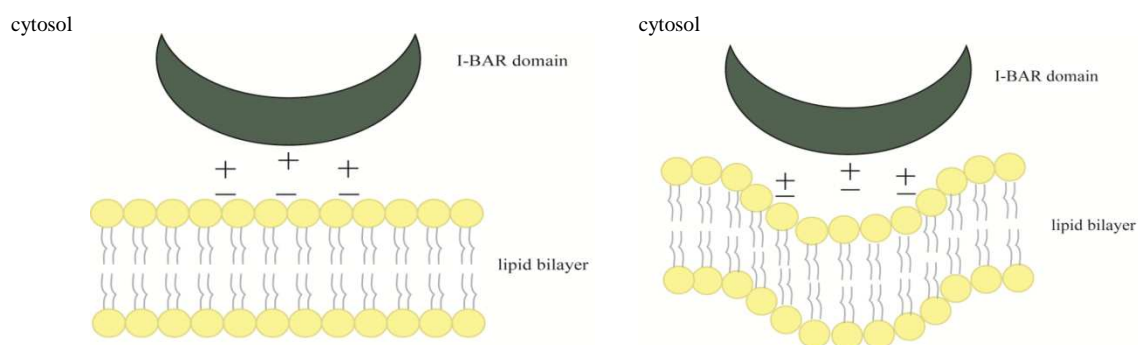


Fig. 3.9: Schematic models for membrane deformation by I-BAR domains

I-BAR domains bind to the negatively charged membrane with their convex surface through electrostatic interaction and lead to membrane protrusions, such as filopodia or lamellipodia.

In contrast to BAR and FBAR domains, I-BAR domains induce filopodia-like membrane protrusions (Mattila et al., 2007; Millard et al., 2005; Saarikangas et al., 2008; Saarikangas et al., 2009). Figure 3.10 shows the putative mechanism of how the BAR/FBAR/I-BAR dimers deform membranes. BAR/FBAR dimers bind to the surface of the membrane, while I-BAR dimers are predicted to bind to the inner side of the protruding membrane. This theory has been confirmed with the help of molecular dynamic simulations by Yu and Schulten in 2013.

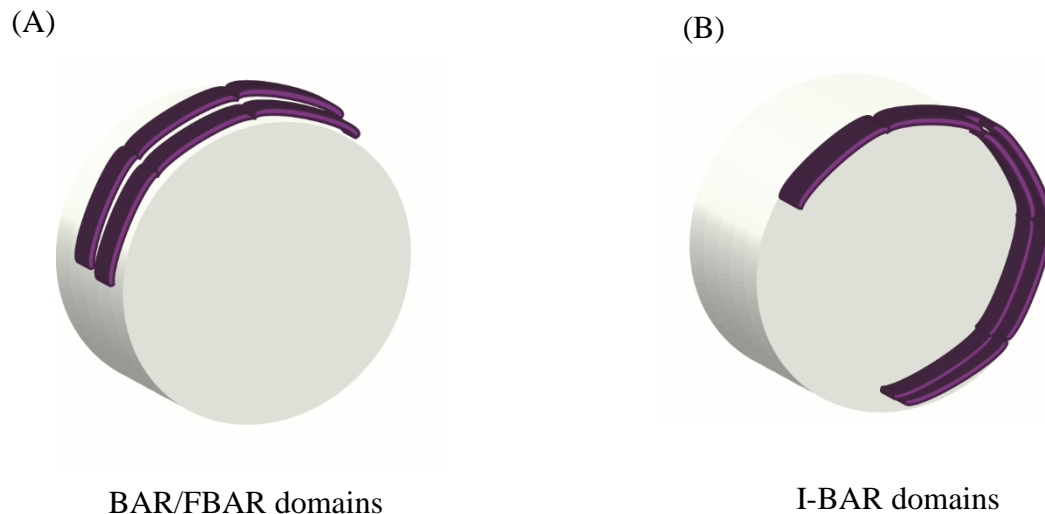


Fig. 3.10: Putative mechanism of membrane deformation for BAR, FBAR and I-BAR domains

(A) The BAR/FBAR dimer spiral is located on the surface of the invaginating membrane. The end-to-end interaction between the homo-dimers can be observed. This interaction facilitates the sensing of the membrane curvature. (B) The I-BAR dimer binds to the inner surface of the protruding membrane (modified, Suetsugu et al., 2010).

Little was known about the FBAR domains of the srGAP family until recently. Studies from the Polleux lab showed for the first time, that the srGAP2 FBAR domain leads to outward membrane protrusions and thereby negatively regulates neuronal migration and induces neurite outgrowth and branching. It was also shown that methylation of srGAP2 plays an important role in cell spreading and cell migration (Guo et al., 2010). Studies on the srGAP3 FBAR domain indicated that it has an inhibitory effect on actin dynamics specifically on lamellipodia formation (Endris et al., 2011). In Cos7 fibroblasts, expression of the full-length FBAR domain of srGAP2 and srGAP3, induce filopodia formation. The deletion of the last 49 amino acids abolishes the effect, though the protein is still located at the cell membrane (Carlson et al. 2011; Guerrier et al., 2009). A more recent study, provided the information that the FBAR domains of the three srGAP family members show a diverse ability to induce filopodia-like protrusions in neuronal and non-neuronal cells. The FBAR domain of srGAP3 induces filopodia in Cos7 cells and in cortical neuron cells, though less potent than the FBAR domain of srGAP2. The FBAR domain of srGAP1 though, prevents filopodia formation in

cortical neuron cells and reduces plasma membrane dynamics. Overall, all results obtained until now point to a unique function of the FBAR domains of the srGAP family through their ability to control membrane deformation (Couthino-Budd et al, 2012).

3.3.1.2 The srGAP GAP domain

The srGAP GTPase activating protein (GAP) domain belongs to the RhoGAP family as it binds and inactivates small GTPases by increasing their intrinsic GTP hydrolysis rate (Schulte and Der, 2006).

3.3.1.2.1 The RhoGTPases

RhoGTPases are a distinct subfamily in the superfamily of Ras-related small GTPases. They are known for their role in actin cytoskeleton regulation, cell growth and differentiation as well as endocytosis (Moon and Zheng, 2003; Threadgill et al., 1997). So far, 22 human members for the RhoGTPase family have been identified (Wennerberg and Der, 2004). Cdc42, RhoA and Rac1 are the best characterized members of this GTPase family (Etienne-Manneville and Hall, 2002). Rac1 has been shown to lead to the formation of lamellipodial protrusions through actin networks, Cdc42 forms filamentous actin bundles, which regulate filopodia formation and RhoA leads to actin depolymerisation (Hall et al., 1994). GTPases act in general as binary switches by cycling between an active and inactive state. In the active state, guanine triphosphate (GTP) is bound to the GTPase. This leads to the association with downstream effectors, which then activate a range of downstream signalling cascades (Bishop and Hall, 2000; Burridge and Wennerberg, 2004). During the inactive state guanine diphosphate (GDP) is bound. The cycle is regulated by GTPase activating proteins (GAPs), which increase the intrinsic GTP hydrolysis rate of the GTPase, and guanine exchange factors (GEFs), which exchange the bound GDP to GTP. Guanine nucleotide dissociation inhibitors (GDIs) bind to prenylated GDP-bound GTPase to control the cycling between the membranes and the cytosol (Schmidt and Hall, 2002) (Fig. 3.11).

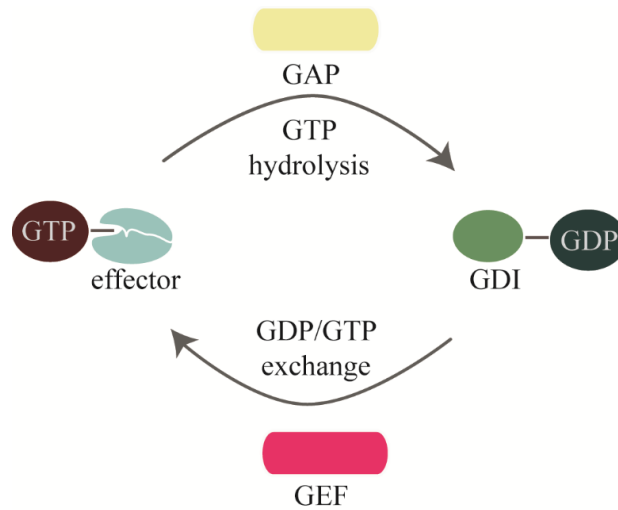


Fig. 3.11: General regulation of RhoGTPases by GEFs, GAPs and GDIs

The RhoGTPases are activated by the GDP/GTP exchange with the help of GEFs (pink) and inactivated by the accelerated GTP hydrolysis by GAPs (yellow). The switch from cytosol to membrane or vice versa is regulated by GDIs (green), (modified, Cherfils and Zeghouf, 2013)

All RhoGTPases are composed of six-stranded β -sheets, which are surrounded by five α -helices, referred as G-domain (Cherfils and Zeghouf, 2013). They contain a guanine nucleotide binding site, which recognizes the guanine base with the N/TKXD motif, in which X stands for any amino acid. The β - and γ -phosphate interact with the phosphate binding loop (P-Loop). Various motifs around these specific regions are also involved in the GTP hydrolysis reaction, for example Switch I and Switch II (Cherfils and Zeghouf, 2003; Vetter and Wittinghofer, 2001). In Fig. 3.12 human Cdc42 with bound GDP is shown as a representative of the three most described members of this GTPase family. The main binding sites are highlighted.

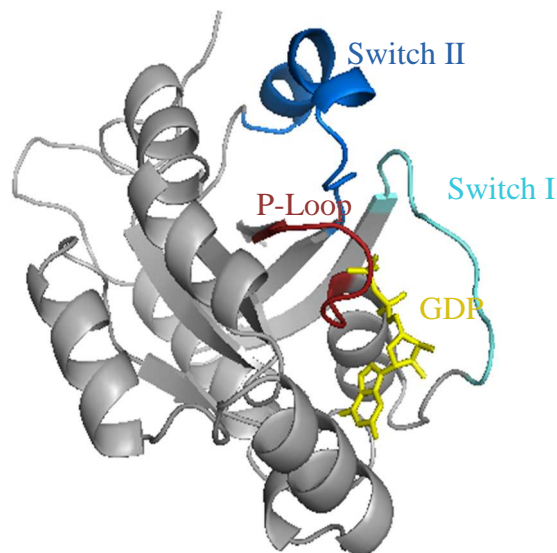


Fig. 3.12: Crystal structure of human GDP-bound Cdc42

Ribbon representation of the human Cdc42 with bound GDP. Switch I (residues 30-38) is highlighted in light blue, Switch II (residues 57-72) is shown in dark blue, the P-loop (residues 9-16) is presented in red and the bound GDP in yellow (PDB: 1GRN, Nassar et al., 1998).

The regulator GEF and GAP proteins are supposed to bind to the Switch I/ Switch II region and stabilize this region (Hakoshima et al., 2003), whereas the nucleotide binds near the P-Loop and is surrounded by the switch regions.

3.3.1.2.2 The RhoGAP family

GTPases have a very slow intrinsic GTPase activity, which is accelerated by its specific GAP protein. GAPs are abundant in eukaryotes ranging from yeast to human. Human genome analysis resulted in 80 RhoGAPs, which outnumber the RhoGTPases comprising 20 members (Moon and Zheng, 2003). This suggests individual roles for the members of the RhoGAP family, while regulating specific RhoGTPases in their activity and function. RhoGAP proteins consist of nine α -helices (Gamblin et al., 1998) and negatively regulate the biological activity of RhoGTPases. Some down-regulate their specific RhoGTPase, while others facilitate the effective cycling of RhoGTPases between the GTP- and the GDP-bound conformation. It is proposed that GAP actively participates in the GTP hydrolysis process by contributing a catalytic residue to the active site (Scheffzek et al., 1998). An important step in solving the mechanism of the GTPase accelerating process came from studies using aluminium fluoride (AlF_x). AlF_x (x represents either aluminium trifluoride (x=3) or aluminium tetrafluoride (x=4)) has been suggested to activate heterotrimeric G-proteins in their GDP-bound inactive state by binding into the γ -phosphate pocket (Chabre et al., 1990). This hypothesis was confirmed by crystal structures of G_α - AlF_x complexes. The data supported the idea that GDP-AlF_x mimics the transition state of the GTPase reaction. This gives more insight into the mechanism of most GAPs. The formation of a stable GTPase/GAP complex in the presence of GDP and AlF_x is used as a reference assay to demonstrate the activity of a GAP domain (Mittal et al., 1996; Wittinghofer et al., 1997). The studies revealed that the GAP domain contains a highly conserved arginine residue, which stabilizes the GTPase stimulation by inserting the arginine residue into the active site (Gamblin and Smerdon et al., 1998; Kosloff and Selinger, 2001; Scheffzek et al., 1998; Vetter and Wittinghofer, 2001). The GAP domain positions the crucial residue Gln61/Gln63 (in RhoA) of the RhoGTPases towards a nucleophile water molecule, which hydrolyses GTP and neutralizes developing negative charges on the leaving group during the phosphoryl-transfer reaction (Ahmadian et al., 1997; Nassar et al., 1998). This has been confirmed with mutation approaches (Li et al., 1997, Nassar et al., 1998). Three binding sites are mentioned in the literature for the RhoGAP domain: the Switch I, the Switch II and the P-Loop region (Dvorsky et al., 2004; Moon and Zheng, 2003).

A previous study in HEK cells reported, that srGAP1 specifically inactivates Cdc42 and RhoA (Wong et al., 2001), whereas srGAP2 and 3 inactivate Rac1 (Guerrier et al., 2009; Soderling et al., 2002). ArhGAP4 can act on both Cdc42 and Rac1 (Vogt et al., 2007). Structurally the srGAP GAP domains are assumed to resemble classical GAP domains, containing nine α -helices, packed together in an anti-parallel arrangement (Dvorsky et al., 2004). In Fig. 3.13 a model of the regulation of the RhoGTPases by the srGAP GAP domain is shown.

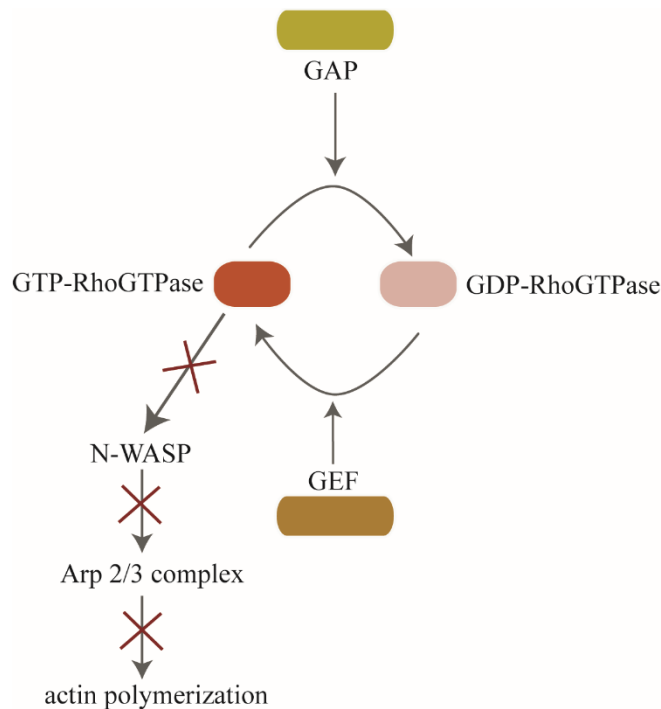


Fig. 3.13: Model for the regulation of the RhoGTPase activity by the srGAP GAP domain

Activation of the GAP domain leads to the inactivation of the RhoGTPase through the increasing intrinsic GTP hydrolysis rate. This leads to the inhibition of downstream effectors, like N-WASP and Arp2/3 complex, which results in less actin polymerization. GEFs activate the RhoGTPases again (modified, Wong et al., 2001).

3.3.1.3 The srGAP SH3 domain

SH3 domains are found in multiple intracellular proteins in living cells. They are ubiquitous protein-interaction modules, which have roles in many aspects of complex signalling networks. The peptide recognition surface contains a hydrophobic cleft, which has variable loops that contribute to the recognition specificity and also determine ligand orientation (Mayer et al., 2001; Li et al., 2006). SH3 domains recognize proline-rich sequence motifs with a PxxP motif, which is classified into class I, RKxxPxxP and class II, PxxPxR motifs. The structure of

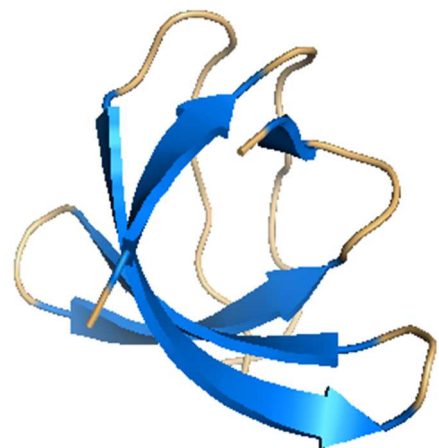


Fig. 3.14: Crystal structure of the srGAP1 SH3 domain

Ribbon representation of the monomer structure of the srGAP1 SH3 domain, containing five β -strands. This figure was drawn using PyMOL (<http://www.pymol.org/>). (PDB: 2GNC, Li et al., 2006)

the srGAP1 SH3 domain (Li et al., 2006) and the srGAP2 SH3 domain (Qin et al., 2006) were solved, showing a classical SH3 domain (Fig. 3.14), containing five β -strands arranged as two orthogonal β -sheets and forming a compact anti-parallel β -sheet (Li et al., 2006). So far, it is known that the SH3 domain of srGAP1 binds to the CC3 of Robo1, hence involving the protein in the Slit-Robo pathway (Fig. 3.15).

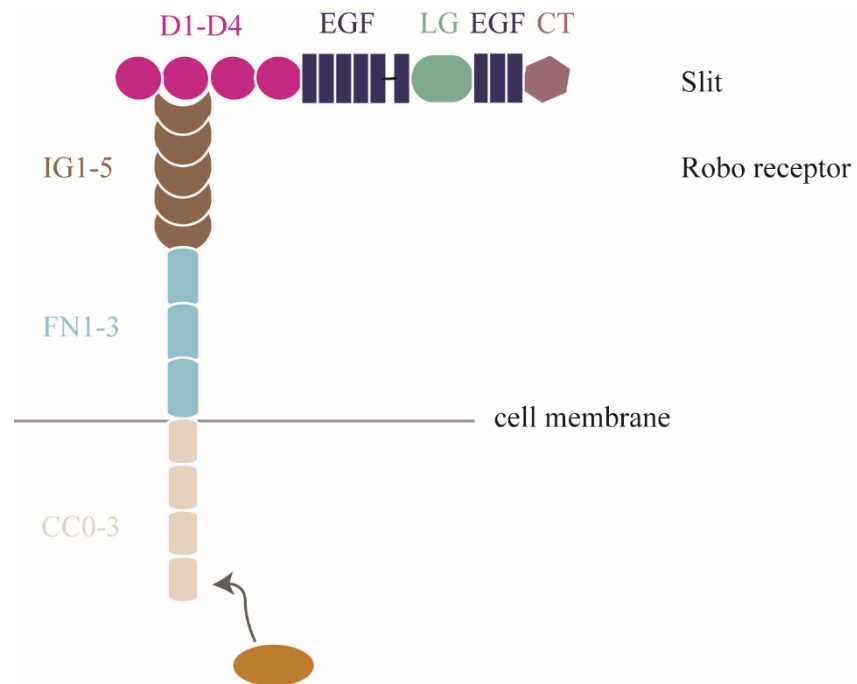


Fig. 3.15: Binding of the srGAP1 SH3 domain to the Robo receptor

The D2 domain of the Slit ligand binds to the IG1 domain of the Robo receptor, hence enhancing its binding to the SH3 domain of srGAP1 via its cytosolic domain 3. Abbreviations: D1-D4: Leucine-rich repeat domains, EGF: epidermal growth factor, LG: laminin G-like domain, CT: C-terminal cysteine knot domain, IG1-5: Immunoglobulin like domain 1-5, FN1-3: fibronectin type 3, CC0-3: cytosolic domain 0-3 (modified, Hohenester et al., 2008).

3.3.1.4 The srGAP C-terminal region

So far, not much is known about the C-terminal region of the srGAP family. It seems to be mainly unstructured, containing a short coiled-coil domain, which is conserved in all organisms. Functionally the C-terminal region is assumed to be involved in protein-protein interaction. *In vitro* studies indicate that the members of the srGAP family play a crucial role in neurological processes during the development of the human brain. srGAP1 transduces Slit signalling in neuronal migration by inactivating Cdc42 (Wong et al., 2001). srGAP2 was shown to be involved in axon regeneration (Madura et al., 2004). Recently, it has also been implicated in a severe neurodevelopmental syndrome, which causes early infantile epileptic encephalopathy and profound psychomotor delay (Saito et al., 2011). srGAP3 is suggested to be involved in a severe form of X-linked mental retardation, the 3p- syndrome, giving srGAP3 the alternate name of mental-disorder associated GAP protein (MEGAP) (Endris et al., 2002). Furthermore, a role for srGAP3 in long term memory has been shown with mice

behaviour tests such as novel object recognition, water maze and passive avoidance (Carlson et al. 2011). Figure 3.16 shows a summary of the known roles for the individual domains of the srGAP family.

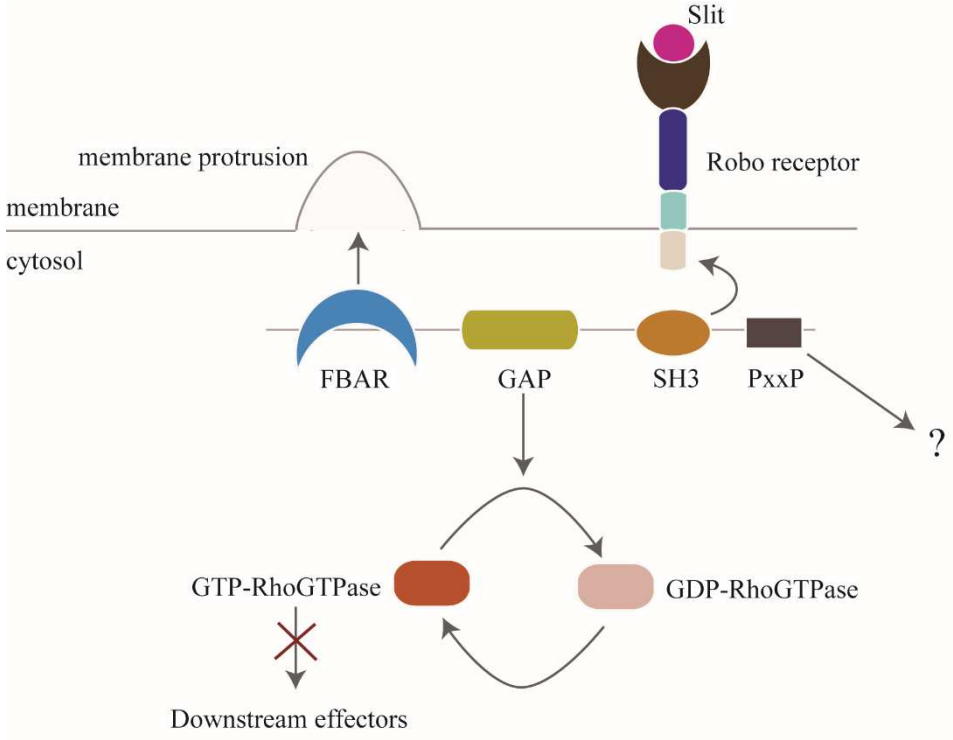


Fig. 3.16: Summary of the individual roles of each domain of srGAP family in the cell
 The members of the srGAP family contain a FBAR, GAP, SH3 and C-terminal domain. The SH3 domain (orange circle) binds to the cytosolic domain of the Robo receptor, thus activating the srGAP protein and involving it in the Slit-Robo-pathway. Activation of the srGAP protein leads to an increasing activity of its GAP domain (yellow box), which specifically binds to members of the RhoGTPase family and increases their intrinsic GTP hydrolysis rate, thus inhibiting all downstream processes. The FBAR domain is responsible for membrane binding and bending (blue half moon). The C-terminal domain contains PxxP motifs and is assumed in protein-protein interaction and for involving the srGAP proteins in new pathways (modified, Wong et al., 2001; Hohenester et al., 2008).

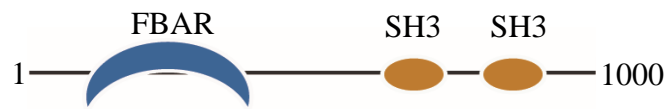
3.4 THE FCH AND DOUBLE SH3 DOMAIN FAMILY- ANOTHER MEMBER OF THE I-FBAR CONTAINING PROTEINS

Intracellular trafficking needs several membrane-shaping proteins, which work together to induce membrane invagination, tubules or vesicle formation. Many of these proteins contain BAR domains, such as the FCH and double SH3 domain family containing a N-terminal FBAR domain. It can be found in various organisms ranging from yeast to mammals and has an evolutionary conserved protein domain composition.

3.4.1 NERVOUS WRECK

Nervous wreck (Nwk) is an FCH and SH3 domain-containing neuronal adaptor protein (Fig. 3.17 A), which localizes to the periaxonal zone of presynaptic terminals and is able to bind to Wsp, the *Drosophila* orthologue of WASP, which is an important regulator of actin polymerization. Nwk was assumed to be a member of a family of adaptor proteins, which include the human srGAP proteins. It is proposed that Nwk controls the endosomal traffic and signalling output of synaptic growth receptors at the presynaptic terminus of the *Drosophila* neuromuscular junction (Coyle et al., 2004; O'Connor-Giles et al, 2008; Rodal et al., 2011). As mentioned above Nwk contains a N-terminal FBAR domain, which is followed by two canonical SH3 domains, recognizing proline-rich consensus sequences (Fig. 3.17 A). The C-terminal domain of Nwk contains additional proline-rich motifs, with five possible SH3 binding sites (Coyle et al., 2004). There are 11 related proteins in yeast, worms and mammals, which include the three members of the human srGAP family (Fig. 3.17 B). In some protein families one of the SH3 domains has been replaced by a GAP domain. Though the sequence identity is not high, Nwk and its 11 homologs share an approximately 60 aa long sequence in the FBAR domain, which is unique for this family. This sequence is referred to as ARNEY domain, for which no relevant function has been described until now (Coyle et al., 2004).

(A)



(B)

HOMOLOGS	FBAR	SH3	SH3
<i>H. sap.</i> FCHSD1	-	55 %	53 %
<i>H. sap.</i> FCHSD2	30 %	47 %	50 %
srGAP1	29 %	-	31 %
srGAP2	32 %	-	30 %
srGAP3	26 %	-	31 %
srGAP4	27 %	-	28 %
<i>M. mus.</i> Nwk	40 %	55 %	53 %
<i>M. mus.</i> RhoGAP4	30 %	-	28 %
<i>M. mus.</i> RhoGAP14	26 %	-	31 %
<i>C. elegans</i> F12F6.5	-	-	-
<i>S. cer.</i> Bzz1p	46 %	35 %	38 %

Fig. 3.17: Domain composition of Nervous Wreck

(A) The *Drosophila* protein Nwk contains a FBAR domain (blue) and two SH3 domains (orange).

(B) Table with the 11 homologs of Nwk. Sequence identities of the individual domains are shown in percentages. Dashes mean either insufficient similarity in BLAST alignment or in case of the first SH3 domain, replacement by a GAP domain. FCHSD1 and FCHSD2 are the human Nwk proteins. The F12F6.5 protein from *C. elegans* shows no specific similarity in domain composition, though it contains the ARNEY domain, which has a sequence identity of 37 %. Abbreviations: *C. elegans*: *Caenorhabditis elegans*, *H. sp.*: *Homo sapiens*, *M. mus.*: *Mus musculus*, *S. cer.*: *Saccharomyces cerevisiae*

The similar domain composition of Nwk and its homologs suggests that all 12 proteins belong to a distinct family of adaptor proteins, which interact with cytoskeletal regulators. Recently, it has been shown that the FBAR domain of Nwk has a membrane deforming activity, which is different from the previously described FBAR proteins. Instead of classical membrane tubules, the Nwk FBAR creates ridges and scallops in *in vitro* assays by assembling into zigzags. In S2 cells, these structures develop into plasma membrane protrusions by actin polymerization, thus showing a negative membrane deforming activity, which is similar to

that of the srGAP family. Analysis of mutations localized in the concave surface indicate, that Nwk exhibits a conventional concave FBAR domain structure. The results of this study suggests that there are unique modes of higher-order assembly, which can define how FBAR proteins sculpt the membrane (Becalska et al., 2013).

3.4.2 THE HUMAN NWK HOMOLOG-THE FCHSD2 PROTEIN

The human Nervous wreck protein, known as FCHSD2 or Carom, shares the same domain composition of Nwk. So far, it is known that the murine FCHSD1 and FCHSD2 form abundant protrusions in S2 cells. Further experiments in HEK293T cells also resulted in F-actin containing protrusions to which the FBAR domains localized. This similar protrusion-generating activity of the *Drosophila* and murine Nwk proteins indicate an evolutionary conserved mechanism (Becalska et al., 2013). The observed membrane deforming activity shows some similarity to that of the srGAP family.

In addition to the information about the FBAR domain, the structures of both SH3 domains have been solved (Qin et al., 2006). Not much is known about their possible interaction partner whereas it is clear that the *Drosophila* Nwk binds to Wsp with its first SH3 domain, and is therefore, involved in actin polymerization (Coyle et al., 2004). Furthermore, it has been shown that Carom interacts with the calcium/calmodulin-dependent serine protein kinase (CASK), which targets junctional components and links them to the cytoskeleton and with myelin-associated glycoprotein 1 (MAGI-1), which is assumed to play a role in the transmission of regulatory signals from the cell surface to the nucleus (Dobrosotskaya et al., 1997; Ohno et al., 2003). Both proteins bind to distinct regions of the C-terminal domain of Carom, whereby CASK inhibits the binding of Carom to MAGI-1. The *in vivo* significance of this interaction is not solved yet, though it is assumed that Carom might be associated with the cytoskeleton and linkage of other proteins to the cytoskeleton (Ohno et al., 2003).

4. GOALS OF THE PROJECT

The goal of this work is to analyse the structural and functional properties of the srGAP1 protein to gain new insight into the characteristics of the srGAP family.

srGAP1 belongs to a novel GTPase activating protein family and is part of the BAR domain superfamily, containing a N-terminal FBAR domain, which belongs to a new class of FBAR domains, termed I-FBAR domains. Characteristic for this new subfamily is the formation of membrane protrusions upon binding of the FBAR domain to the membrane, instead of the classical membrane invagination. This was shown with several *in vivo* experiments with Cos7 and cortical neuron cells. Like many BAR domain containing proteins, the srGAP1 protein has additional protein domains, a GAP and a SH3 domain, as well as several protein binding motifs in its C-terminal region.

To understand the function of the I-FBAR subfamily and their differential behaviour upon membrane binding, the FBAR domain of srGAP1 and the FBAR domain of Carom were analysed with giant unilamellar vesicle based *in vitro* assays for their membrane deforming activity. Furthermore, the affinity of the GAP domain to three members of the Rho family of GTPases was examined using different NMR approaches to gain insight into the structural properties of the acceleration of the intrinsic hydrolysis reaction of the GTPase by the srGAP1 GAP domain. The C-terminal domain, which is rich in protein binding motifs was used to identify potential new interaction partners for the srGAP1 protein, to gain insight into new functions for the protein within the complex protein network.

5. CONTRIBUTIONS

All experiments were discussed with my supervisor Dr. Yvonne Groemping.

7.1.1 Bioinformatical cluster analysis of the srGAP family

The setup and the results of the bioinformatical analysis were discussed with Dr. Moritz Ammelburg. The analysis was carried out by myself with the bioinformatic toolkit of the MPI for Developmental Biology, Tuebingen.

7.1.2 Developmental and tissue-specific expression analysis of *srgap1* in zebrafish embryos

The experimental outline for the analysis of the expression pattern of *srgap1* was discussed with Dr. Christian Soellner and Horst Geiger. Zebrafishes were provided by the fish facility of the Department of Genetics, MPI Tuebingen. I cloned the *srgap1* construct for the *in-situ* hybridization and carried out the *in-situ* experiments by myself. The images of the single *in-situ* experiments were taken by myself. The images of the double *in-situ* experiments were taken together with Dr. Christian Soellner and the results of the analysis were discussed with him as well.

7.1.3 Structural analysis of the srGAP1 FBAR domain

I performed the cloning of all FBAR domain constructs, except the SRGAP1 FBAR domain from *Pristionchus pacificus*, which was done by Martin Schuekel. I carried out all purifications as well as the biochemical analysis of the different srGAP1 FBAR domains. The crystallization screens for the zebrafish srGAP1 FBAR domain were set up by Dr. Reinhard Albrecht and Kerstin Bär.

7.1.4 Functional characterization of the srGAP1 FBAR domain of zebrafish

The liposome mixes for the EM assays were generated by Silvia Wuertenberger. I carried out the EM assays and the images were taken together with Dr. Matthias Floetenmeyer in the beginning, later I took the images by myself. The GUV assays were performed in the research group of Dr. Wolfram Antonin together with Dr. Nathalie Eisenhardt.

7.1.5 Comparison of the binding specificity of the human srGAP1 GAP domain and its zebrafish homolog to three members of the RhoGTPases

I cloned the GAP domains, as well as the zebrafish Cdc42. The human RhoGTPase constructs were already available and were cloned before by Dr. Yvonne Groemping. Dr. Murray Coles conducted all NMR measurements and provided me with the figures, which we discussed together. The mapping of the binding sites on Cdc42 was suggested by my TAC committee members Professor Dr. Andrei Lupas, Professor Dr. Thilo Stehle and Dr. Christian Soellner.

7.1.6 Possible new interaction partners for the human srGAP1 protein and its zebrafish homolog

The C-terminal domain of the human srGAP1 was cloned by Beatrice Laudenschlag. I performed the purification and further characterization of the domain. The setup of the rat brain pulldown was discussed with Silvia Wuertenberger. The mass spectrometry analysis of the rat brain pulldown as well as the zebrafish embryo pulldown were carried out by Johannes Madlung from the Proteome Center in Tuebingen. I carried out further analysis of the mass spectrometry results. The selection of the potential interaction partners were discussed with Dr. Yvonne Groemping.

7.2.1 Biochemical characterization of the FBAR domain of the human Carom protein

Beatrice Laudenschlag and Martin Schueckel cloned the human Carom construct. I performed the purification and further biochemical analysis of the protein. Crystallization screens were set up by Dr. Reinhard Albrecht and Dr. Marcus Hartmann analysed the diffraction data. Further variation of the crystallization screens were carried out by myself.

7.2.2 Membrane deforming activity of the human Carom FBAR domain

The GUV assays in chapter 7.2.2.1 and 7.2.2.3 were performed by Dr. Aleksander Czogalla, Dresden. The GUV assays in chapter 7.2.2.2 were performed by me under the supervision of Dr. Nathalie Eisenhardt.

6. MATERIALS AND METHODS

6.1 MATERIALS

6.1.1 CHEMICALS AND ENZYMES

All chemicals and enzymes which were used in this project were ordered from the following companies: AppliChem GmbH (Darmstadt), Carl Roth GmbH & Co KG (Karlsruhe), Fermentas/Life Technologies Co. (Frankfurt/Main), Merck AG (Darmstadt) and Sigma-Aldrich Chemical GmbH (Steinheim).

6.1.2 USED BACTERIAL STRAINS

Tab. 6.1: *Escherichia coli* (*E. coli*) strains

NAME	GENOTYPE	REFERENCE
BL21 (DE3)	F ⁻ ompT gal dcm lon hsdS _B (r _B ⁻ m _B ⁻) λ(DE3 [lacI lacUV5-T7 gene 1 ind1 sam7 nin5])	Novagen
Rosetta	F ⁻ ompT gal [dcm] [lon] hsdSB (r _B ⁻ ,m _B ⁻) λ(DE3) pRARE(CmR)	Novagen
Lemo21 (DE3)	fhuA2 [lon] ompT gal (λ DE3) [dcm] ΔhsdS/ pLemo(CamR)	New England Biolabs

6.1.3 PLASMIDS

Tab. 6.2: Cloned plasmids

NAME	CHARACTERISTICS	SOURCE
pET28b_FBAR_DR_21-475	srGAP1 FBAR domain of zebrafish with C-terminal 6His-tag in pET-28b, kanamycin resistance	Anitha Jeyanthan
pET47b_FBAR_1-469	human srGAP1 FBAR domain with N-terminal 6His-tag in pET-47b, kanamycin resistance	Anitha Jeyanthan
pET28b_FBAR_PP_20-460	SRGAP1 FBAR domain of <i>Pristionchus pacificus</i> with C-terminal 6His-tag in pET28b, kanamycin resistance	Martin Schueckel
pGEX6P1_GAP_496-695	human srGAP1 GAP domain in pGEX6P1 with N-terminal GST-tag, ampicillin resistance	Anitha Jeyanthan
pGEX6P1_GAP_DR_492-676	srGAP1 GAP domain from zebrafish in pGEX6P1 with N-terminal GST-tag, ampicillin resistance	Anitha Jeyanthan
pGEX6P1_Cterm_799-1085	human srGAP1 C-terminal domain in pGEX6P1 with N-terminal GST-tag, ampicillin resistance	Beatrice Laudenschlager
pGEX6P1_Cterm_DR_782-1073	srGAP1 C-terminal domain, from zebrafish in pGEX6P1 with N-terminal GST-tag, ampicillin resistance	Anitha Jeyanthan
pET28b_Carom_FBAR	Human Carom FBAR domain in pET-28b with C-terminal 6His-tag, kanamycin resistance	Beatrice Laudenschlager, Martin Schueckel
pGEX4T1_Cdc42_Hs_1-178	human Cdc42 in pGEX4T1 with N-terminal GST-tag, ampicillin resistance	Yvonne Groemping
pGEX6P1_Cdc42_DR_1-191	Cdc42 from zebrafish in pGEX6P1 with N-terminal GST-tag, ampicillin resistance	Anitha Jeyanthan
pGEX4T1_Rac1_Hs	human Rac1 in pGEX4T1, with N-terminal GST-tag, ampicillin resistance	Yvonne Groemping
pGEX4T1_RhoA_Hs	human RhoA in pGEX4T1, with N-terminal GST-tag, ampicillin resistance	Yvonne Groemping

6.1.4 OLIGONUCLEOTIDES

Tab. 6.3: Used oligonucleotides for cloning of the FBAR, GAP and the C-terminal constructs

NAME	SEQUENCE	REFERENCE
srGAP1_FBAR_1_fw	CATGCCATGGGAATGTCCACCCCGAGCCGATTCAAG	MWG
srGAP1_FBAR_469_rv	CCGCTCGAGTCATTCTCCCAGGGTCCTCTGCAGCAAGTC	MWG
srGAP1_FBAR_L1_fw	CAGGGACCCGGTATGTCCACCCCGAGCCGATTCAAG	MWG
srGAP1_FBAR_L469_rv	GGCACCAGAGCGTTATTCTCCCAGGGTCCTCTGCAGCAAGTC	MWG
sr1_GAP_496_fw	CGGGATCCCCTCACAGTATAATACTAAGTTGTTTAATG	MWG
sr1_GAP_695_rv	GCGCTCGAGTCATGGGAAAATAGTCTCATGGTGGATGATG	MWG
srGAP1_L799_fw	CAGGGACCCGGTGTGCAGGATATGGATGATACG	MWG
srGAP1_L1085_rv	GGCACCAGAGCGTTACATTGTGCATGACTTGTCTGTG	MWG
SrGp1_DR_1fw	CCAGTTTGTA AACACTCTCATAAC	MWG
SrGp1_DR_2fw	CATGCCATGGTGAAGATGTCGAATCCTCTGTGAAG	MWG
SrGp1_DR_3fw	CATGCCATGGTCAAAGAGATTCGAGCTCAAC	MWG
SrGp1_DR_1rv	ATAGTTTAGCGGCCGCGTCACCGAGGGTTCTCTCAGTAG	MWG
SrGp1_DR_2rv	ATAGTTTAGCGGCCGCGGTGCAGGATTTGTCCAATG	MWG
SrGp1_DR_3rv	GAAATGACTCTGGCTCTGACTG	MWG
SrGP1_DR_ <i>in situ</i> _fw	CAAAATTAACCCTCACTAAAGGGGTCAAAGAGATTTCGAGCTAA	MWG
SrGP1_DR_ <i>in situ</i> _rv	TTGTAACTCCCTATAGTGAGTCGTATTAGCAGCCGGATCTCAG	MWG
sr1drGAPfw1	GAACCGGGCATTGCGGACCTAC	MWG
sr1drGAPrv1	TGAGATGGGTGGACGAGGCAGTG	MWG
sr1drGAPfw2	CGCGGATCCAGACATCAGGACTCTGGTCAAG	MWG
sr1drGAPrv2	CCGCTCGAGAGGAAAGATGGTTTCGTGGTG	MWG
sr1drCtermflfw1	GAGGATGAGGGAGAGCCCATTGAAG	MWG
sr1drCtermflrv1	TACCAAGAGGTTCAAAGCCTGTTGAG	MWG
sr1drCtermflfw2	CCGGAATTCTATGGACGACACGTCTCAGACACTTTG	MWG
sr1drCtermflrv2	CCGCTCGAGTCACATGGTGCAGGATTTGTCCAATG	MWG
Carom fw	CGGGATCCATGCAGCCGCCCGGAG	MWG
Carom rv	ATAGTTTAGCGGCCGCTTAGCGGGCCCATCGCTCATTTC	MWG

6.1.5 CLONING VECTORS

6.1.5.1 pET-28b

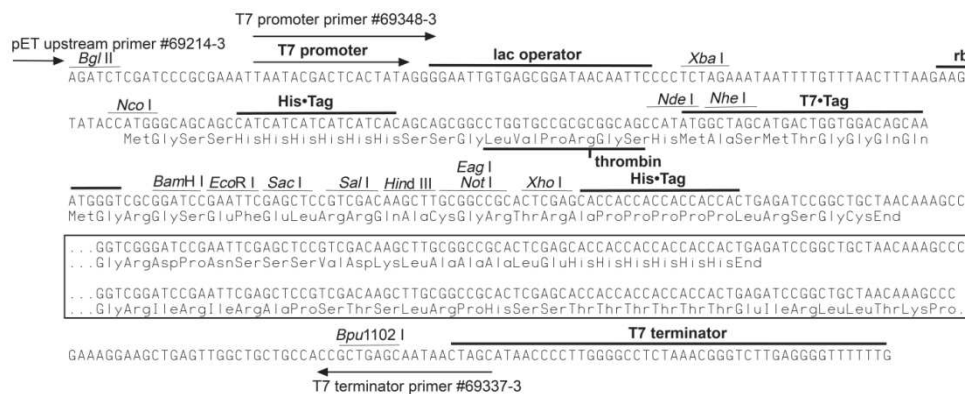


Fig. 6.1: Multiple cloning site of pET-28b from Novagen

6.1.5.2 pET-47b

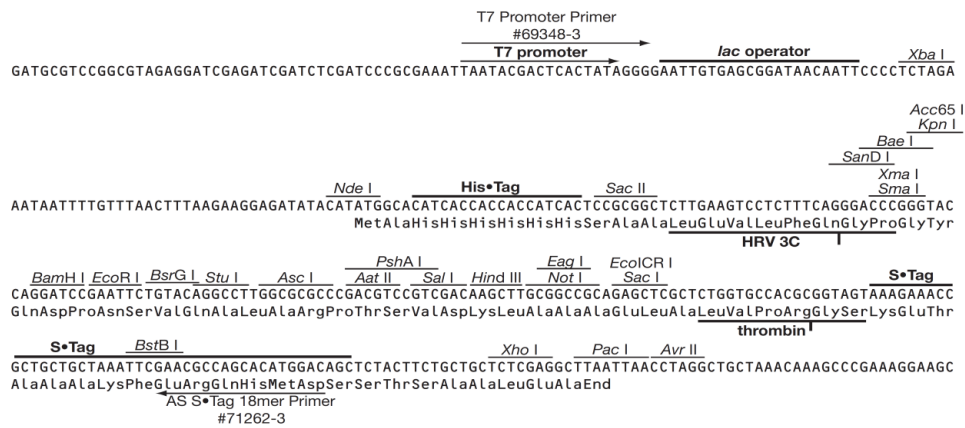


Fig. 6.2: Multiple cloning site of pET-47b from Novagen

6.1.5.3 pGEX4T1

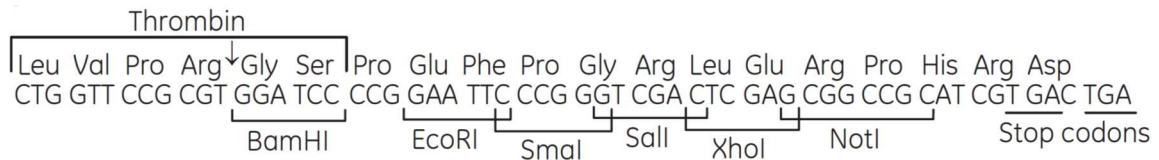


Fig. 6.3: Multiple cloning site of pGEX4T1 from GE Healthcare

6.1.5.4 pGEX6P1

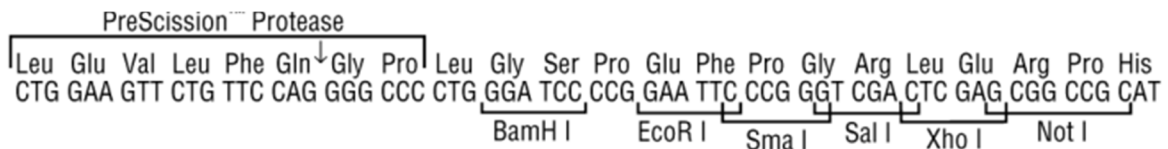


Fig. 6.4: Multiple cloning site of pGEX6P1 from GE Healthcare

6.1.6 MEDIA AND ADDITIVES

Tab. 6.4: Media composition and concentrations of additives

NAME	CONTENTS/USE	CONCENTRATION
LB-Medium	Trypton yeast extract NaCl H ₂ O	10 g 5 g 5 g ad to 1 l
M9 minimal medium	5x M9 Salt* 1 M MgSO ₄ 1 M CaCl ₂ 20 % glucose 1 % thiamin amino acids DL-Selenomethionine	200 ml 2 ml 0.1 ml 20 ml 0.2 ml each 50 mg 50 mg
M9 minimal medium for NMR	5x M9 Salt* ¹⁵ NH ₄ Cl 1 M MgSO ₄ 1 M CaCl ₂ 20 % glucose (¹³ C)	200 ml 1 g 2 ml 0.1 ml 1.25 g ad to 1 l
IPTG (1M)	for induction of bacterial expression	0.1-1 mM
Rhamnose (1M)	for tuning of protein expression with lysozyme level	0.75 mM
Kanamycin sulfate (10 mg/ml)	for resistance	10 µg/ml
Ampicillin (50 mg/ml)	for resistance	50 µg/ml
Chloramphenicol (100 mg/ml)	for resistance	100 µg/ml

* 5x M9 Salt: 64 g Na₂HPO₄ x 7H₂O, 15 g KH₂PO₄, 2.5 g NaCl, 5 g NH₄Cl. For M9 minimal medium labelled ¹⁵NH₄Cl was added instead of unlabelled NH₄Cl.

All additives were filtered and stored at -20 °C or for Rhamnose at room temperature.

6.1.7 BUFFERS

6.1.7.1 Agarose gel buffer

Tab. 6.5: Buffer with components for Agarose gel electrophoresis

NAME	COMPONENTS	
TAE-Buffer (50x)	Tris/HCl pH 7.9 acetic acid 0.5 M EDTA H ₂ O Serva Stain G	242 g 1 ml 100 ml ad 1 l 2 µg/ml
Agarose-gel	agarose in 1x TAE buffer	1 % (w/v)

6.1.7.2 SDS-gel buffer

Tab. 6.6: Buffers for SDS-gel electrophoresis

NAME	COMPONENTS	
Separating-gel buffer	1.5 M Tris/HCl pH 8.8 0,4 % SDS H ₂ O	181.7 g 20 ml (from 20 % stock) ad 1 l
Stacking-gel buffer	0.5 M Tris/HCl pH 6.8 H ₂ O	60 g ad 1 l
Running-buffer (10x)	Tris/HCl pH 8.3 SDS glycerol H ₂ O	151.4 g 50 g 720.6 g ad 5 l
Loading-buffer (4x)	100 mM Tris/HCl pH 6.8 SDS glycerol Bromphenolblue β-ME H ₂ O	1.2 g 4 % (w/v) 20 % (v/v) 0.02 % 30 µl/ml ad 100 ml
Staining solution	Coomassie Brilliant Blue R-250 ethanol acetic acid H ₂ O	2.5 g 400 ml 100 ml ad 1 l
Destaining solution	ethanol acetic acid H ₂ O	300 ml 100 ml ad 1 l

Tab. 6.7: Components for six 10 % SDS gels

NAME	COMPONENTS	
Separation gel	H ₂ O separation gel buffer 30 % Acrylamide APS TEMED	12.3 ml 7.5 ml 10 ml 250 µl 25 µl
Stacking gel	H ₂ O stacking gel buffer 30 % acrylamide APS TEMED	8.9 ml 3.8 ml 2.3 ml 150 µl 15 µl

6.1.7.3 Western Blot

Tab. 6.8: Buffers for Western blotting

NAME	COMPONENTS	
Transfer buffer	20 mM Tris 150 mM glycine 0.1 mM SDS 20 % methanol H ₂ O	30 g 10.5 g 1 g 200 ml ad 1 l
Blocking buffer	PBS Tween BSA	ad 10 ml 1 % (v/v) 5 % (v/v)
Wash buffer	Tween PBS	1 % (v/v) ad 10 ml
Detection solution	Tetramethylbenzidine	1 ml

6.1.7.4 Buffers for silver staining of SDS-gels

Tab. 6.9: Buffers for silver staining

NAME	COMPONENTS	
Fixation buffer	50 % MeOH 12 % Acetic acid 1/2000 37 % Formaldehyde H ₂ O	100 ml 24 ml 0.1 ml ad 200 ml
Post-fixation buffer	0.2 g/l Na ₂ S ₂ O ₃ x 5H ₂ O H ₂ O	0.1 g ad to 500 ml
Developer	60 g/l Na ₂ CO ₃ 1/2000 37 % formaldehyde 1/50 post-fixing H ₂ O	12 g 0.1 ml 4 ml ad to 200 ml
Stop II solution	50 mM EDTA H ₂ O	9.3 g ad to 500 ml
Staining solution	2 g/l AgNO ₃ H ₂ O	0.2 g ad to 100 ml

6.1.7.5 Buffers for protein purification

6.1.7.5.1 srGAP1 FBAR domain 21-469 of *Homo sapiens*

Tab. 6.10: Buffers for purification of the srGAP1 FBAR domain of *Homo sapiens*

NAME	COMPONENTS FOR DETERGENT-APPLIED PURIFICATION	COMPONENTS FOR REFOLDING
Lysis buffer	20 mM Tris pH 8.0 300 mM NaCl 3x protease inhibitor tablets 2 % N-Laurylsarcosine (sarcosyl; added after cell lysis) 2 mM β -Mercapto ethanol (β -ME)	20 mM Tris pH 8.0 300 mM NaCl 3x protease inhibitor tablets 2 mM β -ME
Wash buffer I	20 mM Tris pH 8.0 750 mM NaCl 10 mM MgCl ₂ 50 mM KCl 2 mM ATP 1 % sarcosyl 2 mM β -ME	20 mM Tris pH 8.0 750 mM NaCl 10 mM MgCl ₂ 50 mM KCl 2 mM β -ME
Wash buffer II	20 mM Tris pH 8.0 300 mM NaCl 10 mM imidazole 0.5 % sarcosyl 2 mM β -ME	20 mM Tris pH 8.0 300 mM NaCl 10 mM imidazole 2 mM β -ME
Elution buffer	20 mM Tris pH 8.0 300 mM NaCl 150 mM imidazole 0.2 % sarcosyl 2 mM β -ME	20 mM Tris pH 8.0 300 mM NaCl 150 mM imidazole 2 mM β -ME
Dialysis buffer	20 mM Tris pH 8.0 300 mM NaCl 0.2 % sarcosyl 2 mM β -ME	20 mM Tris pH 8.0 300 mM NaCl 4 M urea/2 M urea 2 mM β -ME
Gelfiltration buffer	20 mM Tris pH 8.0 300 mM NaCl 0.2 % sarcosyl 2 mM β -ME	20 mM Tris pH 8.0 300 mM NaCl 2 mM β -ME

6.1.7.5.2 srGAP1 FBAR domain 20-460 of *Pristionchus pacificus*

Tab. 6.11: Buffers for purification of the srGAP1 FBAR domain from *Pristionchus pacificus*

NAME	COMPONENTS
Lysis buffer	20 mM Tris pH 7,5 400 mM NaCl 2 mM MgCl ₂ 2 mM imidazole 1.0 % CHAPS 2 mM β-ME
Wash buffer I	20 mM Tris pH 7,5 800 mM NaCl 2 mM MgCl ₂ 20 mM KCl 2 mM ATP 0.5 % CHAPS 2 mM β-ME
Wash buffer II	20 mM Tris pH 7,5 300 mM NaCl 10 mM imidazole 0.5 % CHAPS 2 mM β-ME
Elution buffer	20 mM Tris pH 7,5 300 mM NaCl 250 mM imidazole 0.5 % CHAPS 2 mM β-ME
Dialysis buffer	20 mM Tris pH 7.5 300 mM NaCl 0.5 % CHAPS 2 mM β-ME
Gelfiltration buffer	20 mM Tris pH 7,5 300 mM NaCl 0.5 % CHAPS 2 mM β-ME

6.1.7.5.3 srGAP1 FBAR domain 21-475 of zebrafish

Tab. 6.12: Buffers for purification of the srGAP1 FBAR domain from zebrafish

NAME	COMPONENTS
Lysis buffer	20 mM Tris pH 8.0 400 mM NaCl 5 mM imidazole 1.0 % n-Dodecyl β -D-maltoside (β -DDM) 2 mM β -ME
Wash buffer I	20 mM Tris pH 8.0 800 mM NaCl 2 mM MgCl ₂ 20 mM KCl 2 mM ATP 2 mM β -ME
Wash buffer II	20 mM Tris pH 8.0 300 mM NaCl 10 mM imidazole 2 mM β -ME
Elution buffer	20 mM Tris pH 8.0 300 mM NaCl 250 mM imidazole 2 mM β -ME
Dialysis buffer	20 mM Tris pH 8.0 75 mM NaCl 2 mM β -ME
Mono Q buffer 1	20 mM Tris pH 8.0 75 mM NaCl 2 mM β -ME
Mono Q buffer 2	20 mM Tris pH 8.0 1 M NaCl 2 mM β -ME
Dialysis buffer	20 mM Tris pH 8.0 300 mM NaCl 2 mM β -ME

6.1.7.5.4 Purification buffers for GST-tagged proteins

Tab. 6.13: Buffers for purification of GST-tagged proteins

NAME	COMPONENTS
Lysis buffer	20 mM Tris pH 7.5 300 mM NaCl 3x protease inhibitor tablets 2 mM DTT
Wash buffer I	20 mM Tris pH 7.5 750 mM NaCl 10 mM MgCl ₂ 50 mM KCl 2 mM ATP 2 mM DTT
Wash buffer II	20 mM Tris pH 7.5 300 mM NaCl 2 mM DTT
Elution buffer	20 mM Tris pH 7.5 300 mM NaCl 75 mM GSH 2 mM DTT
Dialysis buffer	20 mM Tris pH 7.5 300 mM NaCl 2 mM DTT
Gelfiltration buffer	20 mM Tris pH 7.5 300 mM NaCl 2 mM DTT

The final salt concentration was reduced to 150 mM according to the protein stability.

6.1.7.5.5 Carom FBAR

Tab. 6.14: Buffers for purification of the human Carom FBAR domain

NAME	COMPONENTS
Lysis buffer	20 mM Tris pH 8.0 300 mM NaCl 3x Proteaseinhibitor tablets 2 mM β -ME
Wash buffer I	20 mM Tris pH 8.0 750 mM NaCl 10 mM MgCl ₂ 50 mM KCl 2 mM β -ME
Wash buffer II	20 mM Tris pH 8.0 300 mM NaCl 2 mM β -ME
Elution buffer	20 mM Tris pH 8.0 300 mM NaCl 250 mM imidazole 2 mM β -ME
Dialysis buffer	20 mM Tris pH 8.0 300 mM NaCl 2 mM β -ME
Gelfiltration buffer	20 mM Tris pH 8.0 300 mM NaCl 2 mM β -ME

6.1.7.6 Buffer for rat brain tissue and zebrafish embryos pulldown

Tab. 6.15: Lysis buffer for rat brain and zebrafish embryos

NAME	COMPONENTS
Lysis buffer	20 mM Tris pH 8.0 150 mM NaCl 1 % (v/v) NP-40 2 mM EDTA 1 mM Na ₂ HPO ₄ 5 mM NaF 3 mM Na ₄ P ₂ O ₇ 1 mM Na ₃ VO ₄ 2x proteaseinhibitor tablets PMSF (only in homogenizing buffer 2 μ l/ml) 1 mM DTT

6.1.7.7 Buffers for single and double *in-situ* hybridization

Tab. 6.16: Used buffer and their components for single and double *in-situ* hybridization

NAME	COMPONENTS
PBST pH 7.4	500 ml PBS 0.1 % Tween 20
20x SSC pH 7.0	3 M NaCl 0.3 M Na ₃ -citrate
2x SSCT	20x SSC 0.1 % Tween 20 ad 500 ml H ₂ O
0.2x SSCT	20x SSC 0.1 % Tween 20 ad 500 ml H ₂ O
4 % PFA	20 g Paraformaldehyde ad 500 ml pre-warmed PBS
proteinase K	10 µg/ml proteinase K in PBST
HYB ⁻ pH 6	50 % Formamide 5x 20x SSC 0.1 % of 10 % Tween 20
HYB ⁺	5 mg yeast RNA 50 µg/ml Heparin 100 ml HYB ⁻
Western blocking buffer	500 ml PBS 1 % Tween 20
Blocking bufffer	5 g blocking reagent 50 ml MABT
Glycin	0.05 g glycin 50 ml PBST

6.2 METHODS

6.2.1 METHODS IN MOLECULAR BIOLOGY

6.2.1.1 Polymerase Chain Reaction (PCR)

The target DNA was amplified by PCR with the help of specific oligonucleotides (see chapter 6.1.4). As templates genomic or plasmid DNA were used (Tab. 6.17 and 6.18)

Tab. 6.17: Components of a PCR reaction

	CONCENTRATION	VOLUME
template	5-8 ng	1-2 μ l
MgCl ₂	1 mM	1 μ l
dNTPs	0.5 mM	1 μ l
5x HF Buffer (New England Biolab, Ipswich, USA)		10 μ l
primer fw	1 μ M	1 μ l
primer rv	1 μ M	1 μ l
Phusion High Fidelity DNA Polymerase (New England Biolab, Ipswich, USA)	-	1 μ l

Tab. 6.18: PCR programme

STEPS	TIME	TEMPERATURE
initiation	2 min	98 °C
denaturation	1 min	98 °C
annealing	30 sec	55 °C
elongation	2 min	72 °C
final elongation	1 min	72 °C
Hold	-	8 °C

} 30x

The amplified product was analysed via agarose gel (see chapter 6.1.7.1) and purified either by gel extraction (Qiagen gel extraction kit, Qiagen, Hilden) or with PCR purification (Qiagen PCR purification kit, Qiagen, Hilden).

6.2.1.2 Restriction Digest

The purified PCR product and the specific vector were cut with restriction enzymes (Fast Digest, Fermentas GmbH, Germany) (Tab. 6.19). Vectors were cut for 1 h and PCR products for 30 min at 37 °C. The digested samples were then purified with the gel extraction kit. Ligation independent cloning (LIC) was applied for two constructs. The LIC method uses the 3'→5' exonuclease activity of the T4 DNA polymerase to create 15-base single stranded overhangs in the LIC vector. PCR products with complementary overhangs are created by building appropriate 5' extensions into the primers. The purified PCR product is treated with LIC-qualified T4 DNA polymerase in the presence of dATP to generate specific vector-compatible overhangs. The desired product is formed by annealing.

Tab. 6.19: Target genes with restrictions sites

CONSTRUCT	RESTRICTION SITES
srGAP1_FBAR_DR	NcoI, NotI
srGAP1_GAP_DR	BamHI, XhoI
srGAP1_Cterm_DR	BamHI, XhoI
srGAP1_FBAR_Hs	LIC
srGAP1_GAP_Hs	BamHI, XhoI
srGAP1_Cterm_Hs	LIC
srGAP1_FBAR_PP	NcoI, NotI
Carom_Hs_FBAR	NheI, NotI

6.2.1.3 Ligation

For the ligation of the target insert into the multiple cloning site of a specific vector a ratio of 1:3 was taken. The ligation reaction was set up overnight at room temperature (Tab. 6.20).

Tab. 6.20: Components of the ligation reaction

COMPONENT	VOLUME
insert DNA	5 µl
vector DNA	12 µl
10x T4 Ligase buffer (Fermentas GmbH, Germany)	1 µl
T4 Ligase (Fermentas GmbH, Germany)	1 µl
H ₂ O	ad 20 µl

6.2.1.4 Competent *E. coli* cells

For the transformation, competent *E. coli* cells were used. For making competent cells a 5 ml overnight culture was set up with the required strain from a glycerol stock. 50 ml LB medium were then inoculated with 1:200 of the overnight culture and grown till an OD₆₀₀ of 0.5. Cells were cooled on ice for 30 min and centrifuged at 6000 rpm for 10 min at 4 °C. Then they were resuspended in 10 ml of cold CaCl₂ (100 mM) and incubated one hour at 4 °C. This was followed by another centrifugation step at 6000 rpm for 10 min at 4 °C. Then the cells were resuspended in 2 ml cold CaCl₂ and 416 µl glycerol (to have an end concentration of 15 % of glycerol) and aliquoted à 50 µl.

6.2.1.5 Transformation of competent *E. coli* cells

One 50 µl aliquot of competent cells was thawed on ice. 5 µl of the ligation or plasmid DNA were added and incubated for 12 min on ice. This step was followed by a heat shock at 42 °C for 30 sec. The cells were cooled on ice for 5 min and then 1000 µl of LB medium was added and incubated for 1 h in a 37 °C shaker (Thermomixer compact, Eppendorf AG, Hamburg). After a centrifugation step at 13000 rpm for 10 min, the cells were plated on LB plates with the corresponding antibiotic and incubated overnight in a 37 °C incubator (Heraeus Incubator, Fellbach).

6.2.1.6 Preparation of plasmid DNA

For the isolation of plasmid DNA colonies were picked and grown in 5 ml LB medium containing tubes overnight in a 37 °C shaker. The isolation itself was carried out with a spin column kit containing a silica membrane, which binds DNA in the presence of a high concentration of chaotropic salt and elutes with low-salt buffer. For small scale preparation the QIAprep Spin Miniprep (Qiagen, Hilden) and for large scale preparation the Qiagen Plasmid Midi Kit (Qiagen, Hilden) was used.

6.2.1.7 Sequencing of target DNA

Positive clones were selected and confirmed with DNA sequencing of the target region. For that 150 ng of DNA was mixed with 1 µl of the T7 forward and T7 reverse primer (10 pmol/µl), 0.5 µl BDT mix, 1.9 µl of 5x sequencing buffer (both provided from the sequence facility in house) and H₂O to a total volume of 10 µl. The sequencing reaction was then analysed with the ABI 3730 XL sequencer (Applied Biosystems GmbH, Darmstadt) in the sequence facility of the institute.

6.2.2 Methods in protein biochemistry

6.2.2.1 Overexpression of the proteins in *E. coli* in LB-Medium

The expression of each protein construct was carried out in *E. coli* strains. Table 6.21 shows the used *E. coli* strains, antibiotics and the temperature after induction for each protein construct.

Tab. 6.21: Overexpression of the different protein domain constructs

NAME	LINE	ANTIBIOTICS	TEMPERATURE AFTER INDUCTION
srGAP1_DR_FBAR	BL21 (DE3), Lemo21 (DE3)	kanamycin kanamycin + chloramphenicol	28 °C
srGAP1_DR_GAP	BL21 (DE3)	Ampicillin	28 °C
srGAP1_DR_Cterm	BL21 (DE)	Ampicillin	20 °C
srGAP1_Hs_FBAR	BL21 (DE)	kanamycin	28 °C
srGAP1_Hs_GAP	BL21 (DE3)	Ampicillin	28 °C
srGAP1_Hs_Cterm	BL21 (DE3)	Ampicillin	18 °C
srGAP1_PP_FBAR	BL21 (DE3)	kanamycin	28 °C
Carom_Hs_FBAR	Rosetta II (DE3)	kanamycin + chloramphenicol	28 °C
Cdc42_Hs Isoform 2	BL21 (DE3)	Ampicillin	28 °C
Cdc42_DR Isoform 2	BL21 (DE3)	Ampicillin	28 °C
RhoA_Hs	BL21 (DE3)	Ampicillin	28 °C
Rac_Hs	BL21 (DE3)	Ampicillin	28 °C

The cells were transformed with the plasmids and an overnight culture was set up. In addition to the overnight culture the needed antibiotics (34 µg/mg-100 µg/mg) and in case of the Lemo21 (DE3) cells 750 µM Rhamnose was additionally added to the medium. The cells were grown in 5 l glass flasks in a shaker (Infors Multitron Shaker, INFORS AG, Bottmingen) or in ventilated 1 l bottles at 37 °C up to an OD of 0.6, induced with 0.1 mM IPTG and harvested after 4 hours. The temperature was down regulated for each protein construct after induction, varying from 18-28 °C. For harvesting, the cells were centrifuged at 6000 rpm for 10 min at 4 °C and the pellet was frozen at -20 °C. For purification harvested cells were lysed up to three times with either using the French Press (French Pressure Cell Press, American Thermal Instruments, Dayton, USA) or the sonicator (Branson Sonifier 250, G. Heinemann, Gmuend, Germany). The lysed cells were pelleted by centrifugation in an ultracentrifuge (Beckman Coulter Optima L-80 XP, Beckman Coulter, Krefeld) for 40 min at 104.630 g and 4 °C. The supernatant was filtered (0.22 µM GP Millipore Express Plus Membrane, Millipore Cooperation, Billerica MA, USA) and used as the crude extract.

6.2.2.2 Overexpression in M9-Medium

¹⁵N and ¹³C-labelled recombinant human Cdc42 and Cdc42 from zebrafish were purified from BL21 *E. coli* strain overexpressing the proteins. Cells were grown in 4 l flasks at 37 °C, after induction with 0.1 mM IPTG at 28 °C, in minimal medium containing ¹³C glucose and ¹⁵N NH₄Cl as carbon and nitrogen sources. The cells were grown overnight, harvested and stored at -20 °C.

For selenomethionine labelling the Carom FBAR domain was expressed in M9-Medium with 50 mg of selenomethionine and six additional amino acids (Leu, Ile, Thr, Phe, Lys and Val). Selenomethionine replaces the native methionines in the protein. Cells were grown in 2 l flasks at 37 °C, after induction with 0.1 mM IPTG at 28 °C. The cells were grown overnight, harvested and stored at -20 °C

6.2.2.3 Purification of 6-His-tagged proteins

For the purification of each protein construct a P1 pump was used to load the crude extract on the specific column. Washing and elution steps were carried out on an Aekta FPLC system (GE Healthcare). Hexa-histidine tagged proteins (srGAP_FBAR_Hs, srGAP1_FBAR_DR and Carom_FBAR_Hs) were purified using an immobilized metal ion affinity chromatography (IMAC) column (GE Healthcare). Thereby the protein was eluted with 250 mM imidazole. This purification step was followed by size exclusion on a Sephacryl 200 column (GE Healthcare). At each step the purity of the proteins was examined by SDS-PAGE.

6.2.2.4 Purification of GST-tagged proteins

GST-tagged proteins (srGAP1_GAP_DR, srGAP1_Cterm_DR, srGAP1_GAP_Hs, srGAP1_Cterm_Hs, Cdc42_Hs, zebrafish Cdc42, RhoA_Hs and Rac_Hs) were purified using a GSH affinity column (GE Healthcare). Here the protein was eluted with 50 mM GSH. The purification was generally followed by an overnight dialysis step for the cleavage of the GST-tag with either 3C-Protease or Thrombin. This step was then followed by size exclusion on a Sephacryl 75 column (GE Healthcare).

6.2.2.5 Purification of ¹³C and ¹⁵N labelled proteins for NMR

Purification of ¹³C and ¹⁵N labelled human Cdc42 and Cdc42 from zebrafish were conducted in the same way as the respective unlabelled proteins.

6.2.2.6 Preparation of nucleotide-free RhoGTPases

6.2.2.6.1 Nucleotide-free RhoGTPases with alkaline phosphatase

Preparation of nucleotide-free GTPase is carried out in two steps according to John et al., 1990. In the first step, 1 U alkaline phosphatase and a 1.5 molar excess of GppNHp are added to approximately 1 mg of GDP-bound GTPase to degrade the bound GDP and replace it by its

non-hydrolysable analogue. GppNHp is resistant to alkaline phosphatase, but sensitive to phosphodiesterase. The protein solution is incubated at 4 °C overnight and the degradation process is analysed by a High Performance Liquid Chromatography (HPLC), using an HPLC buffer containing 100 mM potassium phosphate pH 6.5, 10 mM tetrabutylammonium bromide and 7.5 % acetonitrile. After the complete degradation of GDP, 0.002 U snake venom phosphodiesterase per mg GTPase is added to the solution of the GppNHp-bound GTPase to cleave the nucleotide to GMP, G and inorganic phosphate (P_i). Here again, the protein solution was incubated overnight at 4 °C. The degradation process is analysed by HPLC. After the complete degradation of GppNHp, the snake venom phosphodiesterase is separated from the nucleotide-free protein with the help of an analytical gel filtration. The nucleotide-free proteins were stored at – 80 °C.

6.2.2.6.2 Nucleotide-free RhoGTPase with EDTA

Another approach to remove bound nucleotide is to incubate purified protein sample (~100 µM) in buffer containing 50 mM Tris, pH 7.5 and 20 mM EDTA for 20 min at 25 °C. This step is followed by centrifugation in a Centricon 10 concentrator at 4000 x g for 20 min. This was repeated four more times. Then the protein sample was exchanged into buffer containing 50 mM Tris, pH 7.5, 150 mM NaCl and 1 mM DTE (Zhang et al., 2000). The protein sample was examined for the content of remaining nucleotide with ³¹P NMR spectroscopy before the experiment.

6.2.2.7 SDS Polyacrylamide gelelectrophoresis (SDS-PAGE)

The purity of the proteins was analysed with SDS-PAGE. A specific volume of the protein was mixed with 4x SDS buffer and heated up to 95 °C for 5 min. The samples were then loaded on 10 % SDS gels (see chapter 6.1.7.2). Additionally a protein marker (PageRuler Prestained Protein Ladder, Fermentas GmbH, St. Leon-Rot) was loaded. The gels were stained with Coomassie Brilliant Blue R-250 (SERVA Electrophoresis, Heidelberg, Germany) until protein bands became visible and then destained in a destaining solution. The gels were analyzed with the help of a gel documentation system (Fusion SL Vilber Lourmat, pEQLAB, Germany).

6.2.2.8 Silver staining

For more sensitive detection of protein bands silver staining was used. All buffers (see chapter 6.1.7.4) were prepared freshly at the day of use. The 10 % SDS gel was fixated overnight at room temperature. To remove the acetic acid the gel was washed three times with water, 50 % ethanol and again with water. Then the gel was incubated in the post-fixation buffer for 10 min and quickly washed with water afterwards. The silver staining solution was applied to the gel for 0 min, then quickly washed off with water to reduce the staining intensity and developed for 5 min in the developing buffer. When bands started to appear the reaction was stopped by changing to the Stop II solution. The gel was transferred to water after 24 h and analysed with the gel documentation system.

6.2.3 BIOPHYSICAL METHODS

6.2.3.1 Circular Dichroism Spectroscopy

The secondary structure of purified proteins, was examined with Circular dichroism (CD) spectroscopy (Jasco CD Spectropolarimeter J-810). Therefore an aliquot of the protein was dialyzed in buffer with 50 mM NaF. The measurement was blanked with buffer, then the protein was diluted to 0.5 mg/ml and then measured in a 1 mm cuvette (Tab. 6.22).

Tab. 6.22: Parameter for examining the secondary structure

PARAMETER	
band width	1 nm
response	1 sec
sensitivity	Standard
measurement range	260-190 nm
data pitch	0.1 nm
scanning speed	200 nm/min
accumulation	10
cell length	0.1 cm
temperature	20 °C

Additionally heat denaturation of the protein sample was carried out, to examine the melting temperature of the protein. The melting curve was recorded at 220 nm and the denaturation of the protein samples was followed over a temperature gradient from 20 °C- 90 °C. Curves with sigmoidal curvature indicated proper folding of the protein sample.

6.2.3.2 Nuclear Magnetic Resonance

Samples for ^1H and ^{31}P Nuclear Magnetic Resonance (NMR) were prepared at concentrations of 0.15-0.25 mM in their specific buffers. ^{31}P NMR was measured at 243 MHz (i.e. on a 600 MHz spectrometer). Samples for ^{19}F NMR were prepared at a total concentration of 0.15 mM in 20 mM Tris pH 7.5, 150 mM NaCl and 1 mM MgCl_2 with addition of 120 μM AlCl_3 and 5 mM NaF. ^{19}F spectra were recorded at 282 MHz (i.e. at a 300 MHz spectrometer). The binding site mapping for the Cdc42- AlFl_4^- -GAP complex was recorded on 600 or 800 MHz spectrometers. All measurements were carried out at room temperature. Spectra were analysed with Sparky (version 3.113; Goddard/UCLA) or gsim (version 0.20.2b; Zorin/Durham University) and images arranged in Adobe Illustrator 6 (Version 16.0.0, Adobe System Incorporated, USA).

6.2.3.3 Crystallography

In order to determine the molecular structure of the target protein, it was subjected to crystallization. Therefore several screens in 96 well plates (Art-Robbins Intelli Plates, USA) were set up by mixing 0.3 μl of protein with 0.3 μl of the reservoir solution with the help of a Honeybee 963 crystallization robot (Genomic Solution). Images of the drop were obtained with the help of the RockImager 54 (Formulatrix, Waltham MA, USA) and manually inspected. Crystallization conditions were optimized by hanging drop screens varying protein concentration and concentration of the reservoir components. The following eight different crystallization screens (Qiagen Nextal) were applied on the proteins: Classic Suite I and II, PEGs Suite I and II, Protein Complex Suite, Joint Centre for Structural Genomics (JCSG) Suite, PACT Suite and the Cryos Suite. Additionally, heavy metal soaking experiments with platinum and mercury salts were carried out. Here, following platinum and mercury salts from the Hampton Research Heavy Atom Screens were applied to the proteins, according to their minimum pH: Pt1-Pt6, Pt8, Pt10, Pt12, Hg2 and Hg3. For the soaking experiments the crystals were transferred from the mother liquor to the solution with 10 mM of the heavy atom salt and incubated either for few hours or overnight.

Protein crystals were picked with small nylon loops (Hampton) and either frozen in liquid nitrogen at once or immersed in cryo solution before freezing. Measurements of the frozen crystals were carried out at the Beamline PXII at the Swiss Light Source (SLS; Paul-Scherrer-Institut, Villigen, Switzerland).

6.2.3.4 Mass Spectrometry Analysis

For mass spectrometry analysis pulldown samples were submitted to a gel, run on a 1D SDS PAGE (NuPAGE 10 % BisTris gels, Invitrogen). The proteins were visualized by freshly made Coomassie blue staining. Destaining was performed with a destaining solution (see chapter 6.1.7.2). Each lane was divided into three to four sections for in-gel digestion. The gel pieces were dehydrated with acetonitrile (ACN), then swollen at room temperature by adding 13 ng/ml sequencing-grade trypsin (Promega, Germany). The digestion was performed at 37 °C overnight. The resulting peptides were extracted in three subsequent incubation steps with different concentrations of CAN. Supernatants were combined, ACN was evaporated in a vacuum centrifuge and peptides were desalted using C₁₈ StageTips. The digested peptides were separated with the help of a nano-LC (Easy-nLC, Thermo Fisher Scientific, Germany), which is coupled to an LTQ-Orbitrap-XL (Thermo Fisher Scientific, Germany) through a nano-LC-MS interface (Proxeon Biosystems, Germany). Peptides were eluted using a segmented gradient of 5-90 % HPLC solvent B (80 % acetonitrile in 0.5 % acetic acid) at a flow rate of 200 nl/min over 43 min. The data acquisition was conducted in the positive ion mode. The mass spectrometer was operated in the data-dependent mode to automatically switch between MS and MS/MS acquisition. Survey full-scan MS spectra were acquired in the mass range of m/z 300–2000 in the orbitrap mass analyser at a resolution of 60,000. The five most intense ions were sequentially isolated and fragmented in the linear ion trap using collision-induced dissociation (CID) at the ion accumulation target value of 5000 and default CID settings. The ions already selected for MS/MS were dynamically excluded for 90 sec. The resulting peptide fragment ions were recorded in the linear ion trap.

The raw data was analysed using the MaxQuant software version 1.2.2.9 (Cox *et al.*, 2008) to generate peak lists that can be used for database search. A non-linear mass re-calibration for each pre-cursor ion and calculates precise masses as well as individual mass errors. The derived MS data were submitted to the Andromeda search engine (Cox *et al.*, 2011). The acquired MS data was searched against a rat database and in the case of the second pulldown against a zebrafish database plus the sequences of GST_srGAP1_Hs_Cterm/GST-srGAP1_DR_Cterm and 248 common contaminants. The Andromeda database scores calculated by MaxQuant were converted to posterior error probabilities (PEP) and false discovery rates were set to 1 % at peptide and protein group level (Elias *et al.*, 2007).

6.2.4 Bioinformatics

The bioinformatics toolkit of the MPI for Developmental Biology (<http://toolkit.tuebingen.mpg.de/>) served as a platform for a variety of sequence analysis.

Homologs of the target protein sequence were found with PSI-BLAST (Altschul et al., 1997) by searching against a protein database, here the non-redundant sequence database 70 (nr70). nr70 contains representative sequences, which are filtered for a maximum pairwise sequence identity of 70 %. The search was restricted to 2000 sequences at an E-value cut-off of 0.001, which is the threshold for including a sequence to the model created by PSI-BLAST to be used on the next iteration. The result of this search was then subjected to cluster analysis by pairwise BLAST P-values (Altschul et al., 1990) in CLANS (Frickey et al., 2004). Here, the sequences were clustered at a p-value of 10^{-15} .

Multiple sequence alignments were carried out with CLUSTALW. Coiled coil analysis was carried out with the help of the Coil/Pcoil tool (Parry et al., 1982; Lupas et al., 1991; Lupas et al., 1996).

6.2.5 *IN VIVO* AND *IN VITRO* ASSAYS

6.2.5.1 Pulldown

The rat brain was weighed and buffer was added according to the weight. Then it was homogenized with a glass potter and centrifuged for 10 min at 3000 rpm. The supernatant was centrifuged again for 40 min at 164864 g in a Ti70 rotor. Approximately 1 ml of GSH beads were equilibrated with lysis buffer. To pre-clear the lysate, it was added to 600 μ l of the equilibrated GSH beads and then rotated for 30 min at 4 °C. This step was followed by a centrifugation step for 10 min at 13000 rpm and the supernatant was transferred into a new tube. 1 mg of the GST-tagged C-terminus was added to the 400 μ l of equilibrated beads and incubated for 30 min at 4 °C. Before adding 1 ml of the pre-cleared lysate to each bead condition, the beads were washed once with lysis buffer. The incubation took place overnight at 4 °C. The beads were washed 4x with lysis buffer and then taken up in 60 μ l 2x SDS-buffer and heated it up at 90 °C for 10 min. This step was followed by another centrifugation step for 10 min at 13000 rpm at 4 °C and the supernatant transferred into a new tube. 10 μ l were loaded on a BioRad TGX any kD gel (BioRad, Germany) and specific areas cut out and analysed by mass spectrometry. The pulldown with zebrafish embryos was carried out accordingly.

6.2.5.2 *In-situ* hybridization in zebrafish embryos

6.2.5.2.1 Handling of the zebrafish embryos

For the double *in-situ* hybridizations fish pairs from the albino strain were setup. After 2 h, laid eggs were picked in petri dishes and incubated at 28 °C. 1 mM of pronase was added to the medium to dechorinate the embryos. After 48 h the embryos were aliquoted à 100 each into 2 ml Eppendorf tubes and incubated overnight in 4 % Paraformaldehyde (PFA) at 4 °C. After that the embryos were transferred into 100 % MeOH in several steps (25 %, 50 %, 75 %) and frozen at -20 °C.

6.2.5.2.2 Generating template for *in vitro* transcription

The DNA probe of the target domain was generated by PCR amplification from genomic DNA. The product was then cloned into a Topo vector (Invitrogen, Germany), which has a T7 and SP6 recognition site before and after the insertion site (Tab. 6.23).

Tab. 6.23: Different template primers for *in vitro* transcription

PRIMER	SEQUENCE
srGAP1_DR_ <i>insitu</i> _fv	CAAAATTAACCCCTCACTAAAGGGGTCAAAGAGATTCGAGCTAA
srGAP1_DR_ <i>insitu</i> _rev	TTGTAACTCCCTATAGTGAGTCGTATTAGCAGCCGGATCTCAG
Robo_fv	GGATCCTAATACGACTCACTATAGGGAGGCCGTGATGGAGGTCGACGGCG
Robo_rv	ACAGGTGTCCACTCCCAGGTCCAAG

The primers for generating the Robo samples are the same. After analysing the end product via sequencing, antisense RNA was generated for each sample with an *in vitro* transcription kit (Roche, Germany). *srgap1* was labelled with Digoxigenin (Roche, Germany) and *robo1*, 2 and 3 with Fluorescin (Roche, Germany).

6.2.5.2.3 Single *in situ* hybridization

The single *in situ* hybridization assay was carried out at room temperature if not mentioned otherwise in the text. Embryos of different stages (16 hpf, 24 hpf, 30 hpf, 48 hpf and 72 hpf) were rehydrated in a MeOH series (100 %-25 %) and then washed twice in phosphate-buffered saline (PBS) with 0.1 % 10 % Tween 20 (PBST). After digestion with 10 µg/ml proteinase K (Tab. 6.24) the embryos were washed twice in PBST and then incubated 20 min in 4 % PFA to refix the embryos.

Tab. 6.24: Embryonal stages and proteinase K digestion time

EMBRYONAL STAGES	TIME
16 hpf	4 min
24 hpf	7 min
30 hpf	10 min
48 hpf	12 min
72 hpf	20 min

After washing twice in PBST the embryos were divided into different vials and then pre-hybridized in 200 μ l Hyb⁺ buffer for 4 h at 65 °C. Embryos were hybridized overnight at 65 °C with 1 μ g RNA in 200 μ l Hyb⁺ buffer. The RNA sample was taken out and the embryos were washed with 50 % Formamide/SSCT (twice for 30 min), 2 % SSCT (15 min), 0.2 % SSCT (10 min) and then blocked with blocking buffer overnight. All washing steps were carried out at 65 °C in a water bath. For the detection of labelled RNA a 1:5000 dilution of Fab-AP (Roche, Germany) antibody was added overnight and kept at 4 °C. Then NTMT buffer was added to embryos and incubated 4x for 25 min. For staining BM-Purple was added. The embryos were incubated till all stages were stained to the same extent. The staining reaction was stopped with two PBST washing steps. Then the embryos were transferred stepwise into 50 % glycerol for mounting. For microscopy of the embryos lateral and dorsal views were mounted on object slides (Roth, Germany) and then photographed with a Discovery microscope (Zeiss, Germany). The pictures were taken with the AxioVision Software (Zeiss, Germany) and edited with ImageJ 1.42 (National Health Institute, USA).

6.2.5.2.4 Double *in-situ* hybridization

All steps of this process were carried out at room temperature if not mentioned otherwise. 48 h old zebrafish embryos were rehydrated in a stepwise series of MeOH and PBS washes and then washed 4x 5 min in PBST. Digestion of the embryos was performed with 10 μ g /ml proteinase K in PBST for 15 min and washed 3x in PBST. After refixing the embryos in 4 % PFA for 20 min and washing 5x in PBST, the embryos were pre-hybridized in 300 μ l of Hyb⁺ buffer for 4 h at 65 °C. Samples were prepared by adding 200 ng RNA to 200 μ l hybridization buffer. Embryos were hybridized overnight in a 65 °C water bath. Excess of the RNA sample was washed in several washing steps at 65 °C with 2x SSC and 50 % Formamide (15 min), 2x SSC (4x 15 min), 0.2 SSC (4x 15 min). The rest of the washing steps with 3x with PBST were

carried out at room temperature. For the detection of the labelled RNA the embryos were incubated in a western blot reagent, diluted 1:20 in PBST for 2 h at room temperature. The primary antibody sheep anti α -DIG (Roche, Germany) was diluted 1:5000 in western blocking buffer. The embryos were incubated at 4 °C overnight. The incubation step was followed by 6x of 15 min washing steps with PBST. Then the embryos were re-blocked in western blocking buffer for 1 h at room temperature and the second antibody HRP-conjugated rabbit anti-sheep (Roche, Germany) was applied in a 1:200 dilution to the embryos overnight at 4 °C. Again the embryos were washed 6x 15 min with PBST after this incubation step and visualized with TSA Alexa Fluor 647 (Life Technologies, Germany) with HRP goat anti-mouse IgG (Roche, Germany). Therefore the tyramide solution was diluted in 1x amplification buffer. The reaction was setup for 1 h in the dark under agitation and at room temperature. This was followed by 5x of 1 min washing steps with PBST, then the HRP was deactivated by incubating the embryos for 30 min with 6 % H₂O₂ and washed again 3x 10 min in PBST. After reblocking the embryos for 1 h in western blocking buffer, they were incubated in α -Fluorescein-POD (1:500 diluted) overnight at 4 °C. The tyramide signal amplification detection was repeated for the secondary antibody as described for the primary antibody. The fluorescence microscopy was carried out at a LSM 510 Meta (Zeiss, Germany).

6.2.5.3 Assays with liposomes

6.2.5.3.1 Generating the liposomes

A mix of different lipids was used in the assays. Table 6.25 shows the lipid composition of the Endo-Mix liposomes with their molecular mass, stock solution and the used volume for a 2.7 mg/ml (corresponding to 4 mM) lipid mix. The lipids were purchased from Avanti (Avanti, Alabama, USA).

Tab. 6.25: Lipid composition of the Endo-mix liposomes

LIPIDS	MOLAR MASS (G/MOL)	MOLAR CONCENTRATION [%]	LIPID WEIGHT [μ G]
Cholesterol	386.65	35	541.32
Sphingomyelin	760.22	10	304.08
phosphatidylethanolamine (PE)	756.36	10	302.54
phosphatidylserine (PS)	824.96	10	329.98
phosphatidylinositol (PI)	902.13	5	180.42
phosphatidylcholine (PC)	786.64	25	786.64
phosphatidylinositol-4,5- biphosphate (PI(4,5)P ₂)	1096.38	5	219.27
Ø Molar mass	666.03	Total [μ g] of lipids	2664.25

To generate liposomes 1 ml of the lipid mix was transferred into a pear-shaped flask and 1 ml chloroform was added. The solution is then evaporated in a rotary evaporator for 60 min at 90 rpm and 30 mbar. The dried lipid film is then re-suspended in a specific buffer (20 mM HEPES pH 7.5, 140 mM KCl, 10 mM NaCl, 1 mM MgCl₂ to form multilamellar liposomes. The flask is then covered with parafilm and has to undergo a 10x freeze-thaw cycles in liquid nitrogen and 45 °C water bath. The multilamellar liposomes are then aliquoted in Eppendorf tubes and stored at -80 °C.

6.2.5.3.2 Co-sedimentation with high speed centrifugation

First the liposomes were brought to uniform size with a 3 min sonication step. For the co-sedimentation assay 1 mg liposomes were incubated with 5 μ M srGAP1 FBAR domain of zebrafish for 2 h in a table shaker (Eppendorf, Germany) at 37 °C. This step was followed by a high-speed centrifugation step at 21000 g at room temperature for 30 minutes. Supernatant and pellet were analysed with a 10 % SDS gel.

6.2.5.3.3 Negative stain electron microscopy

The liposomes were brought to uniform size with a 3 min sonication step. Then 1 mg of liposomes were incubated with 5 μ M srGAP1 FBAR domain of zebrafish for 15 min. For the liposome assay electron microscopy (EM) carbon coated grids were used. The sample was pipetted on the grids, incubated for a while and then absorbed with a small tissue. The grids were washed 3x to remove probe excess and then stained with 1 % uranylacetate for 30 s. The grids were imaged with a Tecnai Spirit G2.

6.2.5.4 Giant Unilamellar Vesicle (GUV) assay

For the GUV assay different lipids were mixed in different concentrations to mimic the composition of the cell membrane (Tab. 6.26). Calculation of the used volume was done according to Tab. 6.25 in chapter 6.2.5.3.1.

Tab. 6.26: Compositions of the GUVs

COMPONENT	MOLAR CONCENTRATION (%)
Cholesterol	35 %
Sphingomyelin	10 %
PE	10 %
PS	50 %
PC	5 %
PI	25 %
PI(4,5)P ₂	5 %
dicarbocyanine (DiD)	0.5 %

The lipids were dissolved in chloroform to a concentration of 2.7 mg/ml and 15 μ l of the solution were spread on platin (Pt) electrodes and dried in a desiccator for 30 min. The chamber was filled with a 300 osm sucrose solution and the Pt electrodes are connected to a pulse generator and an alternating voltage of 1.2 V and 10 Hz is applied for 1 h 50 min. To detach the GUVs from the electrodes a voltage of 1.2 V and 2 Hz is applied for 20 min. The vesicles are then transferred to an observation chamber, filled with an iso-osmolar buffer and let stay there to sink down to the bottom of the chamber. The proteins (5 μ M) were added to the GUVs and inverse microscopy was carried out at an Olympus Fluoview 1000 with a 60x water objective at different time points. To label the proteins with Alexa-488-C5-maleimide, the proteins were treated with 1 mM DTT and dialyzed in 20 mM Tris and 300 mM NaCl at pH 7.5. 100 μ l of the dialysed protein sample was incubated with the dye for 2 h at 25 °C. To stop the reaction 1 M β -ME is added to the samples and incubated for another 1 h. This is followed by a centrifugation step at 13000 rpm for 5 min. To remove the free dye the sample was purified with a small G50 column, which was equilibrated with the dialysis buffer.

7. RESULTS

7.1 CHARACTERIZATION OF THE SRGAP1 PROTEIN

The srGAP family was first mentioned by Wong et al. in 2001. To date four members (srGAP1-4) have been identified, of which mostly human srGAP1, srGAP2 and srGAP3 have been characterized (Couthino-Budd et al., 2012; Guerrier et al., 2009; Mason et al., 2010; Wong et al., 2001). Excepting the SH3 domain of srGAP1, there is no structural data available for the domains of any member of this protein family.

7.1.1 BIOINFORMATICAL CLUSTER ANALYSIS OF THE SRGAP FAMILY

Homology, described as similarity through common descent, can be observed on a scale ranging from genetic sequence to anatomy. A high degree of protein sequence homology gives a strong expectation, that protein functions will be retained in different species (Tatusov et al., 1997). Here, the homology of the srGAP family to other protein families was analysed. Therefore, the full-length srGAP1 sequence was subjected to cluster analysis. Protein clusters are created using a BLAST p-value, which takes in the length of the hit versus the query and the subject. The top hits of the BLAST search are then clustered together. All sequence similarity searches were carried out in the MPI bioinformatics toolkit (<http://toolkit.tuebingen.mpg.de>; Biegert et al., 2006).

In this query the full-length srGAP1 protein sequence was used to identify homologs of the srGAP proteins, which may help to predict structural and functional characteristics of the srGAP family. First, a PSI-BLAST search (Altschul et al., 1997) was carried out. Thereby, the amino acid sequence is searched against a protein database, here the non-redundant sequence database nr70, for similar sequences. PSI-BLAST performs iterative BLAST searches and builds an alignment from the best hits. This alignment is then used for the next search round. The nr70 data base contains sequences, which are filtered for a maximum pairwise sequence identity of 70 %. The search was restricted to 2000 sequences at an E-value cut-off of 0.001, which is the threshold for including a sequence to the model created by PSI-BLAST to be used on the next iteration. The result of this search was then subjected to cluster analysis by pairwise BLAST p-values (Altschul et al., 1990) in CLANS (CLuster ANalysis of Sequences, Frickey et al., 2004). P-values are defined as the probability that the score of an alignment of an evolutionarily unrelated sequence pair will be higher or at least the same as for a given alignment. Small p-values mean that the alignment of a given sequence pair is statistically relevant and is less likely by chance (Higgs and Atwood, 2005). Here, only

connections of a p-value of 10^{-15} or better were considered. Clusters are formed based on attractive and repulsive forces according to the Fruchterman-Reingold algorithm (Frickey et al., 2004). Similar sequences (represented by dots) locate close together after a few iterations and form one cluster.

The cluster map in Fig. 7.1 shows ten distinct clusters, some containing satellite-clusters. The clusters seem to be not closely related as indicated by the distance of the different clusters. Analysis of the domain composition of each protein family showed that all of them contain a FBAR domain and therefore belong to the BAR superfamily. The srGAP family cluster contains 239 sequences and is well separated from neighbouring clusters. It is connected to the FCH and double SH3 domain protein family as well as the RhoGAP containing protein family and the Tyrosine protein kinase Fer family. The FCH and double SH3 domain protein family consists of three sub-cluster which can be assigned to FCH and double SH3 domain 1, FCH and double SH3 domain 2 and Nervous Wreck, which can be only found in *Drosophila*. The RhoGAP containing protein family can be only found in *Dictyostelium*, whereas tyrosine protein kinase Fer family consists of two sub-clusters, which can be assigned to protein kinases found in insects and in mammals. The tyrosine protein kinase Fer family is an outlier group, which is only connected to the srGAP family and to a not annotated protein in the Cdc42 interacting family. It is also the only protein family with a SH2 domain and a Protein kinase C domain. All homologous protein families, besides the FCH domain only protein family, contain additional domains either SH3 domains or GAP domains. The srGAP family, the RhoGAP containing protein family in *Dictyostelium* and the GTPase activating proteins in fungi are the only protein families with an annotated GAP domain.

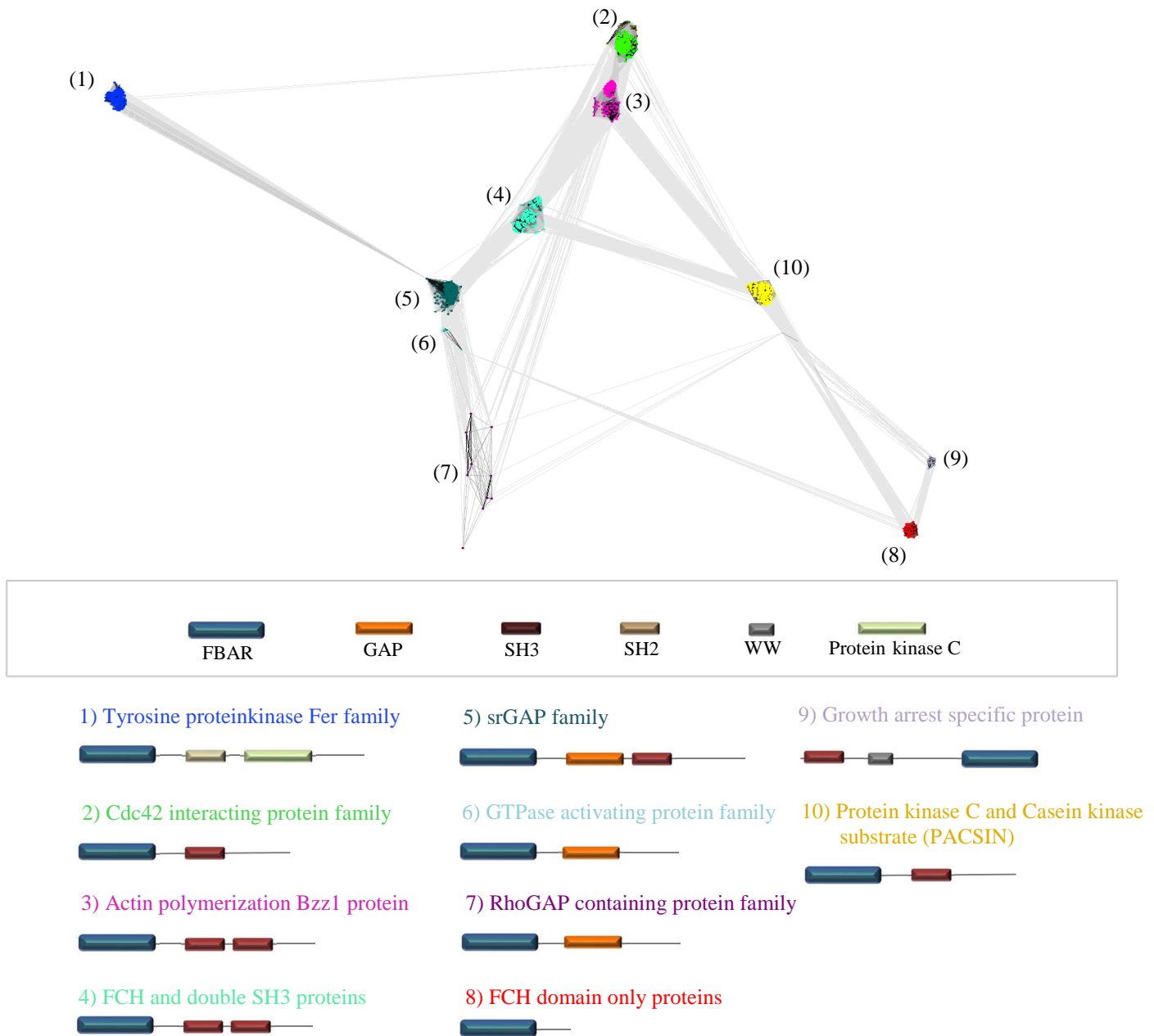


Fig. 7.1: CLANS map of the srGAP family and their related protein families

The sequences were clustered in CLANS at a p-value cut-off of 10^{-15} , based on the all-against-all pairwise similarity as calculated by BLAST p-values. Dots illustrate protein sequences, whereas lines represent p-values. Darker lines represent lower p-values, whereas lighter lines represent higher p-values. Each colour represents one protein family, also indicated by the colour of the labels and each cluster is labelled with a number. A legend of the domains and the domain composition of each protein family is illustrated below the cluster map.

In Tab. 7.1 all protein families found in the cluster map are listed with their known function. Interestingly, most of them are involved in the regulation of the cytoskeleton.

Tab. 7.1 Neighboring protein families with their known function

PROTEIN FAMILY	FUNCTION
srGAP protein family	Regulation of actin dynamics, cell migration and differentiation Role in neuronal morphogenesis and migration
FCH and double SH3 protein family	Regulation of actin polymerization and cell migration Role in neuronal migration
Actin polymerization Bzz1 protein	Actin polymerization and endocytosis in yeast
Cdc42 interacting protein family	Reorganization of actin cytoskeleton
Tyrosine protein kinase Fer family	Regulation of actin cytoskeleton, microtubule assembly, lamellipodia formation and cell migration
Growth arrest specific protein family	Microtubule regulation
FCH domain only protein family	Clathrin-mediated endocytosis
Protein kinase C and Casein kinase substrate family	Reorganization of actin cytoskeleton and neuron morphogenesis
RhoGAP containing protein family	Unknown function in <i>Dictyostelium</i>
GTPase activating proteins	Unknown function in fungi

A closer look at the srGAP family cluster (Nr. 5 in Fig. 7.1) shows that the previously compact cluster (at p-value cut-off of 10^{-15}) disassembles and reveals six sub-clusters when edges with p-values above 10^{-200} are removed (Fig. 7.2).

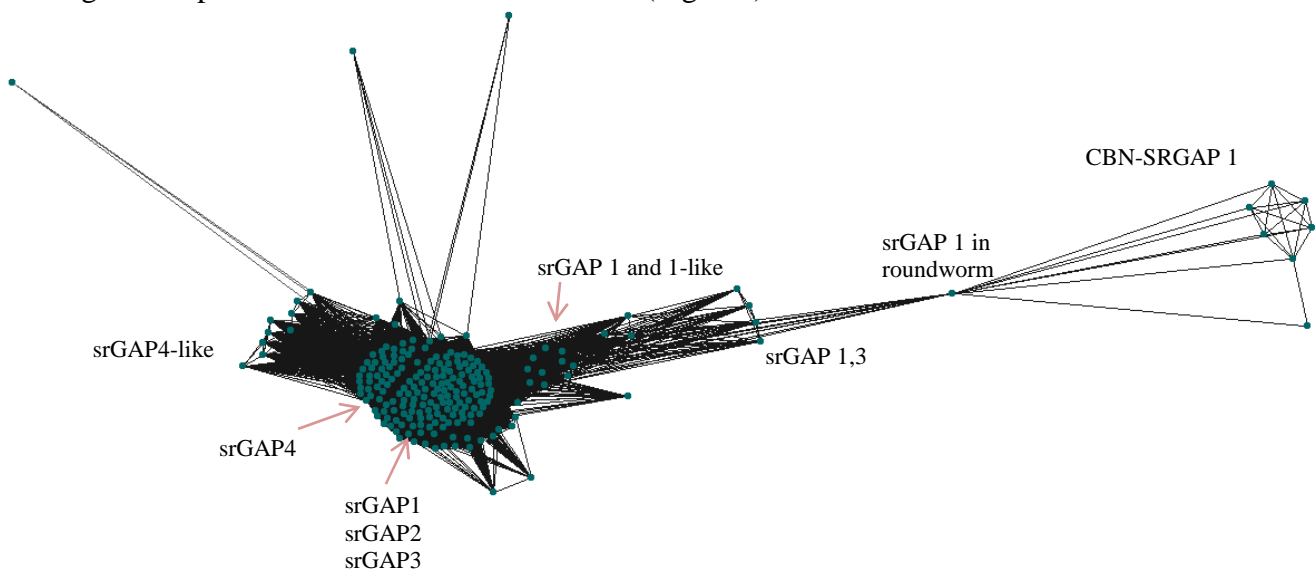


Fig. 7.2: Sub-clusters in the srGAP family cluster

Cluster analysis of the srGAP protein cluster at p-value cut-off of 10^{-200} which separates into six sub-clusters: SRGAP1 from *Caenorhabditis*, srGAP 1,3, srGAP1 and 1-like, srGAP1, srGAP2 and srGAP3, srGAP4 and srGAP 4-like.

The small cluster of the SRGAP1 proteins in *Caenorhabditis* (CBN-SRGAP1) is connected to the bigger cluster through the srGAP1 protein in the roundworm of pigs, which could be the evolutionary link between the *C. elegans* SRGAP1 and the other srGAP proteins. Interestingly srGAP1,3 can be only found in a few organisms: Yellow fever mosquito (*Aedes aegypti*), the southern house mosquito (*Culex quinquefasciatus*) and tick (*Ixodes scapularis*).

The separated part of srGAP1 and srGAP 1-like proteins can be found in some members of the insects. srGAP1, srGAP2 and srGAP3 are too similar and therefore did not collapse into different sub-clusters, whereas srGAP4 differentiates from the big cluster. Also the srGAP4-like proteins separate from the main srGAP4 cluster. Three main outlier sequences can be detected, which can be assigned to srGAP-4 like partial protein in common chimpanzee (*Pan troglodytes*), an unnamed protein in pufferfish (*Tetraodon nigroviridis*) and srGAP1 in atlantic salmon (*Salmo salar*) (dots from left to right). Members of srGAP1-4 have been only identified in eukaryotes. As many genomes, for example that of fish, are not fully sequenced yet, more srGAP proteins and their isoform containing organisms might emerge in the future.

7.1.2 DEVELOPMENTAL AND TISSUE-SPECIFIC EXPRESSION ANALYSIS OF *SRGAP1* IN ZEBRAFISH EMBRYOS

The bioinformatical analysis showed that srGAP1, srGAP2 and srGAP3 are highly similar, as they can be found in one cluster, which does not form subclusters. This also hints a possible conservation of the srGAPs in different organism. On a mRNA level, expression patterns of the *srGAPs* in rat, mice and human foetuses have been shown to be similar (Bacon et al., 2009; Ip et al., 2011; Wong et al., 2001). Here, the expression pattern of *srgap1* in zebrafish embryos was analysed for the first time. Zebrafish is an excellent model system for studying cellular, molecular and genetic developmental mechanisms of vertebrates (Streisinger et al., 1981). So far, there is no information available regarding the mRNA expression pattern of the *srgap* family in developing zebrafish embryos. In the following section, the spatiotemporal gene expression patterns of *srgap1* in different stages and tissues of zebrafish embryos is analysed and described.

7.1.2.1 Gene expression pattern analysis in developing zebrafish embryos

7.1.2.1.1 Expression of *srgap1* in developing zebrafish embryos

The expression of *srgap1* has been studied previously in embryos and juvenile stages of rats, mice and in human foetuses and showed expression in the brain, specifically in retinal ganglion cells of E15 mouse embryos, the olfactory bulb of P2 mouse embryos, as well as in the anterior subventricular zone (SVZa) of the forebrain in P3 rats (Bacon et al., 2009; Ip et al., 2011; Wong et al., 2001). Expression in the spinal cord and the dorsal root ganglia of P2 mouse is also described, though the expression levels are not specified. Human foetuses, ranging from 8-17 post-conceptual week (PCW), show expression in corticospinal axons. However, nothing is known about the expression of *srgap1* in early embryonic and larval stages of zebrafish. In the following the expression of *srgap1* was examined with whole-mount *in-situ* hybridization experiments, which provide information about the timing and localization of the transcribed mRNA in the embryos. For this a 1425 bp long sense and anti-sense probe of *srgap1*, corresponding to the FBAR domain of the srGAP1 protein was generated and labelled with digoxigenin before incubating it with fixed embryos. Figure 7.3 shows lateral views of a 24 hours post fertilization (hpf) zebrafish embryo hybridized with the anti-sense (Fig. 7.3 A) and the negative control sense probe (Fig. 7.3 B). As seen in Fig. 7.3 A, strong *srgap1* expression is concentrated in the fore-, mid-, and hindbrain as well as in the retina, the spinal cord and the tail of the zebrafish embryo. No signal can be observed with the

sense RNA probe (Fig. 7.3 B), thus confirming the specificity of the signal of the anti-sense probe of *srgap1* in Fig. 7.3 A.

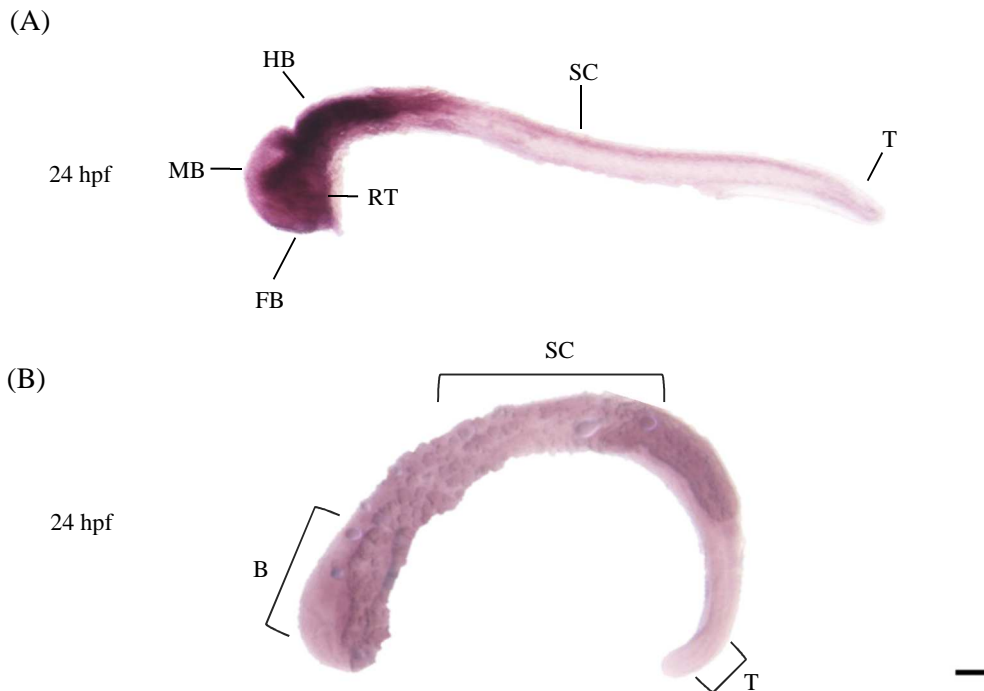


Fig. 7.3: Single *in-situ* hybridization experiment to analyse expression patterns of *srgap1* in different developmental stages of zebrafish embryos

For the single *in-situ* hybridization experiment the *srgap1* RNA was Digoxigenin-labelled, detected with AP-conjugated α -DIG antibody and developed with NBT-BCIP. The stages are indicated in hours post-fertilization. (A) Lateral view of a 24 hpf zebrafish embryo with the anti-sense RNA probe. Labels indicate major expression areas for *srgap1* in fore-, mid- and hindbrain as well as spinal cord and tail. (B) Lateral view of a 24 hpf zebrafish embryo with the sense RNA probe (labels indicate main parts of the embryo) Abbreviations: B, brain; FB, forebrain; HB, hindbrain; MB, midbrain; RT, retina; SC, spinal cord; T, tail. Images were taken with at a Discovery microscope (Zeiss) with 80x resolution. Scale bar: 5 μ m

These results fit well the expression patterns observed in rat and mouse embryos, as well as human foetuses (Bacon et al., 2009; Ip et al., 2011; Wong et al., 2001), leading to the conclusion that the expression sites of *srgap1* are conserved in different vertebrate organisms. The expression of *srgap1* in the central nervous system (CNS) correlates well with the predicted role of *srgap1* in neuronal processes, such as axon guidance and neuron growth (Ip et al., 2011). Therefore, a possible correlation of *srgap1* expression with the expression of its predicted interaction partners *robo1*, *robo2*, *robo3* was investigated in the following.

7.1.2.1.2 Comparison of the expression pattern of *srgap1* with *robo1-3*

The Robo family, cell-surface receptors for Slit ligands, represent possible interaction partners for the srGAP1 protein *in vivo* and play a major role in neuronal migration, axon guidance, vessel integrity and angiogenesis in case of Robo4. In this chapter, the comparison of the expression sites of three zebrafish *robo* genes (*robo1-robo3*) with *srgap1* in zebrafish is described. While the extracellular domains of the *robo 1-3* genes are conserved (see Tab. 7.2), *robo4* shows less similarity with only 48 %-51 %. *robo1*, *robo2* and *robo3* show similar but distinct expression patterns in the zebrafish embryos (Campbell et al., 2007; Lee et al., 2001; Miyasaka et al., 2005; Thisse et al., 2001; Thisse et al., 2008 (direct Zfin database entry)), whereas *robo4* has been described to be expressed in embryonic vasculature (Kaur et al., 2007). This study concentrates on *robo1-3*, as based on literature data they seem to be involved in similar cellular functions as assumed for *srgap1*.

Tab. 7.2: Comparison of the DNA sequence identities of the four *robo* genes of zebrafish

GENE	SEQUENCE IDENTITY
<i>robo1-robo2</i>	65 %
<i>robo1-robo3</i>	63 %
<i>robo1-robo4</i>	48 %
<i>robo2-robo3</i>	65 %
<i>robo2-robo4</i>	51 %
<i>robo3-robo4</i>	49 %

To determine whether *srgap1* expression is similar to one of the three *robo* receptors, zebrafish embryos at 16 hpf, 24 hpf, 30 hpf and 48 hpf were prepared and whole-mount *in situ* hybridization experiments were carried out, using the probes described above. Here, the probes were developed by using BM-Purple as substrate. Fig. 7.4 shows lateral views of 16 hpf, 24 hpf, 30 hpf, and 48 hpf old zebrafish embryos. As seen in Fig. 7.4 column I, *srgap1* expression is detectable in neuronal tissues at all stages of development, with highest expression levels in the brain. The panels in column Fig. 7.4 II display the expression pattern of *robo1*. *robo1* expression sites are in fore-, mid- and hindbrain as well as in the spinal cord. In the 48 hpf stage *robo1* is also expressed in the branchial arches. The expression sites match the data for the *robo1* expression sites in zebrafish published by Lee et al., 2001 and Thisse et al., 2008. For *robo2* (Fig. 7.4 column III) expression sites can be seen in fore-, mid- and hindbrain, as well as in spinal cord (Fig. 7.4 C) and retina (Fig. 7.4 O). Overall, the expression

patterns of *robo2* in the forebrain seem to be more spatially restricted than that of *robo1*, which is especially obvious at 24 hpf (Fig. 7.4 G). Similar observations for *robo2* expression sites in zebrafish embryos were described before (Campbell et al., 2007; Lee et al., 2001 and Miyasaka et al., 2005). In Fig. 7.4 column IV the expression patterns for *robo3* are shown in fore-, mid- and hindbrain, as well as in the retina (Fig. 7.4 P), spinal cord and tail. This pattern is reminiscent of the *robo1* expression pattern. *robo3* exhibits more ubiquitous expression in the brain than *robo2*. Other studies support these data showing similar expression patterns for *robo3* (Campbell et al., 2007, Lee et al., 2001 and Thisse et al., 2001). The expression of *srgap1* resembles that of *robo1* and *robo3*. Absolute expression levels cannot be compared between individual images since signal intensities can vary due to the experimental conditions. For instance, all four genes (Fig. 7.4 row M-P) show weaker expression in the spinal cord at 48 hpf, which could be caused by lack of probe penetration due to insufficient permeabilization by proteinase K or due to further developed muscle tissue. Similar effects can be seen in the data published by Lee et al., 2001. Indeed, this effect is well-known for *in-situ* hybridization experiments, and can be overcome by optimizing proteinase K digestion conditions. To more closely investigate whether *srgap1* expression mimics that of *robo1* and possibly *robo3*, the dorsal view of 30 hpf and 48 hpf heads were studied at higher magnification (Fig. 7.5). Figure 7.5 A shows a schematic view of the zebrafish brain in which fore-, mid- and hindbrain, as well as the retina are labelled in order to aid in the identification.

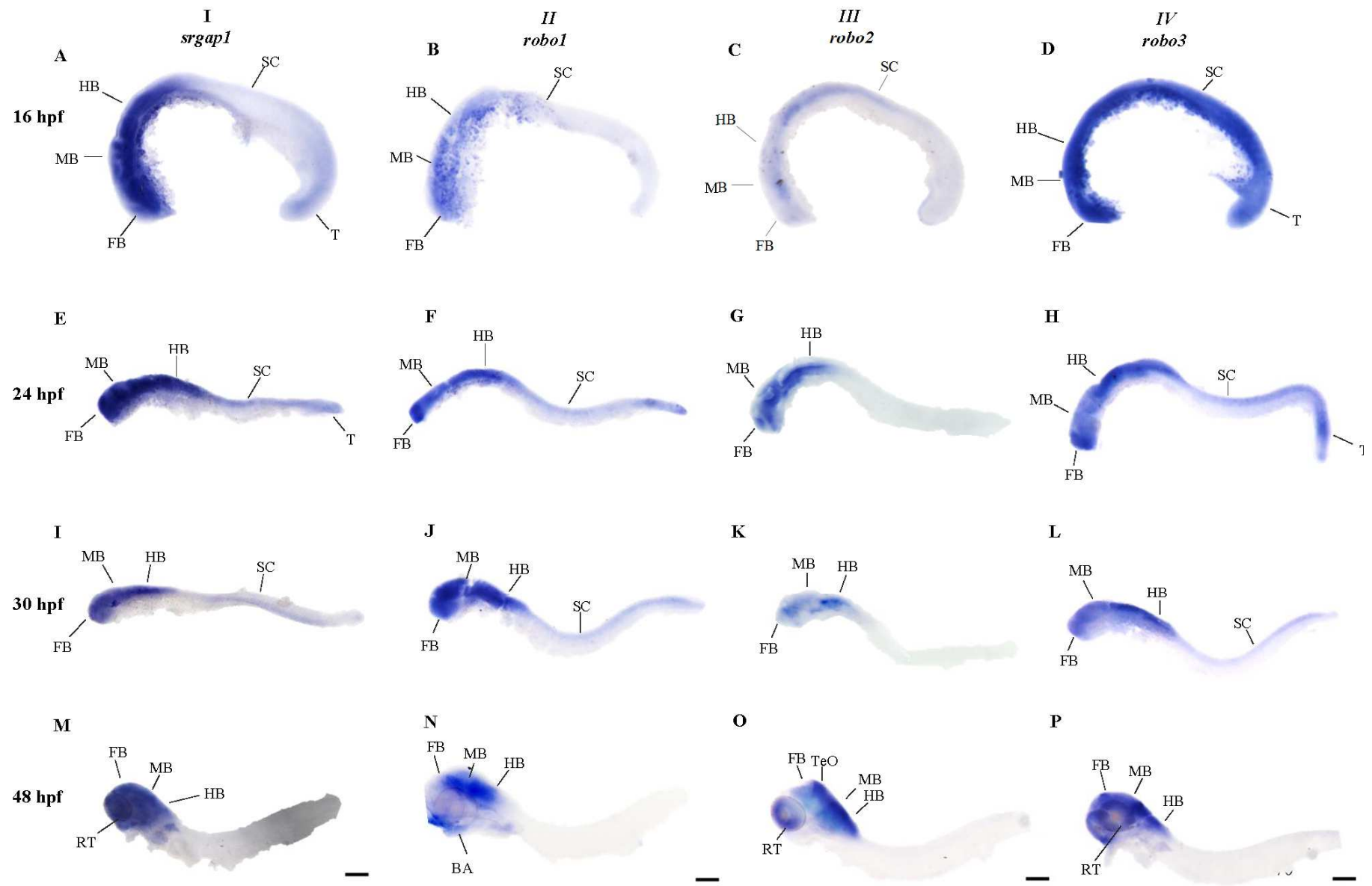


Fig. 7.4: Comparison of the gene expression patterns for *srgap1*, *robo1*, *robo2* and *robo3* at different developmental stages of zebrafish embryos

(A-P) For the single *in-situ* hybridization assays the individual RNA probes were Digoxigenin-labelled, detected with AP-conjugated α -DIG antibody and developed with BM-Purple. The embryos are shown in lateral view. The stages are indicated in hours post-fertilization. Labels show distinct expression patterns of *srgap1*, *robo1*, *robo2* and *robo3* in brain and spinal cord. Abbreviations: BA, branchial arches; FB, forebrain; HB, hindbrain; MB, midbrain; RT, retina; SC, spinal cord; T, tail, TeO, tectum. Images were taken at a Discovery microscope (Zeiss) with 80x resolution. Scale bars: 5 μ m

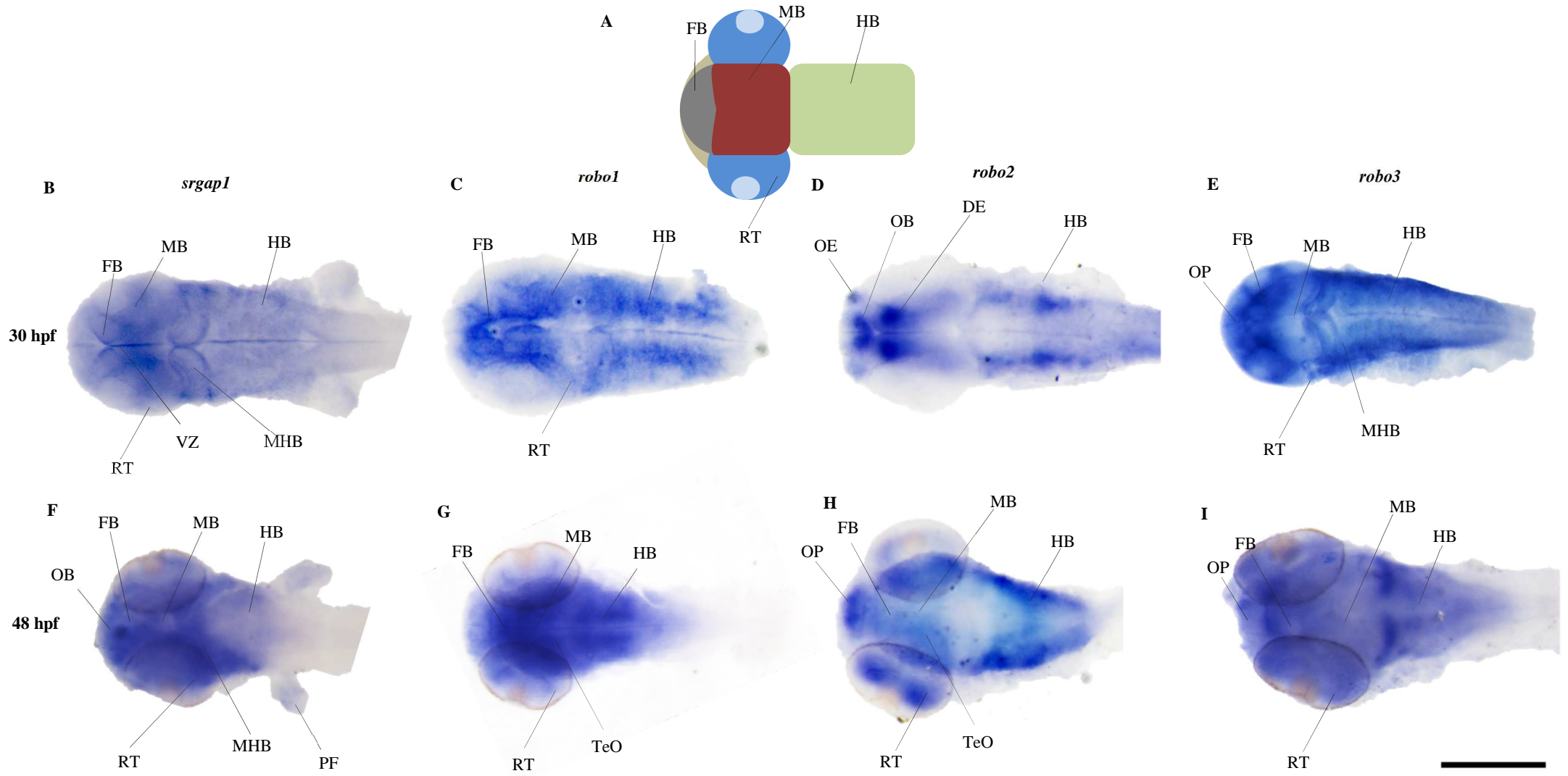


Fig. 7.5: Gene expression patterns of *srgap1*, *robo1*, *robo2* and *robo3* in the brain of developing zebrafish embryos

(A) Scheme of a zebrafish embryo head with labels of the main brain parts. (B-I) In the single *in-situ* hybridization assays the individual RNA probes are digoxigenin-labelled, detected with AP-conjugated α -digoxigenin antibody and developed with BM-Purple. The heads of the embryos are shown in dorsal views. The stages are indicated in hours post-fertilization. Labels show specific expression sites for *srgap1*, *robo1*, *robo2* and *robo3* in the CNS. Abbreviations: FB, forebrain; HB, hindbrain; MB, midbrain; MHB, mid-hindbrain boundary; OB, olfactory bulb; OE, olfactory epithelium; OP, olfactory pit; PF, pectoral fin; RT, retina; TeO, tectum; VZ, ventricular zone. Images were taken at a Zeiss Discovery microscope with 160x resolution. Scale bar: 10 μ m

As seen in Fig. 7.5, even at higher magnification and from a different perspective, *srgap1* expression appears to be ubiquitous, but with higher expression levels in the region posterior to the mid-hindbrain boundary, as well as in the pectoral fins and the retina (Fig. 7.5 B and F). *robo1* expression can be mainly observed in the fore-, mid- and hind brain, as well as in the tectum and the retina (Fig. 7.5 C and G). Especially at 48 hpf, the expression patterns of *srgap1* and *robo1* resemble each other. *robo2* expression sites can be found primarily in fore- and hindbrain, as well as in the olfactory epithelium and the olfactory bulb (Fig. 7.5 D and H). *robo2* shows distinct expression sites in specific nuclei of the fore- and hindbrain, whereas *srgap1* and *robo1* are ubiquitously expressed in fore- and hindbrain. *robo3* appears to be expressed in fore-, mid- and hindbrain, the mid-hindbrain boundary, as well as in the retina and the olfactory pit (Fig. 7.5 E and I). This expression pattern resembles that of *srgap1* and *robo1*. Table 7.3 shows a summary of all expression sites for *srgap1*, *robo1*, *robo2* and *robo3* during early zebrafish embryonic development.

Tab. 7.3: Summary of major expression sites for *srgap1*, *robo1*, *robo2* and *robo3* in developing zebrafish embryos (asterisks mark published expression sites, which are not visible here)

	<i>robo1</i>	<i>robo2</i>	<i>robo3</i>	<i>srgap1</i>
branchial arches				
forebrain				
hindbrain				
midbrain				
olfactory bulb				
olfactory epithelium				
olfactory pit				
pectoral fins	*	*	*	
retina				
spinal cord				
ventricular zone				
tail				
tectum				

The data shows simultaneous expression of all four genes in many areas of the brain. The examination at higher magnification strengthened the hypothesis that *srgap1* and *robo1* are expressed in the same tissues in the zebrafish embryos. To investigate the co-localization of *srgap1*, *robo1* and possibly *robo2* and *robo3* in more detail, I continued with fluorescence double *in-situ* hybridization experiments.

7.1.2.2 *srgap1* co-localizes with *robo1* in developing zebrafish embryos

In the previous section the expression of *srgap1* and *robo1* in overlapping domains in zebrafish embryos was shown. To identify, if both genes are co-expressed and co-localize to identical cells within overlapping expression domains, two-colour-fluorescent *in-situ* hybridization (FISH) was carried out. This method simultaneously visualizes expression patterns of multiple mRNAs in the same tissue or embryo preparation (Fig. 7.6 and Fig 7.7). For this experimental setup the *srgap1* probe was labelled with fluorescein and the *robo1* probe with digoxigenin. Figures 7.6 A-C show dorsal views of the head of a 48 hpf zebrafish embryo. The first two panels (A and B) display the expression sites for *srgap1* and *robo1* individually, whereas the last panel shows both expression sites merged in one image. Panel C in Fig. 7.6 indicates compatible expression sites for *srgap1* and *robo1* in specific nuclei of the fore- and hindbrain, visible through the orange colouring in these regions.

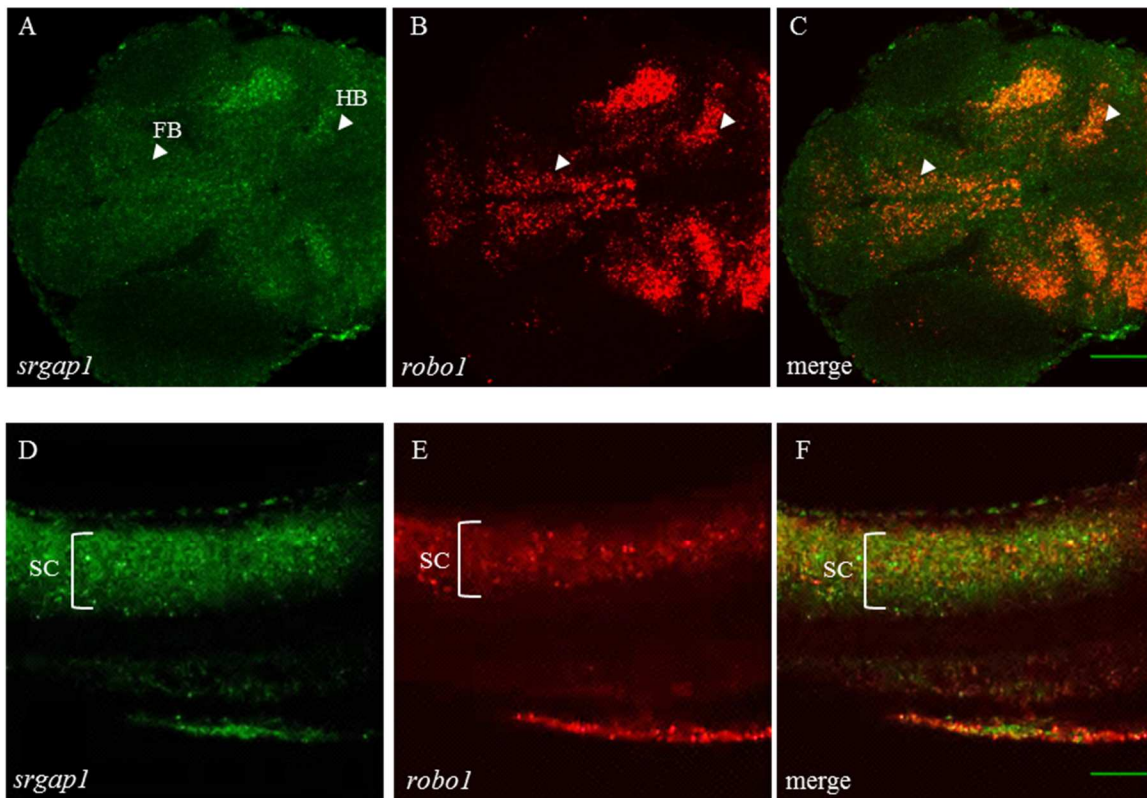


Fig. 7.6: Double *in-situ* hybridization experiments for *srgap1* and the *robo1* receptor gene in 48 hpf zebrafish embryos
Gene expression patterns of *srgap1* and *robo1* in 48 hpf embryos. *srgap1* mRNA is labelled with fluorescein (green). The *robo1* receptor mRNA is labelled with digoxigenin (red). (A-C) Dorsal views of a zebrafish embryo head with expression of *srgap1* and *robo1* in fore- and hindbrain. (D-F) Lateral view of the spinal cord shows expression for both genes. Single channels (A, B, D, E) and overlays of two channels (C and F) are shown. Abbreviations: FB, forebrain; HB, hindbrain; SC, spinal cord. Images were recorded at a Zeiss LSM510 Meta fluorescence microscope, with 40x resolution. Scale bars: 5 μ m.

The panels D-F in Fig. 7.6 show a lateral view of the spinal cord of a zebrafish embryo. Both mRNAs are expressed in the spinal cord and co-localize to a large extent here as well. The expression patterns visualized here with two-colour FISH fit well with my hypothesis of a co-

localization of *srgap1* and *robo1* in zebrafish embryos and are consistent with the results in other vertebrates such as rat, mouse and human (Ip et al., 2011; Wong et al., 2001), suggesting an evolutionary conserved involvement of both partners. The expression pattern of *robo1* is thought to be closely linked to its function in neural development, including neuronal migration and axonal growth. Therefore, it is likely that *srgap1* is also involved in these processes.

Next, the possible co-localization of *srgap1* and *robo2* was examined. For this experiment, a *srgap1* probe labelled with digoxigenin and a *robo2* probe labelled with fluorescein were used. Figures 7.7 A-C show dorsal views of a section of a 48 hpf embryo brain, focusing on the mid- and hindbrain regions. The first two panels (A and B) show the expression patterns for *srgap1* and *robo2*, respectively. Expression of *srgap1* in the tectum and large areas of the hindbrain appears to be very low in this double *in situ* experiment. Stronger expression can be seen in one of the rhombomeres, namely rhombomere 3 of the hindbrain. *robo2* is expressed in the tectum and large parts of the hindbrain and shows specific expression confined to rhombomere 2. The rhombomeres were assigned based on comparisons with published studies (Maves et al., 2002; Moens and Prince., 2002; Prince et al., 1998). To ascertain the assignment, double *in-situ* experiments with rhombomere-specific markers are necessary. An overlay of both signals did not show overlapping expression of *srgap1* and *robo2* in the brain. In Fig 7.7 D-F lateral views of the spinal cord are displayed. *srgap1* shows again very weak expression in this experiment, whereas *robo2* shows a strong expression in the spinal cord. *srgap1* seems to be generally expressed in a lower level than *robo1-3*. Here, in contrast to the *srgap1/robo1* pair, no overlapping expression is observed.

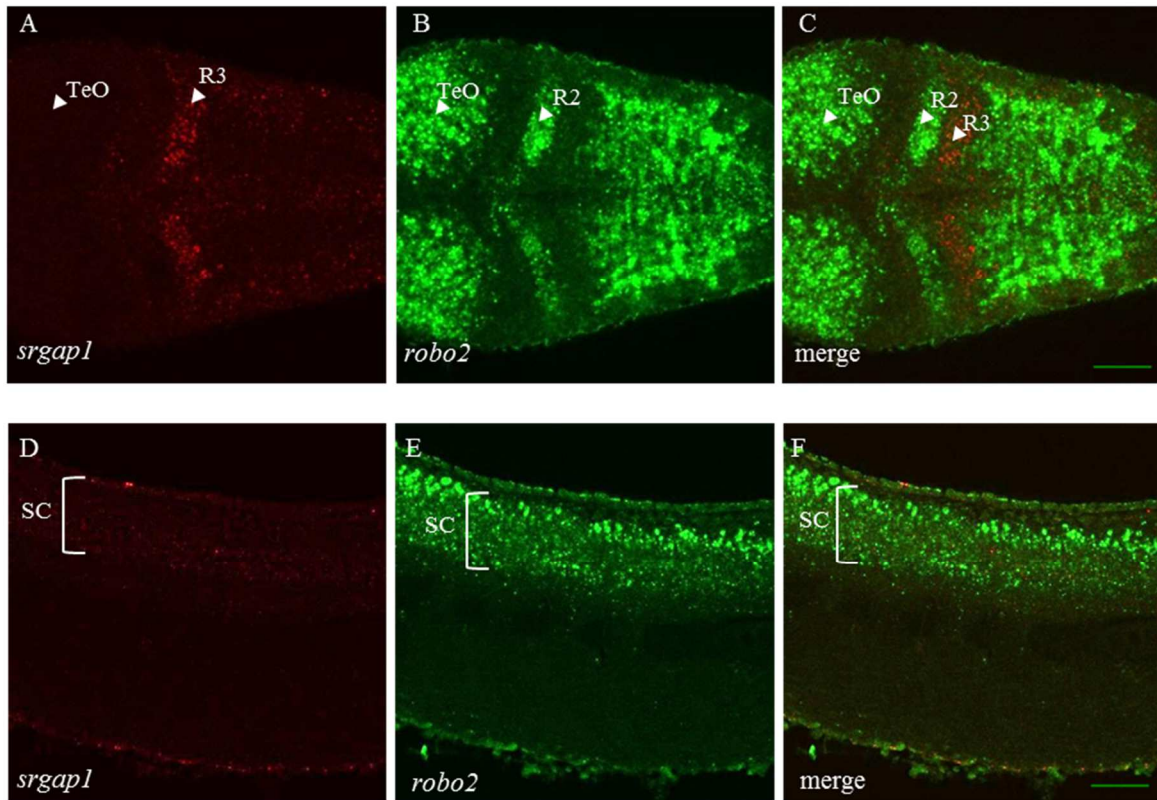


Fig. 7.7: Double *in-situ* hybridization experiments for *srgap1* and the *robo2* receptor gene in 48 hpf zebrafish embryos
 Gene expression patterns of *srgap1* and *robo2* in 48 hpf embryos. *srgap1* mRNA is labelled with digoxigenin (red). The *robo2* receptor mRNA is labelled with fluorescein (green). Expression of *srgap1* seems to be generally lower in two-colour-fluorescent experiments. (A-C) Dorsal views of the hindbrain of a zebrafish embryo, (D-F) Lateral views of the spinal cord. Single channels (A, B, D, E) and overlays of the signals of both channels (C and F) are shown. Abbreviations: R2, rhombomere 2 R3, rhombomere 3, SC, spinal cord; TeO, tectum. Images were recorded at a Zeiss LSM510 Meta fluorescence microscope, with 40x resolution. Scale bars: 5 μ m.

Double *in-situ* experiments rely on the hybridization with a mixture of differently labelled RNA probes. Here, fluorescein-labelled *srgap1* provided strong sensitivity as seen in Fig. 7.6, while digoxigenin-labeled *srgap1* was significantly less sensitive in all performed experiments, as seen in Fig. 7.7 A and D. Therefore, it would be recommendable to use digoxigenin for the strongest expressed transcript, here the *robo* genes, and fluorescein for the weaker *srgap1* probe in two-colour-fluorescent hybridization experiments.

Nevertheless, the results of the double *in-situ* hybridization of *srgap1* and *robo2* indicate that these genes have exclusive expression sites, which can be clearly observed in the differently confined rhombomere expression. This suggests *srgap1* and *robo2* are involved in different steps, at different places during neuronal development.

Since *robo1* and *robo3* show similar mRNA expression patterns, it would have been interesting to determine if both of them also co-localize, hinting a possible interaction of both. However, multiple attempts to carry out double *in-situ* hybridization with *robo3* were not successful, even when every component of the assay (see chapter 6.1.7.7) was exchanged.

The expression patterns of the single *in-situ* experiments for *robo3* suggest possible co-localization with *srgap1*.

Overall, I was able to show that *robo1* co-localizes with *srgap1* in the brain and spinal cord, indicating that the respective proteins have the potential to interact *in vivo*, which is consistent with the results of previous studies (Bacon et al., 2009; Ip et al., 2011; Wong et al., 2001). *robo2*, however does not appear to be a potential interaction partner of *srgap1*, confirming different roles of the *robo* genes during embryonic development (Lee et al., 2001). The analysis of the *srgap1* expression in developing zebrafish embryos confirmed its expression in neuronal tissues, as observed in other species, thus supporting its likely involvement in neuronal processes.






7.1.3 STRUCTURAL ANALYSIS OF THE SRGAP1 FBAR DOMAIN

Membrane sculpting and re-organization of the actin cytoskeleton are crucial steps during important cellular processes like endocytosis, cell migration and cell division. BAR domain containing proteins are central regulators of membrane remodelling. srGAP1 consists of a FBAR domain, a GAP domain, a SH3 domain and a C-terminal domain. As referred to in chapter 3.3 the srGAP family was described as being part of the recently emerged I-FBAR subfamily in the BAR domain superfamily, which are said to functionally mimic I-BARs (Guerrier et al., 2009). The structure of the I-BAR domain differs from the classical BAR and FBAR domains by its shape as it is more zeppelin-like and exhibits less curvature. The positively charged amino acids required for the binding to the negatively charged membrane are located at the convex surface of I-BARs and not on the concave side as for other BAR domains (Millard et al., 2005). This leads to an opposite effect when binding to membranes. The structural mechanism and the membrane binding activity of the I-FBAR domain subfamily has not been solved yet and it is not known how these domains promote membrane protrusions, instead of membrane invaginations *in vivo*. In order to understand this mechanism, I aimed to structurally characterize the FBAR domain of srGAP1.

7.1.3.1 The human srGAP1 FBAR domain

Initially, I started with FBAR fragments of the human srGAP1 protein, as there were already functional characterizations published for the human srGAP2 FBAR domain (Guerrier et al., 2009; Mason et al., 2011). Various constructs of the human srGAP1 FBAR domain were overexpressed in BL21 cells. Table 7.4 summarizes the results achieved with all cloned human FBAR constructs.

Tab. 7.4: List of cloned human srGAP1 FBAR domain constructs with their expression vector and obtained results. The red-labelled construct was used for further analysis

HUMAN SRGAP1 FBAR FRAGMENTS	VECTOR	RESULT
GST-srGAP1_FBAR_1-468 GST-  1 468	pGEX6P1	<ul style="list-style-type: none"> • weak expression
His_srGAP1_FBAR_1-468 6His-  1 468	pET47b	<ul style="list-style-type: none"> • insoluble • refolding with guanidinium chloride, protein not stable • refolding with 8 M urea, degradation • detergent screen: 2.5 % N-lauryl-sarcosyl partly solubilizes the protein
NusA_srGAP1-FBAR_21-468 NusA  21 468	pET-NusA	insoluble
NusA-srGAP1-FBAR_31-510 NusA-  31 510	pET-NusA	insoluble
His_srGAP1_FBAR_1-468_loop mutant 6His-  1 468	pET47b	insoluble

The FBAR fragment (1-468 aa) fused to an N-terminal GST-tag showed weak expression in BL21 cells and was partly soluble. The collected fractions revealed a major protein band with a molecular weight of 55 kDa in the flow-through, but not in the elution fraction. This indicated that the N-terminal GST-tag is probably not accessible and therefore the protein did not bind to the GSH column. I continued with the cloning of a FBAR fragment (1-468 aa) with a N-terminal His-tag yielding a protein fragment that was insoluble as well. Several un- and refolding trials with guanidinium chloride or urea were not successful, as the protein precipitated in lower concentrations of the solubilizing reagents and was not properly folded. This was confirmed by 1D NMR (Dr. Murray Coles, personal communication). In order to identify conditions useful for purification, solubilisation trials with a series of detergents were performed. Among the examined detergents only sarcosyl, an anionic detergent, was able to partly solubilize the protein. Therefore, the purification scheme for the srGAP1 FBAR domain was adapted and the protein purified with a HisTrap column in the presence of 2.5 % sarcosyl, followed by a gel filtration step with a S200 column in the presence of 0.5 %

sarcosyl in the final purification step. Figure 7.8 shows a protein band at approximately 55 kDa on SDS-PAGE as assessed by Coomassie Blue staining. Several bands below the actual protein band suggest degradation of the protein during the course of purification. Sarcosyl represents a non-dialyzable detergent. Therefore, its interference in crystallization screenings makes the use of higher concentrations of the anionic detergent in the final purification step in order to increase the yield of pure protein not applicable.

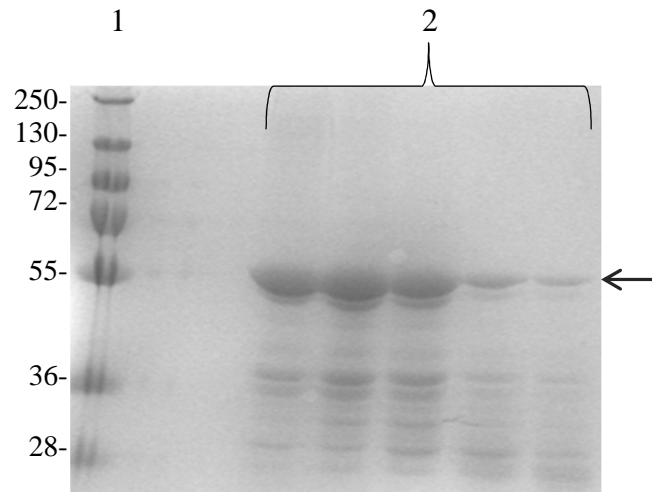


Fig. 7.8: 10 % SDS gel after gel filtration chromatography S75 of the human srGAP1 FBAR domain after detergent-mediated solubilisation of His₆-srGAP1-FBAR domain

The 10 % SDS gel shows the eluted protein after a gel filtration chromatography. Bands occurring lower than 55 kDa, show degradation of the protein. The SDS gel was stained with Coomassie Blue. (1) ProteinPage Plus Ruler, (2) elution fractions of the human srGAP1 FBAR domain (indicated with an arrow).

Despite degradation, the purified His₆-srGAP1 FBAR protein (Fig. 7.8) from independent purification attempts was subjected to multiple crystallization screenings, but even after extensive attempts no protein crystals could be obtained. In order to increase the stability of the protein construct further, the sequence of the human srGAP1 FBAR was re-assessed more closely. Proper determination of the N-terminal as well as the C-terminal boundaries is well known to play an important role in the solubility and expression properties of a protein (Graslund et al., 2008). Using the coils/pcoils tool from the Bioinformatic Toolkit of the MPI Tuebingen (<http://toolkit.tuebingen.mpg.de>) extended coiled coil parts were identified at the N-terminal part of the human srGAP1 FBAR domain (Fig. 7.9). Comparisons with known structures of BAR domains revealed the absence of these types of N-termini in most of the BAR domains starting from around amino acids number 20 (for example pdb: 2EFK, Shimada et al., 2007; 2EFL, Shimada et al., 2007; 3M3W, Bai et al., 2012).

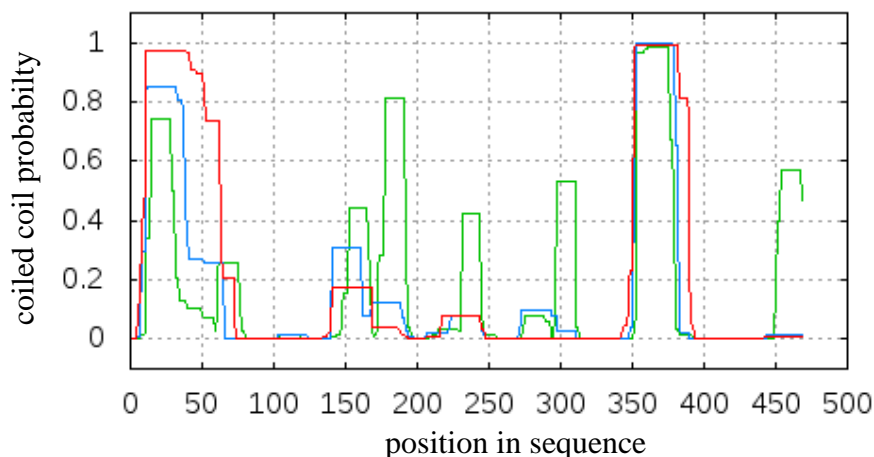


Fig. 7.9: Coiled coil sites in the human srGAP1 FBAR domain sequence

Prediction of coiled coil sites in the human srGAP1 FBAR domain sequence with coiled coil areas at the N-terminal region from 1-50 aa, three smaller areas between 150-300 aa and another site at the C-terminus from 350-400 aa can be observed. The colours correspond to different sliding windows with 14 (green), 21 (blue) and 24 (red) residues (<http://toolkit.tuebingen.mpg.de>).

Based on the results of this analysis, shorter constructs were designed and expressed. In addition, a FBAR fragment containing a mutation in the loop region from 190-220 aa, which is composed of a large fraction of hydrophobic residues, was cloned. However, no soluble protein was obtained from the cloned FBAR constructs again (see Tab. 7.4). Taken together, all types of constructs of the human srGAP1 FBAR domain did not yield soluble protein, which could be used for subsequent structural analysis of the domain.

7.1.3.2 The SRGAP1 FBAR domain of *Pristionchus pacificus*

As no structural data could be obtained from the human srGAP1 FBAR domain, the work was focused in the following on the FBAR domains of two other organisms: *Pristionchus pacificus* and *Danio rerio*. Table 7.5 shows a sequence comparison between the FBAR domains of all three organisms.

Tab. 7.5: Comparison of the sequence identities of the srGAP1 FBAR domain of *Homo sapiens*, *Pristionchus pacificus* and *Danio rerio*

NAME	SEQUENCE IDENTITY FOR THE FBAR DOMAIN
<i>Homo sapiens-Pristionchus pacificus</i>	33 %
<i>Homo sapiens-Danio rerio</i>	92 %
<i>Danio rerio-Pristionchus pacificus</i>	32 %

Human srGAP1 FBAR domain and the SRGAP1 FBAR domain of *Pristionchus pacificus* share a mere sequence identity of 33 %, whereas then human and zebrafish FBAR domains are 92 % identical. The level of sequence identity of *Pristionchus pacificus* and zebrafish corresponds with 32 % to the grade of sequence identity between the human and *Pristionchus* srGAP1 FBAR domain. So, by choosing these organisms, highly similar and distantly related srGAP1 FBAR domains were covered with the intention to get protein fragments that can be more easily handled during purification and functional characterization of the srGAP1 FBAR domain.

In a next step the SRGAP1 FBAR domain of *Pristionchus pacificus* was overexpressed and purified. The FBAR domain border was designed according to the results of the coils/pcoils analysis (Fig. 7.9). Hence, the FBAR domain was truncated at the N-terminus, resulting in a fragment from 20-460 aa with a molecular weight of 48 kDa. However, the FBAR fragment of *Pristionchus pacificus* was also not soluble. Solubilisation trials with a number of detergents were performed. The zwitterionic detergent CHAPS showed the best result and partly solubilized the protein. The purification was carried out with 1 % of the detergent. Unfortunately, the FBAR domain was degraded during the purification process. In order to yield properly folded protein and to reduce degradation, the protein was unfolded in 8 M urea. Subsequent refolding with lower concentrations of the solubilizing reagent, lead to degradation during the purification process as well.

7.1.3.3 The srGAP1 FBAR domain of zebrafish

In addition to the srGAP1 FBAR domain of *Homo sapiens* and *Pristionchus pacificus*, I overexpressed and purified the FBAR domain from zebrafish. Corresponding to the FBAR domain from *Pristionchus pacificus*, the first 25 aa at the N-terminal part of the domain were truncated, resulting in a fragment from amino acids 25-473 with a molecular weight of 53 kDa. This protein construct was not soluble either. Therefore, a detergent screening was carried out. Similar to the human construct, here as well only the anionic detergent sarcosyl was able to solubilize the protein. Hence, 1 % of sarcosyl was used in the early purification steps. The concentration of the detergent was reduced to a final concentration of 0.25 % during the subsequent gelfiltration step. In a second approach the protein was unfolded with 8 M urea and refolded by dialysis with stepwise reduction of the urea concentration. For both purified samples, the first in the presence of 1 % sarcosyl and the latter refolded, secondary structure determination was performed via CD spectroscopy. CD spectroscopy is defined as

the measurement of unequal absorption of left-handed and right-handed circularly polarized light. When light is polarized by passing through prisms or filters its electric field will oscillate sinusoidally in a single plane. When a molecule interacts with the light, it will absorb right and left handed circularly polarized light to different extents (Greenfield, 2006). Figure 7.10 shows the secondary structure analysis after both purification methods.

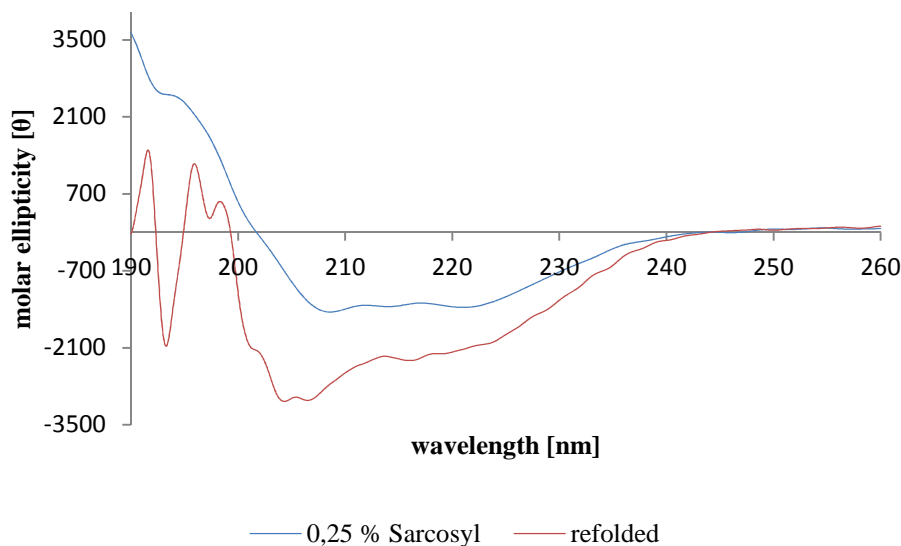


Fig. 7.10: Comparison of CD-spectra representing secondary structure of the FBAR domain from zebrafish purified by detergent or by Urea unfolding

The blue line shows the CD spectrum of the srGAP1 FBAR domain after purification with sarcosyl. The final concentration of sarcosyl is 0.25 %. The red line shows the CD spectrum after refolding. For the measurement the srGAP1 FBAR protein was diluted to 1 mg/ml in 20 mM Tris pH 8.0 and 50 mM NaF buffer. 10 spectra were recorded on a Jasco Spectrometer J-810 at room temperature. The resulting spectra were averaged.

The CD spectrum of the protein purified in the presence of sarcosyl resembles a folded α -helical protein with two minima at 208 and 222 nm (blue line), whereas the refolded F-BAR domain appears to be only partly folded, which becomes apparent by shifts of the two minima to 205 and 215 nm (red line). As mentioned in chapter 7.1.4.1 the protein sample containing sarcosyl did not yield any protein crystals for the human srGAP1 FBAR domain. Sarcosyl is also known to be a harsh detergent with possible interference in lipid-based *in vitro* assays, which are used to test the activity of the srGAP1 FBAR domain. As an alternative strategy and to obtain detergent-free protein, the protein was overexpressed in *E. coli* LEMO21 (DE3) cells. These cells are specifically designed for membrane proteins and proteins with solubility issues. The overexpression resulted in partly soluble protein, in the case that another, weaker detergent (1 % n-Dodecyl β -D-maltoside; β -DDM) was used after the cell lysis and during the purification process. β -DDM is a non-ionic, less harsh detergent, which does not interfere in crystallization setups and lipid-based *in vitro* assays. The concentration of β -DDM was reduced to 0.1 % in the final protein pool. The secondary structure analysis by CD

spectroscopy clearly shows α -helical secondary structure elements with two minima at 208 and 222 nm (Fig. 7.11). Additionally, 1D NMR measurements confirmed proper folding of the FBAR domain (Dr. Murray Coles, personal communication).

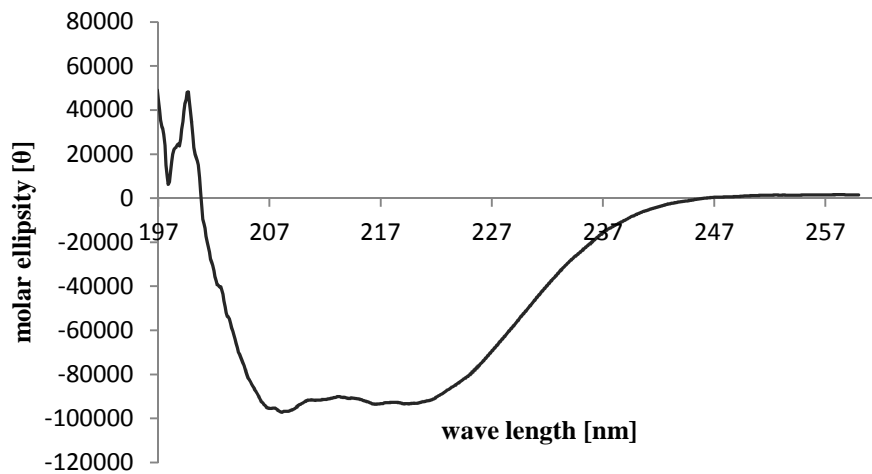


Fig. 7.11: Secondary structure analysis of the srGAP1 FBAR domain of zebrafish with CD-spectroscopy

For the secondary structure analysis of the srGAP1 FBAR domain of zebrafish 1 mg/ml of the srGAP1 FBAR protein was diluted in 20 mM Tris pH 8.0 and 50 mM NaF buffer. 10 spectra were recorded on a Jasco Spectrometer J-810 at room temperature. The resulting spectrum was averaged.

In order to analyse the oligomeric state of this purified FBAR domain in detail, a static light scattering experiment was carried out (Fig. 7.12). Light scattering is an optical technique that measures the intensity of the scattered light in dependence of the scattering angle to obtain information on the molecular weight of a polymer. The protein was loaded on a size exclusion column and eluted in one peak with a calculated molecular weight of 110 kDa, indicating the presence of dimers.

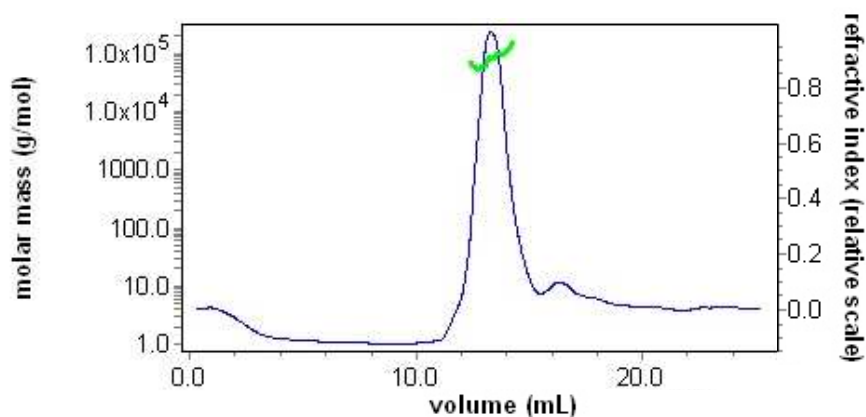


Fig. 7.12: Static light scattering profile of the srGAP1 FBAR domain of zebrafish

For determining the molecular mass the protein (1 mg/ml) was loaded on a Wyatt SEC column and run with 0.5 ml/min at 4 °C. The FBAR domain of srGAP1 eluted in one peak with a calculated size of 100 kDa (green line), which indicates the presence of dimers. The chromatogram displays two graphs: in blue the refractive index and in the green the molecular weight.

The result of the light-scattering experiment confirmed that FBAR domains have the tendency to dimerize. In the next step, the purified recombinant protein was setup for several crystallization screenings, but all attempts to obtain crystals for the srGAP1 FBAR domain of zebrafish, were not successful.

Taken together, the srGAP1 FBAR domain was proven to be a domain difficult to analyse structurally as proteins from different organisms and with different tags did not yield diffracting crystals. Screening more constructs with varying N- and C-termini might succeed in obtaining more stable protein fragments with an increased tendency to crystallize.

In the following functional characterization of the srGAP1 FBAR domain of zebrafish were carried out, to examine the activity and the effect of the FBAR domain.

7.1.4 FUNCTIONAL CHARACTERIZATION OF THE SRGAP1 FBAR DOMAIN OF ZEBRAFISH

Classical FBAR domains bind to the negatively charged membrane and lead to membrane invagination, whereas I-FBARs have a contrary effect by inducing membrane protrusion. When expressed in Cos7 or cortical neuron cells FBAR domains of the srGAP family led to filopodia formation (Coutinho-Budd et al., 2012; Guerrier et al., 2009), instead of invaginations, as it would occur for a classical FBAR domain like FBP17 (Kamioka et al., 2004). In a previous study it was also reported that the human FBAR domain of srGAP2 binds to brain-derived liposomes and leads to the formation of tubules when it is introduced into liposomes through sonication (Guerrier et al., 2009). To understand how FBAR domain proteins interact with the membrane and how they are regulated, the membrane binding properties of the FBAR domain of srGAP1 from zebrafish was examined using different *in-vitro* assays. For this purpose I used liposomes and giant unilamellar vesicles, both frequently employed as models for biological membranes in biochemical and biophysical studies (Hotani et al., 1999; Lasic et al., 1995). The effect of the FBAR domain was monitored by electron microscopy and later fluorescence microscopy. A co-sedimentation assay with negatively charged liposomes was also carried out, to determine the liposome binding activity of the srGAP1 FBAR domain.

7.1.4.1 The srGAP1 FBAR domain of zebrafish co-sediments with negatively charged liposomes

As mentioned above, liposomes are used as models of biological membranes, to examine *in vitro* effects of membrane-binding proteins. In order to analyse, if the purified FBAR domain

of srGAP1 can directly bind to liposomes a co-sedimentation assay was used. Co-sedimentation assays are based on the sedimentation of interacting proteins with liposomes during high-speed centrifugation. This was previously shown for cofilin-1, which is involved in cell motility and endocytosis (Zhao et al., 2010). For this assay a lipid mix, which physiologically mimics the composition of the negatively charged cell membrane, called Endomix was used.

The liposomes were made from cholesterol/sphingomyelin/PE/PS/PI/PC/PI(4,5)P₂ in a ratio of 1:0.28:0.28:0.28:0.14:0.02 (Corbin et al., 2007). First, 5 μM of purified srGAP1 FBAR domain were incubated with 1 mg/ml of liposomes for 2 h at 37 °C. Then, the protein-liposome mixture was centrifuged at high-speed (13000 rpm). The supernatants were removed and the pellets were resuspended in the original volume of 30 μl. As no sucrose layer was used, the liposomes should sediment to the pellet during the centrifugation step. Aliquots of the supernatant and pellet fraction were subjected to a 10 % SDS gel and stained with silver staining (Fig. 7.13).

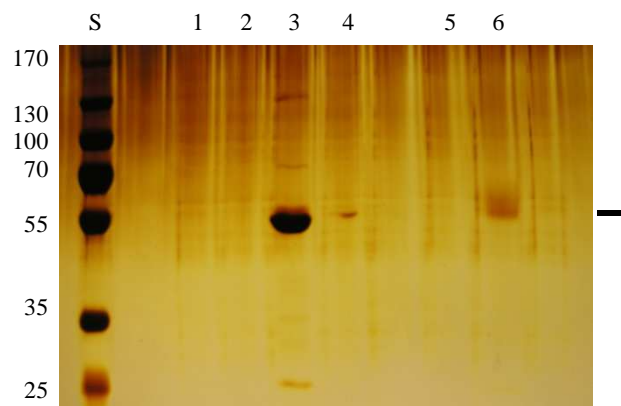


Fig. 7.13: Binding of the srGAP1 FBAR domain of zebrafish to negatively charged liposomes

The ability of the FBAR domain of srGAP1 to bind to liposomes was evaluated using co-sedimentation. The FBAR domain (5 μM) was incubated with 1 mg/ml of the liposome mix for 2 h at 37 °C. After centrifugation at 13000 rpm for 10 min, supernatants and pellets were analysed by 10 % SDS PAGE. The gel was stained with silver staining. (S) Standard, (1) 1 mg/ml liposomes alone, (2) 1 mg/ml liposomes with protein buffer (20 mM Tris, pH 8, 300 mM NaCl), (3) supernatant of the srGAP1 FBAR domain protein (5μM), (4) pellet of the srGAP1 FBAR domain protein (5μM), (5) supernatant of 1 mg/ml liposomes and 5 μM of the srGAP1 FBAR domain, (6) pellet with 1 mg/ml liposomes and 5 μM of the srGAP1 FBAR domain. Black label indicates molecular weight of the srGAP1 FBAR domain (54 kDa)

As controls, liposomes alone (Fig. 7.13, lane 1-2) and the FBAR domain in buffer (Fig. 7.13, lane 3-4) were subjected to the same steps as the sample. Both controls serve to identify, if the liposomes alone or the protein itself have the tendency to precipitate. The strong band in lane 3 indicates that the srGAP1 FBAR domain can be found in the supernatant. As shown in Fig. 7.13, lane 6 the FBAR domain of srGAP1 sedimented with the liposomes. A blurred band can be observed in the pellet fraction. This band is approximately at the molecular weight of the srGAP1 FBAR domain (54 kDa, indicated with black line). The blurred and

weaker band can be explained by the presence of the liposomes and the volume of the samples which were used on the SDS gel. The result of the co-sedimentation suggests that the FBAR domain of srGAP1 binds to negatively charged liposomes. With this first indication and to further support this result, the effect of the FBAR domain of srGAP1 on preformed liposomes was examined with negative stain electron microscopy.

7.1.4.2 The srGAP1 FBAR domain of zebrafish leads to indentations of charged liposomes

FBAR domains have been shown to bind to liposomes and lead to deformation or tubulation (Frost et al., 2008; Shimada et al., 2007). Multiple publications use negative stain electron microscopy to analyse the effect of FBAR domains on liposomes (Boucrot et al., 2012; Guerrier et al., 2009; Shimada et al., 2007). To directly examine the membrane deforming properties of the srGAP1 FBAR domain the purified srGAP1 FBAR domain of zebrafish was incubated with preformed liposomes. The samples were pipetted on carbon coated grids and stained with 1 % uranylacetate to visualize them by negative stain electron microscopy (Fig. 7.14).

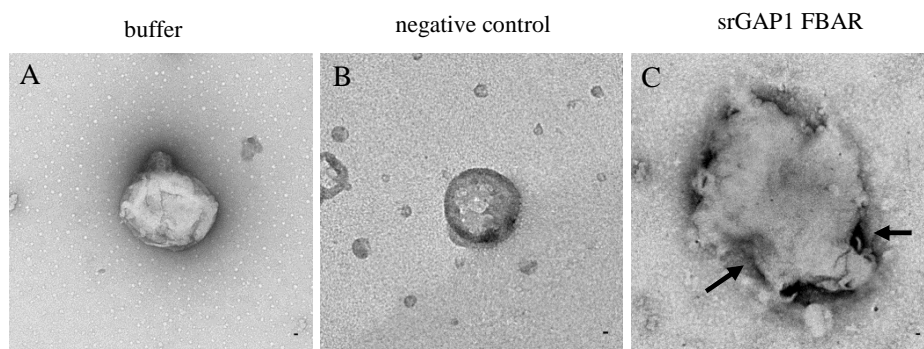


Fig. 7.14: Deformation of negatively charged liposomes by the srGAP1 FBAR domain

Negative stain electron microscopy of negatively charged liposomes incubated with (A) buffer, (B) liposomes incubated with DHPH domain of Intersectin as negative control and (C) liposomes incubated with the FBAR domain of srGAP1. All grids were stained with 1 % uranylacetate. Arrows indicate deformation. Scale bars: 2 μ m.

In Fig 7.14 A liposomes were incubated with buffer alone. When liposomes were incubated with the DHPH domain of the adaptor protein Intersectin, no deformation was observed. The DHPH domain is known to bind to membranes without inducing a deforming effect (Zamanian and Kelly, 2003). Figure 7.14 C displays liposomes incubated with the srGAP1 FBAR domain. Interestingly, no tubulation of the liposomes can be seen as reported for the FBAR domains of FBP17, CIP4 and Syndapin (Itoh et al., 2005; Shimada et al., 2010), but slight indentations of the preformed liposomes. This result supports an inverse FBAR activity of the srGAP1 FBAR domain, as suggested for IRSp53 and Missing in Metastasis (MIM)

(Mattila et al., 2007, Millard et al., 2007; Saarikangas et al., 2009). Unfortunately, this experimental setup turned out to be not the best approach to examine indentations, as control liposomes without the incubation with the srGAP1 FBAR domain were sometimes also deformed during the experimental procedure, thus not facilitating the quantification of deformed liposomes. Therefore, I continued studying the effect of the srGAP1 FBAR domain *in vitro*, by using giant unilamellar vesicles, which allow a better observance of vesicle deformation in contrast to the smaller-sized liposomes.

7.1.4.3 The srGAP1 FBAR domain of zebrafish causes invagination of giant unilamellar vesicles

Giant unilamellar vesicles are cell-sized vesicles, which consist of a phospholipid bilayer and are large enough to be observed with optical microscopes. In recent publications an assay with giant unilamellar vesicles was described, to directly show invagination activities of the BAR/FBAR domains of Pinkbar and Nervous wreck (Becalska et al., 2013; Pykäläinen et al., 2010). In order to visualize the effect of the srGAP1 FBAR domain, I established a GUV assay, with the help of Dr. Nathalie Eisenhardt (MPI for Developmental Biology, Tuebingen). To generate the GUVs, two different lipid-mixes labelled with 0.5 % dicarbocyanine were used, here DiD (DiI_{C18}), to examine if different lipid-mixes have an effect on the FBAR domain activity. The first lipid-mix consisted of lipids, which mimic the negatively charged composition of the cell membrane (as described in chapter 7.1.4.1). The second lipid-mix contained Folch I lipids, which are brain derived lipids with 5 % PIP₂ as an additional component. The generated GUVs were incubated with the following components in different reaction chambers overnight: buffer alone (10 mM HEPES pH 7.5, 140 mM KCl, 10 mM NaCl and 1 mM MgCl₂), DHPH domain of the adaptor protein Intersectin as a negative control, human Carom FBAR domain as a positive control (see chapter 7.2.2.1) and srGAP1 FBAR domain of zebrafish (Fig. 7.15).

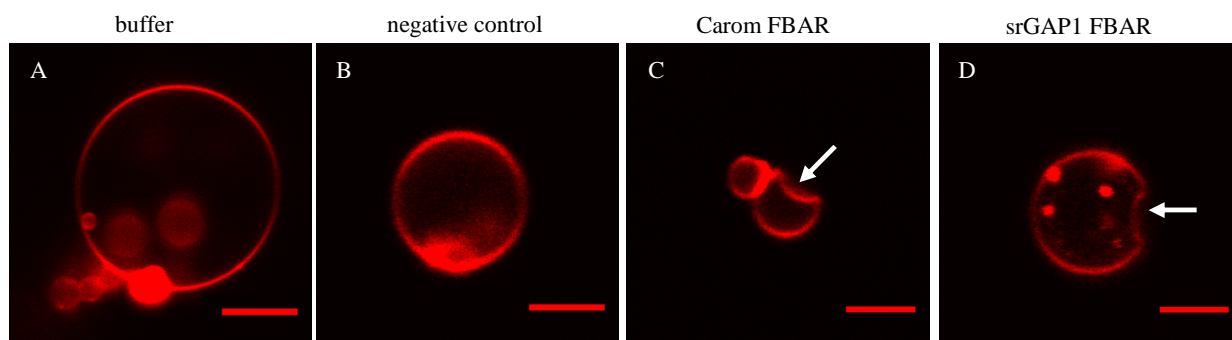


Fig 7.15: Invagination of giant unilamellar vesicles by the srGAP1 FBAR domain

Deformation of DiD-labelled GUVs (red) after an overnight incubation with (A) buffer (10 mM HEPES pH 7.5, 140 mM KCl, 10 mM NaCl and 1 mM MgCl₂), (B) DHPH domain of Intersectin, as negative control, (C) the human Carom FBAR domain and (D) the FBAR domain of srGAP1. Arrows point to deformation. Scale bars: 5 μm.

As shown in Fig. 7.15 A incubation of GUVs with buffer alone has no effect. In Fig. 7.15 B the DHPH domain of Intersectin, with no membrane deforming activity is added to the vesicles as a negative control and shows no visible effect either. Fig. 7.15 C displays GUVs incubated with the Carom FBAR domain, the human homolog of the *Drosophila* Nervous wreck protein (Becalska et al., 2013). The FBAR domain of Carom is used as a positive control in this experimental setup as it has a scalloping effect on vesicles (see chapter 7.2.2.1 for more detail). Here, invagination of the giant unilamellar vesicles were observed as expected. The FBAR domain of the srGAP1 protein also generates invaginations of the vesicles, though only 40 - 50 % of the vesicles were deformed (Fig. 7.15 D). Compared to the positive control, the invaginations induced by the srGAP1 FBAR domain are weaker, indicating the possibility of less induced curvature.

7.1.4.4 Time-dependent invagination of giant unilamellar vesicles by the srGAP1 FBAR domain

To determine the time-frame of the invagination process, images of the vesicles incubated with srGAP1 FBAR domain were taken after certain time points (0, 5 min, 40 min and 24 h). Figure 7.16 shows the respective images for the srGAP1 FBAR domain.

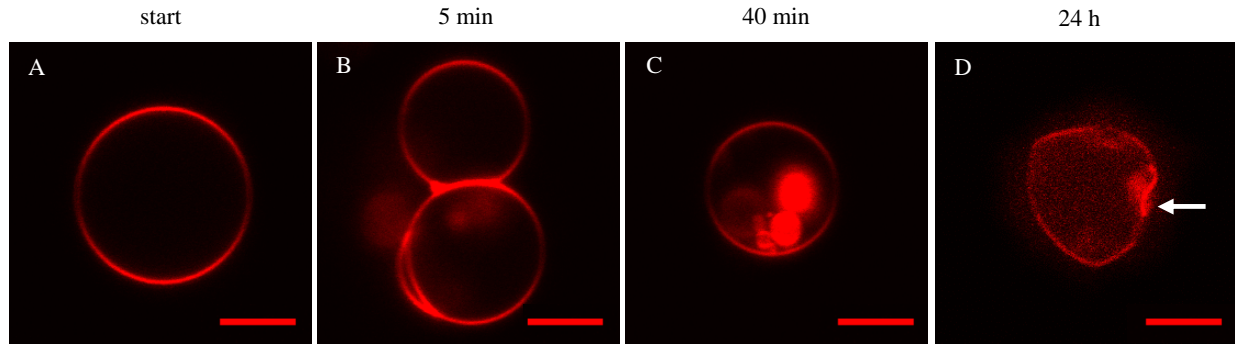


Fig 7.16: Time-dependent deformation of giant unilamellar vesicles by the FBAR domain of srGAP1

Deformation of DiD-labelled GUVs (red) over time, (A) GUV immediate after adding of the srGAP1 FBAR domain, (B) protein-GUV mix after 5 min of incubation, (C) GUV after 40 min of incubation and (D) after an overnight incubation at 4 °C with the FBAR domain of srGAP1. Arrow points to deformation. Scale bars: 5 μ m.

Taken together, the co-sedimentation assay, the negative stain EM assay and the GUV assay demonstrate, that unlike previously described FBAR domains of FBP17, CIP4 and Syndapin (Henne et al., 2007; Itoh and De Camilli, 2006; Peter et al., 2004; Shimada et al., 2007) the FBAR domain of the srGAP1 protein is not a classical FBAR domain, but rather belongs to the I-FBAR subfamily. Members of this subfamily cause invaginations, when incubated with liposomes and giant unilamellar vesicles, instead of forming tubules. Interestingly, the srGAP family is not the only family with a predicted functional I-FBAR domain: PSTPIP2 and Gas7 have also been shown to induce filopodia in *in vivo* experiments (Chitu et al., 2005; She et al., 2002). Therefore, more members of the I-FBAR family could emerge in the future.

In summary the results of the functional analysis of the FBAR domain suggest an inverse FBAR function. In order to prove this hypothesis structural information for the srGAP1 FBAR domain is essential, as it might give insight of how the structure and the function of the FBAR domains are related. At the same time, in an attempt to characterize the structural properties of I-FBARs, I concentrated on the FBAR domain of an analogous but distantly related protein, the human adaptor protein Carom (chapter 7.2).

7.1.5 COMPARISON OF THE BINDING SPECIFICITY OF THE HUMAN SRGAP1 GAP DOMAIN AND ITS ZEBRAFISH HOMOLOG TO THREE MEMBERS OF THE RHOGTPASES

Many FBAR-containing proteins are involved in the regulation of Rho-GTP binding proteins (Habermann et al., 2004; Ho et al., 2004; Kanoh et al., 1997; Peter et al., 2004; Van Aelst et al., 1996). In addition to its FBAR domain, its SH3 domain and its C-terminal domain, the srGAP1 protein contains a GAP domain. Small guanine nucleotide-binding proteins, like the members of the Rho family of GTPases, act as molecular switches in cellular signalling pathways controlling cell proliferation, differentiation and apoptosis. Conversion from the GDP-bound to the GTP-bound state is controlled either positively or negatively by GEFs or GAPs, respectively (Corbett, and Alber, 2001, Vetter and Wittinghofer, 2001). GAP domains increase the intrinsic hydrolysis rate of GTPases by inserting a catalytic residue into the active site of the GTPase (Ahmadian et al., 1997, Mittal et al., 1996, Rensland et al., 1991). In a previous study with HEK cells it was reported, that the human srGAP1 GAP domain specifically inactivates Cdc42 and RhoA.

In this present study, the human and zebrafish srGAP1 GAP domains were examined with different NMR methods to determine their activity towards three members of the Rho GTPase family, Cdc42, RhoA and Rac1. Attempts to measure this interaction with other methods, like, HPLC or fluorescence spectroscopy did not yield any results. First, the binding of the human srGAP1 GAP domain to the three members of the RhoGTPases was examined via ¹⁹F-NMR spectroscopy, to analyse if there is aluminium fluoride-activated complex formation between the srGAP1 GAP domain and the RhoGTPase as this would indicate an interaction between both components. With ³¹P-NMR the activity of the srGAP1 GAP domain was examined, by following the acceleration of the intrinsic hydrolysis rate of the RhoGTPases. This experiment was carried out for the human srGAP1 GAP domain and its zebrafish homolog. In the last step, the binding sites of the GAP domain on ¹⁵N and ¹³C labelled Cdc42 were mapped. All experiments were carried out in collaboration with Dr. Murray Coles (MPI for Developmental Biology, Tuebingen).

7.1.5.1 The human srGAP1 GAP domain binds to the human Cdc42, but not to human RhoA and Rac1

In a previous study srGAP1 and myc-tagged Cdc42, RhoA and Rac1 were co-transfected in HEK cells and interaction between srGAP1 and Cdc42 as well as RhoA was detected using

co-immunoprecipitation (Wong et al., 2001). Here, the interaction of the srGAP1 GAP domain with Cdc42, RhoA and Rac is analysed with a structural approach, using different NMR methods. Figure 7.17 displays the domain borders of the human srGAP1 GAP domain, the human Cdc42, RhoA and Rac1.

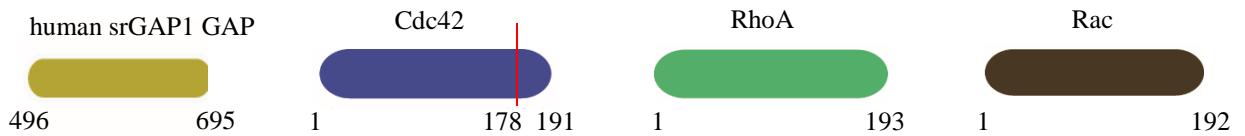


Fig. 7.17: Domain boundaries of the human srGAP1 protein and the human RhoGTPases

The human srGAP1 protein consists of a FBAR domain, a SH3 and a C-terminal domain with protein binding motifs. Its GAP domain (496-695 aa) is reported to bind to two members of the RhoGTPase family, Cdc42 and RhoA (Wong et al., 2001). For RhoA and Rac the full-length protein was used, for Cdc42 the last 13 amino acids, which were highly hydrophobic, were truncated due to solubility issues. The red line indicates the domain boundary for the used Cdc42 construct

The srGAP1 GAP domain (496-695 aa) was cloned into a pGEX_6P1 vector with a N-terminal GST-tag. The protein was purified with a GSH column, followed by the cleavage of the GST-tag with TEV-protease. The purification was finalized by a gel filtration step with a S75 column (Fig. 7.18).

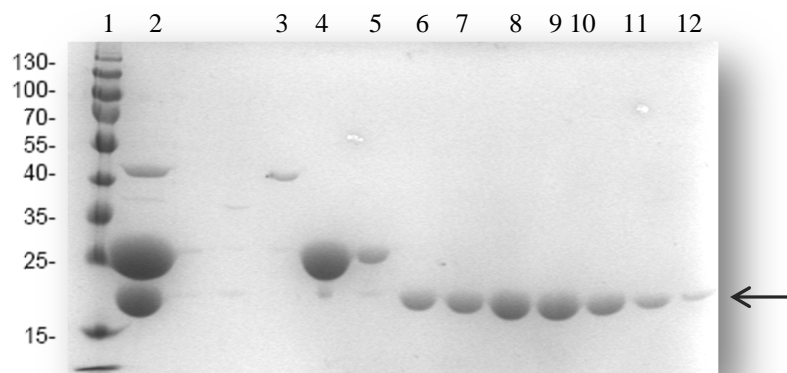


Fig. 7.18: 10 % SDS gel after gel filtration chromatography S75 of the human srGAP1 GAP domain

The 10 % SDS gel shows the eluted protein after a gel filtration chromatography. The SDS gel was stained with Coomassie Blue. 1) ProteinPage Plus Ruler, 2) fractions after cleavage with TEV-protease, 3) non-cleaved fusion protein, 4-5) GST protein, 6-12) elution fractions of the human srGAP1 GAP domain (22 kDa, indicated with an arrow).

The human RhoGTPases, Cdc42 (1-178 aa), RhoA (1-193 aa) and Rac (1-192 aa) were purified following the same protocol.

An important finding in the studies regarding GAP binding was the application of AlF_4^- . This compound mimics the transition state during the GTP hydrolysis process of heterotrimeric G-proteins (Chabre, 1990). AlF_4^- forms a complex with the GDP-bound α -subunit of heterotrimeric G-proteins by binding into the pocket that usually accommodates the γ -phosphate of the bound GTP (Coleman *et al.*, 1994; Sondek *et al.*, 1994). This method was successfully used in a previous study to analyse the interaction of AlF_4^- and α -transducin (Higashijima *et al.*, 1991; Hoffmann *et al.*, 1998). Figure 7.19 presents the possible binding mechanism of AlF_4^- in the RhoGTPase-GAP complex.

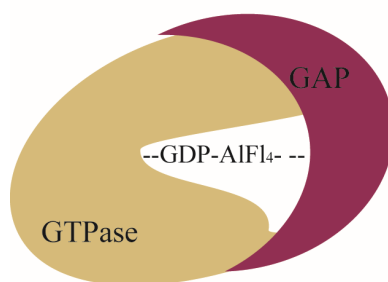


Fig. 7.19: Model of the potential AlF_4^- -induced binding mechanism

AlF_4^- -induced transition state of a GDP-bound GTPase (brown) and a GAP domain (purple). Thereby, the AlF_4^- binds into the pocket, which is usually occupied by the γ -phosphate of the bound GTP (modified, Hoffman *et al.*, 1998).

Here, ^{19}F -NMR spectroscopy was applied to probe the fluoride binding directly and determine if the human srGAP1 GAP domain can form complexes with one of the three RhoGTPases. Figure 7.20 shows the obtained experimental data for the human GAP domain with human Cdc42, RhoA and Rac1.

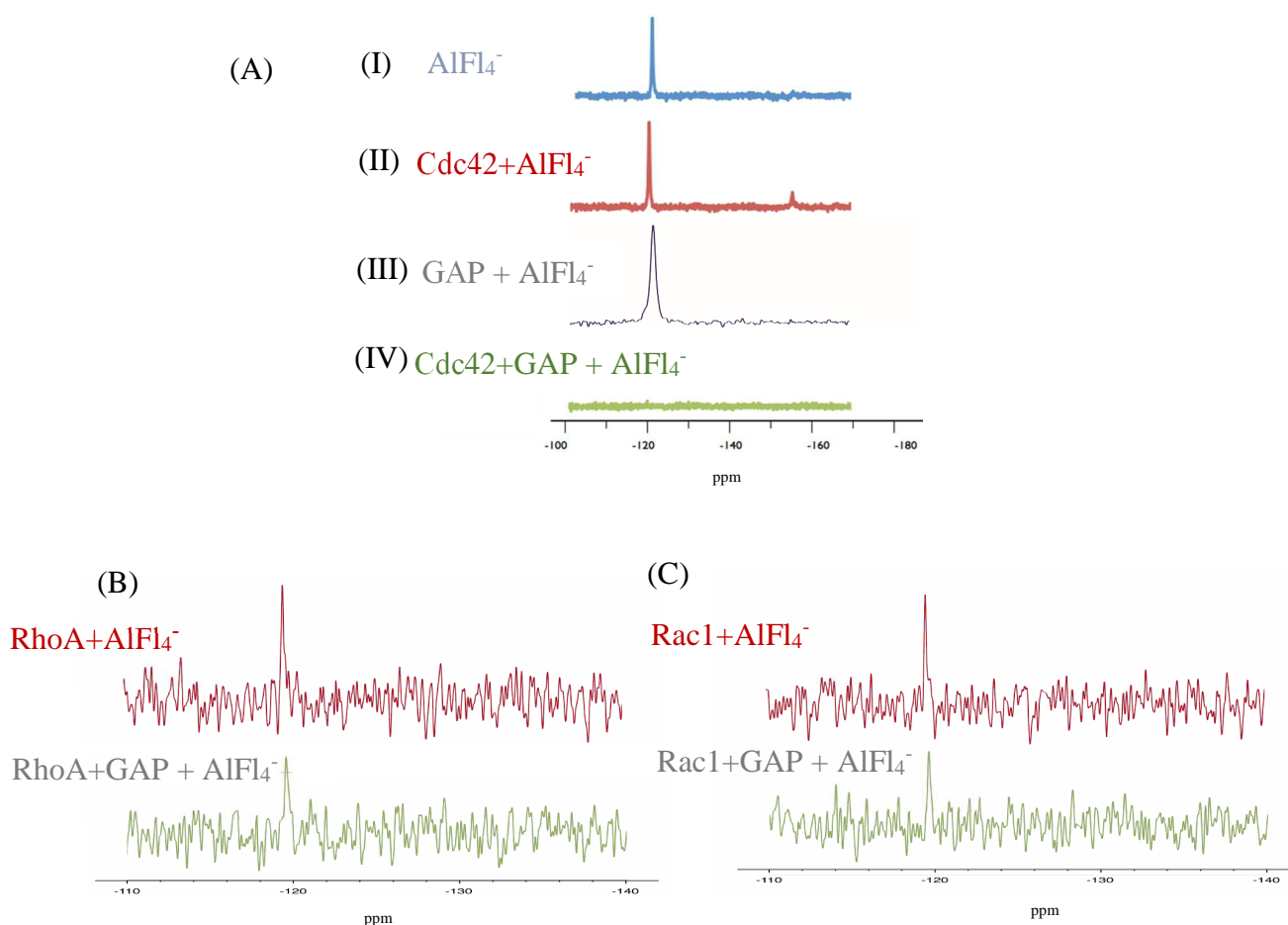


Fig. 7.20: Analysis of AlF_4^- -induced complex formation between the RhoGTPases and the srGAP1 GAP domain

^{19}F -NMR spectra (282 MHz) of protein samples in AlF_4^- -containing NMR buffer. Spectra were measured at a Bruker 600 at room temperature. Chemical shifts were measured relative to free fluoride (-120 ppm). (A) Spectrum of AlF_4^- alone (I), spectrum of GDP-bound Cdc42 with AlF_4^- (II), spectrum of srGAP1 GAP domain with AlF_4^- (III), spectrum of GDP-bound Cdc42 (0.15 mM) with AlF_4^- and equimolar concentration of human srGAP1 GAP domain (0.15 mM; IV). (B) Spectrum of GDP-bound RhoA and AlF_4^- alone (red) and spectra of GDP-bound RhoA with the srGAP1 GAP domain and AlF_4^- (green). (C) Spectrum of GDP-bound Rac1 with AlF_4^- alone (red) and Rac1 with the srGAP1 GAP domain and AlF_4^- .

The ^{19}F -spectra of AlF_4^- shows a sharp peak at -120 ppm (Fig. 7.20 A I). The spectrum of GDP-bound Cdc42 and AlF_4^- shows no change in the signal at -120 ppm, suggesting that free GDP-bound Cdc42 did not bind to AlF_4^- (Fig. 7.20 A II). The small peak at -160 ppm is an artefact of the measurement and can be disregarded. The spectrum of the srGAP1 GAP domain with AlF_4^- also shows a peak at -120 ppm, indicating that the domain alone also does not interact with AlF_4^- (Fig. 7.20 A III). In Fig. 7.20 A IV the ^{19}F -NMR spectrum obtained when both GDP-bound Cdc42 and equimolar srGAP1 GAP domain are added together in the presence of AlF_4^- , is shown. The disappearance of the signal at -120 ppm suggest stable complex formation between the GDP-bound form of the human Cdc42 and the human srGAP1 GAP domain. In contrast to the Cdc42 measurements, RhoA and Rac1 show weak signals and no binding to the srGAP1 GAP domain as the signal of AlF_4^- does not disappear

when the GAP domain of srGAP1 is added (Fig. 7.20 B and C). However, both proteins, RhoA and Rac1, show proper folding in $^1\text{H-NMR}$ measurements, in which the hydrogen-1 nuclei of a molecule are analysed. In a previous study, the AlF_4^- signal does not disappear, but shifts instead. This could be due to the bigger size difference between the GAP domain and the GTPase or due to different measurement set up (Hoffmann et al., 1998). The first structural analysis confirmed the binding of the srGAP1 GAP domain to Cdc42, but not to RhoA, although both interactions were shown with HEK cell assays (Wong et al., 2001).

7.1.5.2 The human srGAP1 GAP domain is active and increases the intrinsic hydrolysis rate of the human Cdc42

As described in chapter 7.1.5.1, the human srGAP1 GAP domain specifically binds to the human GDP-bound Cdc42 in the presence of AlF_4^- . To confirm this interaction and to examine the activity of the human GAP domain, $^{31}\text{P-NMR}$ spectroscopy was carried out. With $^{31}\text{P-NMR}$ spectroscopy it is possible to probe the conformational states of nucleotide-binding proteins, dependent on the type of nucleotide present in their active centre (Spoerner et al., 2005). Here, the state of GTP was followed overtime (Fig. 7.21).

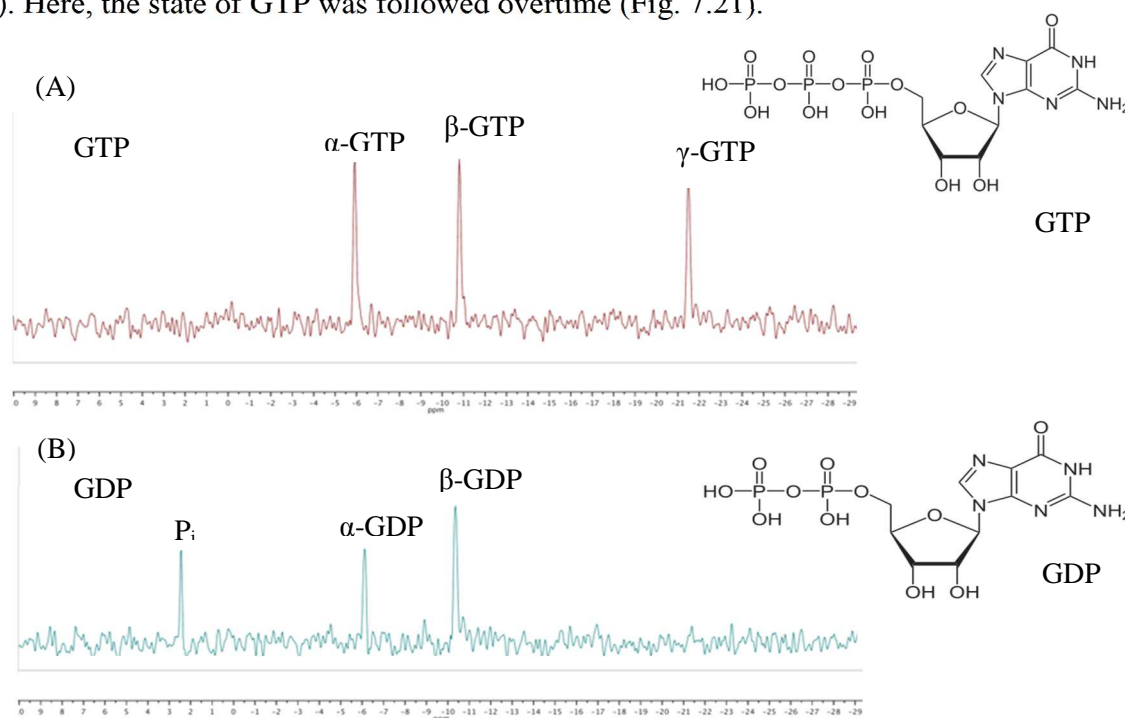


Fig. 7.21: $^{31}\text{P-NMR}$ spectra of GTP and GDP

The $^{31}\text{P-NMR}$ spectra (243MHz) were measured at a Bruker 600 at room temperature. For the measurements 1 mM of GTP and 1 mM GDP and inorganic phosphate were used. (A) The spectrum of GTP shows three peaks, which were assigned to γ -phosphate at -22 ppm, β -phosphate at -11 ppm and α -phosphate at -6 ppm. (B) The spectrum of GDP and inorganic phosphate has three peaks as well, which were assigned to β -phosphate at -10 ppm, α -phosphate at -6 ppm and inorganic phosphate at -3 ppm.

For GTP three distinct peak positions were assigned as γ -phosphate (-22 ppm), β -phosphate (-11 ppm) and α -phosphate (-6 ppm) (Fig. 7.21). The ^{31}P spectrum of GDP and inorganic phosphate contains a new peak at 3 ppm, which was assigned as inorganic phosphate, while the resonance of γ -phosphate disappeared completely (Fig. 7.21 B). The signal of γ -phosphate is well resolved, therefore GTP hydrolysis can be unambiguously measured by analysing the decline of the γ -phosphate over time and steady increase of free inorganic phosphate and β -GDP phosphate peaks (Fig. 7.21 B).

For the measurements, nucleotide-free Cdc42 was used, which was obtained with two different methods. In the first approach nucleotide-free GTPase was prepared in two steps according to John et al., 1990. First, bound GDP was degraded by alkaline phosphatase and replaced by GppNHp, a non-hydrolysable GTP analogue, resistant to alkaline phosphatase, but sensitive to phosphodiesterase (Fig. 7.22). The completion of the degradation process was determined by a High Performance Liquid Chromatography (HPLC). After the complete degradation of GDP, snake venom phosphodiesterase was added to the solution to cleave GppNHp to GMP, G and P_i . The snake venom phosphodiesterase was then removed from the nucleotide-free protein by analytical gel filtration. The second approach for removal of bound GDP is based on serial dilution (Zhang et al., 2000). The protein sample was examined for the content of the remaining nucleotide with ^{31}P NMR spectroscopy before the experiment.

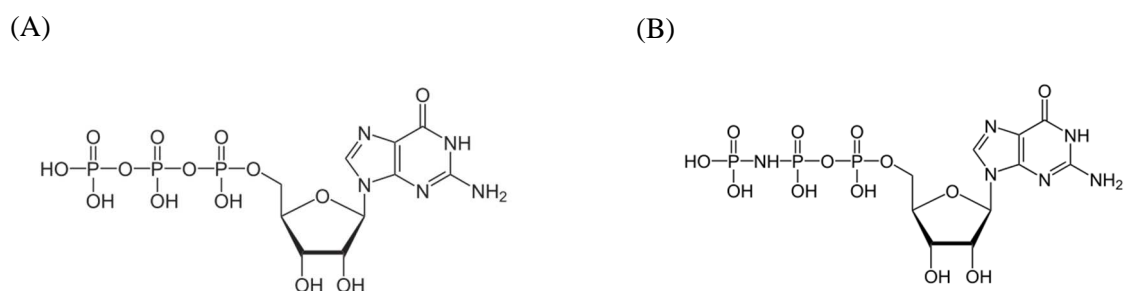


Fig. 7.22: GTP and its non-hydrolysable analogue GppNHp

(A) Chemical formula of GTP, (B) Chemical formula of GppNHp, the non-hydrolysable analogue of GTP, in which the oxygen atom bridging the β - to the γ -phosphate is replaced by a nitrogen atom.

To assess the activity of the srGAP1 GAP domain, the intrinsic hydrolysis activity of Cdc42 was measured first. Therefore, nucleotide-free Cdc42 and an excess of GTP were monitored over time till GTP was completely hydrolysed to GDP and inorganic phosphate. Then, an equimolar concentration of the srGAP1 GAP domain and additional GTP were added. Here again, the hydrolysis reaction was measured over time. Figure 7.23 presents a work chart for the measurement.

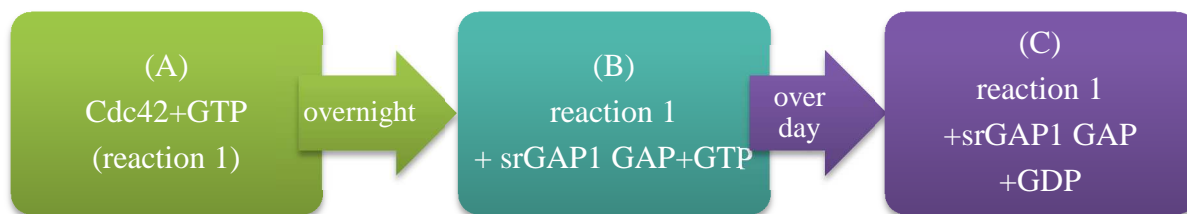


Fig. 7.23: Work chart for the ^{31}P -NMR measurement

(A) Intrinsic hydrolysis rate of Cdc42 was measured over time. Complete hydrolysis of added GTP after overnight incubation. (B) Addition of srGAP1 GAP domain and additional GTP to the overnight reaction and hydrolysis of GTP was monitored again over day. (C) After approximately 1 h complete hydrolysis of GTP to GDP and inorganic phosphate can be observed after the addition of GAP.

In Fig. 7.24 the intrinsic hydrolysis rate of Cdc42 is shown over a time period of 12 h. Four signals can be observed, which correspond to γ -phosphate, β -phosphate, α -phosphate and inorganic phosphate.

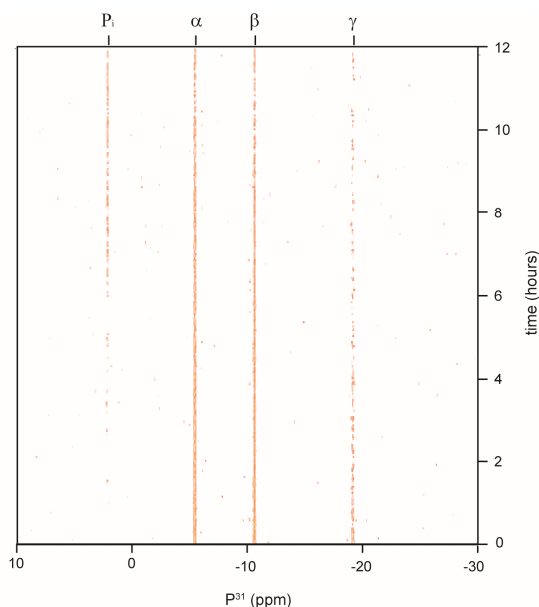


Fig. 7.24: Intrinsic hydrolysis activity of Cdc42

^{31}P NMR spectra (243 MHz) of 0.15 mM Cdc42 in 20 mM Tris pH 7.5, 150 mM NaCl and 1 mM MgCl_2 buffer and 1 mM GTP were measured at a Bruker 600 spectrometer at room temperature. The signal of γ -phosphate, β -phosphate and α -phosphate are followed over time (orange).

At time point 0, no signal for inorganic phosphate can be observed. After 6 h the signal for inorganic phosphate is increasing, whereas the signal for γ -phosphate is decreasing gradually. After 12 h there is still a signal for γ -phosphate visible, implying a slow intrinsic hydrolysis rate for Cdc42. Therefore, Cdc42 and GTP were incubated overnight, which resulted in the complete hydrolysis of GTP to GDP and inorganic phosphate (Fig. 7.25 A). The labelling in Fig. 7.25 correspond to the labels used in the work chart (Fig. 7.23). Addition of the human srGAP1 GAP domain accelerated the GTP hydrolysis reaction. Within one hour newly added GTP was converted into GDP and inorganic phosphate, indicated by the decline of the γ -

phosphate and the increase of the inorganic phosphate and the β -GDP phosphate (Fig. 7.25 C).

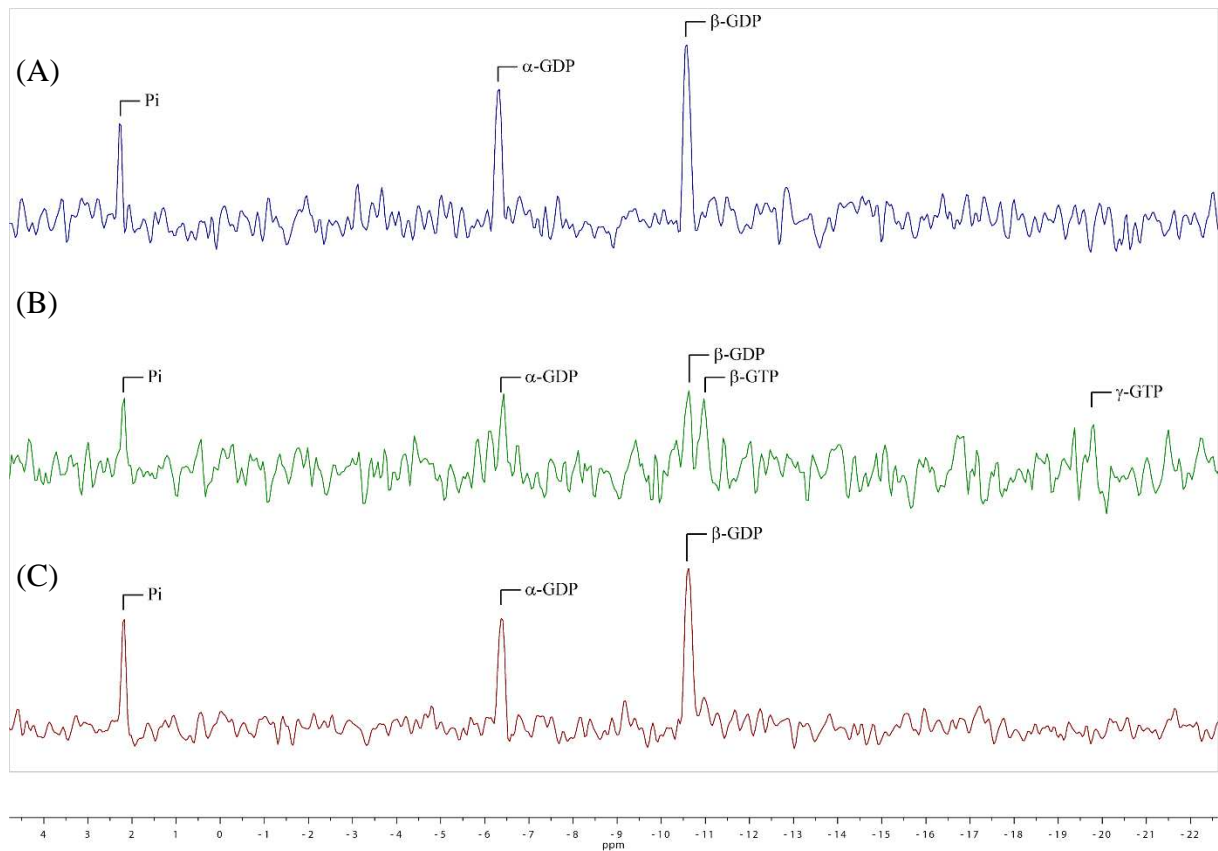


Fig. 7.25: ^{31}P -NMR spectroscopy showing accelerated GTP hydrolysis by Cdc42 affected by the GAP domain of srGAP1

^{31}P -NMR spectra (243 MHz) of samples in 20 mM Tris pH 7.5, 150 mM NaCl and 1 mM MgCl_2 buffer were measured at a Bruker 600 spectrometer at room temperature. (A) Spectrum of 0.15 mM nucleotide-free human Cdc42 with 1 mM GTP. Slow intrinsic GTP hydrolysis activity of the human Cdc42 (blue). Complete conversion of GTP to GDP and inorganic phosphate after overnight incubation. (B) Addition of 0.15 mM srGAP1 GAP domain and additional 1 mM of GTP (green) to the human Cdc42. (C) Total conversion of GTP to GDP and inorganic phosphate after approximately 1 h after adding the srGAP1 GAP domain.

For the calculation of the hydrolysis time the number of scans is multiplied by the time for 1 slice, which corresponds to a single 1D experiment. In Fig. 7.26, a scheme of the calculation is presented.

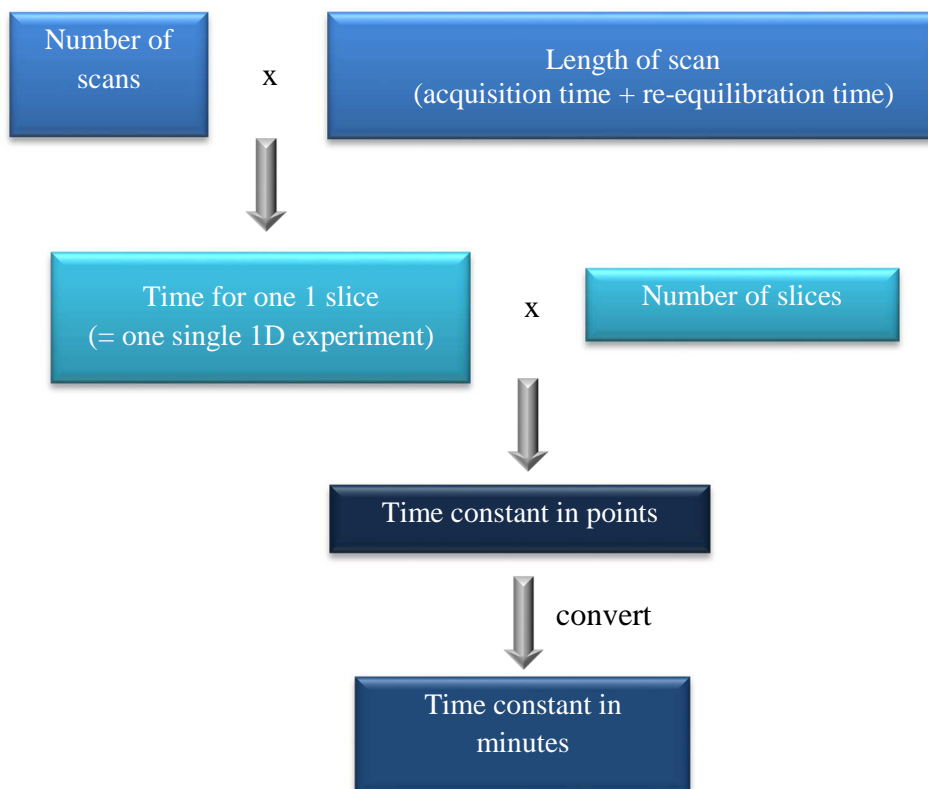


Fig. 7.26: Calculation scheme for calculating the accelerated hydrolysis time for Cdc42

The number of scans are multiplied by the time which corresponds to the length of the scan. The resulting time is for one slice, which is one single 1D experiment. This is then multiplied by the number of scans for each slice. This results into the time constant in points, which then can be converted into the time constant in minutes.

With this calculation scheme the time for the accelerated intrinsic hydrolysis reaction was calculated to be 16 min, whereas the value calculated for the intrinsic hydrolysis activity of Cdc42 is more than 12 h.

7.1.5.3 The zebrafish srGAP1 GAP domain increases the intrinsic hydrolysis rate of the zebrafish Cdc42

The srGAP1 protein can be found in various organisms. The srGAP1 protein from zebrafish has with 80 %, a high sequence identity to the human srGAP1 protein. To test if the interaction between the srGAP1 GAP domain and Cdc42 is conserved, analogous ^{31}P -NMR measurements, were carried out with the zebrafish srGAP1 GAP domain and zebrafish Cdc42 as described in the previous section. Figure 7.27 shows the domain boundaries for both proteins.



Fig. 7.27: Domain boundaries for the zebrafish srGAP1GAP domain and the zebrafish Cdc42

The domain boundary for the zebrafish srGAP1 GAP domain was designed according to the boundary set for the human srGAP1 GAP domain (see Fig. 6.17). For the zebrafish Cdc42 the full-length protein was used.

The zebrafish srGAP1 GAP domain (492-676 aa) was cloned into a pGEX6P1 vector with a N-terminal GST-tag. The protein was purified with a GSH column, followed by the cleavage of the GST-tag with TEV-protease and a second GSH column. The purification was finalized by a gelfiltration step with a S75 column (Fig. 7.28).

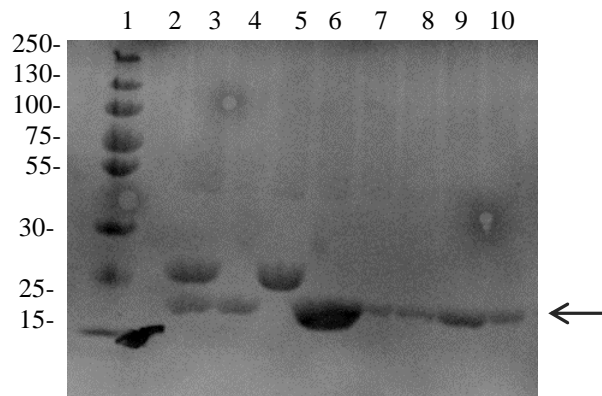


Fig. 7.28: 10 % SDS gel after the second GSH column and gelfiltration chromatography S75 of the zebrafish srGAP1 GAP domain

The 10 % SDS gel shows the eluted protein after a gelfiltration chromatography. The SDS gel was stained with Coomassie Blue. 1) ProteinPage Plus Ruler, 3) fractions after cleavage with TEV-protease, 4) srGAP1 GAP domain in the flow-through of the second GSH column, 5) GST protein, 6-10) elution fractions of the zebrafish srGAP1 GAP domain (21 kDa, indicated with an arrow).

The zebrafish Cdc42 was purified following the same protocol. Both proteins were analysed regarding their folding state with 1D NMR and proper folding was confirmed (Dr. Murray Coles, personal communication). For the ^{31}P -NMR measurement, the intrinsic hydrolysis activity of the nucleotide-free Cdc42 with an excess of GTP was measured first (Fig. 7.29).

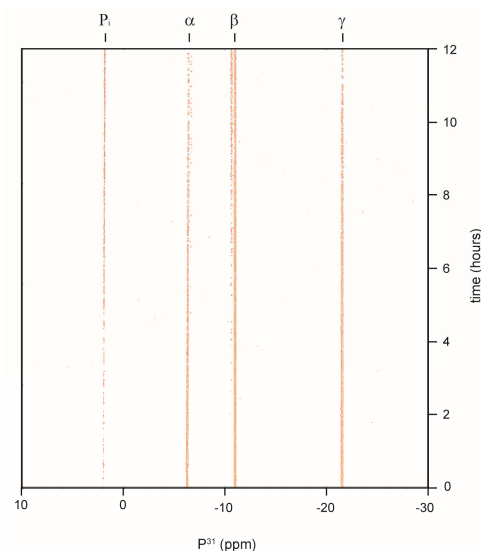


Fig. 7.29: Intrinsic hydrolysis activity of Cdc42

³¹P NMR spectra (243 MHz) of 0.15 mM Cdc42 in 20 mM Tris pH 7.5, 150 mM NaCl and 1 mM MgCl₂ buffer and 1 mM GTP were measured at a Bruker 600 spectrometer at room temperature. The signal of γ-phosphate, β-phosphate and α-phosphate are followed over time (orange).

Four signals can be observed in the graph, which correspond to γ-phosphate, β-phosphate, α-phosphate and inorganic phosphate. Here, the signal for inorganic phosphate appears to be present from a very early time point. This can be attributed to a not complete nucleotide-free Cdc42. Therefore, the decline of the γ-phosphate and the increase of β-GDP phosphate was monitored. In comparison to the intrinsic hydrolysis rate of the human Cdc42, the intrinsic hydrolysis rate of the zebrafish Cdc42 seems to be very slow, as the signal for γ-phosphate is still clearly visible after 12 h (Fig. 7.29). A complete conversion of GTP into GDP and P_i cannot be observed even after an overnight measurement (Fig. 7.30 A). The zebrafish GAP domain and additional GTP were added to the overnight reaction and the hydrolysis process was monitored over time (Fig. 7.30 B). No peak for free inorganic phosphate can be detected at 3 ppm, which could be explained by weaker signals and the high signal/noise ratio in contrast to Fig. 7.25.

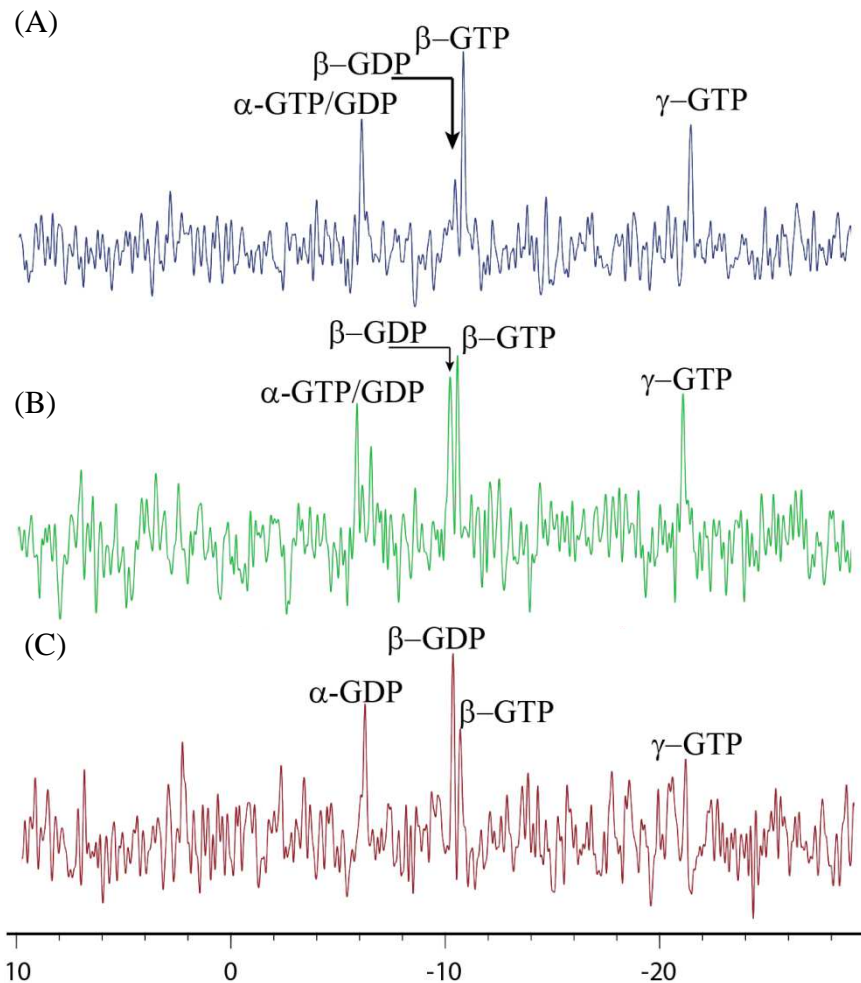


Fig. 7.30: ^{31}P -NMR spectroscopy showing accelerated GTP hydrolysis by the zebrafish Cdc42 affected by the GAP domain of the zebrafish srGAP1

^{31}P -NMR spectra (243 MHz) of samples in 20 mM Tris pH 7.5, 150 mM NaCl and 1 mM MgCl_2 buffer were measured at a Bruker 600 spectrometer at room temperature. (A) Spectrum of 0.10 mM nucleotide-free zebrafish Cdc42 with 1 mM GTP. (B) Addition of 0.15 mM srGAP1 GAP domain and additional 1 mM of GTP, (C) Conversion of GTP to GDP and inorganic phosphate 1 h after adding the zebrafish srGAP1 GAP domain.

The basal GTP turnover for the zebrafish Cdc42 is lower than the human Cdc42, as the γ -phosphate signal can be still detected after overnight incubation of the reaction. Within one hour, newly added GTP was hydrolysed to GDP and inorganic phosphate in the presence of equimolar concentration of the srGAP1 GAP protein (Fig. 7.30 C). This can be seen in the decline of the γ -phosphate (-21 ppm) and the increase of β -GDP (-10 ppm), indicating the srGAP1 GAP domain activity. Taken together, the results of the hydrolysis experiments indicate that both, the human and the zebrafish srGAP1 GAP domains are active and bind to Cdc42, increasing its intrinsic GTP hydrolysis rate.

7.1.5.4 No effect observed on the intrinsic hydrolysis activity of Cdc42 domains in cross-organism ³¹P-NMR measurements

As both human srGAP1 GAP domain and human Cdc42 as well as zebrafish srGAP1 GAP domain and zebrafish Cdc42 show interaction, which can be observed through the accelerated intrinsic hydrolysis activity of Cdc42, I examined if cross-organism measurements have an effect on the respective Cdc42 activity. The measurements were carried out analogous to the measurements described in 7.1.5.2 and 7.1.5.3.

First the activity of the human Cdc42 with the zebrafish srGAP1 GAP domain was measured (Fig. 7.31).

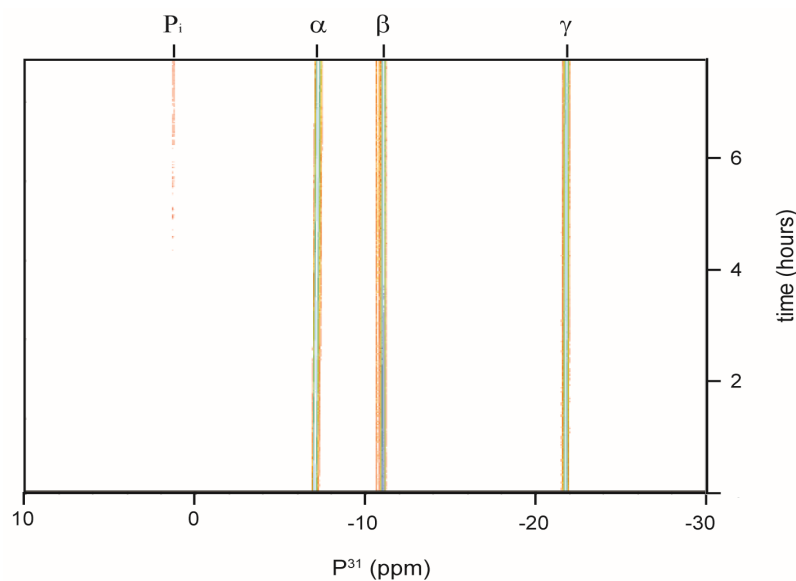


Fig. 7.31: ³¹P-NMR spectroscopy showing GTP hydrolysis by the human Cdc42 affected by the GAP domain of the zebrafish srGAP1

³¹P-NMR spectra (243 MHz) of samples in 20 mM Tris pH 7.5, 150 mM NaCl and 1 mM MgCl₂ buffer were measured at a Bruker 600 spectrometer at room temperature. 0.10 mM nucleotide-free human Cdc42 was measured with 1 mM GTP and 0.15 mM zebrafish srGAP1 GAP domain.

Signals for α-, β-, γ-phosphate and inorganic phosphate are observed. Compared to the results presented in Fig. 7.25 and 7.30 the signal for inorganic phosphate did not decrease even after 8 h of incubation. The signal for inorganic phosphate starts to appear after almost 5 h. This would indicate that the zebrafish srGAP1 GAP domain has no effect on the intrinsic hydrolysis rate of the human Cdc42.

In the next step zebrafish Cdc42 was measured with human srGAP1 GAP domain (Fig. 7.32).

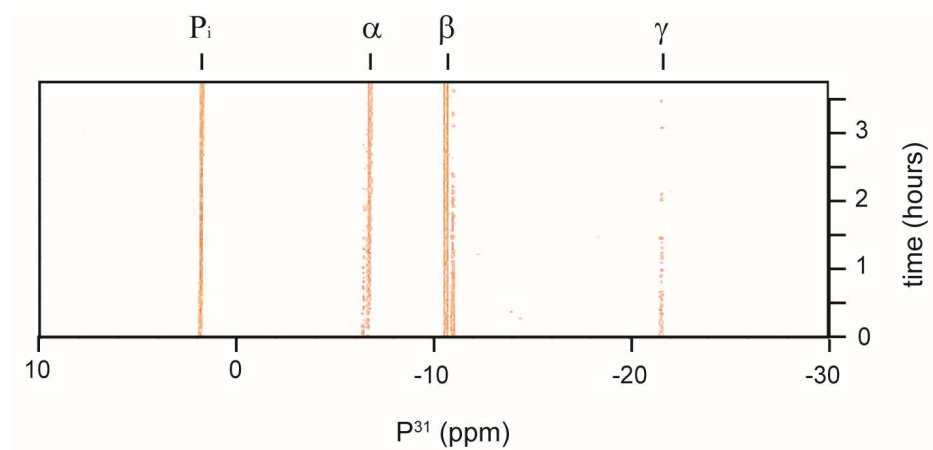


Fig. 7.32: ^{31}P -NMR spectroscopy showing GTP hydrolysis by the zebrafish Cdc42 affected by the GAP domain of the human srGAP1

^{31}P -NMR spectra (243 MHz) of samples in 20 mM Tris pH 7.5, 150 mM NaCl and 1 mM MgCl_2 buffer were measured at a Bruker 600 spectrometer at room temperature. 0.10 mM nucleotide-free zebrafish Cdc42 was measured with 1 mM GTP and 0.10 mM zebrafish srGAP1 GAP domain.

Here as well signals for α -, β -, γ -phosphate and inorganic phosphate can be observed. Signal for inorganic phosphate can be observed at early time points. One explanation for this could be a not complete nucleotide-free GTPase. The γ -phosphate decreases over time and the signal for inorganic phosphate increases steadily. After almost 4 h a complete turnover of the γ -phosphate can be observed indicating a low effect of the human srGAP1 GAP domain on the zebrafish Cdc42 compared to the measurement in Fig. 7.31. Species cross-over measurements showed either no effect on the acceleration of the intrinsic hydrolysis reaction of the RhoGTPase, in the case of human Cdc42 and zebrafish srGAP1 GAP domain (Fig. 7.32), or a very low effect on the hydrolysis rate, in the case of human Cdc42 and zebrafish srGAP1 GAP domain (Fig. 7.31). These results lead to the assumption that both srGAP1 GAP domains are active and specific for Cdc42. But reach full activity in accelerating GTP hydrolysis only in the presence of Cdc42 proteins of their own species.

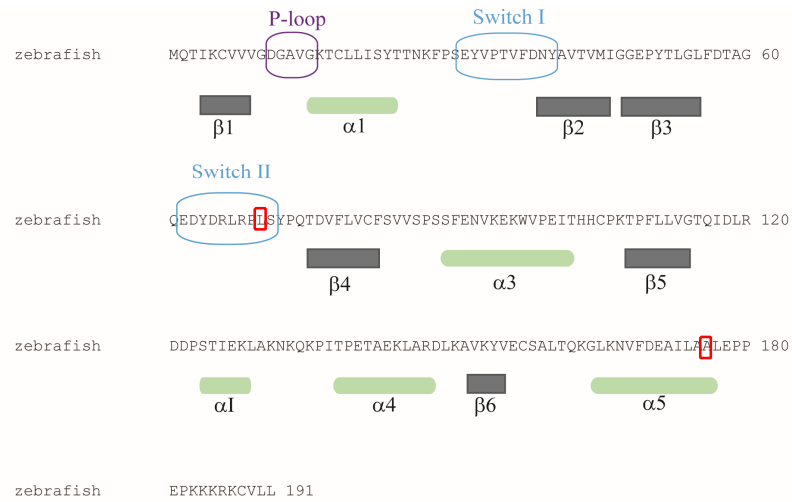
7.1.5.5 Mapping of the srGAP1 GAP domain binding sites on the homologous Cdc42 proteins

Cdc42 has a low intrinsic GTPase activity, which is significantly enhanced by the GAP domain, as seen in the ^{31}P -NMR measurement series. To identify the regions of human and zebrafish Cdc42, which are involved in the binding of their respective GAP domains, ^{15}N HSQC spectra were measured. HSQC measurements permit to obtain a 2D heteronuclear chemical shift correlation map between directly-bonded ^1H and X-heteronuclei (commonly, ^{13}C and ^{15}N). To assess the chemical shifts both Cdc42 proteins were measured alone and then with added GppNHp or GTP. The respective GAP domains were then added to the sample, until equimolar concentrations were reached. Chemical shifts were then recorded and mapped to a structural model of the RhoGTPase.

7.1.5.5.1 Mapping of the human srGAP1 GAP domain binding sites on the human Cdc42

First the binding sites for human Cdc42 and srGAP1 GAP domain were examined. Therefore, ^{15}N and ^{13}C labelled Cdc42 was prepared and ^{15}N HSQC spectra were measured on a Bruker 600 MHz spectrometer at room temperature. HSQC stands for Heteronuclear Single Quantum Coherence spectrum. It is a two-dimensional spectrum with one axis for ^1H and the other for a heteronucleus ^{13}C or ^{15}N . The spectrum contains a peak for each unique proton attached to the heteronucleus being considered. The assignment of the backbone ^1H , ^{13}C , and ^{15}N resonances of Cdc42 was carried out based on the already published assignment of human GDP-bound Cdc42 (Feltham et al., 1997) and additional HNCO (amide proton-to-nitrogen-to-carbonyl-carbon correlation) and HNCA (amide proton-to-nitrogen-to- α -carbon correlation) experiments, which make it easier to distinguish between all $\text{C}\alpha_i$ and $\text{C}\alpha_{i-1}$ peaks. Feltham et al. were not able to fully assign the GDP-bound human Cdc42. Several residues in the loops were not observed, presumably due to unfavourable water exchange, and residues at the C-terminal end were missing due to proteolysis, as confirmed by mass spectrometry (Feltham et al., 1997). Also, the proline residues P32, P87 and P99 do not appear in ^1H - ^{15}N correlation spectra, as they lack an amide proton. Nevertheless, 80 % of backbone amide resonances of the human Cdc42 could be assigned, providing good coverage of the protein surface. Figure 7.33 A shows the sequence of the human Cdc42 protein with its P-loop, Switch I and Switch II binding sites. The secondary structure is indicated below the sequence.

(A)



(B)

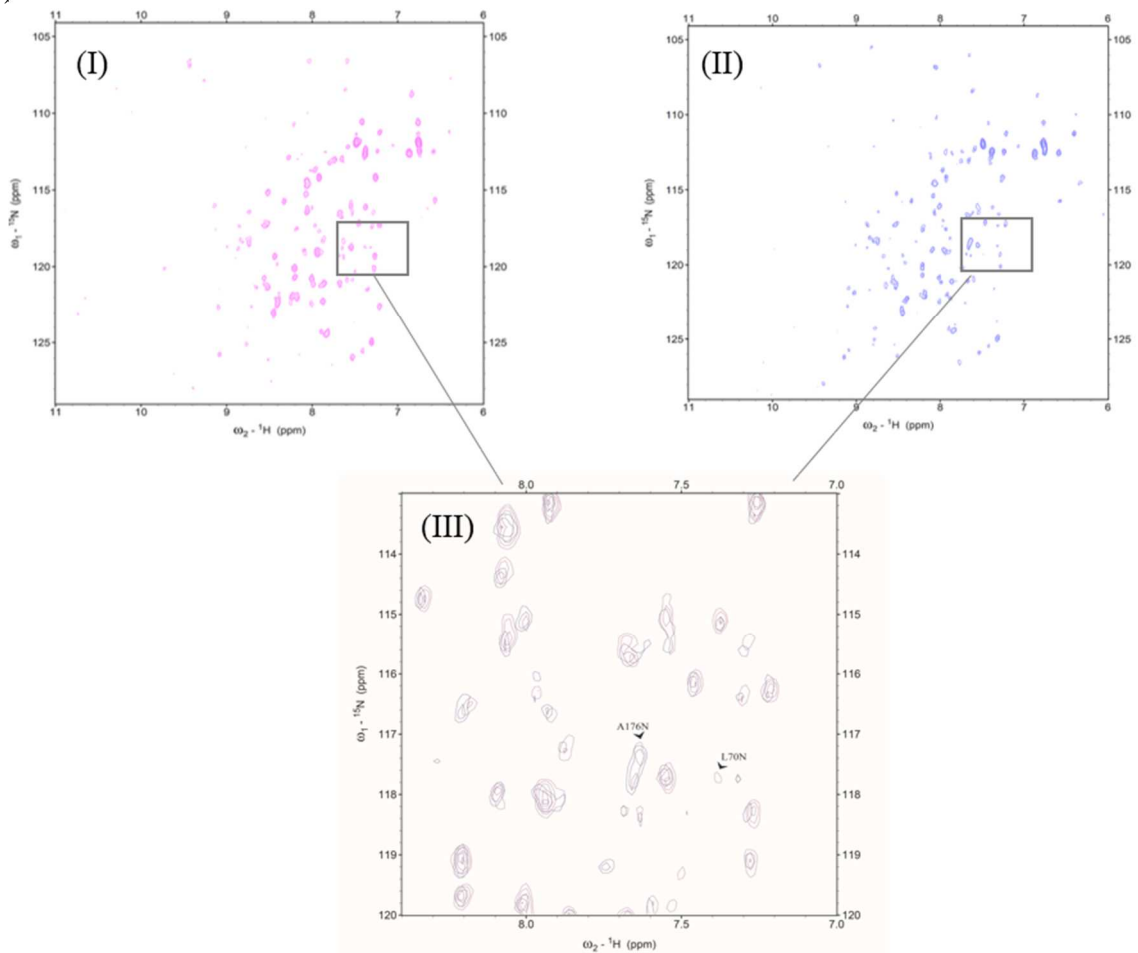


Fig. 7.33: Structural motifs of the human Cdc42 and ¹⁵N HSQC spectrum of the bound complex human Cdc42 and human srGAP1 GAP domain

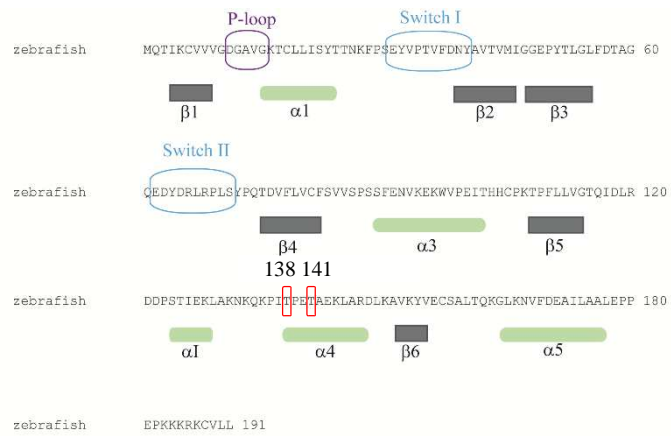
(A) Sequence of the human Cdc42 protein with the potential binding sites, P-loop, Switch I and Switch II, for the srGAP1 GAP domain (shown with coloured boxes). The secondary structure is indicated below the sequence. α -helices are represented as green cylinders and β -strands as grey boxes. (B) ¹H, ¹⁵N HSQC spectrum collected on human Cdc42-GTP (pink, I) and after addition of human srGAP1 GAP domain (blue, II). The box below (III) shows a zoomed view of the overlaid spectra, emphasizing the changes in the spectrum. Amino acid residue A176N is labelled as an example for an increasing and shifting signal, amino acid L70N for a disappearing signal after addition of the human srGAP1 GAP domain. Both amino acid residues are highlighted with red boxes in 7.33 (A).

Figure 7.33 B presents ^1H - ^{15}N correlation spectra of the human Cdc42 before (Fig. 7.33 BI) and after adding the srGAP1 GAP domain (Fig. 7.33 BII). In Fig. 7.33 BIII a zoomed view of the overlaid spectra is presented to highlight the changes in the spectra after adding the srGAP1 GAP domain. This led either to increasing and shifting signals, as seen for A176N or disappearing signals, as seen for L70N. Based on the NMR spectra, it was attempted to map the binding sites of the srGAP1 GAP domain. This proved to be difficult as the complex was actively hydrolysing GTP. However, it was possible to narrow the binding site to the Switch I region. The same experiment was carried out with zebrafish Cdc42 and its respective GAP domain.

7.1.5.5.2 Mapping of the zebrafish srGAP1 GAP domain binding sites on the zebrafish Cdc42 protein

As mapping of the binding sites for the human Cdc42 and human srGAP1 GAP domain proved to be difficult, due to the active complex and only implicated binding to the Switch I region. The same experiment was carried out for the zebrafish proteins to compare the results and examine if the binding sites are similar. Here, GppNHP was used instead of GTP to form a non-hydrolysable complex between the zebrafish Cdc42 and zebrafish GAP domain. Figure 6.33 A shows the sequence of the zebrafish Cdc42 protein with its P-loop, Switch I and Switch II binding sites. The secondary structure is indicated below the sequence. The ^1H - ^{15}N correlation spectrum of nucleotide-free zebrafish Cdc42 (1-191) is in good agreement with the data set published for human Cdc42 (pdb: 1GRN, Nassar et al., 1998). However, the spectrum shows considerable differences to that for the GTP/GDP bound protein. Signals for many residues assigned in the earlier analysis were not observed and others were of considerably lower intensity. Figure 7.34 B presents ^1H - ^{15}N correlation spectra of the zebrafish Cdc42 before (Fig. 7.34 BI) and after adding the srGAP1 GAP domain (Fig. 7.34 BII). In Fig. 7.34 BIII a zoomed view of the superimposed spectra is presented to highlight the changes in the spectra after adding the srGAP1 GAP domain. This led either to increasing and shifting signals, as seen for T141N or disappearing signals, as seen for T138N.

(A)



(B)

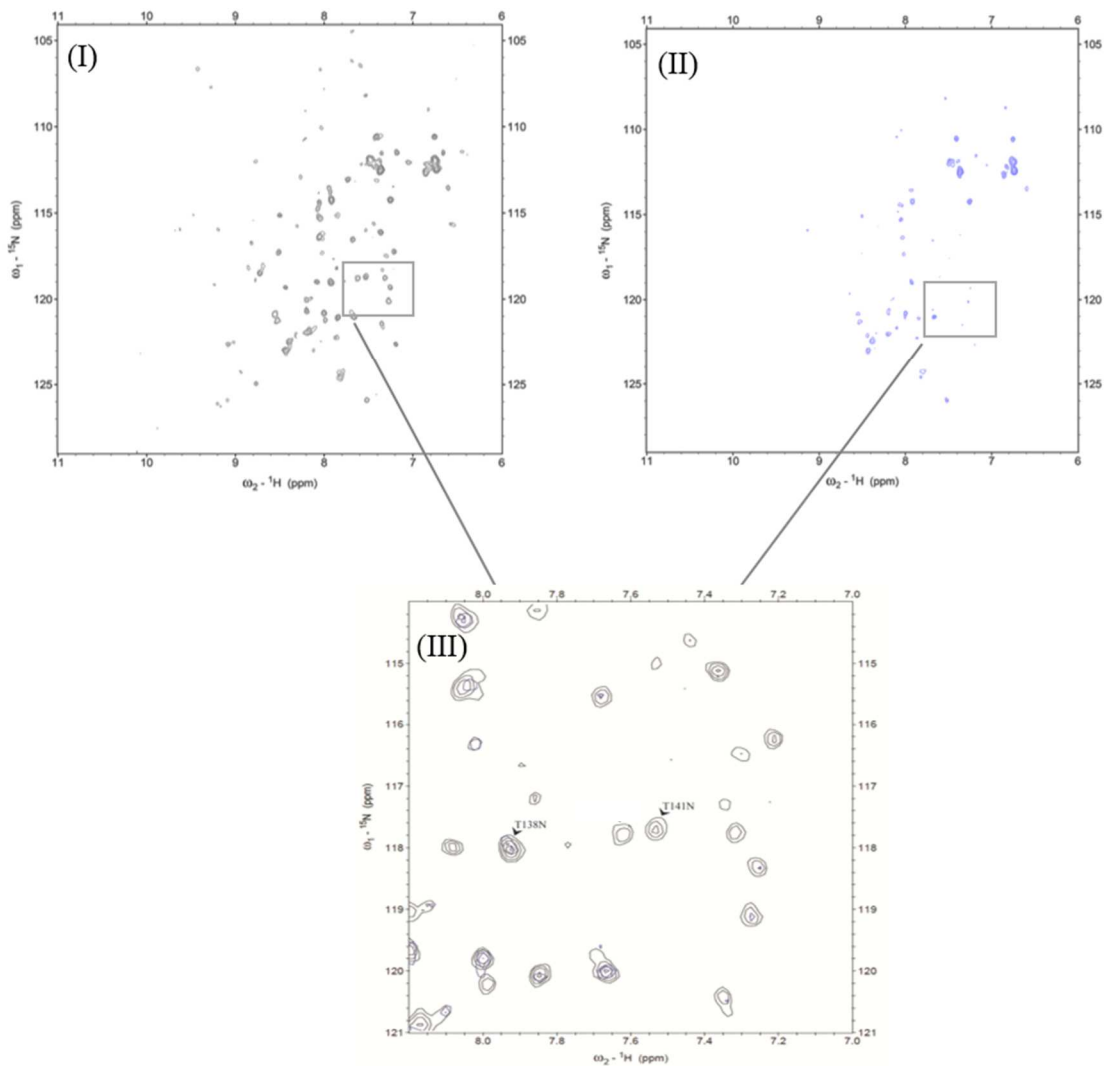


Fig. 7.34: Structural motif of the zebrafish Cdc42 and ^{15}N HSQC spectrum of the bound complex

(A) Sequence of the zebrafish Cdc42 protein and its potential binding sites for the srGAP1 GAP domain are shown with coloured boxes. The secondary structure is indicated below the sequence. α -helices are represented as green cylinders and β -strands as grey boxes. (B) ^1H , ^{15}N HSQC spectrum collected on zebrafish Cdc42-GppNHp (grey, I) and after addition of the zebrafish srGAP1 GAP domain (blue, II). Small box below (III) shows a zoomed view of the overlaid spectrum, emphasizing the changes in the spectrum. Amino acid residue T138N is labelled as an example for decreasing signal and amino acid T141N for a disappeared signal after addition of the zebrafish srGAP1 GAP domain. Both amino acid residues are highlighted with red boxes in 7.34 (A).

Figure 7.35 shows a model of the zebrafish Cdc42 highlighting the regions of the protein, which undergo conformational changes upon activation, as evidenced by chemical shift changes. Cdc42 consists of a central 6-stranded β -sheet. Helix $\alpha 1$ lies perpendicular to the β -strands at the concave side. The convex surface is flanked by $\alpha 3$ and $\alpha 4$, which are parallel to the β -strands. There is no structural evidence for an $\alpha 2$ helix, which cannot be found in Cdc42, in contrast to other GTP-binding proteins. αI is a less stable insert, forming a compact loop structure and lies adjacent to the loop between $\beta 4$ and $\alpha 3$. Mapping the unobserved residues in white on to this structure (PDB: 1GRN) in Fig. 7.35 shows them to cluster on one face of the protein.

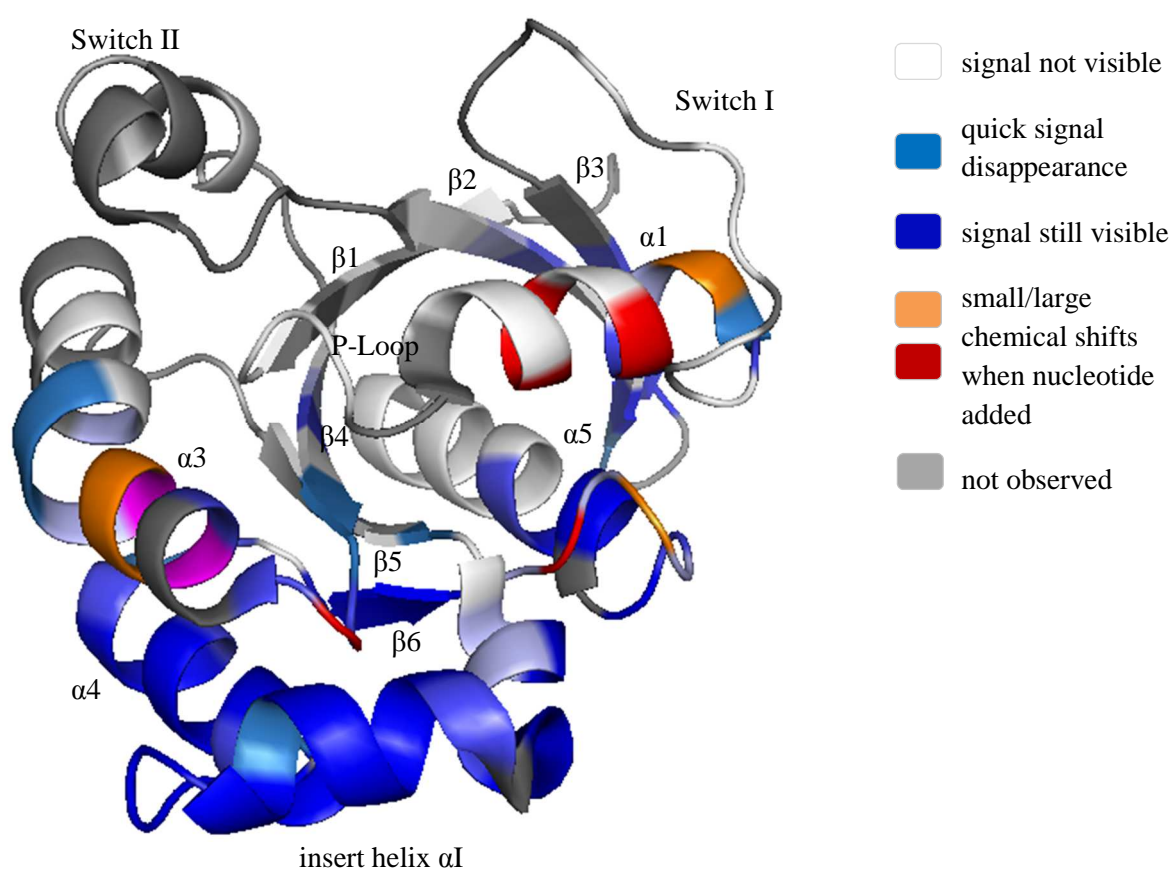


Fig. 7.35: Mapping the binding site for the GAP protein on the homologous RhoGTPase Cdc42

Model of the zebrafish Cdc42 based on the pdb structure 1GRN. The mapping of the binding site was acquired through ^1H , ^{15}N HSQC spectra. Upon adding the non-hydrolysable analogue of GTP, GppNHp, which binds into the P-Loop between $\beta 1$ and $\alpha 1$, small/large shifts are observed in the near surroundings of the nucleotide binding site (coloured in orange and red). Dark blue regions at the C-terminal region of Cdc42 are not involved in the binding of the nucleotide or the GAP domain and are not affected by the short-termed complex formation. Light blue areas undergo quick signal changes, when the GAP domain is added. White regions, which include the Switch I, Switch II and P-loop region were barely visible. Grey areas were not detected at all.

For both organisms the hydrolysis complex seems to be very short-lived and instable as the interaction itself is very hard to detect when GTP is added instead of GppNHp.

When nucleotide is added, small to large changes are observed in the orange/red coloured areas (residues 20-22, residues 84 and 90-91 and residues 157 and 159). When the srGAP1 GAP domain is added, further residues in $\alpha 3$, αI and $\beta 4$ showed decreased intensity with increasing GAP concentration (e.g. T138N, see the enlargement to Fig. 7.34), many of them disappear completely (e.g. T141N, see Fig. 7.33). A large area on the C-terminal surface of Cdc42, which corresponds to the insert helix αI , is not involved in any interaction (dark blue). It is possible that this region has a role in mediating the binding of the target and regulatory proteins as it is relatively close to the switch surface (Feltham et al., 1997). Several residues in the Switch I, Switch II and the P-loop region are barely visible or have unassigned peaks. The switch binding regions are unstructured and very flexible, yet important for the interaction of Cdc42 with effectors. A possible explanation for the observed data is a dimerization of nucleotide-free Cdc42, leading to low intensities of the signals highlighted in white. Such dimerization was suggested by Zhang et al., 1998 and leads to a negative regulation of the RhoGTPase. Addition of GAP leads to complex formation utilizing a similar binding surface (light blue areas in the figure). It can be assumed that binding of GAP disrupts the dimerization, promoting the active form.

Grey coloured regions were not detectable at all. This could be due to either unstructured flexible regions and/or internal dynamics, when the protein is in solution. This phenomenon was also described by Feltham et al., 1997, when the structure of the human GDP-bound Cdc42 was solved. Most of the potential affected residues lie on the surface of the protein.

The results of the human and zebrafish proteins emphasize the importance of flexible regions in the N-terminus of Cdc42 in the interaction. At least one specific region of the flexible switch region contributes to the binding of the GAP domain, possibly Switch I (residues 31-40 aa). From the NMR data it can be expected, that the GAP domains bind primarily to those regions of Cdc42, which change conformation upon GTP/GppNHp binding. This result fits well with studies for other GAP domains with members of the RhoGTPase family (Feltham et al., 1997; Nassar et al., 1998; Dvorsky et al., 2004; Chandrashekar et al., 2011).

7.1.6 POSSIBLE NEW INTERACTION PARTNERS FOR THE HUMAN SRGAP1 PROTEIN AND ITS ZEBRAFISH HOMOLOG

An essential step in understanding protein function is the identification of relevant interacting proteins. Based on structural and functional characteristics protein interactions can be classified as stable or transient, whereby the stable interaction will form protein complexes and the transient interaction will form signalling pathways (Rao et al., 2014). Only few binding partners for the srGAP1 protein are known so far. The RhoGTPase Cdc42 binds to the srGAP1 GAP domain, whereas Robo1 and possibly Robo3 bind to the srGAP1 SH3 domain (Wong et al., 2001). The C-terminus of srGAP1 has received less attention so far, although it is expected to enable association of srGAP1 with other proteins. In a previous study it was shown that members of the srGAP family might interact with 14-3-3 proteins, though not much detail is provided about the interaction site (Blasutig et al., 2008). In this present study an approach to identify possible new interaction partners for the human and zebrafish srGAP1 C-terminal domains is described.

7.1.6.1 Prediction of protein binding motifs in the human srGAP1 C-terminus

The C-terminal domain of the human srGAP1 contains 286 residues (799-1085 aa) and is less conserved across different species, suggesting functional diversity (Fig. 7.36). However, no functional and biochemical data are available for the srGAP1 C-terminus. Comparison of the three human srGAP C-termini resulted in a sequence identity of 21 %. Compared with the sequence identities of the other domains, this region of the srGAP family has the highest sequence variation. Secondary structure analysis of the srGAP1 C-terminal domain does not reveal any elements of specific secondary structure, besides a short α -helical motif (955-979 aa), which is conserved in all organisms.


```

srGAP1 VQDMDDTFSDTLSQKADSEASSGQVTEDEKSSSKD-MNSPTDR-HPDGYLARQQRKGEPPP
srGAP2 -----GVVERSSPKSEIEVI SEPEEKVTARAG-ASCPGSGGHVADIYLANINKQRKRPE
srGAP3 -----SLSQKADSEASSGQLLDDKASSKNDLQSPTEHISDYGGVGMGRVRLRSD
          * *:: * * * * .. :: ..* : : . :
          * *:: * * * * .. :: ..* : : . :

srGAP1 PVRPRGRTSDGHCPLHPPHALSNSSVDLGSPLASH---PRGLLQNRGLNNDSPERRRRP
srGAP2 -----SGSIRKTFRSDSHGLSSSLTDSSSPGVGASCRPSSQPIMSQSLPKGPDKCSIS
srGAP3 GAAIPRRRS-GGDTHSPPRGLGPSI---DTPPRAAACPSSPHKIPLTRGRIESPEKRMA
          * :.* * :* . : : : :.*::
          * :.* * :* . : : : :.*::

srGAP1 GHGSLTNSRHDSLK-KIDSPPIRRSTSSGQYTGFNDRKPLDPETIAQDIEETMNTALNE
srGAP2 GHGSLNSISRHSSLKNRLDSPQIRKTATAGRSKSFNNHRPMDPEVIAQDIEATMNSALNE
srGAP3 TFGSAGSINYPDKK-ALSEGHSMRSTCGSTRHSSLGDHKSLEAEALAEDEKTMSTALHE
          .** *. . . :. :* : : : . : :* : : * : : * * : * * *
          .** *. . . :. :* : : : . : :* : : * : : * * : * * *

srGAP1 LRELERQSTAKHAPDVVLDLTLEQVNSPTPATSTESLSPLHNVALRSSEPQIRRSTSSSS
srGAP2 LRELERQSSVKTHTPDVVDLTLEPLKTSFVVAPTSEPSPLHTQLLKDPEPAFQRSASTAG
srGAP3 LRELERONTVKQAPDVVLDLTLEPLKNPBGV-SSEPASPLHTIVIRDPDAAMRRSSSSST
          ***** . : * : : ***** : * . * . : : * ***** . : . : : : * : : :
          ***** . : * : : ***** : * . * . : : * ***** . : . : : : * : : :

srGAP1 DTMSTFKPMVAPRM-GVQLKPPALRPKPAVLPKTNPTIG--PAPPP-----QGPT
srGAP2 DIACAPRPVKSVM-AAPVKPPATRPKPTVFPKTNATSP--GVNSS-----TSPQST
srGAP3 EMMTTFKPAALSARLAGAQLRPPMPVRPVVQHRSSSSSSSGVGSAPVTPTEKMFNPSSA
          : : * : * : : . . : : * * * * . : . : . : : : : : : :
          : : * : * : : . . : : * * * * . : . : . : . : : : : :

srGAP1 DKSCIM
srGAP2 DKSCIV
srGAP3 DKSGIM
          *** * :

```

Fig. 7.36: Sequence comparison for the C-termini of the three members of the human srGAP family

The C-terminus is the less conserved domain of the srGAP family. Comparison of the C-termini of srGAP1, srGAP2 and srGAP3 resulted in a sequence identity of 21 %.

To detect potential protein binding motifs in the C-terminal part of the srGAP1 protein, the primary sequence of the srGAP1 C-terminus was analysed. It is well known that protein-protein interactions are mediated through binding of modular domains to characteristic short sequence motifs. For the analysis, Scansite, a program, developed to predict short sequence motifs (Oberbauer and Yaffe, 2004; <http://scansite.mit.edu/>) was used. Several motifs likely to be phosphorylated or harbouring consensus binding sequences for proteins such as 14-3-3 and SH3 domains, were identified. In Fig. 7.37 specific binding motifs for potential binding partners in the C-terminal domain are shown. The binding motif search with Scansite was divided in three sections: the phosphoserine/threonine binding group, the SH3 group and different kinase binding groups. Here, the focus lies on the binding sites of 14-3-3 proteins and SH3 domains, as their possible relevance is indicated by previous publications (Blasutig et al., 2008; Tzivion et al., 2001; Weng et al., 1995).

SH3

799 VQDMDDTFSDTLSQKADSEASSGPVTEDEKSSSKDMNSPTDRHPDGYLARQRKRGEPPP

PVRRPGRTS¹⁴⁻³⁻³GDGHCPLHPPHALSNSSVDLGSPSLASHPRGLLQNRGLNNDSPERRRRPG

HGSLTNISRHDSLKKIDSPPIRRSTSSGQYTG¹⁴⁻³⁻³FNDHKPLDPETIAQDIEETMNTALNE

LRELERQSTAKHAPDVVLD¹⁴⁻³⁻³TLEQVKNSPTPATSTESLSPLHNVALRSSEPQIRRSTSS

SH3

SSDTMSTFKPMVAPRMGVQLKPPALRPKPAVL^{SH3}PKTNPTIGPAPPQGPTDKSCTM 1085

Fig. 7.37: Binding sites for putative interaction partners of the human srGAP1 C-terminus

The C-terminal domain of srGAP1 contains several binding motifs for 14-3-3 proteins (orange) and various SH3 domains (blue). Sequence motifs are underlined.

The results indicate that there are possible binding motifs for different proteins in the C-terminal domain of the human srGAP1 protein. 14-3-3 protein binding was suggested in a previous study for the srGAP protein family (Blasutig, 2008). 14-3-3 proteins recognize two common recognition motifs containing phosphorylated serine or threonine residues: RSxpSxP (mode 1) and RxxxpSxP (mode 2). “pS” represents a phosphorylated serine residue and “x” represents any amino acid residue (Tzivion et al., 2001). Two potential mode 1 binding sites can be found in the C-terminal domain of srGAP1. Besides the binding sites for 14-3-3 proteins, binding motifs for SH3 domains and different classes of kinases were also detected. SH3 domains recognize two classes of binding motifs: R/KxxPxxP (class I) and PxxPxR (class II). The binding motifs in the C-terminus of srGAP1 are class 2 motifs. Different types of kinase binding sites were also detected, with binding motifs containing serine or threonine residues. In this context it should be noted, that the predicted binding sites are exclusively based on the predictions using Scansite. In order to identify protein complexes associated with the human srGAP1, rat brain tissue pulldown assays were combined with mass spectrometry analysis.

7.1.6.2 Rat brain pulldown with the human srGAP1 C-terminus hints to possible new interaction partners for srGAP1

Previous studies indicate the involvement of srGAP1 in neuronal processes, as well as cytoskeletal regulation and endocytosis. As shown in previous studies and in this thesis (chapter 7.1.2), srGAP1 is mainly expressed in the brain during development (Bacon et al., 2011; Couthino-Budd et al., 2012; Ip et al., 2010; Wong et al., 2001). To identify putative binding partners of srGAP1, a GST-fusion pulldown with brain tissue from rats at the

developmental stage P14 was carried out. First, the C-terminal domain of the human srGAP1 (799-1085 aa) was cloned and purified as a GST-fusion protein. Then brain tissue from P14 rats was homogenized in lysis buffer and the lysate pre-cleared with glutathione-sepharose (GSH) beads. The GST-srGAP1 C-terminus was bound to GSH beads and incubated with the pre-cleared lysate overnight. GST protein alone was used as a negative control. After extensive washing steps, the beads were heated to 90 °C, to release the proteins bound to the GSH beads, centrifuged and the supernatant was separated on a 10 % SDS gel (Fig. 7.38). The gel was stained with Coomassie Blue, destained and selected areas on the gel were cut out, digested with trypsin and the resulting peptides were submitted to nano-LC MS/MS. The acquired MS data were pre-processed with MaxQuant (v.1.2.2.9) to generate peak lists, which were submitted to the Andromeda search engine and searched against a rat protein database. In addition the data were analysed for the presence of peptides of the human srGAP1 C-terminus as a positive control. Proteins identified with a minimum of one peptide were taken into consideration.

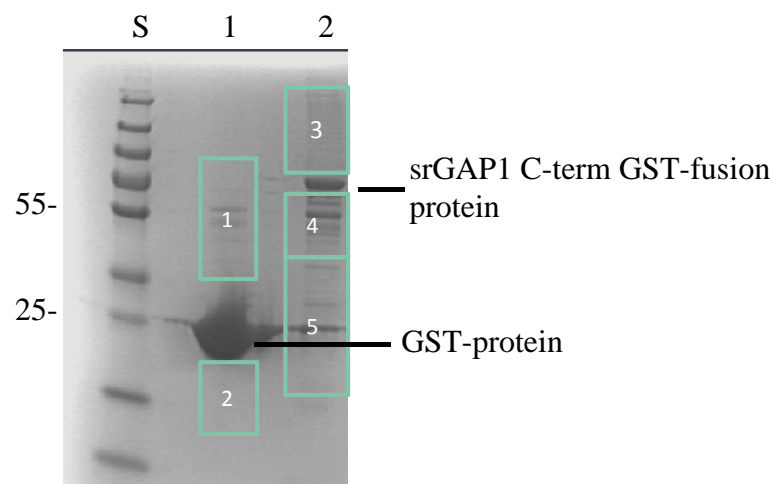


Fig. 7.38: GST-pulldown assay of human srGAP1 C-terminal fusion protein with P14 rat brain tissue

The C-terminal GST-fusion protein of srGAP1 and GST protein alone were bound to GSH beads and incubated with rat brain lysate. The samples were washed and separated on a 10 % SDS gel. The gel was stained with Coomassie Blue and destained in destaining solution. (S) Standard, (1) negative control: GST (24 kDa). GST 1 and 2 correspond to the framed areas in lane 1. (2) GST-srGAP1_C-terminus fusion protein (55 kDa). Similarly, GST-srGAP1_Cterm3-5 correspond to the specific framed areas in lane 2 on the 10 % SDS-gel. Framed and numbered areas (1-5) in the 10 % SDS gel were digested with trypsin and analysed with nano LC-MS.

807 proteins were identified based on the MS/MS spectra of the peptides. To filter out non-specific contaminants the results of the sample were compared to the GST negative control. A protein was not considered, if the negative control showed the same amount of identified peptides as the sample of the candidate protein. Proteins such as ribosomal proteins or heat shock proteins were identified in both samples to the same extent and thus were considered as background proteins. Proteins, which were detected in only one of two independent experiments, were also eliminated. To decide how reliable a protein is identified, the posterior

error probability (PEP) score in combination with the intensity and the number of identified peptides for the corresponding proteins was considered. The PEP score is calculated for each peptide. A PEP score lower than 0.01 indicates that the peptide was identified with a probability of more than 99 %. Using this approach, 14 putative interaction partners with the lowest PEP scores and the highest number of detected peptides were selected and analysed regarding their domain composition and function. Table 7.6 shows the raw data of the mass spectrometry analysis for the 14 selected proteins. The labelling of the intensities in the table corresponds to the selected regions on the 10 % SDS in Fig. 7.38.

Tab. 7.6: Raw data of the 14 putative interaction partners for the GST-srGAP1_C-terminus as identified in the rat brain pulldown experiment and mass spectrometry analysis, sorted with regard to the PEP score. Proteins of interest are highlighted in purple.

Protein Names	Peptides (negative control GST)	Peptides (GST-srGAP1 Cterm)	Sequence Coverage [%]	PEP Score	Intensity GST 1	Intensity GST 2	Intensity GST-srGAP1_Cterm3	Intensity GST-srGAP1_Cterm4	Intensity GST-srGAP1_Cterm5
Dynamin-1-like protein	9	16	47,8	7,13E-269	3x10 ⁶	0	1.2x10 ⁷	0	0
Dynactin subunit 1	1	12	38,6	6,28E-245	3x10 ⁴	0	4.5x10 ⁶	0	0
Endophilin A1	2	7	58,8	2,12E-216	0	9.2x10 ⁵	0	0	9.2x10 ⁶
Nck-1	1	23	36	6,52E-214	7x10 ⁴	0	2.2x10 ⁷	0	0
Cyfp2	0	21	38,3	1,26E-210	0	0	3x10 ⁷	0	0
AP-2 complex subunit alpha-2	8	27	34,9	2,72E-188	2.9x10 ⁶	1.6x10 ⁵	3.8x10 ⁷	0	0
14-3-3 protein zeta	9	13	38,4	5,04E-96	0	2.1x10 ⁷	0	0	4.8x10 ⁷
14-3-3 protein gamma	8	13	34,8	4,48E-76	0	2.3x10 ⁷	0	0	6x10 ⁷
LIM and SH3 domain protein 1	7	12	67,3	5,54E-66	0	6.5x10 ⁶	0	0	3.1x10 ⁷
Synapsin 2	4	9	19,8	1,67E-60	2.7x10 ⁶	0	0	1.2x10 ⁷	0
Neuronal migration protein doublecortin	1	5	27	3,23E-51	0	1.2x10 ⁶	0	0	1.4x10 ⁶
Cortactin	0	4	23,3	5,21E-42	0	0	1.5x10 ⁶	0	0
14-3-3 protein theta	4	7	15,9	2,23E-29	0	2.8x10 ⁶	0	0	5.2x10 ⁶
Abi1 protein	0	3	9,6	1,54E-25	0	0	0	1.8x10 ⁶	0

For some candidate proteins peptides were also detected in the negative control, but the number of the detected peptides and their measured intensity was lower in comparison to values obtained for the srGAP1 C-terminus, thus indicating specific binding to the C-terminal region. For other proteins, peptides were only detected in the sample. These proteins were also considered for further examination (not highlighted). In Fig. 7.39 the function of the identified binding partners are listed.

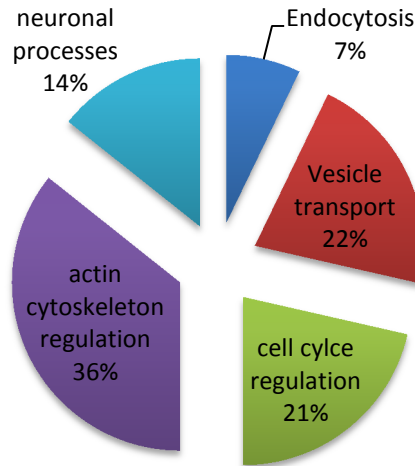
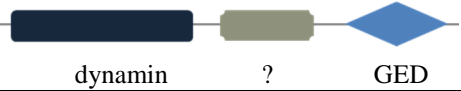

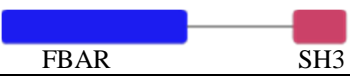


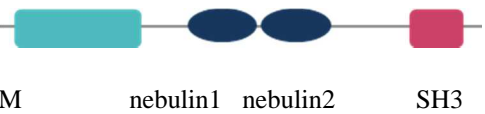

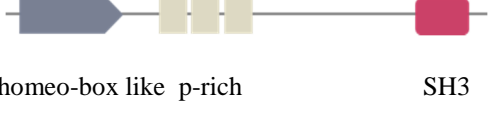






Fig. 7.39: Functional categorization of potential interaction partners of the C-terminal domain of srGAP1. Proteins were identified by nano LC-MS/MS analysis of a rat brain tissue pulldown with GST-tagged srGAP1 C-terminal fusion protein. The biological functions were assigned as referred to in the universal protein resource database (<http://uniprot.org>) and protein- specific publications.

Many SH3 domain containing proteins as well as subunits of the 14-3-3 proteins, which binding sites were indicated in the analysis of the primary sequence of the srGAP1 C-terminus, were found in the mass spectrometry analysis. Interestingly, most of the identified candidates seemed to be involved in actin cytoskeleton regulation (39 %), vesicle transport (22 %) or neuronal processes (26 %). A lower number of proteins are involved in endocytosis (9 %) and cell cycle regulation (4 %).

In the following table (Tab. 7.7) proteins belonging to the different categories are analysed regarding their domain composition and function:

Tab. 7.7: Identified potential interaction partners for the human srGAP1 protein with their domain composition and detailed function

CATEGORY	DOMAIN COMPOSITION	FUNCTION
VESICLE TRANSPORT		
Dynamin-1-like protein	 dynamin ? GED	Key player in fission process of mitochondria (Froehlich et al., 2013)
Dynactin subunit 1	 CAP-Gly dynactin	Organization of microtubules and transport of vesicles (Zhapparova et al., 2009)
Endophilin A1	 FBAR SH3	Synaptic vesicle transport (Bai et al., 2010)
ACTIN CYTOSKELETON REGULATION		
Nck-1	 SH3 SH3 SH3 SH2	Binding of to effector proteins involved in cytoskeletal dynamics (Jones et al., 2009)
Cyfp-2	 Cyfp	Scaffolding protein for complexes associated with Rac pathway (Jackson et al., 2007)
Lasp1	 LIM nebulin1 nebulin2 SH3	Involvement in cell migration, signalling and stabilization of cytoskeleton (Pappas et al., 2011).
Cortactin	 NTA repeats helical p-rich SH3	Regulation of cortical actin assembly (Weed et al., 2001)
Abi1	 homeo-box like p-rich SH3	Involvement in actin reorganization, lamellopodia formation and part of WAVE2 complex (Echarri et al., 2004)
ENDOCYTOSIS		
Assembly protein-2 complex subunit alpha 2	 adaptin-N α-adaptin C	Involvement in clathrin-mediated endocytosis and cargo recognition (Nakatsu et al., 2003)
NEURONAL PROCESSES		
Synapsin-2 Isoform a	 A B C G H E	Modulation of neurotransmitter release at the presynaptic terminal (Medrihan et al., 2013)
Neuronal migration protein doublecortin	 DCX1 DCX2	Neuronal migration and neurite branching (Gleeson et al., 1999)
CELL CYCLE CONTROL		
14-3-3 proteins	 14-3-3- gamma or zeta or theta	Mitotic signal transduction, apoptose and cell cycle control (Meek et al., 2004; Tzivion et al., 2001)

In order to determine if the srGAP1 C-terminus from zebrafish has similar or different putative interaction partners, a pull-down with whole zebrafish embryos at the developmental

stage of 48 hpf was carried out on the basis of the data obtained from the pulldown with the C-terminal domain of the human srGAP1 protein. Similar results would indicate a conserved role for the human and zebrafish srGAP1 in multiple pathways besides the Slit-Robo pathway, like endocytosis or the regulation of the actin cytoskeleton.

7.1.6.3 Prediction of protein binding motifs in the C-terminal domain of the zebrafish srGAP1

As described in chapter 7.1.6.1 proteins recognize specific linear binding motifs for binding to other proteins in signalling pathways. To assess the existence of such motifs in the C-terminal domain of the zebrafish srGAP1 protein, I analysed the primary sequence with Scansite. In Fig. 7.40 the predicted binding motifs are highlighted and the putative interaction partners are indicated. The binding motif search with Scansite was divided in three sections: the phosphoserine/threonine binding group, the SH3 group and different kinase binding groups. The focus of the analysis was put on binding sites for 14-3-3 proteins and SH3 domains as kinase motifs are too abundant.

14-3-3

782 DMDDTFSDTLSQKADSEASSGHGGEKCSSRDMGSPDTSRLPDAYISRHRKRSDP

SH3

PTRRPPARPTDTHCLVHPSHHSSHTNPDLGSPVMGHYSPRDMLRGRGHMPMDSPE

SH3 14-3-3

RRRRTGHGSLTNISRHESIKKMESPPIRSTSSGQYSSFNEPHVKSLDPESIAQD

IEETMNTALNELKELERQSSAKHAPDVVLDTLEQMKNAPTPASSTESLSQLHGLL

14-3-3 SH3 SH3

LRPAGTELHMRRSTSSSSDTMSTFKPAVAPRMGVQLKPPTLRPKPMVVPVKTGAA

QHPAAPPQDPLDKSCTM 1073

Fig. 7.40: Binding sites for putative interaction partners of the zebrafish srGAP1 C-terminus

The C-terminal domain of srGAP1 contains several binding motifs for 14-3-3 proteins (orange) and various SH3 domains (blue). Sequence motifs are underlined.

The results of the binding motif search indicate several possible short sequence motifs that might be recognized by different proteins. The identified sequence motifs are similar to them of the human srGAP1 C-terminal domain and indicate a possible conserved binding region (see chapter 7.1.6.1). Although, for the srGAP1 C-terminus of zebrafish more SH3 and 14-3-3 binding motifs in comparison to its human equivalent are predicted. In order to identify

potential binding partners for the srGAP1 C-terminal domain, as pulldown assay with whole 48 hpf zebrafish embryos.

7.1.6.4 No relevant hints for potential interaction partners for the zebrafish srGAP1 C-terminus

In chapter 7.1.6.1 the pulldown with P14 rat brain tissue revealed several potential binding candidates for the human srGAP1. Here, I searched for potential interaction partners for the C-terminal domain of the zebrafish srGAP1 with a zebrafish embryo pulldown followed by a mass spectrometry analysis. The experimental design of the pulldown followed the protocol of the rat brain tissue pulldown with GST-tagged srGAP1 C-terminus as bait. First, the C-terminal domain of the zebrafish srGAP1 (782-1083 aa) was cloned and purified as a GST-fusion protein. 48 hpf embryos were collected, removed from their chorion, washed and homogenized in lysis buffer. The lysate was pre-cleared with glutathione-sepharose (GSH) beads. The GST-fusion protein of the srGAP1 C-terminus was bound to GSH beads and incubated with the pre-cleared lysate overnight, while GST alone was used as a negative control. After several washing steps, the beads were heated at 90 °C, to release bound proteins from the GSH beads. The samples were centrifuged and the supernatant separated with SDS-PAGE (Fig. 7.41). The gel was stained with Coomassie Blue and destained in destaining solution. As seen on the 10 % SDS gel the sample of the srGAP1 C-terminus (Fig. 7.41, lane 2) was apparently degraded during the pulldown process. Despite the degradation the samples were analysed by the mass spectrometry facility after trypsin digest as it was considered that the amount of the bait protein might be enough to identify possible interacting proteins. The resulting peptides were submitted to nano-LC MS/MS. Identified peptides were pre-processed by MaxQuant (v.1.2.2.9) to generate peak lists, which were then submitted to the Andromeda search engine and searched against a zebrafish protein database. In addition, the data were analysed for the presence of the zebrafish srGAP1 C-terminal peptides as a positive control.

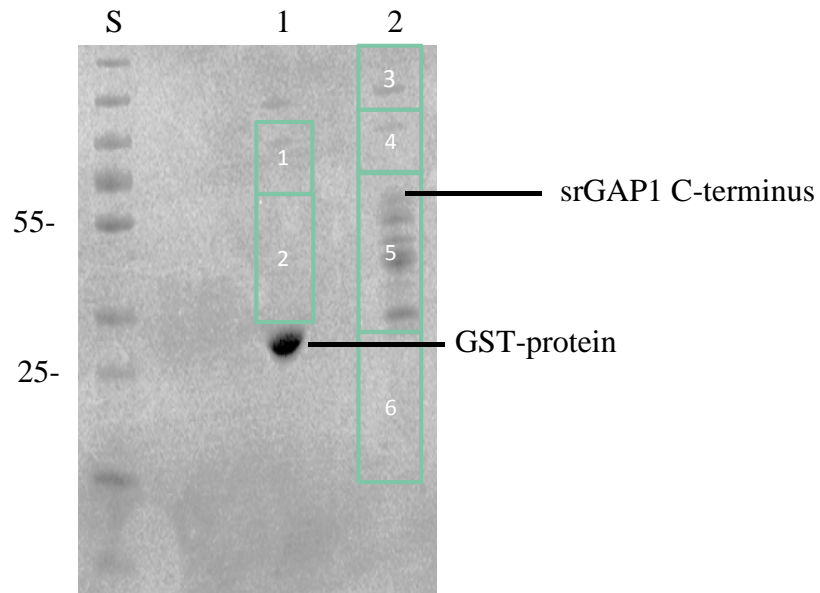


Fig. 7.41: GST-pulldown assay of the C-terminal fusion protein of srGAP1 with 48 hpf zebrafish embryos.

The GST-fusion protein of the C-terminal srGAP1 protein and GST protein alone were bound to GSH beads and incubated with zebrafish embryo lysate. The samples were washed and separated on a 10 % SDS gel. The gel was stained with Coomassie Blue and destained in destaining solution. (S) Standard, (1) negative control: GST (24 kDa) (2) GST-srGAP1_C-terminus fusion protein (55 kDa). Framed and numbered areas (1-6) on the 10 % SDS gel were digested with trypsin and analysed with nano LC-MS.

Based on the MS/MS spectra analysis 571 proteins were identified. From them 141 proteins with the lowest PEP score were selected and examined for their peptide coverage in comparison to the GST negative control. Figure 7.42 shows a chart with the identified proteins. Unlike the pulldown with the rat brain tissue for the human srGAP1 C-terminal fusion protein, the majority of the proteins are non-specific contaminants, like ribosomal proteins (13 %), yolk-derived proteins (6 %), proteins from the eyes (3 %) or muscle tissues (8 %) as they were detected in the negative control and the sample to the same extent. The annotation of the zebrafish genome is not complete yet, which might explain the 21 % of uncharacterized proteins. Furthermore, proteins with unknown function were detected (34 %).

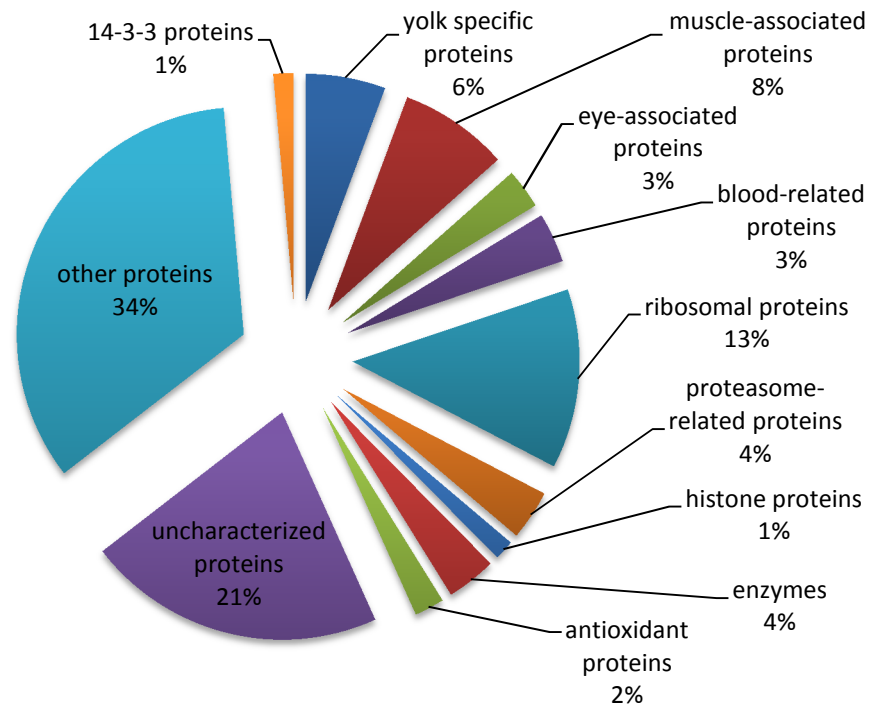


Fig. 7.42: Categorization of identified proteins in the zebrafish embryo pulldown.

Proteins were identified through a pulldown with zebrafish embryos, using GST-tagged srGAP1 C-terminal fusion protein and analysed by nano LC-MS/MS. The categorization was assigned according to the Universal protein resource database (<http://uniprot.org>).

In conclusion, no specific interaction partner could be identified by the GST-pulldown with zebrafish embryos. One obvious reason for this might be the degradation of the bait protein by contamination with proteases. srGAP1 is mainly expressed in the brain, a pulldown with zebrafish brain tissue should be considered. This might be more successful in the assessment of similar candidates as it was done for the human srGAP1 C-terminus. So far, it can be assumed that the srGAP1 protein is not only a crucial factor in the Slit-Robo pathway, but possibly also in multiple other pathways, like actin cytoskeleton regulation, endocytosis and vesicle transport.

7.2 STRUCTURAL AND FUNCTIONAL CHARACTERIZATION OF THE FBAR DOMAIN OF THE HUMAN CAROM PROTEIN

As mentioned before the BAR superfamily contains three subfamilies. Recently, the subfamily of I-FBARs was described (Couthino-Budd et al., 2011; Guerrier et al., 2009). Though several FBAR containing proteins have been solved (Syndapin (PDB: 3I2W, Edling et al., 2009), CIP4 (PDB: 2EFK, Shimada et al., 2007), FPB17 (PDB: 2EFL, Shimada et al., 2007), the structural properties of I-FBAR domains have not been determined yet. Furthermore, the mechanism of how they induce membrane invagination remains unknown. A recent study about the to the srGAP family phylogenetically related Nwk protein, which also contains a N-terminal FBAR domain, reported inverse FBAR activity (Becalska et al., 2013). To understand the difference between “classical” FBAR domains and inverse FBAR domains structural and functional studies were performed on the human homolog of Nwk, Carom.

7.2.1 BIOCHEMICAL CHARACTERIZATION OF THE FBAR DOMAIN OF THE HUMAN CAROM PROTEIN

carom encodes a protein, composed of a conserved FBAR domain and two SH3 domains. The protein is so far poorly characterized, but its function seems to be connected to endocytosis and cell migration. According to a study of its *Drosophila* homolog, Nwk, this FBAR domain is assumed to have a membrane deforming activity differing from previously described BAR and FBAR proteins and sharing similarity to the activity described for the srGAP protein family (Becalska et al., 2013).

7.2.1.1 Purification and biochemical analysis of the FBAR domain of the human Carom protein

The recombinant FBAR domain of the human Carom protein comprising amino acid residues 1-424, was overexpressed in *E. coli* Rosetta DE3 cells (Fig. 7.42). This construct contains a C-terminal α -helical extension, which has been shown to be dispensable for filopodia formation in S2 cells in a previous study (Becalska et al., 2013). To be able to compare the results of the functional analysis of the Carom FBAR domain with them obtained for the srGAP1 FBAR domain containing this extension, the longer FBAR fragment was chosen.

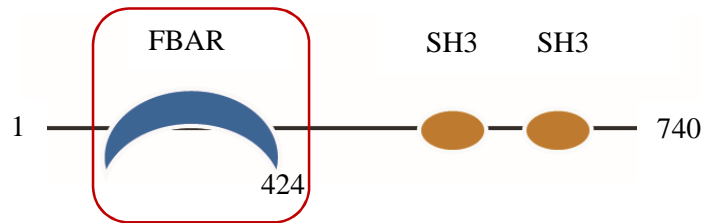


Fig. 7.42: Domain composition of the full-length human Carom protein

The human Carom protein consists of a FBAR domain and two SH3 domains. Its FBAR domain (1-424 aa, highlighted with a red box) is presumed to bind to membranes and induce membrane protrusions.

The Carom FBAR domain, with a molecular weight of 54 kDa, was purified in a two-step purification by affinity chromatography using NiNTA and size exclusion S75 (Fig. 7.43).

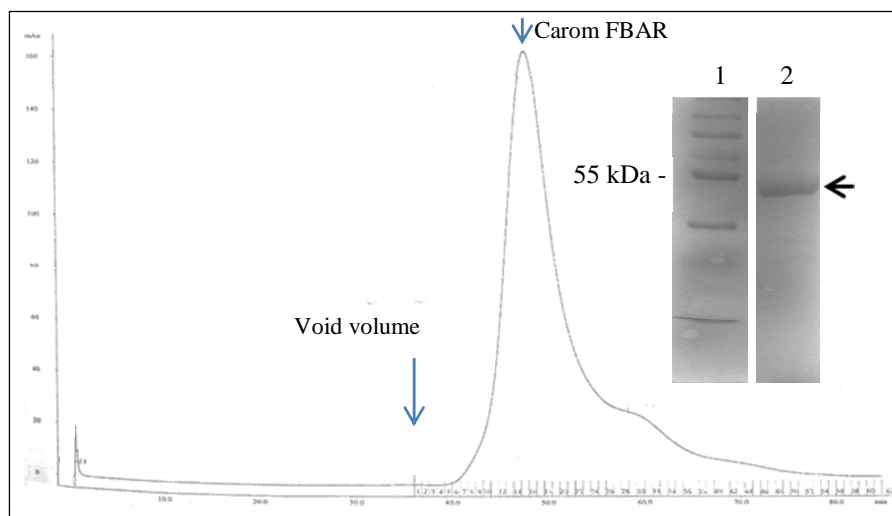


Fig. 7.43: Gelfiltration chromatography profile and 10 % SDS gel of the FBAR domain of the human Carom protein

The Carom FBAR domain elutes in one peak. This corresponds to the band on the 10 % SDS gel at a molecular weight of 54 kDa (indicated by an arrow). The 10% SDS gel was stained with Coomassie Blue. Insert 1) ProteinPage Plus Ruler, insert 2) concentrated fraction from the elution peak.

In order to analyse the oligomeric state of the FBAR domain in detail, a chromatography-mode static light scattering was performed. The protein (1 mg/ml) was loaded on a size exclusion column and subjected to analysis. The Carom FBAR domain eluted in two peaks, the first one at 100 kDa and the second one at 51 kDa, implying that it probably exists as a mix of monomers and dimers in solution (Fig. 7.44).

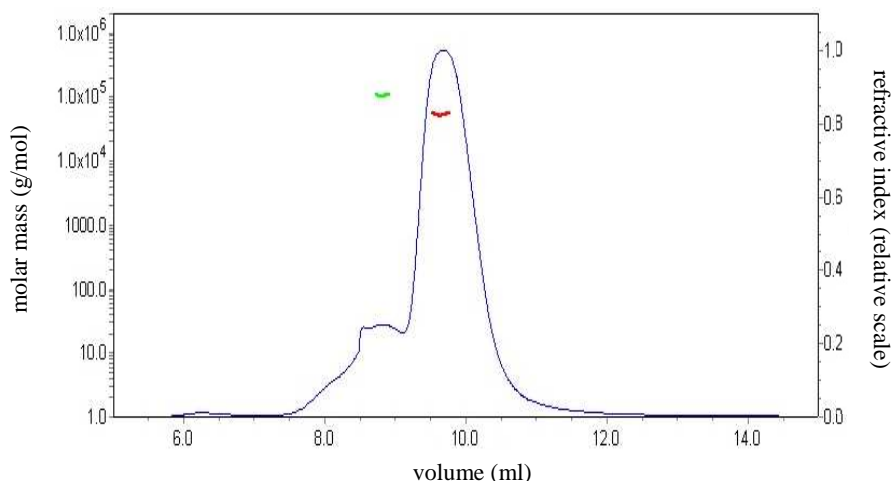


Fig. 7.44: Static light scattering profile for the human Carom FBAR domain

For determining the molecular mass, the protein (1 mg/ml) was injected on a Wyatt size exclusion column and run with 0.5 ml/min at 4 °C. The FBAR of the Carom protein eluted in two peaks: the first one with a calculated size of 100 kDa (green line) and the second with a size of 51 kDa (red line). The chromatogram displays two graphs: in blue the refractive index and in green and red the molecular weight.

Using published structures of the FBAR domains of CIP4 (PDB: 2EFL, Shimada et al., 2007) and FBP17 (PDB: 2EFK, Shimada et al., 2007) as templates, a structural model of the Carom FBAR domain has been built (Fig. 7.45). This suggests that the Carom FBAR domain shows the typical FBAR domain fold with six anti-parallel α -helices.

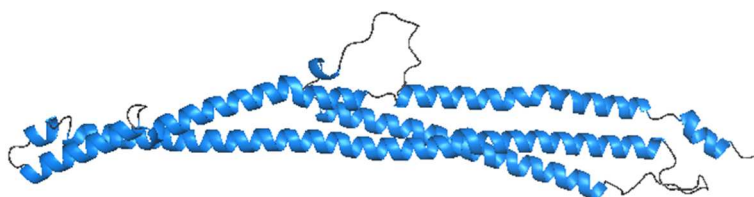


Fig. 7.45: PDB-based model for the human Carom FBAR domain

The PDB-based model shows the potential structure of the human Carom FBAR domain, based on the structural data of the FBAR domain of CIP4 (PDB: 2EFL, Shimada et al., 2007) and FBP17 (PDB: 2EFK, Shimada et al., 2007). The sequence data base research was conducted with HHpred and the model created with Modeller and edited with OpenSource Pymol 1.3.

The model coincides with the secondary structure analysis performed by CD spectroscopy (Fig. 7.46). The CD spectrum was recorded at room temperature at a wavelength ranging from 190 to 260 nm.

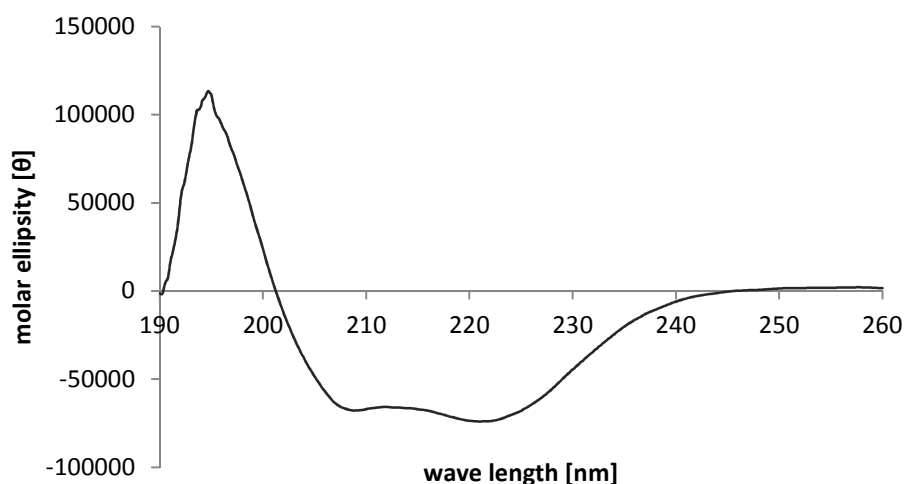


Fig. 7.46: Secondary structure analysis of the human Carom FBAR domain by CD-spectroscopy

For the measurement the Carom FBAR protein (0.5 mg/ml) was diluted in 20 mM Tris pH 8.0 and 50 mM NaF buffer and 10 spectra were recorded on a Jasco Spectrometer J-810 at room temperature. The resulting spectrum was averaged.

The obtained spectrum shows a curve with two minima at 208 and 222 nm that is typical for α -helical proteins.

7.2.1.2 First crystals for the human Carom FBAR domain

Since the biophysical characterization of the Carom FBAR domain showed the protein to be properly folded, it was set up for crystallization. This was done using the following Qiagen Nextal Screens: Classic Suite I and II, PEGs Suite I and II, Protein Complex Suite, JCSG Suite, PACT Suite and the Cryos Suite. The crystallisation set up yielded small rectangular native crystals. Analysis of the crystals presented the best data set at 2.8 Å in 0.1 M Bis-Tris pH 5.5, 25 % PEG 3350 and 0.1 M NH₄OAc (highlighted in Tab. 7.8).

Tab. 7.8: Crystallization conditions with Carom FBAR domain crystals

CRYSTALLIZATION CONDITIONS	DIFFRACTION
0.1 M HEPES 1.4 M tri-sodium citrate	no diffraction
0.1 M sodium cacodylate 5% PEG 800 40% 2-methyl-2,4-pentanediol	3.5 Å
0.1 M Bis-Tris pH 5.5 25% PEG 3350 0.1 M NH ₄ OAc	2.8 Å
30% PEG 1500	6 Å
0.1 M Bis-Tris pH 6.5 0.2 M NaCl 25% PEG 3350	no diffraction
0.1 M HEPES pH 7.5 0.1 M NaOAc 22% PEG 4000	no diffraction
2.1 M DL-malic acid pH 7.0	no diffraction

To increase the quality of the diffracting crystals, the purified Carom FBAR domain was subjected to extensive crystallisation screens with different buffers, salts as well two differently sized PEGs (Tab. 7.9). The initial condition is highlighted in Tab. 7.8 and was varied in its buffer concentrations (0.1 M - 0.4 M), its pH range (pH 5 - 7.2) as well as in the precipitant concentration (18 % - 33 %). All conditions were set up as duplicates at room temperature and at 4 °C. Despite this effort, no better diffracting crystals were obtained by varying the initial condition.

Tab. 7.9: Variation of the crystallization conditions for initial set up of the Carom FBAR domain

BUFFER	Bis-Tris	Acetate	Phosphate	Citrate
CONCENTRATION	0.1 M-0.4 M	0.1 M-0.4 M	0.1 M-0.4 M	0.1 M-0.4 M
PH RANGE	5.0-7.2	3.6-5.6	5.0-8.0	3.0-6.2

SALT	NH ₄ OAc	NaOAc	Mg(OAc) ₂
CONCENTRATION	0.1 M-0.4 M	0.1 M-0.4 M	0.1 M-0.4 M

PRECIPITANT	18%-33% PEG 3350	28%-32% PEG 1500	28%-32% PEG 6000
-------------	---------------------	---------------------	---------------------

TEMPERATURE	room temperature	4 °C
-------------	---------------------	------

An attempt was made to resolve the 2.8 Å crystal data set by molecular replacement with the help of the available structures of the FBAR domains of CIP4 (PDB: 2EFK, Shimada et al., 2007) and FBP17 (PDB: 2EFL, Shimada et al., 2007) as search models. Both proteins are related FBAR domains to the human Carom FBAR domain, with a mere sequence identity of 12 % and 17 % and a shorter length compared to the FBAR domain of Carom. Unfortunately, the molecular replacement effort did not lead to any results.

Another approach to solve the structure of the Carom FBAR domain was applied by soaking experiments with platinum and mercury salts with reproduced crystals from the native condition, which originally yielded the 2.8 Å data set. Heavy metal soaking relies on the fact that molecules diffuse into the protein crystal and bind to the crystal lattice. Typically, numerous heavy atom salts must be screened before one is found to bind to the crystal without damaging the crystal lattice. Here, platinum and mercury salts from the Hampton Research Heavy Atom Screens were applied, according to their minimum pH (Tab. 7.10). This screen was designed to offer convenient sets of popular heavy atom compounds. For the soaking experiments the crystals were transferred from the mother liquor to the solution with 10 mM of the heavy atom salt and incubated either for few hours or overnight.

Tab. 7.10: Heavy atom screen for the Carom FBAR domain

HEAVY ATOM SCREEN	DIFFRACTION
PLATINUM	
Pt1	4.5 Å
Pt2	7 Å
Pt3	4-5 Å
Pt4	3.5-4 Å
Pt5	no diffraction
Pt6	no diffraction
Pt8	5-6 Å
Pt10	no diffraction
Pt12	no diffraction
MERCURY	
Hg2	no diffraction
Hg3	no diffraction

Even though several platinum salts bound to the protein and crystals were obtained, the structure could not be solved from the resulting crystallisation data.

Therefore, selenomethionine-labelled protein was purified and subjected to crystallization screenings for experimental phasing. The protein was overexpressed in bacteria, grown in medium containing selenomethionine as the only source of methionine. This allows for the complete replacement of the methionine residues by selenomethionine in the protein. Selenomethionine-substituted proteins can be solved with the multi-wavelength anomalous dispersion (MAD) method. This method resulted in the growth of small rectangular crystals in different crystallization setups (Tab. 7.11).

Tab. 7.11: Crystallization conditions of the selenomethionine-substituted Carom FBAR domain and the obtained diffraction data sets

CRYSTALLIZATION CONDITIONS	DIFFRACTION	RESULT
0.2 M Ca(OAc) ₂ 0.1 HEPES pH 7.5 10% PEG 8000	10 Å	could not be solved
0.2 M CaCl ₂ 0.1 M HEPES pH 7.5 28% PEG 400	3 Å too small cell?	could not be solved
0.1 M Tris pH 8.5 0.2 M MgCl ₂ 15% PEG 4000	9 Å	could not be solved

Crystals from 0.1 M Tris pH 8.5, 0.2 M MgCl₂ and 15 % PEG 4000 diffracted to a resolution of 9 Å. Another crystal from 0.2 M CaCl₂, 0.1 M HEPES pH 7.5 and 28 % PEG 400 diffracted to a resolution of 3 Å. But processing of the data set resulted in a small unit cell, which did not fit the Carom FBAR domain. However, performed mass spectrometry analysis of the selenomethionine crystals showed that the crystals were indeed composed of the Carom FBAR domain. Additional screenings did not lead to any crystals providing better diffraction by using the selenomethionine labelled crystals.

Finally, the obtained native crystals were identified with molecular replacement as tetrameric *E. coli* beta carbonic anhydrase, a contaminating protein co-purified from the expression host. This was also confirmed with mass spectrometry analysis.

By varying the crystallization conditions more precisely for the selenomethionine labelled protein, it may be possible to define the structure of the Carom FBAR domain. This information would give new insight into the structural properties and functional mechanism of I-FBAR domains.

7.2.2 MEMBRANE DEFORMING ACTIVITY OF THE HUMAN CAROM FBAR DOMAIN

The FBAR domain of Nervous Wreck from *Drosophila* has been shown to have a negative membrane deforming activity (Becalska et al., 2013). This deforming activity is similar to that of the srGAP family. Both FBAR domains functionally mimic I-BAR domains though they do not bear any detectable sequence homology. To determine the role of the Carom FBAR domain and to compare its function with that of the FBAR domain of srGAP1, *in vitro* assays with GUVs in cooperation with Dr. Aleksander Czogalla (Hertie Institute, Dresden) and Dr. Nathalie Eisenhardt (MPI for Developmental Biology, Tuebingen) were performed.

7.2.2.1 The Carom FBAR domain induces scalloping of giant unilamellar vesicles

The main characteristic of FBAR domains is to bind and bend membranes. In chapter 7.1.3.3 it is shown that the FBAR domain of the zebrafish srGAP1 induces membrane deformations of giant unilamellar vesicles (see Fig. 7.11). The human Carom FBAR domain is implicated to have a similar functional role. To confirm this assumption a GUV assay was performed by Dr. Aleksander Czogalla. GUVs were incubated with the FBAR protein overnight and the reaction chambers were examined with confocal fluorescence microscopy. Figure 7.47 shows the effect

of the human Carom FBAR domain on 0.5 % DiD-labelled, vesicles in comparison to a buffer control.

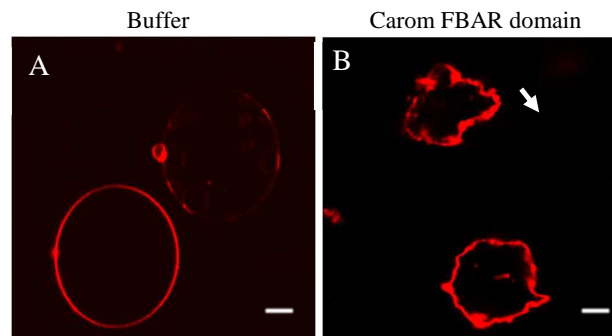


Fig. 7.47: Scalloping of giant unilamellar vesicles by the human Carom FBAR domain

Deformation of DiD-labelled giant unilamellar vesicles (red) after overnight incubation with (A) buffer (20 mM Tris pH 7.5, 300 mM NaCl) and with (B) Carom FBAR domain. Arrows point to deformation. Scale bars: 20 μm.

When incubated with the Carom FBAR domain, vesicles show a strong scalloping (Fig. 7.47 B), compared to the buffer control showing circular GUVs (Fig. 7.47 A). After an overnight incubation at 4 °C, almost 80 % of the giant unilamellar vesicles were deformed in comparison to the control vesicles in buffer. This result supports the assumption that the Carom FBAR domain, like the FBAR domain of the srGAP family, belongs to the novel I-FBAR domain subfamily.

7.2.2.2 The Carom FBAR domain binds to giant unilamellar vesicles

By varying the experimental set up, I wanted to examine if the deformations of the GUVs are specifically induced upon binding of the Carom FBAR domain. For this I performed an additional GUV assay with Alexa-488-labelled FBAR protein with the help of Dr. Nathalie Eisenhardt. Two different kind of vesicles were generated: first using vesicles from the Endo-Mix, containing negatively charged lipids, (Fig. 7.48) and secondly vesicles containing Folch I + 5 % PIP₂ (Fig. 7.49). Both were labelled with 0.5 % DiD. I then used Alexa-488-C5-maleimide to label the thiol groups of the 7 cysteine residues in the Carom FBAR domain. The protein was incubated with the dye for 2 h at 25 °C. Then the reaction was inhibited with 1 M β-ME and free dye was separated from the labelled protein by a Sephadex G50 column. The vesicles were incubated overnight at 4 °C with buffer or the Carom FBAR domain. The reaction chambers containing the vesicles were imaged with two channels, Alexa-488 and DiD.

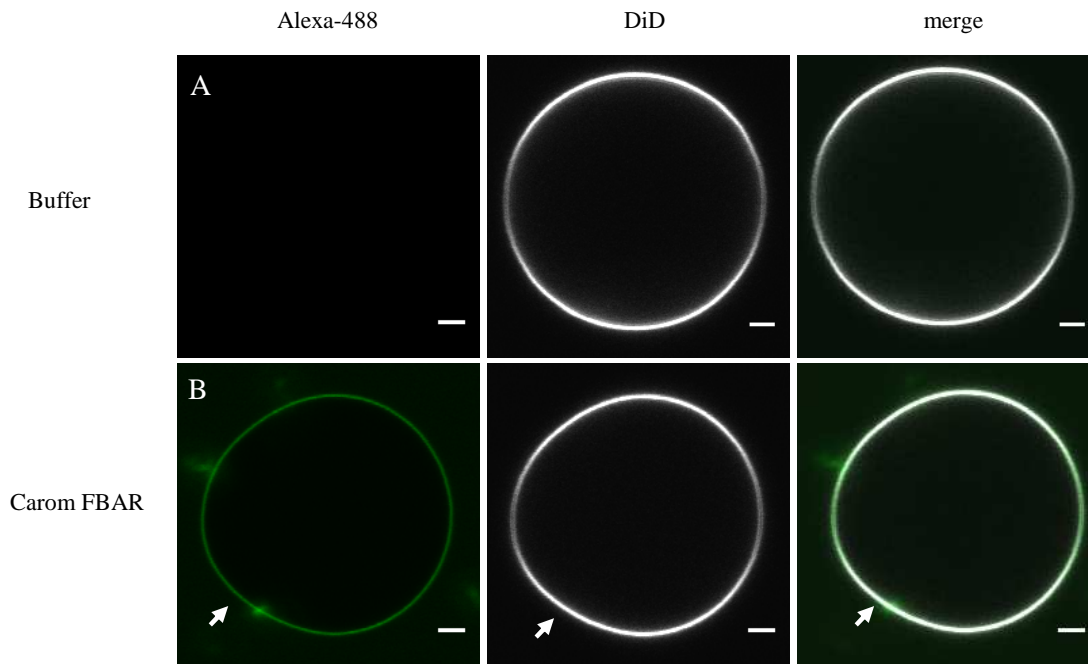


Fig. 7.48: The Carom FBAR domain deforms giant unilamellar vesicles composed of negatively charged lipids

For the GUV assay Endo-Mix DiD-labelled giant unilamellar vesicles (white) were incubated with (A) buffer (20 mM Tris pH 7.5, 300 mM NaCl) as negative control and (B) the Alexa-488 labelled FBAR domain of the human Carom protein (green). Binding of the Carom FBAR domain to vesicles is accompanied by slight deformation effects, indicated with an arrow. Scale bars: 20 μ m.

Control vesicles generated from negatively charged lipids show no signal in the Alexa-488 channel (Fig. 7.48 A). Incubation with the FBAR domain lead to slight deformations of the vesicles (Fig. 7.48 B). This can be attributed to the FBAR domain, which is observed as a clear signal in the Alexa-488 channel. In the next step, the effect of the Carom FBAR domain on vesicles generated from Folch I with 5 % PIP₂ was examined, in order to determine if vesicles composed of a different lipid mix show the same effect when incubated with the human Carom FBAR (Fig. 7.49).

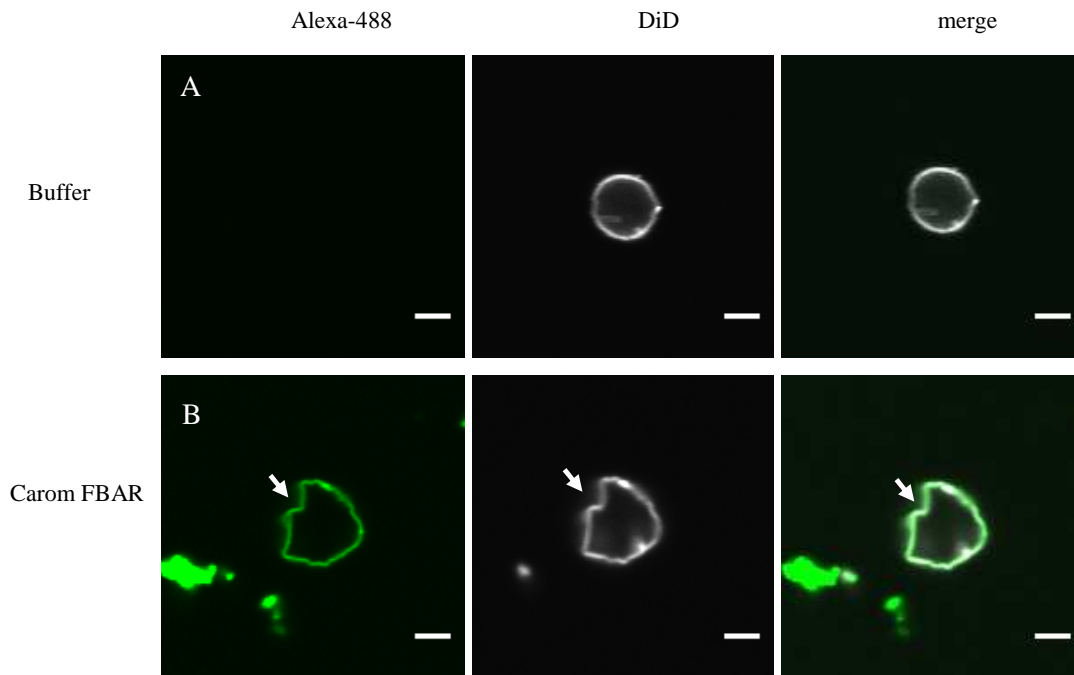


Fig. 7.49: Scalloping of giant unilamellar vesicles composed of Folch I and 5 % PIP₂ by the human Carom FBAR domain
 Giant unilamellar vesicles were generated from Folch I + 5 % PIP₂ and labelled with 0.5 % DiD. (A) Vesicles incubated with buffer (20 mM Tris pH 7.5, 300 mM NaCl) (B) Vesicles incubated with Alexa-488 labelled Carom FBAR domain. Arrows point to deformation. Scale bars: 20 μm.

GUVs containing labelled Carom FBAR domain are clearly visible in the Alexa-488 channel showing severe deformation (Fig. 7.49 B), whereas the control is not affected (Fig. 7.49 A). The results indicate that the FBAR domain binds to the vesicles and induces scalloping. The higher level of deformation for the Folch I and 5 % PIP₂ generated GUVs can be explained by the higher amount of PIP₂ in the vesicle preparation and a higher affinity to Folch I lipids. With the Alexa-488-labelled protein it could be clearly shown, that the deformation of the vesicles is indeed induced by the FBAR domain of the human Carom protein.

7.2.2.3 Time-dependence of the deformation of giant unilamellar vesicles by the Carom FBAR domain

In the following, the time frame, in which the deformations of the GUVs become apparent was examined. The assay was carried out by Dr. Aleksander Czogalla. Vesicles were generated from negatively charged lipids. The assay was performed in a time frame of 24 h and images were taken after 5 h, >5 h and 24 h incubation with the Carom FBAR domain (Fig. 7.50).

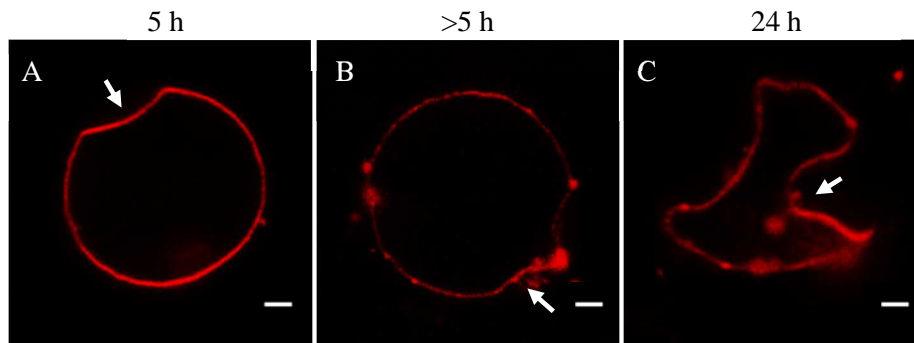


Fig. 7.50: Time-dependent deformation of giant unilamellar vesicles by the Carom FBAR domain

Vesicles (red), generated from negatively charged lipids and labelled with 0.5 % DiD were incubated with the Carom FBAR domain for 5h (A), >5h (B) and overnight (C) at 4 °C. Deformation are indicated with an arrow. Scale bars: 20 μ m.

Strong deformation was observed after an overnight incubation (Fig. 7.50 C). Figure 7.50 A shows a slight deformation after 5 h, though it is possible that the deforming processes start earlier. It seems that the Carom FBAR domain induces deformations of vesicles in a time-dependent manner.

Taken together, the functional analysis of the FBAR domain of the human Carom protein implicated a negative membrane deforming activity. I was able to show this in *in vitro* assays with GUVs. The different degree of scalloping in the performed experiments could be attributed to different stocks of lipids used for generating the vesicles. All results indicate an inverse FBAR activity for the FBAR domain of Carom, similar to the results of the Nervous Wreck FBAR domain scalloping and the srGAP1 FBAR domain. The membrane deforming activity of the Carom FBAR domain seems to be stronger, than the activity of the srGAP1 FBAR domain and more comparable to the scalloping induced by the FBAR domain of Nervous Wreck (Becalska et al., 2013). Determination of the structure of the Carom FBAR domain would have supplemented detailed information about the shape of the FBAR domain. The current findings indicate a potential new member in the inverse FBAR subfamily.

8. DISCUSSION

The srGAP family is known to be involved in Slit-dependent axon repulsion as well as in the regulation of neuronal migration, neuronal morphology, spine maturation and synaptic plasticity (Bacon et al., 2011; Carlson et al., 2011; Charrier et al., 2012; Guerrier et al., 2009; Soderling et al., 2002; Soderling et al., 2007, Wong et al., 2011). Two members of the srGAP family, srGAP2 and 3 have been implicated in severe mental illnesses, such as mental retardation and the neurodevelopmental syndrome, indicating a crucial role of this protein family during brain development (Carlson et al., 2011; Saitsu et al., 2011). The FBAR domain of this family shares functional properties with the I-BAR domains of IRSp53 and MIM by inducing membrane protrusion instead of membrane invaginations as observed for classical FBAR domains (Couthino-Budd et al., 2011; Frost et al., 2007; Itoh et al., 2005; Mattila et al., 2007; Millard et al., 2007; Saarikangas et al., 2009). Recent studies functionally define the srGAP family as part of a new subgroup in the BAR superfamily, the I-FBAR domain containing proteins (Carlson et al., 2011; Couthino Budd et al., 2011).

In this thesis, I focused on the biochemical, structural and functional characterization of human and zebrafish srGAP1 proteins as well as on the FBAR domain of human Carom. In the following chapters the role of the srGAP1 protein and the resulting function will be highlighted and critically analysed.

8.1 *SRGAP1* IS EXPRESSED IN NEURONAL TISSUES OF ZEBRAFISH EMBRYOS

Members of the srGAP family are involved in neuronal processes, such as repulsive axon guidance and neuronal migration (Endris et al., 2011). Few studies show information about the expression and distribution of *srgaps*, though this might provide us with new clues to the function of this family. In this thesis, the expression sites of *srgap1* were analysed for the first time in zebrafish embryos. The developmental and tissue-specific expression analysis showed that *srgap1* is mainly expressed in neuronal tissues in zebrafish embryos supporting its involvement in neuronal processes. In previous studies the expression patterns of *srgap1* were analysed in mouse and rat embryos as well as human foetuses, showing preferential expression in neuronal tissue as well, indicating a conserved expression pattern for *srgap1* (Tab. 8.1) (Bacon et al., 2009; Ip et al., 2011; Wong et al., 2001).

Tab. 8.1: Summary of known expression sites of *srgap1*

	zebrafish (this thesis)	Mice	rats	Human
Expression sites	Forebrain	Cerebellar plate	Subventricular zone (forebrain)	Subventricular zone
	Hindbrain	Cortical plate		Intermediate zone
	Midbrain	Dorsal root ganglia		Corticospinal axons
	Olfactory bulb	Olfactory bulb		
	Pectoral fins	Spinal cord		
	Retina			
	Spinal cord			
	Ventricular zone			
	Tail			

In this work it is shown that in early hours of the zebrafish development (16 hpf) *srgap1* is expressed more broadly, whereas in later stages (24 - 48 hpf) the expression sites concentrate to the head region. The expression of *srgap1* appears to be evenly distributed and not to be localized to specific areas, such as in the olfactory epithelium and specific nuclei in the hindbrain, as it could be shown for *robo2*. When later stages than 48 hpf were analysed the expression sites of *srgap1* were hardly detectable. This can be either caused by less penetration of the mRNA probe or a reduced level of *srgap1* expression. Analysis of co-localization with *robo1*, *robo2* and *robo3* resulted in distinct overlapping expression sites with *robo1* in the fore- and hind brain area as well as in the spinal cord. This might be an indication for a possible interaction of both proteins or at least the participation of srGAP1 in pathways in which Robo1 is involved in, such as axon pathfinding and axon branching.

8.2 THE SRGAP1 FBAR DOMAIN BELONGS TO THE INVERSE-FBAR SUBFAMILY

An important aspect of neuronal migration including motility, cell division and cell communication is the remodelling of membranes. Proteins can bind to membranes, impose, stabilize or preferentially bind specific membrane curvatures. Besides this, they can recruit additional effector functions to specific regions of the cell (Henne et al., 2007). There are several known membrane binding domains C1, C2, PH, FYVE, PX and ENTH (Hurley et al.,

2006). Lately, proteins with a membrane binding BAR domain have emerged (Chitu and Stanley, 2007; Itoh and De Camilli, 2006; McMahon and Gallop 2005). BAR domain containing proteins bind to membranes and induce in dependence of the type of the BAR domain membrane invaginations or membrane protrusions (Fig. 8.1). BAR, N-BAR and FBAR domains induce tubular membrane invaginations, whereas I-BAR domains lead to membrane protrusions.

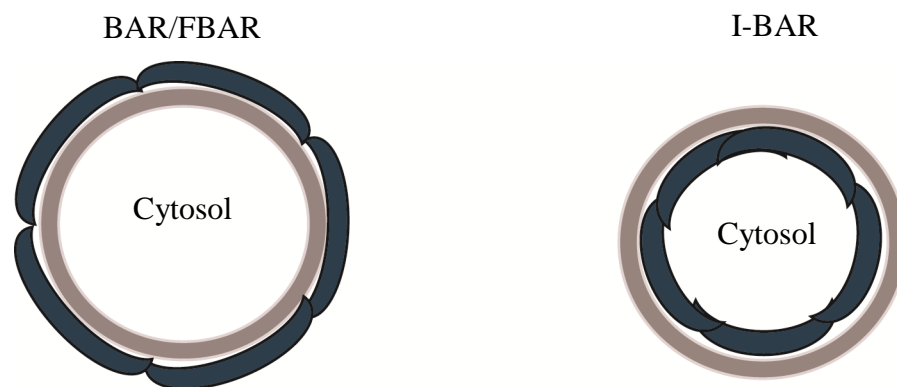


Fig. 8.1: Model of membrane deformation

Possible mechanism for membrane deformation by BAR/FBAR domains and I-BAR domains. The membrane is depicted in brown and the membrane binding domain in blue. Classical BAR or FBAR domains bind with their concave surface to the membrane and thereby lead to membrane invagination, whereas I-BAR domains bind to the inner-leaflet of the membrane with their convex interface and lead to membrane protrusion (modified, Scita et al., 2007).

In this thesis, the FBAR domain of srGAP1 has been characterised biochemically and functionally. Using a GUV-based *in vitro* system, a negative regulation of membrane deformation by the FBAR domain of srGAP1 has been demonstrated. When incubated with GUVs the srGAP1 FBAR domain leads to inward deformations of the vesicles. This observation coincides with functional *in vivo* studies concerning other members of the srGAP family, which show that the srGAP FBAR domain acts not in its classical way by inducing membrane invagination, but rather leads to membrane protrusions upon binding. A recent *in vivo* study in cortical neuron and Cos7 cells with all three members of the srGAP family, demonstrated that the degree of membrane protrusion varies among the members. In this context it was shown that srGAP2 seems to induce stronger filopodia formation compared to srGAP1 and 3 (Couthino-Budd et al., 2012; Endris et al., 2011; Guerrier et al., 2009). In general it was noted, that srGAP1 is less potent in inducing filopodia like structures when expressed in cells. Therefore, it seems to be more important for membrane stabilization as opposed to membrane deformation during expression in cortical neuron cells (Couthino-Budd et al., 2012). The ability of the srGAP1 FBAR domain to induce membrane invagination, when incubated with liposomes or giant unilamellar vesicles, is reminiscent of the activity of the presumably structurally related I-BAR domain containing proteins (Mattila et al., 2007, Millard et al., 2007, Saarikangas et al., 2009 and Scita et al., 2008). The I-BAR domain

of Pinkbar induces planar or gently curved membrane structures similar to the srGAP1 FBAR domain. It was suggested that the Pinkbar I-BAR domain oligomerizes, thus deforming cellular membranes (Pykäläinen et al., 2011). This result is consistent with the proposed mechanism of coat formation of F-BAR domains, in which multiple interactions, including lateral and tip-to-tip contacts, contribute to the stabilization of F-BAR domain coats on membranes (Frost et al., 2008). If this is also the case for the srGAP1 FBAR domain has to be examined.

One explanation for the behaviour of the srGAP FBAR domains, deviating from other BAR domains could be a different curvature of the FBAR domains, which lead to a different distribution of positively charged residues on the surface, similar to that of the I-BARs (Guerrier et al., 2009). The extent of membrane deformation seems to be also dependent on the flanking sequences of the FBAR domain. For Amphiphysin it was reported that it performs different functions in cellular context depending on its flanking sequences (Itoh and Camilli, 2006). To analyse this in more detail, structural data of the srGAP1 FBAR domain are necessary. In a previous study a structural model for the srGAP3 FBAR domain was created based on alignments with the FBAR domains of FBP17, CIP4, and FCHo2. Divergence from the canonical FBAR domains was suggested through multiple sequence alignments, which showed that residues which were identified to interact with membrane lipids were not conserved in the srGAP3 FBAR domain. The structural model provides an estimation of the srGAP3 FBAR domain, which seems to be less curved compared to the solved FBAR domains (Carlson et al., 2011). From the obtained functional data in this thesis, it can be assumed that this FBAR domain, therefore, might be less curved and more planar than other characterized FBAR domains.

Another factor, which could influence the membrane binding activity of the FBAR domain, is a potential autoinhibition. A mutation in the SH3 domain of srGAP2 reduced neurite branching. A complete lack of the SH3/C-terminal part restored the ability to inhibit neurite branching. This contradictory finding suggested that the SH3 and C-terminal domain could block the srGAP2 FBAR dimerization and thus prevent binding to the membrane (Coutinho-Budd et al., 2011) (Fig. 8.2). This autoinhibitory mechanism is observed for FBAR domain-containing proteins, like syndapin 1, endophilin and amphiphysin (Meinecke et al., 2013; Rao et al., 2010), as well as RhoGAP proteins, like GRAF and Oligophrenin-1 (Eberth et al., 2009). For the FBAR domain of syndapin 1 crystallographic analysis revealed a basic interaction surface on the FBAR domain, which interacts with the acidic surface on the SH3 domain. Also cell assays with Cos7 cells showed that the full-length syndapin 1 shows no

membrane tubule formation in contrast to the truncated syndapin 1, containing only the FBAR domain. Binding of dynamin to the SH3 domain releases the inhibition of the SH3 domain on the syndapin 1 FBAR domain (Rao et al., 2010). Similar results were described for the FBAR domains of endophilin and amphiphysin, which also contain a C-terminal SH3 domain (Meinecke et al., 2013). Oligophrenin-1 and GRAF contain a GAP domain instead of a SH3 domain. Here, a fluorescence-based GTP-hydrolysis assay showed that the GAP domains alone increased the intrinsic hydrolysis rate of the GTPase Cdc42, whereas a longer protein construct with the FBAR and the GAP domain reduced the stimulation of the intrinsic hydrolysis rate of the GTPase by 50-fold. In this case the BAR domain itself is the inhibiting factor, though it is also suggested that the GAP domain binding stabilizes the dimerization state of the FBAR domain (Eberth et al., 2009).

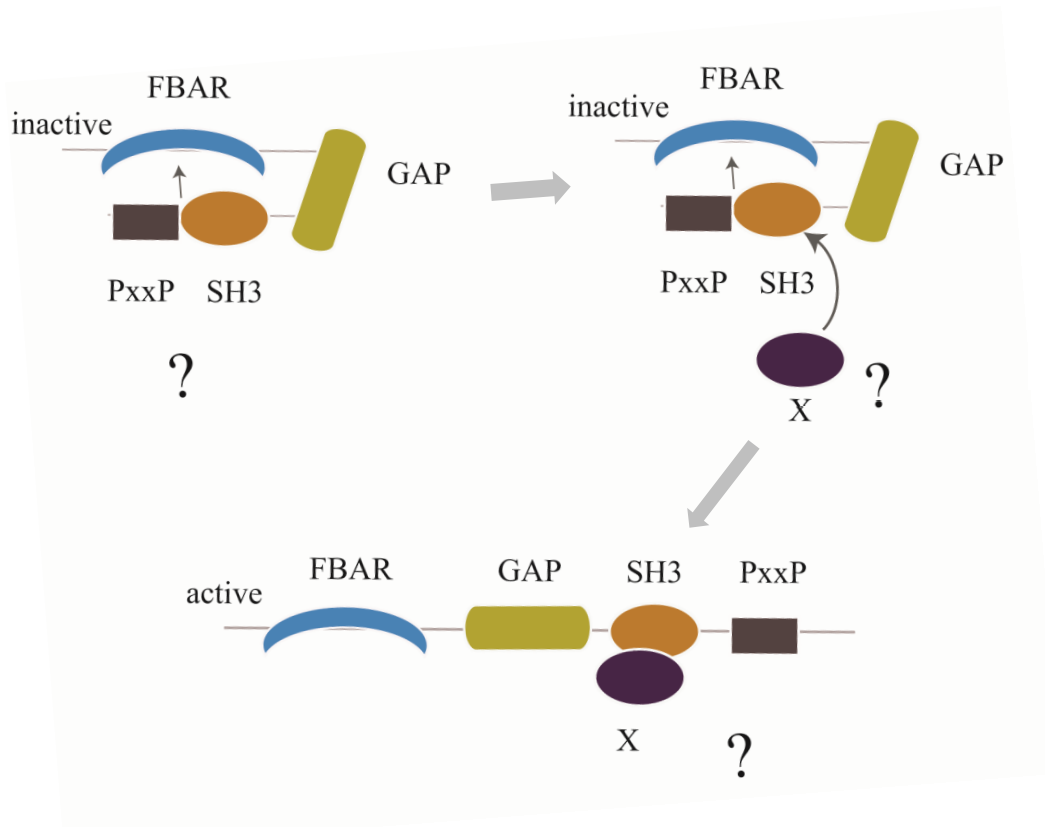


Fig. 8.2: Possible autoinhibition mechanism for the srGAP FBAR domain

Model for the auto-inhibition mechanism of the srGAP FBAR domain by SH3 and C-terminal domain. The autoinhibition is abolished upon binding of an effector X to the SH3 domain (modified, Guerrier et al., 2012).

For the srGAP family it is assumed that the autoinhibition is probably abolished through effector binding to the SH3/C-terminal domain. Whether the proposed mechanism is indeed the case for the srGAP1 has to be investigated. It would be also interesting to examine if the FBAR of the srGAP1 protein has an inhibitory effect on its GAP domain, like it is described for GRAF and Oligophrenin-1 (Meinecke et al., 2013).

The GUV-based *in vitro* analysis of the FBAR domain of the human Carom protein, led to scalloping of the GUVs upon incubation with the FBAR domain. When the srGAP1 FBAR domain was incubated with GUVs under same condition a lower extent of deformation could be observed, which would confirm the assumption that the srGAP1 FBAR domain might be less curved and might have a weaker affinity to the vesicles. For both proteins the GUV assay was more suitable than EM assays with liposomes. The bigger size of the vesicles in the GUV assay, allowed a better observation of the deformation than it was possible in the EM assays with the much smaller liposomes. Liposomes are more suitable to visualize outward tubulation than inward deformation. Early 2013, a novel study described the FBAR domain of the *Drosophila* protein-Nwk, which is phylogenetically closely related to the srGAP family and which is an orthologue of Carom. It reported flattening and scalloping of GUVs, when incubated with the FBAR domain of Nwk (Becalska et al., 2013). This suggested a novel higher order structure and membrane-deforming activity for the Nwk FBAR domain separating it from previously described FBAR proteins and demonstrating relation to the activity of the FBAR domain of the srGAP family and the Carom protein.

In my *in vitro* assays using a higher amount of PIP₂ led to a stronger deformation of the vesicles in contrast to assays with a lower amount of PIP₂. Previous *in vitro* studies with BAR domain containing proteins, suggested a high affinity of BAR domains to phospholipid-containing liposomes (Itoh et al., 2005). Association with PIP₂ is highly favoured by BAR domains and the extent of tubulation is dependent on the PIP₂ concentration. Based on the fact that PIP₂ shows a 25fold higher abundance in the plasma membrane, the latter is most likely the physiological binding partner of FBARs in the cell (Mattila et al., 2007). For the FBAR domains of srGAP1 and Carom this specificity has not been confirmed so far by measuring dose-dependent binding of both FBAR domains to PIP₂ containing membranes.

The BAR domain is a dimerization, membrane-binding and curvature-sensing domain, which can be found in many different protein contexts. Its ability to sense membrane curvature led to the assumption of a specific mechanism for spatial and temporal compartmentalisation of proteins to specific membrane domains. With the results obtained in this project an I-FBAR activity for the srGAP1 FBAR domain as well as for the Carom FBAR domain could be shown. The observation that both proteins do not exhibit inward tubulation on GUVs as shown for IRSp53 (Saarikangas et al., 2009) and also do not show the outward tubulation typical for other FBAR domains, makes them unique in their membrane binding activity. However, the mechanism of the FBAR assembly and the way, they control membrane deformation, is still unknown and needs further investigation.

8.3 THE SRGAP1 GAP DOMAIN BINDS TO THE RHO GTPASE CDC42 AND INCREASES ITS INTRINSIC HYDROLYSIS RATE

GTPases are low molecular weight guanine nucleotide binding proteins, which function as binary switches by cycling between an active and an inactive state. The activity of the GTPases is dependent on the GTP/GDP ratio in the cell and can be influenced by different regulatory proteins (Schmidt and Hall, 2002). It has been reported that BAR domain containing proteins interact with GTPases through their BAR domains. The GTPases Arf and Rac, both bind to the BAR domain of Arfaptin (Habermann et al., 2004; Kanoh et al., 1997; Peter et al., 2004; Van Aelst et al., 1996). Members of the Toca family, CIP4 and Toca-1, contain a Cdc42 binding module, called HR1 at the C-terminal part of the FBAR domain (Ho et al., 2004). Several BAR domain containing proteins, like PACSIN2, IRSp53, MIM and Abba show interaction with GTPases as well. However, it is reported that the binding sites for GTPases overlap with the site for PIP₂ binding, hinting towards a competing interaction (Lee et al., 2007; Matilla et al., 2007). There are also several BAR domain-containing protein families having flanking domains, which specifically bind to GTPases. The srGAP family contains a GAP domain next to the FBAR domain. In a previous study using HEK cell assays it was shown that the srGAP1 GAP domain tends to interact with Cdc42 and RhoA (Wong et al., 2001).

In my experiments the srGAP1 FBAR domain does not show any signs of interaction with RhoGTPases, Cdc42, RhoA and Rac1, in GST-pulldown analysis as well as co-expression and co-purification experiments, indicating a specific role for the GAP domain. Several methods were applied, to examine whether a RhoGTPase exists which is specific for the srGAP1 GAP domain. This included the stopped-flow method, fluorescence spectroscopic measurements and HPLC. Unfortunately, none of them showed a clear effect of the GAP domain on the acceleration of the intrinsic GTP hydrolysis activity of any of the RhoGTPases. An explanation for this could be that the used rhodamine labelled nucleotides are not suitable as no significant change of the fluorescence signal could be detected. To determine the activity and specificity of the srGAP1 GAP domain a structural approach based on different NMR methods, here ¹⁹F and ³¹P-NMR, was applied. Using this approach, activity of the srGAP1 GAP domain and a specific interaction with Cdc42 could be shown. Table 8.2 summarizes the specificity of all three members of the srGAP family for one of the three RhoGTPases, Cdc42, RhoA and Rac.

Tab. 8.2: Summary of RhoGTPase family specificity and their detection method for the three members of the srGAP family

srGAP family member	RhoGTPase	Detection method
srGAP1	Cdc42, RhoA only Cdc42	<ul style="list-style-type: none"> • HEK cell assay (Wong et al., 2001) • ³¹P-NMR, ¹⁹F-NMR (this thesis)
srGAP2	Rac1	<ul style="list-style-type: none"> • fluorescent-based GAP assay with purified srGAP2 GAP protein (Guerrier et al., 2009)
srGAP3	Rac1	<ul style="list-style-type: none"> • ³²P labelled GTPase assay (Soderling et al., 2002) • cerebellar granular neuron assay (Soderling et al., 2002)

The specificity for Cdc42 seems to be conserved in different organisms as both, the zebrafish and the human srGAP1 GAP domains show the same specific interaction with Cdc42. It seems that both GAP domains show full activity only in the presence of species specific Cdc42. The human srGAP1 GAP domain affects the intrinsic hydrolysis rate of the zebrafish Cdc42 to a lower extent with less than 10 % activity compared to the human Cdc42, while the zebrafish srGAP1 GAP domain shows no effect on the intrinsic hydrolysis rate of the human Cdc42. The species specific binding is surprising as the sequence identity between the human and zebrafish Cdc42 is 98 %. Whether this is caused by the last 13 aa, which are missing at the C-terminus of the human Cdc42 protein construct is unclear. Due to its flexibility the C-terminal region of the zebrafish Cdc42 cannot be observed in the HSQC spectrum. This is consistent with a previous published result (Feltham et al., 1997). No peaks emerge in this region after we added the srGAP1 GAP domain. Therefore, it might be assumed that the 13 aa are not important as they are beyond the binding site, which was narrowed down to the Switch I region. In a previous study, in which the crystal structure of Cdc42 was solved, it was noted that the C-terminal region of the protein was disordered and only partly visible in the electron density map. Therefore, it has been assumed that the C-terminal part of the protein is only providing a tail, which anchors the protein in the membrane compartment, a prerequisite for its biological function (Rudolph et al., 1999).

The interaction with Cdc42 possibly connects srGAP1 to processes taking place during cell polarity determination, cell cycle regulation and spine formation. Moreover, through this interaction srGAP1 would be involved in severe illnesses, like cancer by affecting cell migration and invasion and also mental retardation, which is caused by abnormalities during spine formation (Newey et al., 2004; Ramackers et al., 2002; Schmidt and Hall, 2002;).

Affiliation of members of the srGAP family in mental retardation has already been shown for srGAP3 (Endris et al., 2002).

8.4 IDENTIFICATION OF POTENTIAL NEW PATHWAYS FOR THE SRGAP1 PROTEIN

The function of the C-terminal domain of srGAP1 has not been characterized so far. It is assumed that it might act as a protein binding anchor, connecting srGAP1 to other unknown pathways. Bioinformatical analysis of the C-terminal domain of the srGAP1 protein predicted several protein binding motifs for SH3 domains or 14-3-3 proteins. In this study, a screen with GST-tagged srGAP1 C-terminus was performed, to find novel interaction partners for srGAP1. The pull-down was carried out with rat brain tissue and was analysed by mass spectrometry, to identify potential binding partners for the human srGAP1 protein.

Several potential candidates involved in neuronal processes, endocytosis, vesicle transport, cell cycle and actin cytoskeleton regulation have been identified (Fig. 8.3). Some of these proteins have been already reported as potential binding partners for members of the srGAP family.

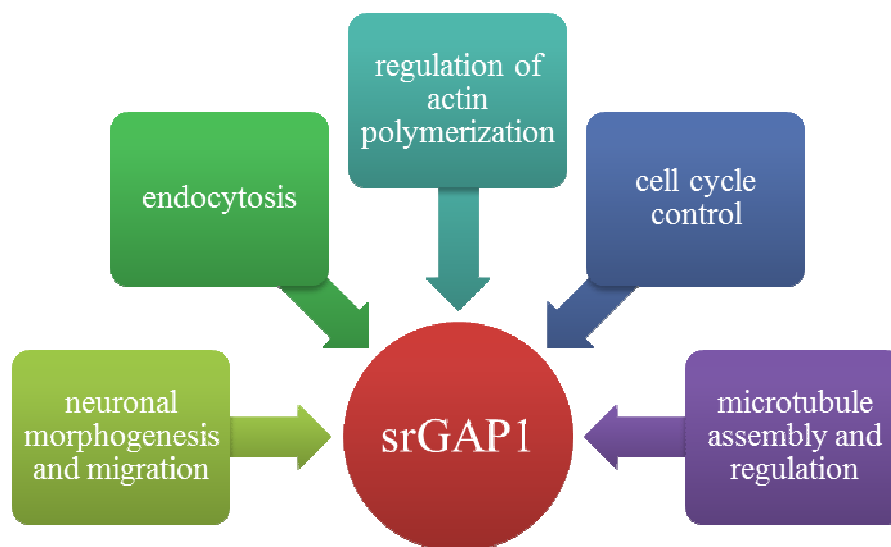


Fig. 8.3: Potential pathway involvements for the srGAP1 protein

The pull-down with rat brain tissue and the analysis of the pull-down with mass spectrometry identified several potential binding partners for srGAP1, which are involved in neuronal morphogenesis and migration, endocytosis, regulation of actin polymerization, cell cycle control and microtubule assembly and regulation.

Many FBAR containing proteins, like FBP17, CIP4, Nwk, Syndapin 1 and PSTPIP bind to N-WASP and Dynamin (Coyle et al., 2004; Itoh et al., 2005; Kessels et al., 2002; Merilainen et al., 1997; Qualmann et al., 1999 and 2000; Tsujita et al., 2006; Wu et al., 1998). Previous

studies also indicated interaction of srGAP2 with the WASP complex, which is involved in filopodia formation (Miki et al., 1998). For srGAP3 an interaction with the related WAVE1 protein was reported (Endris et al., 2011). In this pulldown, members of the WAVE complex, Nck1 and Abi1, have been identified. Although a direct interaction of srGAP1 with both proteins has to be confirmed, it appears to be likely. WAVE is a small G-protein effector that has been shown to be important for actin nucleation, branching of the actin meshwork in lamellipodia (Suetsugu et al., 2003, Yamazaki et al., 2005), which activates the RhoGTPase Rac and the Arp2/3 complex. Other possible interaction partners are different subunits of the 14-3-3 protein family, which are mostly involved in mitotic signal transduction, apoptosis and cell cycle control (Fu et al., 2000; Meek et al., 2004; Tzivion et al., 2001). Here, the subunits gamma, theta and zeta have been identified. For all selected proteins (Tab. 7.6) the identified interaction has to be verified with other methods to show direct interaction. In comparison, the pulldown with zebrafish embryos did not yield a conclusive result as most of the identified proteins were contaminants. One reason for this high number of contaminants might be the degraded target protein. An explanation for this rapid and almost complete degradation of the target protein, can be the presence of mere concentrations of pronase that is applied to the zebrafish embryos for dechorination. Although the embryos are washed afterwards extensively, this does obviously not completely remove the protease. A control gel with the purified fusion protein appeared to be stable. For a future experiment it should be considered to carry out a pulldown with adult zebrafish brains to avoid pronase treatment as well as contamination with muscle tissue and eye-associated proteins as well as yolk-specific proteins. A classical problem of protein mass spectrometry in the assessment of protein complexes is, the difficulty to distinguish real from adventitious protein associations. To verify *in vivo* interaction of the selected mass spectrometry candidates identified in this project, several approaches can be pursued. Performance of co-expression and co-immunoprecipitation assays in HEK or Cos7 cells represent one possibility to eliminate false positive candidates. In such experiments, srGAP1 and its potential interaction partner will be tagged with two different markers, for example GFP and mCherry, and their localization can be analysed with the help of fluorescence microscopy. Co-expressing candidates can then be verified by co-immunoprecipitation experiments or the proteins can be purified and binding affinities could be determined with isothermal titration calorimetry (ITC) or microscale thermophoresis (MST).

In Fig. 8.4 a model showing the possible functions of each domain of the srGAP1 protein is presented. The data obtained within this project clearly show that the FBAR domain of the

srGAP1 protein differs in its membrane binding activity clearly from classical FBAR domains. The extent of the invagination observed in *in vitro* assays, is indicative for a less curved shape of the FBAR domain. This is confirmed with the results obtained for the Carom FBAR domain, showing a complete deformation of giant unilamellar vesicles in contrast pointing to a probably highly curved FBAR domain. The srGAP1 GAP domain specifically binds to Cdc42 and increases its intrinsic hydrolysis activity. The binding site was mapped to the Switch I region of the Cdc42 protein. An additional involvement of the srGAP1 protein in other pathways, like cell migration, signal transduction process, vesicle transport and organization of microtubules besides the Slit-Robo pathway are indicated by the potential binding partners identified by mass spectrometry.

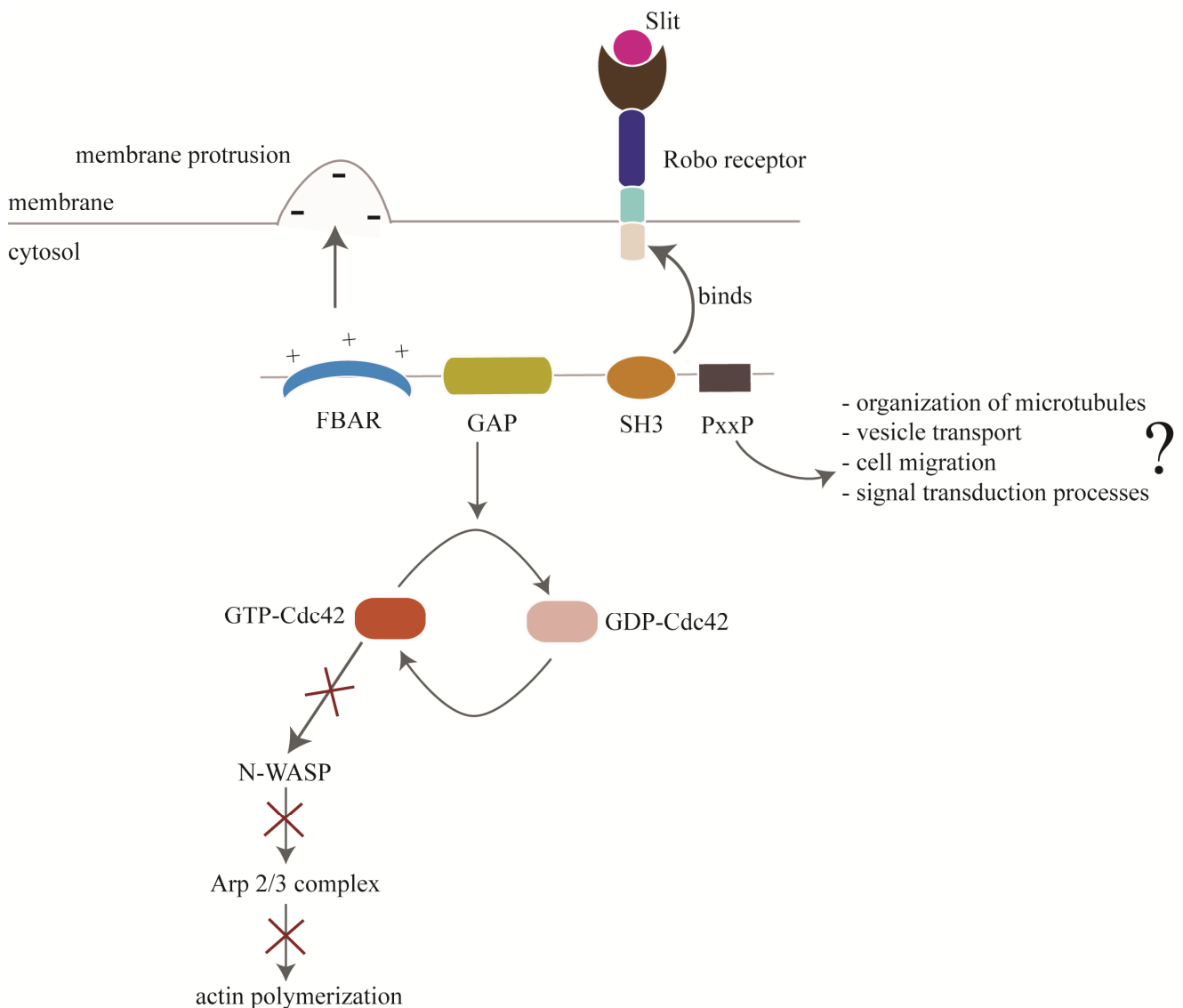


Fig. 8.4: Role of the individual srGAP1 FBAR domains

The members of the srGAP family contain a FBAR, GAP, SH3 and C-terminal domain. The SH3 domain (orange circle) binds to the cytosolic domain of the Robo receptor, thus activating the srGAP1 protein and involving it in the Slit-Robo-pathway, leading to axon repulsion during neuronal development. Activation of the srGAP1 protein leads to an increased activity of its GAP domain (yellow box), which specifically binds to a member of the RhoGTPase family, Cdc42, and increases its intrinsic GTP hydrolysis rate, thus inhibiting all downstream processes and preventing actin polymerization. The FBAR domain (blue half moon) binds with its negatively charged concave surface to the positively charged membrane and leads to membrane bending/deformation. The C-terminal domain contains a PxxP motif and is assumed in protein-protein interaction and thus involving the srGAP1 protein in new pathways (modified, Wong et al., 2001; Hohenester et al., 2008).

The srGAP proteins can be linked to different signal cascades. This is supported by their distinct expression sites in neuronal tissue of mouse and rat embryos as well as human foetuses (Bacon et al., 2009; Ip et al., 2011; Wong et al., 2001) and as shown for *srgap1* in zebrafish embryos in this thesis. The different protein domains of the protein, not only the FBAR domain but also the GAP and C-terminal domain, might work together to implement the srGAP1 protein in signal cascades downstream of Slit and Robo1, as well as connect it to other, related pathways; allowing the control of membrane deformation during neuronal migration.

8.5 OUTLOOK

The results of this thesis confirm and complement previously published data about the srGAP1 protein, which indicated a different membrane binding activity for this protein, and provide new data about the Carom FBAR domain. Here, in contrast to previous studies different types of *in vitro* approaches with GUVs were performed to visualize differences in the membrane binding activities of the srGAP1 and Carom FBAR domain. Both FBAR domains lead to inward vesicle deformation instead of tubule formation. Additional *in vivo* assays with *Cos7* cells or neuronal cells and the structural characterization of these FBAR domains would help to get a deeper understanding of this complex mechanism of membrane binding and deformation, which differs from other examined FBAR domains, such as FBP17 and CIP4. A differently shaped FBAR domain, in contrast to the already known canonical FBAR domains could explain the membrane protruding activity of the srGAP family members. Also the possible autoinhibition of the FBAR domain should be analysed in cell assays with full-length srGAP1 protein and a truncated srGAP1 protein with the FBAR domain only. Similar experiments should be carried out for the Carom protein. When an autoinhibitory effect, possibly indicated by less tubulation of the cells, which express the full-length protein, is observed, direct binding of the FBAR domain to the SH3/C-terminal domain should be examined. Additionally, the effect of the srGAP1 FBAR domain on the activity of its GAP domain should be examined. Therefore, a protein construct with both domains should be purified and its activity tested with the already established ³¹P-NMR measurements. It can be assumed that the activity of the srGAP1 protein relies on the cooperation of its different domains. Furthermore, the characterization of the potential interaction partners, which were identified by mass spectrometry analysis, regarding their binding affinity to srGAP1 would provide new information about possible unknown functions of the srGAP1 protein and contribute to a better understanding of the complex protein network in the cell.

9. REFERENCES

- Ahmadian, M.R., Stege, P., Scheffzek, K., and Wittinghofer, A. (1997). Confirmation of the arginine-finger hypothesis for the GAP-stimulated GTP-hydrolysis reaction of Ras. *Nature structural biology* 4, 686-689.
- Altschul, S.F., Madden, T.L., Schaeffer, A.A., Zhang, J., Zhang, Z., Miller, W. and Lipman D.J. (1997). Gapped BLAST and PSI-BLAST: a new generation of protein data base search programs. *Nucleic Acids Research*, 25 (17), 3389-3402.
- Aspenstrom, P. (2010). Formin-binding proteins: modulators of formin-dependent actin polymerization. *Biochimica et biophysica acta* 1803, 174-182.
- Avci, M.E., Konu, O., and Yagci, T. (2008). Quantification of SLIT-ROBO transcripts in hepatocellular carcinoma reveals two groups of genes with coordinate expression. *BMC cancer* 8, 392.
- Ayala, R., Shu, T., and Tsai, L.H. (2007). Trekking across the brain: the journey of neuronal migration. *Cell* 128, 29-43.
- Bacon, C., Endris, V., and Rappold, G. (2009). Dynamic expression of the Slit-Robo GTPase activating protein genes during development of the murine nervous system. *The Journal of comparative neurology* 513, 224-236.
- Bai, J., Hu, Z., Dittman, J., Pym, E.C.G and Kaplan, J.M. (2010). Endophilin functions as a membrane-bending molecule and is delivered to endocytic zones by exocytosis. *Cell* 143, 430-441.
- Bai, X., Meng, G., Luo, M. and Zheng, X. (2012). Rigidity of wedge loop in PACSIN3 protein is a key factor in dictating diameters of tubules. *Journal of Biological Chemistry*, 287 (26), 22387-96.
- Barnes, A.P., and Polleux, F. (2009). Establishment of axon-dendrite polarity in developing neurons. *Annual review of neuroscience* 32, 347-381.
- Battye, R., Stevens, A., and Jacobs, J.R. (1999). Axon repulsion from the midline of the Drosophila CNS requires slit function. *Development* 126, 2475-2481.
- Becalska, A.N., Kelley, C.F., Berciu, C., Stanishneva-Konovalova, T.B., Fu, X., Wang, S., Sokolova, O.S., Nicastro, D., and Rodal, A.A. (2013). Formation of membrane ridges and scallops by the F-BAR protein Nervous Wreck. *Molecular biology of the cell* 24, 2406-2418.
- Biegert, A., Mayer, C., Remmert, M., Soeding, J., and Lupas, A. (2006). The MPI bioinformatics toolkit for protein sequence analysis. *Nucleic Acids Research*, 34 (web service issue), W137-142.
- Bishop, A.L., and Hall, A. (2000). Rho GTPases and their effector proteins. *The Biochemical journal* 348 Pt 2, 241-255.
- Blasutig, I. (2008). Phosphorylated motif recognition and mechanisms of cell signaling in actin-cytoskeletal regulation.
- Bos, J.L., Rehmann, H., and Wittinghofer, A. (2007). GEFs and GAPs: critical elements in the control of small G proteins. *Cell* 129, 865-877.
- Boucrot, E., Pick, A., Camdere, G., Liska, N., Evergren, E., McMahon, H.T., and Kozlov, M.M. (2012). Membrane fission is promoted by insertion of amphipathic helices and is restricted by crescent BAR domains. *Cell* 149, 124-136.
- Brose, K., Bland, K.S., Wang, K.H., Arnott, D., Henzel, W., Goodman, C.S., Tessier-Lavigne, M., and Kidd, T. (1999). Slit proteins bind Robo receptors and have an evolutionarily conserved role in repulsive axon guidance. *Cell* 96, 795-806.

- Bulow, H.E., and Hobert, O. (2004). Differential sulfations and epimerization define heparan sulfate specificity in nervous system development. *Neuron* 41, 723-736.
- BurrIDGE, K., and Wennerberg, K. (2004). Rho and Rac take center stage. *Cell* 116, 167-179.
- Campbell, D.S., Stringham, S.A., Timm, A., Xiao, T., Law, M.Y., Baier, H., Nonet, M.L., and Chien, C.B. (2007). Slit1a inhibits retinal ganglion cell arborization and synaptogenesis via Robo2-dependent and -independent pathways. *Neuron* 55, 231-245.
- Carlson, B., and Soderling, S.H. (2009). Mechanisms of cellular protrusions branch out. *Developmental cell* 17, 307-309.
- Chabre, M. (1990). Aluminofluoride and beryllifluoride complexes: a new phosphate analogs in enzymology. *Trends in biochemical sciences* 15, 6-10.
- Chandrashekar, R., Salem, O., Krizova, H., McFeeters, R. and Adams P.D. (2011). A switch I mutant of Cdc42 exhibits less conformational freedom. *Biochemistry* 50 (28), 6196-6207.
- Chen, J.H., Wen, L., Dupuis, S., Wu, J.Y., and Rao, Y. (2001). The N-terminal leucine-rich regions in Slit are sufficient to repel olfactory bulb axons and subventricular zone neurons. *The Journal of neuroscience : the official journal of the Society for Neuroscience* 21, 1548-1556.
- Cherfils, J., and Zeghouf, M. (2013). Regulation of small GTPases by GEFs, GAPs, and GDIs. *Physiological reviews* 93, 269-309.
- Chitu, V., Pixley, F.J., Macaluso, F., Larson, D.R., Condeelis, J., Yeung, Y.G., and Stanley, E.R. (2005). The PCH family member MAYP/PSTPIP2 directly regulates F-actin bundling and enhances filopodia formation and motility in macrophages. *Molecular biology of the cell* 16, 2947-2959.
- Chitu, V., and Stanley, E.R. (2007). Pombe Cdc15 homology (PCH) proteins: coordinators of membrane-cytoskeletal interactions. *Trends in cell biology* 17, 145-156.
- Coleman, D.E., Berghuis, A.M., Lee, E., Linder, M.E., Gilman, A.G., and Sprang, S.R. (1994). Structures of active conformations of Gi alpha 1 and the mechanism of GTP hydrolysis. *Science* 265, 1405-1412.
- Cooper, J.A. (2013). Cell biology in neuroscience: mechanisms of cell migration in the nervous system. *The Journal of cell biology* 202, 725-734.
- Corbett, K.D. and Alber, T. (2001). The many faces of Ras: recognition of small GTP-binding proteins. *Trends in Biochemical Science* 12, 710-716.
- Corbin, J.A., Evans, J.H., Landgraf, K.E., and Falke, J.J. (2007). Mechanism of specific membrane targeting by C2 domains: localized pools of target lipids enhance Ca²⁺ affinity. *Biochemistry* 46, 4322-4336.
- Coutinho-Budd, J., Ghukasyan, V., Zylka, M.J., and Polleux, F. (2012). The F-BAR domains from srGAP1, srGAP2 and srGAP3 regulate membrane deformation differently. *Journal of cell science* 125, 3390-3401.
- Cox, J. and Mann, M. (2008). MaxQuant enables high peptide identification rates, individualized p.p.b.-range mass accuracies and proteome-wide protein quantification. *Nature Biotechnology* 26, 1367-1372
- Cox, J., Neuhauser, N., Michalski, A., Scheltema, R. A., Olsen, J. V. and Mann, M. (2011) Andromeda: a peptide search engine integrated into the MaxQuant environment. *Journal of Proteome Research* 10, 1794-1805

- Coyle, I.P., Koh, Y.H., Lee, W.C., Slind, J., Fergestad, T., Littleton, J.T., and Ganetzky, B. (2004). Nervous wreck, an SH3 adaptor protein that interacts with Wsp, regulates synaptic growth in *Drosophila*. *Neuron* 41, 521-534.
- Di Paolo, G., Sankaranarayanan, S., Wenk, M.R., Daniell, L., Perucco, E., Caldarone, B.J., Flavell, R., Picciotto, M.R., Ryan, T.A., Cremona, O., et al. (2002). Decreased synaptic vesicle recycling efficiency and cognitive deficits in amphiphysin 1 knockout mice. *Neuron* 33, 789-804.
- Dickson, B.J., and Gilestro, G.F. (2006). Regulation of commissural axon pathfinding by slit and its Robo receptors. *Annual review of cell and developmental biology* 22, 651-675.
- Dobrosotskaya, I., Guy, R.K., and James, G.L. (1997). MAGI-1, a membrane-associated guanylate kinase with a unique arrangement of protein-protein interaction domains. *The Journal of biological chemistry* 272, 31589-31597.
- Dooley, K., and Zon, L.I. (2000). Zebrafish: a model system for the study of human disease. *Current opinion in genetics & development* 10, 252-256.
- Dvorsky, R., and Ahmadian, M.R. (2004). Always look on the bright site of Rho: structural implications for a conserved intermolecular interface. *EMBO reports* 5, 1130-1136.
- Eberth, A., Lundmark, R., Gremer, L., Dvorsky, R., Koessmeier, K.T., McMahon, H.T., and Ahmadian, M.R. (2009). A BAR domain-mediated autoinhibitory mechanism for RhoGAPs of the GRAF family. *Biochemical Journal* 417, 371-377.
- Echarri, A., Lai, M.J., Robinson, M.R. and Pendergast, A.M (2004). Abl interactor 1 (Abi-1) wave-binding and SNARE domains regulate its nucleocytoplasmic shuttling, lamellipodium localization, and wave-1 levels. *Molecular Cell Biology* 24 (11), 4979-4993.
- Edeling, M.A., Sanker, S., Shima, T., Umasankar, P.K., Höning, S., Kim, H.Y., Davidson, L.A., Watkins, S.C., Tsang, M., Owen, D.J. and Traub, L.M. (2009). Structural requirements for PACSIN/Syndapin operation during zebrafish embryonic notochord development. *PLoS One* 4 (12), e8150.
- Elias, J. E. and Gygi, S. P (2007). Target-decoy search strategy for increased confidence in large scale protein identifications by mass spectrometry. *Nature Methods* 4, 207–214.
- Endris, V., Haussmann, L., Buss, E., Bacon, C., Bartsch, D., and Rappold, G. (2011). SrGAP3 interacts with lamellipodin at the cell membrane and regulates Rac-dependent cellular protrusions. *Journal of cell science* 124, 3941-3955.
- Endris, V., Wogatzky, B., Leimer, U., Bartsch, D., Zatyka, M., Latif, F., Maher, E.R., Tariverdian, G., and Rappold, G.A. (2002). The novel Rho-GTPase activating gene MEGAP has a putative role in severe mental retardation. *Proc Natl Acad Sci U S A* 99: 11754–11759. doi: 10.1073/pnas.162241099
- Etienne-Manneville, S., and Hall, A. (2002). Rho GTPases in cell biology. *Nature* 420, 629-635.
- Fan, X., Labrador, J.P., Hing, H., and Bashaw, G.J. (2003). Slit stimulation recruits Dock and Pak to the roundabout receptor and increases Rac activity to regulate axon repulsion at the CNS midline. *Neuron* 40, 113-127.
- Feltham, J.L., Doetsch, V., Raza, S., Manor, D., Cerione, R.A., Sutcliffe, M.J., Wagner, G., and Oswald, R.E. (1997). Definition of the switch surface in the solution structure of Cdc42Hs. *Biochemistry* 36 (29), 8755-8766.
- Frickey, T. and Lupas, A. (2004). CLANS: a Java application for visualizing protein families based on pairwise similarity. *Bioinformatics* 20, 3702-3704.

- Fröhlich, C., Grabiger, S. Schwefel, D. Faelber, K. and Rosenbaum. E. (2013). Structural insights into oligomerization and mitochondrial remodelling of dynamin 1-like protein. *EMBO Journal* 32 1280–1292.
- Frost, A., De Camilli, P., and Unger, V.M. (2007). F-BAR proteins join the BAR family fold. *Structure* 15, 751-753.
- Frost, A., Perera, R., Roux, A., Spasov, K., Destaing, O., Egelman, E.H., De Camilli, P., and Unger, V.M. (2008). Structural basis of membrane invagination by F-BAR domains. *Cell* 132, 807-817.
- Frost, A., Unger, V.M., and De Camilli, P. (2009). The BAR domain superfamily: membrane-molding macromolecules. *Cell* 137, 191-196.
- Fu, H.A., Subramanian, R.R., and Masters, S.C. (2000). 14-3-3 proteins: Structure, function, and regulation. *Annu Rev Pharmacol* 40, 617-647.
- Gamblin, S.J., and Smerdon, S.J. (1998). GTPase-activating proteins and their complexes. *Current opinion in structural biology* 8, 195-201.
- Gleeson, J.G., Lin, P.T., Flanagan, L.A and Walsh C.A. (1999). Doublecortin is a microtubule-associated protein and is expressed widely by migrating neurons. *Neuron* 23, 257-271.
- Govek, E.E., Newey, S.E., and Van Aelst, L. (2005). The role of the Rho GTPases in neuronal development. *Genes & development* 19, 1-49.
- Graslund, S., Sagemark, J., Berglund, H., Dahlgren, L.G., Flores, A., Hammarstrom, M., Johansson, I., Kotenyova, T., Nilsson, M., Nordlund, P., et al. (2008). The use of systematic N- and C-terminal deletions to promote production and structural studies of recombinant proteins. *Protein expression and purification* 58, 210-221.
- Greenfield, N.J. (2006). Using circular dichroism spectra to estimate protein secondary structure. *Nature Protocols*, 1 (6), 2876-90.
- Grieshammer, U., Le, M., Plump, A.S., Wang, F., Tessier-Lavigne, M., and Martin, G.R. (2004). SLIT2-mediated ROBO2 signaling restricts kidney induction to a single site. *Developmental cell* 6, 709-717.
- Guerrier, S., Coutinho-Budd, J., Sassa, T., Gresset, A., Jordan, N.V., Chen, K., Jin, W.L., Frost, A., and Polleux, F. (2009). The F-BAR domain of srGAP2 induces membrane protrusions required for neuronal migration and morphogenesis. *Cell* 138, 990-1004.
- Guo, S., and Bao, S. (2010). srGAP2 arginine methylation regulates cell migration and cell spreading through promoting dimerization. *The Journal of biological chemistry* 285, 35133-35141.
- Gupta, A., Tsai, L.H., and Wynshaw-Boris, A. (2002). Life is a journey: a genetic look at neocortical development. *Nature reviews. Genetics* 3, 342-355.
- Gupton, S.L., and Gertler, F.B. (2007). Filopodia: the fingers that do the walking. *Science's STKE: signal transduction knowledge environment* 2007, re5.
- Habermann, B. (2004). The BAR-domain family of proteins: a case of bending and binding? *EMBO reports* 5, 250-255.
- Heath, R.J., and Insall, R.H. (2008). F-BAR domains: multifunctional regulators of membrane curvature. *Journal of cell science* 121, 1951-1954.
- Henne, W.M., Kent, H.M., Ford, M.G., Hegde, B.G., Daumke, O., Butler, P.J., Mittal, R., Langen, R., Evans, P.R., and McMahan, H.T. (2007). Structure and analysis of FCHo2 F-BAR domain: a dimerizing and membrane recruitment module that effects membrane curvature. *Structure* 15, 839-852.

- Higashijima, T., Graziano, M. P., Suga, H., Kainosho, M. and Gilman, A. G. (1991) *Journal of Biological Chemistry* 266, 3396–3401
- Ho, H.Y., Rohatgi, R. Lebensohn, A.M., Le, M., Li, J., Gygi, S.P. and Kirschner, M.W. (2004) Toca-1 mediates Cdc42-dependent actin nucleation by activating the N-WASP–WIP complex. *Cell* 118, 203–216
- Hoffman, G.R., Nassar, N., Oswald, R.E. and Cerione, R.A. (1998). Fluoride activation of the Rho family GTP-binding protein Cdc42Hs*. *Journal of biological chemistry* 273 (8), 4392-4399.
- Hohenester, E. (2008). Structural insight into Slit-Robo-signalling. *Biochemical Society transactions* 36, 251-256.
- Hotani, H., Nomura, F., and Suzuki, Y. (1999). Giant liposomes: from membrane dynamics to cell morphogenesis, *Current Opinions Colloid Interface Science* 4, 358-368
- Howitt, J.A., Clout, N.J., and Hohenester, E. (2004). Binding site for Robo receptors revealed by dissection of the leucine-rich repeat region of Slit. *The EMBO journal* 23, 4406-4412.
- Hu, H. (2001). Cell-surface heparan sulfate is involved in the repulsive guidance activities of Slit2 protein. *Nat. Neurosci.* 4, 695-701.
- Humniecki, L., Gorn, M., Suchting, S., Poulosom, R., and Bicknell, R. (2002). Magic roundabout is a new member of the roundabout receptor family that is endothelial specific and expressed at sites of active angiogenesis. *Genomics* 79, 547-552.
- Hummel, T., Schimmelpfeng, K., and Klampt, C. (1999). Commissure formation in the embryonic CNS of *Drosophila*. I. Identification of the required gene functions. *Dev. Biol.*, 381-398.
- Hurley, JH., (2006). Membrane binding domains. *Biochim. Biophys. Acta.* 1761 (8), 805-811.
- Hussain, S.A., Piper, M., Fukuhara, N., Strohlic, L., Cho, G., Howitt, J.A., Ahmed, Y., Powell, A.K., Turnbull, J.E., Holt, C.E., et al. (2006). A molecular mechanism for the heparan sulfate dependence of slit-robo signaling. *The Journal of biological chemistry* 281, 39693-39698.
- Inatani, M., Irie, F., Plump, A.S., Tessier-Lavigne, M., and Yamaguchi, Y. (2003). Mammalian brain morphogenesis and midline axon guidance require heparan sulfate. *Science* 302, 1044-1046.
- Insall, R.H., and Weiner, O.D. (2001). PIP3, PIP2, and cell movement--similar messages, different meanings? *Developmental cell* 1, 743-747.
- Ip, B.K., Bayatti, N., Howard, N.J., Lindsay, S., and Clowry, G.J. (2011). The corticofugal neuron-associated genes *ROBO1*, *SRGAP1*, and *CTIP2* exhibit an anterior to posterior gradient of expression in early fetal human neocortex development. *Cerebral cortex* 21, 1395-1407.
- Itoh, T., and De Camilli, P. (2006). BAR, F-BAR (EFC) and ENTH/ANTH domains in the regulation of membrane-cytosol interfaces and membrane curvature. *Biochimica et biophysica acta* 1761, 897-912.
- Itoh, T., and De Camilli, P. (2006). BAR, F-BAR (EFC) and ENTH/ANTH domains in the regulation of membrane-cytosol interfaces and membrane curvature. *Biochimica et biophysica acta* 1761, 897-912.
- Itoh, T., Erdmann, K.S., Roux, A., Habermann, B., Werner, H., and De Camilli, P. (2005). Dynamin and the actin cytoskeleton cooperatively regulate plasma membrane invagination by BAR and F-BAR proteins. *Developmental cell* 9, 791-804.
- Itoh, T., Erdmann, K.S., Roux, A., Habermann, B., Werner, H., and De Camilli, P. (2005). Dynamin and the actin cytoskeleton cooperatively regulate plasma membrane invagination by BAR and F-BAR proteins. *Developmental cell* 9, 791-804.

- Jackson, R.S., Cho, Y.-J., Stein, S. and Liang P. (2007). Cyfip, a direct p53 target, is leptomycin-B sensitive. *Cell cycle* 6:1, 95-103.
- Janmey, P.A., and Kinnunen, P.K. (2006). Biophysical properties of lipids and dynamic membranes. *Trends in cell biology* 16, 538-546.
- John, J., Sohmen, R., Feuerstein, J., Linke, R., Wittinghofer, A. and Goody, R.S. (1990). Kinetics of interaction of nucleotides with nucleotide-free H-ras p21. *Biochemistry* 29 (25), 6058-6065.
- Jones, N., New, L.A., Fortino, M.A, Eremina, V., Ruston, J., Blasutig, I.M., Aoudjit, L., Zou, Y., Liu, X., Yu, G.L., Takano, T., Quaggin, S.E. and Pawson, T (2009). Nck proteins maintain the adult glomerular filtration barrier. *Journal of the American Society of Nephrology* 20 (7). 1533-1543.
- Kamioka, Y., Fukuhara, S., Sawa, H., Nagashima, K., Masuda, M., Matsuda, M., and Mochizuki, N. (2004). A novel dynamin-associating molecule, formin-binding protein 17, induces tubular membrane invaginations and participates in endocytosis. *The Journal of biological chemistry* 279, 40091-40099.
- Kanoh, H., Williger, B.T., and Exton, J.H. (1997). Arfaptin 1, a putative cytosolic target protein of ADP-ribosylation factor, is recruited to Golgi membranes. *The Journal of biological chemistry* 272, 5421-5429.
- Kaur, S., Abu-Asab, M.S., Singla, S., Yeo, S.Y., and Ramchandran, R. (2007). Expression pattern for *unc5b*, an axon guidance gene in embryonic zebrafish development. *Gene expression* 13, 321-327.
- Keleman, K., Rajagopalan, S., Cleppien, D., Teis, D., Paiha, K., Huber, L.A., Technau, G.M., and Dickson, B.J. (2002). Comm sorts robo to control axon guidance at the *Drosophila* midline. *Cell* 110, 415-427.
- Kessels, M.M., and Qualmann, B. (2002). Syndapins integrate N-WASP in receptor-mediated endocytosis. *The EMBO journal* 21, 6083-6094.
- Kidd, T., Bland, K.S., and Goodman, C.S. (1999). Slit is the midline repellent for the robo receptor in *Drosophila*. *Cell* 96, 785-794.
- Kidd, T., Brose, K., Mitchell, K.J., Fetter, R.D., Tessier-Lavigne, M., Goodman, C.S., and Tear, G. (1998). Roundabout controls axon crossing of the CNS midline and defines a novel subfamily of evolutionarily conserved guidance receptors. *Cell* 92, 205-215.
- Kidd, T., Russell, C., Goodman, C.S., and Tear, G. (1998). Dosage-sensitive and complementary functions of roundabout and commissureless control axon crossing of the CNS midline. *Neuron* 20, 25-33.
- Kimmel, C.B., Ballard, W.W., Kimmel, S.R., Ullmann, B., and Schilling, T.F. (1995). Stages of embryonic development of the zebrafish. *Developmental dynamics: an official publication of the American Association of Anatomists* 203, 253-310.
- Kosloff, M., and Selinger, Z. (2001). Substrate assisted catalysis -- application to G proteins. *Trends in biochemical sciences* 26, 161-166.
- Lasic, D.D. (1995) *Liposomes: from physics to applications*. Elsevier, Amsterdam, 2nd Ed., 63-107.
- Lee, J.S., Ray, R., and Chien, C.B. (2001). Cloning and expression of three zebrafish roundabout homologs suggest roles in axon guidance and cell migration. *Developmental dynamics: an official publication of the American Association of Anatomists* 221, 216-230.
- Lee, S.H., Kerff, F., Chereau, D., Ferron, F., Klug, A., and Dominguez, R. (2007). Structural basis for the actin-binding function of missing-in-metastasis. *Structure* 15, 145-155.

- Li, R., Zhang, B., and Zheng, Y. (1997). Structural determinants required for the interaction between Rho GTPase and the GTPase-activating domain of p190. *The Journal of biological chemistry* 272, 32830-32835.
- Li, R., and Zheng, Y. (1997). Residues of the Rho family GTPases Rho and Cdc42 that specify sensitivity to Dbp-like guanine nucleotide exchange factors. *The Journal of biological chemistry* 272, 4671-4679.
- Li, X., Chen, Y., Liu, Y., Gao, J., Gao, F., Bartlam, M., Wu, J.Y., and Rao, Z. (2006). Structural basis of Robo proline-rich motif recognition by the srGAP1 Src homology 3 domain in the Slit-Robo signaling pathway. *The Journal of biological chemistry* 281, 28430-28437.
- Liu, Z., Patel, K., Schmidt, H., Andrews, W., Pini, A., and Sundaresan, V. (2004). Extracellular Ig domains 1 and 2 of Robo are important for ligand (Slit) binding. *Molecular and cellular neurosciences* 26, 232-240.
- Long, H., Sabatier, C., Ma, L., Plump, A., Yuan, W., Ornitz, D.M., Tamada, A., Murakami, F., Goodman, C.S., and Tessier-Lavigne, M. (2004). Conserved roles for Slit and Robo proteins in midline commissural axon guidance. *Neuron* 42, 213-223.
- Lowery, A. L. and Van Vector, D. (2009). The trip of the tip: understanding the growth cone machinery. *Nature Reviews. Molecular cell biology* 10, 332-343-
- Luo, L. (2002). Actin cytoskeleton regulation in neuronal morphogenesis and structural plasticity. *Annual review of cell and developmental biology* 18, 601-635.
- Lupas, A. N., Van Dyke, M., and Stock, J. (1991). Predicting coiled coils from protein sequences. *Science*, 252 (5009), 1162-1164.
- Lupas, A. (1996) Coiled coils: New structures and new functions. *TIBS* 21, 375-382.
- Madura, T., Yamashita, T., Kubo, T., Tsuji, L., Hosokawa, K., and Tohyama, M. (2004). Changes in mRNA of Slit-Robo GTPase-activating protein 2 following facial nerve transection. *Brain research. Molecular brain research* 123, 76-80.
- Marin, O., Valiente, M., Ge, X., and Tsai, L.H. (2010). Guiding neuronal cell migrations. *Cold Spring Harbor perspectives in biology* 2, a001834.
- Mason, F.M., Heimsath, E.G., Higgs, H.N., and Soderling, S.H. (2011). Bi-modal regulation of a formin by srGAP2. *The Journal of biological chemistry* 286, 6577-6586.
- Mattila, P.K., and Lappalainen, P. (2008). Filopodia: molecular architecture and cellular functions. *Nature reviews. Molecular cell biology* 9, 446-454.
- Mattila, P.K., Pykalainen, A., Saarikangas, J., Paavilainen, V.O., Vihinen, H., Jokitalo, E., and Lappalainen, P. (2007). Missing-in-metastasis and IRSp53 deform PI(4,5)P2-rich membranes by an inverse BAR domain-like mechanism. *The Journal of cell biology* 176, 953-964.
- Maves, L., Jackman, W. and Kimmel C.B. (2002). FGF3 and FGF8 mediate a rhombomere 4 signaling activity in the zebrafish hindbrain. *Development* 129, 3825-3837.
- Mayer, B.J. (2001). SH3 domains: complexity in moderation. *Journal of cell science* 114, 1253-1263.
- McLaughlin, S., Wang, J., Gambhir, A., and Murray, D. (2002). PIP(2) and proteins: interactions, organization, and information flow. *Annual review of biophysics and biomolecular structure* 31, 151-175.

- McMahon, H.T., and Gallop, J.L. (2005). Membrane curvature and mechanisms of dynamic cell membrane remodelling. *Nature* 438, 590-596.
- Medrihan, L., Cesca, F., Raimondi, A., Lignani, G., Baldelli, P. and Benfenati, F. (2013). Synapsin II desynchronizes neurotransmitter release at inhibitory synapses by interacting with presynaptic calcium channels. *Nature Communications* 4:1512.
- Meek, S.E.M., Lane, W.S., and Piwnicka-Worms, H. (2004). Comprehensive proteomic analysis of interphase and mitotic 14-3-3-binding proteins. *Journal of Biological Chemistry* 279, 32046-32054.
- Meinecke, M., Boucrot, E., Camdere, G., Hon, W.C., Mittal, R., and McMahon, H.T. (2013). Cooperative Recruitment of Dynamin and BIN/Amphiphysin/Rvs (BAR) Domain-containing Proteins Leads to GTP-dependent Membrane Scission. *Journal of Biological Chemistry* 288, 6651-6661.
- Merilainen, J., Lehto, V.P., and Wasenius, V.M. (1997). FAP52, a novel, SH3 domain-containing focal adhesion protein. *The Journal of biological chemistry* 272, 23278-23284.
- Miki, H., Suetsugu, S., and Takenawa, T. (1998). WAVE, a novel WASP-family protein involved in actin reorganization induced by Rac. *The EMBO journal* 17, 6932-6941.
- Millard, T.H., Bompard, G., Heung, M.Y., Dafforn, T.R., Scott, D.J., Machesky, L.M., and Futterer, K. (2005). Structural basis of filopodia formation induced by the IRSp53/MIM homology domain of human IRSp53. *The EMBO journal* 24, 240-250.
- Mim, C., Cui, H.S., Gawronski-Salerno, J.A., Frost, A., Lyman, E., Voth, G.A., and Unger, V.M. (2012). Structural Basis of Membrane Bending by the N-BAR Protein Endophilin. *Cell* 149, 137-145.
- Mittal, R., Ahmadian, M.R., Goody, R.S., and Wittinghofer, A. (1996). Formation of a transition-state analog of the Ras GTPase reaction by Ras-GDP, tetrafluoroaluminate, and GTPase-activating proteins. *Science* 273, 115-117.
- Moens, C.B. and Prince, V.E. (2002). Constructing the hindbrain: insights from the zebrafish. *Development Dynamics* 224 (1), 1-17.
- Miyasaka, N., Sato, Y., Yeo, S.Y., Hutson, L.D., Chien, C.B., Okamoto, H., and Yoshihara, Y. (2005). Robo2 is required for establishment of a precise glomerular map in the zebrafish olfactory system. *Development* 132, 1283-1293.
- Moon, S.Y., and Zheng, Y. (2003). Rho GTPase-activating proteins in cell regulation. *Trends in cell biology* 13, 13-22.
- Morlot, C., Thielens, N.M., Ravelli, R.B., Hemrika, W., Romijn, R.A., Gros, P., Cusack, S., and McCarthy, A.A. (2007). Structural insights into the Slit-Robo complex. *Proceedings of the National Academy of Sciences of the United States of America* 104, 14923-14928.
- Nakatsu, F. and Ohno H., (2003). Adaptor protein complexes as the key regulators of protein sorting in the post-golgi network. *Cell structure and function* 28, 419-429.
- Nassar, N., Hoffman, G.R., Manor, D., Clardy, J.C., and Cerione, R.A. (1998). Structures of Cdc42 bound to the active and catalytically compromised forms of Cdc42GAP. *Nature structural biology* 5, 1047-1052.
- Newey, S.E., Velamoor, V., Govek, E.E., and Van Aelst, L. (2005). Rho GTPases, dendritic structure, and mental retardation. *Journal of neurobiology* 64, 58-74.
- Ng, J., and Luo, L. (2004). Rho GTPases regulate axon growth through convergent and divergent signaling pathways. *Neuron* 44, 779-793.

- Nguyen Ba-Charvet, K.T., Brose, K., Marillat, V., Kidd, T., Goodman, C.S., Tessier-Lavigne, M., Sotelo, C., and Chedotal, A. (1999). Slit2-Mediated chemorepulsion and collapse of developing forebrain axons. *Neuron* 22, 6181-6186.
- Noctor, S.C., Martinez-Cerdeno, V., Ivic, L., and Kriegstein, A.R. (2004). Cortical neurons arise in symmetric and asymmetric division zones and migrate through specific phases. *Nature neuroscience* 7, 136-144.
- Nuesslein-Volhard, C., Wieschaus, E., and Kluding, H. (1984). Mutations affecting the pattern of the larval cuticle in *Drosophila melanogaster*. *Roux Arch. Dev. Biol.* 193, 267-282.
- Obenauer, J.C., Cantley, L.C. and Yaffe, M.B. (2003). Scansite 2.0: Proteome-wide prediction of cell signaling interaction using short sequence motifs. *Nucleic Acids Research* 31 (13), 3635-3641.
- O'Connor-Giles, K.M., Ho, L.L., and Ganetzky, B. (2008). Nervous wreck interacts with thickveins and the endocytic machinery to attenuate retrograde BMP signaling during synaptic growth. *Neuron* 58, 507-518.
- Ohno, H., Hirabayashi, S., Kansaku, A., Yao, I., Tajima, M., Nishimura, W., Ohnishi, H., Mashima, H., Fujita, T., Omata, M., et al. (2003). Carom: a novel membrane-associated guanylate kinase-interacting protein with two SH3 domains. *Oncogene* 22, 8422-8431.
- Ohshima, T., Hirasawa, M., Tabata, H., Mutoh, T., Adachi, T., Suzuki, H., Saruta, K., Iwasato, T., Itohara, S., Hashimoto, M., et al. (2007). Cdk5 is required for multipolar-to-bipolar transition during radial neuronal migration and proper dendrite development of pyramidal neurons in the cerebral cortex. *Development* 134, 2273-2282.
- Pappas, C.T., Bliss, K.T., Zieseniss, A. and Gregorio, C.C (2011). The Nebulin family: an actin support group. *Trends in Cell biology* 21, 29-37.
- Parry, D. A. D. (1982). Coiled-coils in α -helix-containing proteins - analysis of the residue types within the heptad repeat and the use of these data in the prediction of coiled-coils in other proteins. *Bioscience Reports*, 2(12), 1017-1024.
- Peter, B.J., Kent, H.M., Mills, I.G., Vallis, Y., Butler, P.J., Evans, P.R., and McMahon, H.T. (2004). BAR domains as sensors of membrane curvature: the amphiphysin BAR structure. *Science* 303, 495-499.
- Piper, M., Anderson, R., Dwivedy, A., Weinl, C., van Horck, F., Leung, K.M., Cogill, E., and Holt, C. (2006). Signalling mechanisms underlying Slit2-induced collapse of *Xenopus* retinal growth cones. *Neuron* 49, 215-228.
- Prince, V. E., Moens, C. B., Kimmel, C. B. and Ho, R. K. (1998). Zebrafish hox genes: expression in the hindbrain region of wild-type and mutants of the segmentation gene, valentino. *Development* 125, 393-406.
- Purves, D., Fitzpatrick, D., Hall, C.D., LaMantia, A.-S., McNamara, O. J., White, E. L. (2008). *Neuroscience Fourth Edition*
- Pykalainen, A., Boczkowska, M., Zhao, H.X., Saarikangas, J., Rebowski, G., Jansen, M., Hakanen, J., Koskela, E.V., Peranen, J., Vihinen, H., et al. (2011). Pinkbar is an epithelial-specific BAR domain protein that generates planar membrane structures. *Nat Struct Mol Biol* 18, 902-U959.
- Qualmann, B., and Kelly, R.B. (2000). Syndapin isoforms participate in receptor-mediated endocytosis and actin organization. *The Journal of cell biology* 148, 1047-1062.

- Qualmann, B., Roos, J., DiGregorio, P.J., and Kelly, R.B. (1999). Syndapin I, a synaptic dynamin-binding protein that associates with the neural Wiskott-Aldrich syndrome protein. *Molecular biology of the cell* 10, 501-513.
- Ramakers, G.J. (2002). Rho proteins, mental retardation and the cellular basis of cognition. *Trends in neurosciences* 25, 191-199.
- Rao, Y., Ma, Q., Vahedi-Faridi, A., Sundborger, A., Pechstein, A., Puchkov, D., Luo, L., Shupliakov, O., Saenger, W. and Haucke, V. (2010). Molecular basis for SH3 domain regulation of F-BAR-mediated membrane deformation. *Proc. Natl. Acad. Sci. USA* 107 (18): 8213-8218.
- Rensland, H., Lautwein, A., Wittinghofer, A. and Goody, R.S. (1991). Is there a rate-limiting step before GTP cleavage by H-ras p21? *Biochemistry* 30, 111181-11185.
- Rodal, A.A., Blunk, A.D., Akbergenova, Y., Jorquera, R.A., Buhl, L.K., and Littleton, J.T. (2011). A presynaptic endosomal trafficking pathway controls synaptic growth signaling. *The Journal of cell biology* 193, 201-217.
- Rothberg, J.M., Jacobs, J.R., Goodman, C.S., and Artavanis-Tsakonas, S. (1990). slit: An extracellular protein necessary for development of midline glia and commissural axon pathways contains both EGF and LRR domains. *Genes Dev.* 4, 2169-2187.
- Rudolph, M.G., Wittinghofer, A., and Vetter, I.R. (1999). Nucleotide binding to the G12V-mutant of Cdc42 investigated by X-ray diffraction and fluorescence spectroscopy: two different nucleotide states in one crystal. *Protein science: a publication of the Protein Society* 8, 778-787.
- Saarikangas, J., Hakanen, J., Mattila, P.K., Grumet, M., Salminen, M., and Lappalainen, P. (2008). ABBA regulates plasma-membrane and actin dynamics to promote radial glia extension. *Journal of cell science* 121, 1444-1454.
- Saarikangas, J., Zhao, H., Pykalainen, A., Laurinmaki, P., Mattila, P.K., Kinnunen, P.K., Butcher, S.J., and Lappalainen, P. (2009). Molecular mechanisms of membrane deformation by I-BAR domain proteins. *Current biology: CB* 19, 95-107.
- Saengsawang, W., Mitok, K., Viesselmann, C., Pietila, L., Lombard, D.C., Corey, S.J., and Dent, E.W. (2012). The F-BAR protein CIP4 inhibits neurite formation by producing lamellipodial protrusions. *Current biology: CB* 22, 494-501.
- Saitsu, H., Osaka, H., Sugiyama, S., Kurosawa, K., Mizuguchi, T., Nishiyama, K., Nishimura, A., Tsurusaki, Y., Doi, H., Miyake, N., et al. (2012). Early infantile epileptic encephalopathy associated with the disrupted gene encoding Slit-Robo Rho GTPase activating protein 2 (SRGAP2). *American journal of medical genetics. Part A* 158A, 199-205.
- Scheffzek, K., Ahmadian, M.R., Wiesmuller, L., Kabsch, W., Stege, P., Schmitz, F., and Wittinghofer, A. (1998). Structural analysis of the GAP-related domain from neurofibromin and its implications. *The EMBO journal* 17, 4313-4327.
- Schmidt, A., and Hall, A. (2002). Guanine nucleotide exchange factors for Rho GTPases: turning on the switch. *Genes & development* 16, 1587-1609.
- Schuske, K.R., Richmond, J.E., Matthies, D.S., Davis, W.S., Runz, S., Rube, D.A., van der Blik, A.M., and Jorgensen, E.M. (2003). Endophilin is required for synaptic vesicle endocytosis by localizing synaptojanin. *Neuron* 40, 749-762.
- Scita, G., Confalonieri, S., Lappalainen, P., and Suetsugu, S. (2008). IRSp53: crossing the road of membrane and actin dynamics in the formation of membrane protrusions. *Trends in cell biology* 18, 52-60.

- Scott, E.K., Reuter, J.E., and Luo, L. (2003). Small GTPase Cdc42 is required for multiple aspects of dendritic morphogenesis. *The Journal of neuroscience: the official journal of the Society for Neuroscience* 23, 3118-3123.
- Seeger, M., Tear, G., Ferres-Marco, D., and Goodman, C.S. (1993). Mutations affecting growth cone guidance in *Drosophila*: genes necessary for guidance toward or away from the midline. *Neuron* 10, 409-426.
- She, B.R., Liou, G.G., and Lin-Chao, S. (2002). Association of the growth-arrest-specific protein Gas7 with F-actin induces reorganization of microfilaments and promotes membrane outgrowth. *Experimental cell research* 273, 34-44.
- Shimada, A., Niwa, H., Tsujita, K., Suetsugu, S., Nitta, K., Hanawa-Suetsugu, K., Akasaka, R., Nishino, Y., Toyama, M., Chen, L., et al. (2007). Curved EFC/F-BAR-domain dimers are joined end to end into a filament for membrane invagination in endocytosis. *Cell* 129, 761-772.
- Shimada, A., Takano, K., Shirouzu, M., Hanawa-Suetsugu, K., Terada, T., Toyooka, K., Umehara, T., Yamamoto, M., Yokoyama, S., and Suetsugu, S. (2010). Mapping of the basic amino-acid residues responsible for tubulation and cellular protrusion by the EFC/F-BAR domain of pacsin2/Syndapin II. *FEBS letters* 584, 1111-1118.
- Soderling, S.H., Binns, K.L., Wayman, G.A., Davee, S.M., Ong, S.H., Pawson, T., and Scott, J.D. (2002). The WRP component of the WAVE-1 complex attenuates Rac-mediated signalling. *Nature cell biology* 4, 970-975.
- Sondek, J., Lambright, D.G., Noel, J.P., Hamm, H.E. and Sigler, P.B. (1994). GTPase mechanism of G proteins from the 1.7-Å crystal structure of transducin α -GDP-AlF₄. *Nature* 372, 276-279.
- Spoerner, M., Prisner, T.F., Bennati, M., Hertel, M.M., Weiden, N., Schweins, T. and Kalbitzer, H.R. (2005b). Conformational states of human H-Ras detected by high-field EPR, ENDOR, and 31P NMR spectroscopy. *Magnetic Resonance in Chemistry* 43, 74-83
- Streisinger, G., Walker, C., Dower, N., Knauber, D., and Singer, F. (1981). Production of clones of homozygous diploid zebra fish (*Brachydanio rerio*). *Nature* 291, 293-296.
- Suetsugu, S. (2009). The direction of actin polymerization for vesicle fission suggested from membranes tubulated by the EFC/F-BAR domain protein FBP17. *FEBS letters* 583, 3401-3404.
- Suetsugu, S., Murayama, K., Sakamoto, A., Hanawa-Suetsugu, K., Seto, A., Oikawa, T., Mishima, C., Shirouzu, M., Takenawa, T., and Yokoyama, S. (2006). The RAC binding domain/IRSp53-MIM homology domain of IRSp53 induces RAC-dependent membrane deformation. *The Journal of biological chemistry* 281, 35347-35358.
- Suetsugu, S., Toyooka, K., and Senju, Y. (2010). Subcellular membrane curvature mediated by the BAR domain superfamily proteins. *Seminars in cell & developmental biology* 21, 340-349.
- Tatusov, R.L., Koonin, E.V. and Lipman, D.J. (1997). A genomic perspective on protein families. *Science* 278 (5338), 631-637
- Tessier-Lavigne, M., and Goodman, C.S. (1996). The molecular biology of axon guidance. *Science* 274, 1123-1133.
- Thisse, B., Pflumio, S., Fürthauer, M., Loppin, B., Heyer, V., Degraeve, A., Woehl, R., Lux, A., Steffan, T., Charbonnier, X.Q. and Thisse, C. (2001). Expression of the zebrafish genome during embryogenesis. *Direct zfin entry*.
- Thisse, B., Thisse, C. and Wright, G.J. (2008). Embryonic and larval expression patterns from large scale screening for novel low affinity extracellular protein interactions. *Direct zfin entry*.

- Threadgill, R., Bobb, K., and Ghosh, A. (1997). Regulation of dendritic growth and remodeling by Rho, Rac, and Cdc42. *Neuron* 19, 625-634.
- Tsujita, K., Suetsugu, S., Sasaki, N., Furutani, M., Oikawa, T., and Takenawa, T. (2006). Coordination between the actin cytoskeleton and membrane deformation by a novel membrane tubulation domain of PCH proteins is involved in endocytosis. *Journal of Cell Biology* 172, 269-279.
- Tzivion, G., Shen, Y.H., and Zhu, J. (2001). 14-3-3 proteins; bringing new definitions to scaffolding. *Oncogene* 20, 6331-6338.
- Van Aelst, L., Joneson, T., and Bar-Sagi, D. (1996). Identification of a novel Rac1-interacting protein involved in membrane ruffling. *The EMBO journal* 15, 3778-3786.
- Vetter, I.R., and Wittinghofer, A. (2001). The guanine nucleotide-binding switch in three dimensions. *Science* 294, 1299-1304.
- Vetter, I.R., and Wittinghofer, A. (2001). The guanine nucleotide-binding switch in three dimensions. *Science* 294, 1299-1304.
- Vogt, D.L., Gray, C.D., Young, W.S., 3rd, Orellana, S.A., and Malouf, A.T. (2007). ARHGAP4 is a novel RhoGAP that mediates inhibition of cell motility and axon outgrowth. *Molecular and cellular neurosciences* 36, 332-342.
- Weed, S.A. and Parsons, J.T. (2001). Cortactin: coupling membrane dynamics to cortical actin assembly. *Oncogene* 20, 6418-6434.
- Wennerberg, K., and Der, C.J. (2004). Rho-family GTPases: it's not only Rac and Rho (and I like it). *Journal of cell science* 117, 1301-1312.
- Weng, Z., Rickles, R.J., Feng, S., Richard, S., Shaw, A.S., Schreiber, S.L., and Brugge, J.S. (1995). Structure-function analysis of SH3 domains: SH3 binding specificity altered by single amino acid substitutions. *Molecular and cellular biology* 15, 5627-5634.
- Wittinghofer, A., Scheffzek, K., and Ahmadian, M.R. (1997). The interaction of Ras with GTPase-activating proteins. *FEBS letters* 410, 63-67.
- Wong, K., Ren, X.R., Huang, Y.Z., Xie, Y., Liu, G., Saito, H., Tang, H., Wen, L., Brady-Kalnay, S.M., Mei, L., et al. (2001). Signal transduction in neuronal migration: roles of GTPase activating proteins and the small GTPase Cdc42 in the Slit-Robo pathway. *Cell* 107, 209-221.
- Wu, Y., Dowbenko, D., and Lasky, L.A. (1998). PSTPIP 2, a second tyrosine phosphorylated, cytoskeletal-associated protein that binds a PEST-type protein-tyrosine phosphatase. *The Journal of biological chemistry* 273, 30487-30496.
- Xian, J., Aitchison, A., Bobrow, L., Corbett, G., Pannell, R., Rabbitts, T., and Rabbitts, P. (2004). Targeted disruption of the 3p12 gene, Dutt1/Robo1, predisposes mice to lung adenocarcinomas and lymphomas with methylation of the gene promoter. *Cancer research* 64, 6432-6437.
- Yamagishi, A., Masuda, M., Ohki, T., Onishi, H., and Mochizuki, N. (2004). A novel actin bundling/filopodium-forming domain conserved in insulin receptor tyrosine kinase substrate p53 and missing in metastasis protein. *The Journal of biological chemistry* 279, 14929-14936.
- Yang, L., and Bashaw, G.J. (2006). Son of sevenless directly links the Robo receptor to rac activation to control axon repulsion at the midline. *Neuron* 52, 595-607.
- Yoshihara, Y., De Roo, M., and Muller, D. (2009). Dendritic spine formation and stabilization. *Current opinion in neurobiology* 19, 146-153.

- Yoshikawa, M., Mukai, Y., Okada, Y., Yoshioka, Y., Tsunoda, S., Tsutsumi, Y., Okada, N., Aird, W.C., Doi, T., and Nakagawa, S. (2008). Ligand-independent assembly of purified soluble magic roundabout (Robo4), a tumor-specific endothelial marker. *Protein expression and purification* 61, 78-82.
- Yu, H., and Schulten, K. (2013). Membrane sculpting by F-BAR domains studied by molecular dynamics simulations. *PLoS computational biology* 9, e1002892.
- Zamanian, J.L., and Kelly, R.B. (2003). Intersectin 1L guanine nucleotide exchange activity is regulated by adjacent src homology 3 domains that are also involved in endocytosis. *Molecular biology of the cell* 14, 1624-1637.
- Zapparova, O.N, Bryantseva, S.A, Dergunova, L.V., Raevskaya, N.M, Burakov, A.V, Bantysh, O.B, Shanina, N.A and Nadezhdina, E.S. (2009). Dynactin subunit p150Glued isoforms notable for differential interaction with microtubules. *Traffic* 10 (11), 1635-1646.
- Zhang, B. and Zheng, Y. (1998). Negative regulation of Rho family GTPases Cdc42 and Rac2 by homodimer formation. *Journal of Biological Chemistry* 273, 25728–25733.
- Zhang, B., Zhang, Y., Wang, Z.-X. and Zheng, Y. (2000). The role of Mg²⁺ cofactor in the guanine nucleotide exchange and GTP hydrolysis reactions of the Rho GTP-binding proteins. *The Journal of Biochemistry* 275, 25299-25307.
- Zhao, H. Hakala, M. and Lappalainen, P. (2010). ADF/cofilin binds phosphoinositides in a multivalent manner to act as a PIP(2)-density sensor. *Biophysical Journal* 98, 2327–2336.
- Zheng, W., Geng, A.Q., Li, P.F., Wang, Y., and Yuan, X.B. (2012). Robo4 regulates the radial migration of newborn neurons in developing neocortex. *Cerebral cortex* 22, 2587-2601.